

JAERI-Review
2001-003



JP0150335



ANNUAL REPORT OF KANSAI RESEARCH ESTABLISHMENT 1999
OCTOBER 1, 1995-MARCH 31, 2000

March 2001

Kansai Research Establishment

日本原子力研究所
Japan Atomic Energy Research Institute

本レポートは、日本原子力研究所が不定期に公刊している研究報告書です。
入手の問い合わせは、日本原子力研究所研究情報部研究情報課（〒319-1195 茨城県那珂郡東海村）あて、お申し越し下さい。なお、このほかに財団法人原子力弘済会資料センター（〒319-1195 茨城県那珂郡東海村日本原子力研究所内）で複写による実費頒布を行っております。

This report is issued irregularly.
Inquiries about availability of the reports should be addressed to Research Information Division, Department of Intellectual Resources, Japan Atomic Energy Research Institute, Tokai-mura, Naka-gun, Ibaraki-ken 〒319-1195, Japan.

Annual Report of Kansai Research Establishment 1999
October 1, 1995—March 31, 2000

Kansai Research Establishment

Japan Atomic Energy Research Institute
Kizu-cho, Souraku-gun, Kyoto-fu

(Received January 15, 2001)

This report is the first issue of the annual report of Kansai Research Establishment, Japan Atomic Energy Research Institute. It covers status reports of R&D and results of experiments conducted at the Advanced Photon Research Center and the Synchrotron Radiation Research Center during the period from October 1, 1995 to March 31, 2000.

Keywords: Annual Report, Kansai Research Establishment, JAERI, R&D, Advanced Photon Research Center, Synchrotron Radiation Research Center

Board of Editors for Annual Report

Editors: Takashi ARISAWA (Chief editor), Osamu SHIMOMURA, Akira NAGASHIMA, Norio OGIWARA,
Mitsuru YAMAGIWA, Masato KOIKE, Kazuhisa NAKAJIMA, Eisuke MINEHARA, Teikichi
SASAKI, Jun-ichiro MIZUKI, Yuji BABA, Atsushi FUJIMORI

Editorial assistants: Noboru TSUCHIDA, Sayaka HARAYAMA, Shuichi FUJITA, Tsutomu WATANABE,
Hironobu OGAWA

関西研究所年報 1999
1995年10月1日-2000年3月31日

日本原子力研究所
関西研究所

(2001年1月15日受理)

本報告書は、日本原子力研究所関西研究所の最初の年報であり、1995年10月から2000年3月31日までの期間に行われた光量子科学研究センター及び放射光科学研究センターの研究活動をまとめたものである。

関西研究所：〒619-0215 京都府相楽郡木津町梅美台8-1
年報編集委員会

(編集委員) 有澤孝(委員長)、下村理、長島章、荻原徳男、山極満、小池雅人、中島一久、峰原英介、
佐々木貞吉、水木純一郎、馬場祐治、藤森淳

(事務局) 土田昇、原山清香、藤田修一、渡邊勉、小川弘伸

Contents

Preface-----	ix
1. Summary-----	1
2. Facilities of Advanced Photon Research Center-----	3
3. Facilities of Synchrotron Radiation Research Center-----	4
4. Advanced Photon Science-----	5
4.1 High Peak Power Laser Development-----	7
4.1.1 Development of Ultrahigh Peak Power Lasers -----	7
Koichi YAMAKAWA, Makoto AOYAMA, Shin-ichi MATSUOKA, Yutaka AKAHANE, Fumihiko NAKANO	
4.1.2 High Repetition High Peak Power Laser -----	10
Yoichiro MARUYAMA, Masaaki KATO, Kazuyoku TEI, Hiromitsu KIRIYAMA, Fumiaki MATSUOKA, Tohru MATOBA, Takashi ARISAWA	
4.1.3 Characterization of Phase and Contrast for High Peak Power Laser with Ultrashort Pulse Width-----	13
Akito SAGISAKA, Makoto AOYAMA, Shin-ichi MATSUOKA, Yutaka AKAHANE, Fumihiko NAKANO, Koichi YAMAKAWA	
4.1.4 Wave Front Compensation by Deformable Mirror-----	14
Katsuaki AKAOKA, Takashi ARISAWA, Yoichiro MARUYAMA	
4.1.5 Wave-front Reconstruction of TW-class Ultrashort Laser Pulses using Fresnel Phase Retrieval Method-----	15
Shin-ichi MATSUOKA, Koichi YAMAKAWA	
4.1.6 Wave Front Correction by Photorefractive Crystal -----	16
Fumiaki MATSUOKA, Kazuyoku TEI, Masaaki KATO, Yoichiro MARUYAMA, Takashi ARISAWA	
4.1.7 Second Harmonic Generation by Quadrature Configuration-----	17
Hiromitsu KIRIYAMA, Shin-ichi MATSUOKA, Fumihiko NAKANO, Koichi YAMAKAWA	
4.1.8 Efficient Noncollinear Second Harmonic Generation with Proper Frequency Chirp and Tilted Pulse Fronts of Femtosecond Laser Pulses-----	18
Makoto AOYAMA, Fumihiko NAKANO, Yutaka AKAHANE, Koichi YAMAKAWA	
4.1.9 Ti:sapphire Free Running Laser for Pumping Yb Material-----	19
Akira OHZU, Akihiko NISHIMURA, Tsutomu USAMI, Tohru MATOBA	
4.1.10 Measurement of Thermal Lens Effects on Highly Pumped Ytterbium Glass-----	20
Akihiko NISHIMURA, Katsuaki AKAOKA, Akira SUGIYAMA, Akira OHZU, Tsutomu USAMI	
4.1.11 Laser Oscillation with Cooled Yb:YLF-----	21
Junji KAWANAKA, Koichi YAMAKAWA, Hajime NISHIOKA, Ken-ichi UEDA	
4.1.12 Dynamic Imaging using a Laser Pumped Soft X-ray Source -----	22
Yoji SUZUKI, Takashi ARISAWA, Akira OHZU, Yoichiro MARUYAMA	
4.1.13 Generation of Short Pulse Hard X-Ray by a Laser Assisted Discharge -----	23
Akira OHZU, Kazunori ITO	
4.2 X-ray Laser Development -----	24
4.2.1 The Outline of X-ray Laser Research in APRC -----	24
Akira NAGASHIMA, Keisuke NAGASHIMA, Masataka KADO, Tetsuya KAWACHI, Noboru HASEGAWA, Momoko TANAKA, Kouta SUKEGAWA, Peixiang LU, Akito SAGISAKA, Tomonao HOSOKAI, Kenjiro TAKAHASHI, Yoshiaki KATO	

4.2.2	X-ray Laser Generation with Transient Collisional Excitation Scheme -----	25
	Masataka KADO, Tetsuya KAWACHI, Noboru HASEGAWA, Momoko TANAKA, Kouta SUKEGAWA, Keisuke NAGASHIMA, Akira NAGASHIMA, Yoshiaki KATO	
4.2.3	Calculation of Populations of the Lithiumlike and Berylliumlike Ions in Low Temperature Dense Recombining Plasma -----	27
	Tetsuya KAWACHI	
4.2.4	Development of CPA Glass Laser System -----	29
	Kouta SUKEGAWA, Masataka KADO, Tetsuya KAWACHI, Noboru HASEGAWA, Momoko TANAKA, Keisuke NAGASHIMA, Akira NAGASHIMA, Yoshiaki KATO	
4.2.5	Design of Pulse Compressor of CPA Glass Laser System for X-ray Laser Research -----	30
	Tetsuya KAWACHI, Masataka KADO, Kouta SUKEGAWA, Noboru HASEGAWA, Momoko TANAKA, Keisuke NAGASHIMA, Akira NAGASHIMA, Yoshiaki KATO	
4.2.6	Line Focusing System for the Transient X-ray Laser -----	31
	Noboru HASEGAWA, Tetsuya KAWACHI, Masataka KADO, Momoko TANAKA, Kouta SUKEGAWA, Akira NAGASHIMA, Yoshiaki KATO	
4.2.7	Near Field Pattern of Transient Collisional Excitation X-ray Laser -----	32
	Momoko TANAKA, Tetsuya KAWACHI, Masataka KADO, Noboru HASEGAWA, Kouta SUKEGAWA, Akira NAGASHIMA, Yoshiaki KATO, Hisataka TAKENAKA	
4.2.8	Cold-electron Production for Optical-field Ionization X-ray Lasers using Mixed Gases -----	33
	Keisuke NAGASHIMA, Tohru MATOBA, Hiroshi TAKUMA	
4.2.9	Observation of X-ray Spectra from Nitrogen Clusters Irradiated with High-intensity Ultrashort Laser Pulses -----	34
	Akito SAGISAKA, Hiroshi HONDA, Kiminori KONDO, Hajime SUZUKI, Keisuke NAGASHIMA, Tetsuya KAWACHI, Akira NAGASHIMA, Yoshiaki KATO, Hiroshi TAKUMA	
4.2.10	Collisional Effects on Population Inversion in Optical-field-ionized Plasmas -----	35
	Akito SAGISAKA, Keisuke NAGASHIMA, Mitsuru YAMAGIWA, Tohru MATOBA, Hiroshi TAKUMA	
4.2.11	Short Pulse X-ray Source by Inverse-Compton Scattering -----	36
	Kenjiro TAKAHASHI, Masataka KADO, Akira NAGASHIMA, Yoshiaki KATO	
4.3	Free Electron Laser Development -----	37
4.3.1	The JAERI Industrial 1.3 micron 40 kW Highly-efficient FEL Driven by the Superconducting RF Linac -----	37
	Eisuke MINEHARA, Toshihiko YAMAUCHI, Masayoshi SUGIMOTO, Masaru SAWAMURA, Ryoichi HAJIMA, Ryoji NAGAI, Nobuhiro KIKUZAWA, Nobuyuki NISHIMORI, Toshiyuki SHIZUMA	
4.3.2	Optimization of an Optical Resonator with Insertable Scraper Output Coupler for the JAERI Far-infrared Free-electron Laser -----	39
	Ryoji NAGAI, Ryoichi HAJIMA, Nobuyuki NISHIMORI, Masaru SAWAMURA, Nobuhiro KIKUZAWA, Toshiyuki SHIZUMA, Eisuke MINEHARA	
4.3.3	Decomposition Experiment of Dioxins by IR Laser Irradiation -----	40
	Toshihiko YAMAUCHI, Eisuke MINEHARA, Nobuhiro KIKUZAWA, Takehito HAYAKAWA, Masaru SAWAMURA, Ryoji NAGAI, Nobuyuki NISHIMORI, Ryoichi HAJIMA, Toshiyuki SHIZUMA, Yasutaka KAMEI, Hisato IKAI, Shin-ichi ITOH, Yukio FURUKAWA	
4.3.4	Second Harmonic Generation in CdTe Plate by Free Electron Laser -----	41
	Toshihiko YAMAUCHI, Nobuhiro KIKUZAWA, Eisuke MINEHARA, Ryoji NAGAI, Nobuyuki NISHIMORI, Masaru SAWAMURA, Ryoichi HAJIMA, Toshiyuki SHIZUMA, Takehito HAYAKAWA	
4.3.5	Study on Recirculating Beam Transport and RF Instability for the Energy-recovery	

Experiment at JAERI-FEL-----	42
Ryoichi HAJIMA, Toshiyuki SHIZUMA, Eisuke MINEHARA	
4.3.6 Development of SHG Autocorrelator for Far Infrared JAERI-FEL-----	43
Nobuhiro KIKUZAWA, Toshihiko YAMAUCHI, Ryoji NAGAI, Eisuke MINEHARA	
4.3.7 Injector Design for the Energy-recovery Transport at JAERI-FEL-----	44
Toshiyuki SHIZUMA, Ryoichi HAJIMA, Nobuyuki NISHIMORI, Ryoji NAGAI, Eisuke MINEHARA	
4.3.8 Simulated Performance for the Present JAERI-FEL Injection System-----	45
Toshiyuki SHIZUMA, Ryoichi HAJIMA, Nobuyuki NISHIMORI, Ryoji NAGAI, Eisuke MINEHARA	
4.3.9 Interband E1 Transitions of ¹⁵⁷ Gd-----	46
Takehito HAYAKAWA, Yosuke TOH, Masumi OSHIMA, Yuichi HATSUKAWA, Makoto MATSUDA, Nobuo SHINOHARA, Hideki IIMURA, Yu Hu ZHANG, Hideshige KUSAKARI	
4.3.10 Temperature Characteristics of RF Control System for the JAERI-FEL-----	47
Masaru SAWAMURA, Ryoji NAGAI, Nobuhiro KIKUZAWA	
4.3.11 A Stable and Bright DC Electron Gun System with a Thermionic Cathode for the JAERI Far-infrared Free-electron Laser-----	48
Nobuyuki NISHIMORI, Ryoji NAGAI, Ryoichi HAJIMA, Toshiyuki SHIZUMA, Eisuke MINEHARA	
4.4 Optics Research and Development-----	49
4.4.1 Optics Development-----	49
Masato KOIKE	
4.4.2 Development of High Quality Large Laser Crystals for a CPA Laser System-----	50
Akira SUGIYAMA	
4.4.3 Development of Multilayer Mirrors for Soft X-rays-----	51
Osamu YODA, Masahiko ISHINO	
4.4.4 Evaluation of a Laminar-type Holographic Grating for the Soft X-ray Flat-field Spectrograph-----	52
Masato KOIKE, Yoshihisa HARADA, Eric GULLIKSON, Kazuo SANO, Sadayuki ISHIKAWA, Takashi IMAZONO, Stanley MROWKA, Mihiro YANAGIHARA, James. H. UNDERWOOD, Osamu YODA, Siro NAGAI, Takeshi NAMIOKA	
4.4.5 Femtosecond Time-resolved Fluorescence Spectra of a Coumarin Dye in Glass-forming Liquids-----	53
Hiroshi MURAKAMI	
4.4.6 Time-resolved UV-visible Absorption Spectroscopic Study on Fs Laser Ablation-----	54
Nobuyuki ICHINOSE, Shun-ichi KAWANISHI, Koji HATANAKA, Tamitake ITOH, Tsuyoshi ASAHI, Tsuneo SASUGA, Hiroshi FUKUMURA, Hiroshi MASUHARA	
4.4.7 UV Photochemical Oxygenation and Cross-linking of Thin Polymer Film-----	55
Nobuyuki ICHINOSE, Shun-ichi KAWANISHI, Toshiyuki TAMAI, Kazuhiko MIZUNO	
4.4.8 Energy Transfer Quenching of a Fluorescent Excited Radical Cation-----	56
Nobuyuki ICHINOSE, Tomoko TANAKA, Shun-ichi KAWANISHI, Tetsuro MAJIMA	
4.4.9 Development of Debris-free Target for Laser-plasma X-ray Source-----	57
Norio OGIWARA, Kazuaki SUGANUMA, Yoji SUZUKI	
4.4.10 Application to Chiral Chemistry-----	58
Yuichi SHIMIZU	
4.5 Laser Driven Particle Acceleration Development-----	59
4.5.1 Laser Driven Particle Acceleration Research-----	59
Kazuhisa NAKAJIMA, Tomonao HOSOKAI, Shuhei KANAZAWA, Masaki KANDO, Shuji KONDO,	

	Hideyuki KOTAKI, Takashi YOKOYAMA	
4.5.2	First Commissioning of 150 MeV Microtron Injected by Photocathode RF Gun -----	61
	Masaki KANDO, Hideyuki KOTAKI, Shuji KONDO, Tomonao HOSOKAI, Takashi YOKOYAMA, Shuhei KANAZAWA, Tohru MATOBA, Kazuhisa NAKAJIMA	
4.5.3	Experimental Characterization of Photocathode RF Gun -----	63
	Hideyuki KOTAKI, Masaki KANDO, Shuji KONDO, Hideki DEWA, Shuhei KANAZAWA, Takashi YOKOYAMA, Tomonao HOSOKAI, Fumio SAKAI, Kazuhisa NAKAJIMA	
4.5.4	Optical Guiding of Terrawatt Laser Pulses by Fast Z-pinch -----	65
	Tomonao HOSOKAI, Masaki KANDO, Hideki DEWA, Hideyuki KOTAKI, Shuji KONDO, Kazuhiko HORIAKA, Kazuhisa NAKAJIMA	
4.6	Advanced Photon Simulation Research -----	67
4.6.1	Development of Hydrodynamic Code for the Simulation of the Laser-Matter Interaction-----	68
	Takayuki UTSUMI	
4.6.2	Plasma Simulation with the Differential Algebraic Cubic Interpolated Propagation Scheme -	69
	Takayuki UTSUMI	
4.6.3	Molecular Dynamics Simulation on Laser Ablation due to Ultra-short pulse Laser Irradiation-----	70
	Ichirou FUKUMOTO, Etsuji OHMURA	
4.6.4	Laser Acceleration and Laser Propagation -----	71
	James KOGA, Susumu KATO, Levan N. TSINTSADZE, Yasuaki KISHIMOTO	
4.6.5	Calculation of the High Gain of the Transient Collisional X-ray Laser using a Thin Foil Target-----	73
	Akira SASAKI, Takayuki UTSUMI, Kengo MORIBAYASHI	
4.6.6	Inner-shell Ionization and Hollow Atom X-ray Lasers -----	74
	Kengo MORIBAYASHI, Akira SASAKI, Yutaka UESHIMA, Toshiki TAJIMA	
4.6.7	Development of an Atomic Model for X-ray Lasers-----	75
	Akira SASAKI, Takayuki UTSUMI, Kengo MORIBAYASHI	
4.6.8	Calculations of the Wavelengths of Ni-like 4d to 4p X-ray Laser Lines -----	76
	Takayuki UTSUMI	
4.6.9	Generation of High Energy Photons, Electrons, and Ions by Short-pulse Laser -----	77
	Mitsuru YAMAGIWA, Yutaka UESHIMA, Alexei ZHIDKOV, James KOGA, Akira SASAKI, Levan N. TSINTSADZE, Takuya ARAKAWA, Keisuke NAKAGAWA, Yasuaki KISHIMOTO, Toshiki TAJIMA	
4.6.10	Short-laser-pulse Driven Emission of Energetic Ions into a Solid Target from a Surface Layer Spalled by a Laser Prepulse-----	79
	Alexei ZHIDKOV, L.V. ZHIGILEI, Akira SASAKI, Toshiki TAJIMA	
4.6.11	Energy Distribution of Particles Accelerated During the Interaction of Intense Femtosecond Laser Pulses with Solids -----	80
	T. AUGUSTE, P. D'OLIVERA, S. HULIN, P. MONOT, Alexei ZHIDKOV, Akira SASAKI, Toshiki TAJIMA, Ya. FAENOV, T.A. PIKUZ, I. Yu. SKOBELEV	
4.6.12	Effect of Amplified Spontaneous Emission on the Interaction of Intense Femtosecond Laser Pulses with High-Z Solids -----	81
	Alexei ZHIDKOV, Akira SASAKI, Takayuki UTSUMI, Ichirou FUKUMOTO, Toshiki TAJIMA, F. SAITO, Y. HIRONAKA, K. G. NAKAMURA, K. KONDO, M. YOSHIDA	
5.	Synchrotron Radiation Science-----	83
5.1	Beamline -----	85

5.1.1 Construction of JAERI Beamline III (BL11XU) at SPring-8-----	85
Hideaki SHIWAKU	
5.1.2 Bending Magnet Beamline BL14B1 at SPring-8-----	86
Yasuo NISHIHATA, Hiroyuki KONISHI, Jun-ichiro MIZUKI	
5.1.3 Soft X-ray Beamline -BL23SU- at the SPring-8-----	87
Akane AGUI, Akitaka YOSHIGOE, Yuji SAITOH, Yuden TERAOKA, Akinari YOKOYA	
5.1.4 Construction of Public Beamlines in SPring-8-----	88
Hiroyuki KONISHI	
5.1.5 Present Status of BL-27 at the Photon Factory of KEK and Recent Highlights-----	90
Yuji BABA, Tetsuhiro SEKIGUCHI, Iwao SHIMOYAMA, Hiroyuki YAMAMOTO, Hideo OHTSUKA, Yoshihiro OKAMOTO, Tsuyoshi YAITA, Haruhiko MOTOHASHI	
5.2 High Pressure Science-----	91
5.2.1 <i>In situ</i> Observation of Diamond Formation Process under High Pressures and High Temperatures-----	91
Wataru UTSUMI, Takashi TANIGUCHI, Ken-ichi FUNAKOSHI, Osamu SHIMOMURA	
5.2.2 Construction of the Laser-heated Diamond Anvil Cell System-----	92
Tetsu WATANUKI, Takehiko YAGI, Tadashi KONDO, Osamu SHIMOMURA	
5.2.3 A First-order Liquid-Liquid Phase Transition in Phosphorus-----	93
Yoshinori KATAYAMA, Takeshi MIZUTANI, Wataru UTSUMI, Osamu SHIMOMURA, Masaaki YAMAKATA, Ken-ichi FUNAKOSHI	
5.3 Structural Physics Research-----	94
5.3.1 Pseudomorphic Growth of Pd Monolayer on Au(111) Electrode Surface-----	94
Masamitsu TAKAHASHI, Yukio HAYASHI, Jun-ichiro MIZUKI, Kazuhisa TAMURA, Toshihiro KONDO, Hideo NAOHARA, Kohei UOSAKI	
5.3.2 X-ray Diffraction Study on Quadrupolar Order in DyB ₂ C ₂ -----	95
Toshiya INAMI, Yoshikazu TANAKA, Tetsuya NAKAMURA, Hiroki YAMAUCHI, Hideya ONODERA, Kenji OHYAMA, Yasuo YAMAGUCHI	
5.3.3 High Real-space Resolution Structure of Oxide Glasses by High-energy X-ray Diffraction --	96
Kentaro SUZUYA, Yasuhiro YONEDA, Norimasa MATSUMOTO, Shinji KOHARA	
5.3.4 XAFS in the High-energy Region-----	97
Yasuo NISHIHATA, Jun-ichiro MIZUKI	
5.3.5 Crystal Structure of Pd-perovskite Catalyst in Redox Fluctuating Atmospheres-----	98
Yasuo NISHIHATA, Jun-ichiro MIZUKI, Takahiro AKAO, Hirohisa TANAKA, Mari UENISHI, Mareo KIMURA, Tokuhiko OKAMOTO	
5.3.6 Magnetic Properties of Some Perovskite Cobalt Oxides-----	99
Kenji YOSHII, Masaichiro MIZUMAKI, Yuji SAITOH, Takayuki MURO, Akio NAKAMURA	
5.3.7 Dielectric Investigation of Nanostructured Ferroelectrics-----	100
Yasuhiro YONEDA, Hikaru TERAUCHI	
5.3.8 Crystal Orientation Dependence of Spin Polarization on Cu in Single Crystal Co/Cu Multilayers by MCD Method-----	101
Jun-ichiro MIZUKI, Tatsuo FUKUDA, Hideaki YAMAMOTO, Atsushi KAMIJO, Motohiro SUZUKI, Naomi KAWAMURA, Masaichiro MIZUMAKI, Shunji GOTO	
5.3.9 X-ray and Neutron-scattering Studies of Orbital Order in Lightly Doped La _{1-x} Sr _x MnO ₃ -----	102
Tatsuo FUKUDA, Kazuma HIROTA, Kazuo TAKAHASHI, Yasuo ENDOH, Youichi MURAKAMI	
5.4 Surface Chemistry Research-----	103

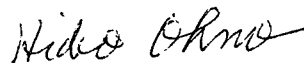
5.4.1	Desorption of Fragment Ions from Mono- and Multilayered Si(OCH ₃) ₄ Following Localized Inner-shell Electron Excitation-----	103
	Yuji BABA, Guohua WU, Iwao SHIMOYAMA, Tetsuhiro SEKIGUCHI	
5.4.2	Construction of Surface Reaction Analysis Apparatus and its Application to Initial Oxidation of Silicon Surfaces -----	104
	Yuden TERAOKA, Akitaka YOSHIGOE	
5.4.3	X-ray Absorption Near Edge Structures (XANES) Spectral Changes of 2-deoxy- <i>D</i> -ribose by Irradiation within Energy Region around Oxygen <i>K</i> -shell Absorption Edge-----	105
	Ken AKAMATSU, Akinari YOKOYA	
5.4.4	Orientation-selective Surface Photochemistry using Linearly Polarized Synchrotron Radiation-----	106
	Tetsuhiro SEKIGUCHI, Yuji BABA, Iwao SHIMOYAMA, Guohua WU	
5.5	Heavy Atom Science -----	107
5.5.1	Performance of Soft X-ray Emission Spectrometer Employing CCD Camera -----	107
	Teikichi A. SASAKI, Nobuhiko CHUGAN, Yasuji MURAMATSU	
5.5.2	Probing Bulk Electronic States of Solids by High-resolution Photoemission Spectroscopy ---	108
	Yuji SAITOH, Akira SEKIYAMA, Shigemasa SUGA	
5.6	Electronic Material Science -----	109
5.6.1	Photoelectron Spectroscopy for Strongly Correlated Electron Systems -----	109
	Tetsuo OKANE, Shin-ichi FUJIMORI, Akihiro INO, Atsushi FUJIMORI	
5.6.2	Synchrotron Radiation Mössbauer Spectroscopy of BL11XU in SPring-8 -----	110
	Takaya MITSUI	
5.7	Experimental Facilities Development -----	111
5.7.1	Investigation of an Effect of Gas Bremsstrahlung Due to Stored Electron Beam Condition of SPring-8 -----	111
	Yoshihiro ASANO, Toru MATSUMURA	
5.7.2	Development of X-ray Beam Position Monitor for Bending Magnet Beamline at SPring-8 ----	112
	Hideaki SHIWAKU	
6.	List of Publications -----	113
6.1	List of Publications on Advanced Photon Research Center -----	113
6.2	List of Publications on Synchrotron Radiation Research Center -----	139
Appendix A	Activities of the Research Committee -----	154
Appendix B	Organization of Kansai Research Establishment -----	158
Appendix C	Personnel -----	164
Appendix D	Symposia -----	167

Preface

Kansai Research Establishment of the Japan Atomic Energy Research Institute was established in October 1995 to promote the research and development of advanced lasers (Advanced Photon Research) and the third generation synchrotron radiation (Synchrotron Radiation Research). Its facilities are located in the Kansai area which is blessed with a long history and tradition, filled with frontier spirit and creativity. Its activity is devoted to innovation in technology, pioneering of new science, and creation of new industry.

“Advanced Photon Research” is conducted at the Advanced Photon Research Center in Kansai Science City, Kyoto Prefecture and “Synchrotron Radiation Research” at the Synchrotron Radiation Research Center in the SPring-8 (Super Photon ring – 8 GeV) facility in Harima Science Park City, Hyogo Prefecture.

Kansai Research Establishment is a unique and active research center in Japan as well as in the world, because high quality and high performance advanced photon sources are available in both laser and synchrotron radiation, such as 100 TW T-cube laser, X-ray laser, super conducting linac-based free electron laser, and the world’s brightest synchrotron radiation sources, SPring-8, covering from the soft and hard X-ray ranges (0.5 keV to 300 keV).



Hideo Ohno

Director General

Kansai Research Establishment, JAERI

This is a blank page.

1. Summary

Since its discovery in 1894, X-rays have been extensively applied not only to scientific research but also to medical and industrial uses. The 21st century is often referred to be an era of light, due to the progress achieved in the 20th century where new technologies such as fine fabrication, structural analysis, and information processing have been developed utilizing excellent properties of light. Development of new light sources have been continuously pursued: for example, the brilliant and high quality synchrotron radiation source, and the shorter-wavelength coherent laser beam with high brilliance and ultra short pulse width. These new light sources are expected to play important roles for observing and controlling nano- to atomic-scale phenomena such as the biological properties of DNA in a living cell and the physical properties of materials under extreme conditions. Therefore the 21st century will be an era of nano-technology. Where the versatility of the advanced synchrotron and laser technologies will prevail in many fields including material science, biological science, and industrial and medical applications.

For promoting the research on advanced laser sources, an Advisory Committee on the Advanced Photon Research was organized at Science and Technology Agency in 1995 to investigate 'Present and Future Prospect of Advanced Photon Research'.¹⁾ A preparatory organization for founding Kansai Research Establishment has started its activities in 1996 at Tokai (Tokai Research Establishment) and at Neyagawa (Osaka Laboratory for Radiation Chemistry).

In this 1st publication of the Annual Report, we summarize the research activities at both Advanced Photon Research Center and Synchrotron Radiation Research Center for the last 5 years since the foundation of Kansai Research Establishment in 1995. Brief history of Kansai Research Establishment is described below with emphases on construction of buildings and facilities.

Most of the research groups in the Advanced Photon Research Center have been moved from Tokai and Neyagawa to Kizu, the new site established in July 1999. During these 5 years, we have succeeded in operating an ultra high-peak-power laser with the world shortest pulse width, a superconducting linear-accelerator free electron laser with the world highest average power, and a laser driven X-ray laser with high efficiency. In addition to these laser development, the simulation group started using a super parallel computer at Neyagawa branch office in 1995, and a newer computer will be installed at the Kizu site by the end of March 2001.

Synchrotron Radiation Science at JAERI was started in 1990 by constructing the SPring-8 at Harima under cooperation with RIKEN. Three JAERI beamlines have been constructed since October 1997, and JASRI (Japan Synchrotron Radiation Research Institute) is now in charge of operation. By the end of 1999 forty-one beamlines have been constructed including public beamlines, specific beamlines, JAERI beamlines, and RIKEN beamlines. The Synchrotron Radiation Research Center is now promoting synchrotron radiation science in cooperation with the staffs at Tokai and Takasaki Research Establishments and Advanced Science Research Center by using the three JAERI beamlines and public beamlines. As of the year 1999, 40 JAERI staffs are working in 6 groups at the Advanced Photon Research Center, 47 in 6 groups at the Synchrotron Radiation Research Center, and 24 at the Administrative Department.

In parallel with the facility construction and operation, Kansai Research Establishment is promoting comprehensive light science based on the advanced lasers and the 3rd generation synchrotron radiation under close collaboration with academic, governmental and private research organizations.

In the Advanced Photon Science, a CPA (chirped pulse amplification) Ti:sapphire laser with 100 TW

1) "Present and Future Prospect of Advanced Photon Research", Published by the Japan Foundation of Public Communication on Science and Technology, Nov. 1996 (in Japanese)

peak power, 19fs pulse width and 10 Hz repetition rate has been development. Also an all solid-state high peak power laser pumped by laser diode array has been developed with sub-TW, 100 fs and 100 Hz performances. Together with these developments, the laser beam quality has been improved by way of several wave-front correction methods. As the next generation short pulse laser, Yb medium has been tested using strong excitation by a free-running Ti:sapphire pump laser. With LD-pumping of cooled Yb medium, we showed low oscillation threshold and broad-band oscillation. The X-ray laser program is undertaken for developing a compact and practical coherent X-ray source. A CPA Nd:glass has been used to drive the transient collisional excitation X-ray lasers. X-ray lasings have been obtained in 1999 in dense plasmas of Ti, Ag and Sn down to 12 nm wavelength. Under the free electron laser development program, we have achieved world-highest 2.34 kW average power at 23 micrometer wavelength, which has been applied to decomposition of dioxin by taking advantage of high power in the IR region. Under the optics research and development program, diffusion bonding of laser crystals to obtain large aperture high quality optical crystals, fabrication of multilayer mirrors for soft X-rays and development of a new flat-field soft X-ray diffraction grating with laminar structure grooves have been succeeded. In the laser driven particle acceleration development program, electron acceleration to over 200 MeV by the laser-induced wake field has been achieved. Based on this experience, a 150 MeV microtron with a photo-cathode RF gun has been developed in order to improve the electron beam quality and to rest a long acceleration channel with a Z-pinch guiding channel. Under the Advanced Photon Simulation Research program, simulation codes have been developed for laser-matter interaction studies under ultra short pulse, high intensity irradiation. These codes have been used for analyses and new proposals in laser acceleration, X-ray lasers, and atomic physics.

In the Synchrotron Radiation Science, we employ SPring-8 featured by its high brilliance, high energy photon, low emittance for material science to investigate the strongly correlated materials, random materials, actinide materials and so on in order to open the door to the advanced material science as well as emerge new materials. These efforts are useful to give positive effects even to the nuclear engineering materials. Beam lines constructed so far for JAERI in SPring-8 are the X-ray undulator beam line BL11XU, bending magnet beam line BL14B1, and soft X-ray undulator beam line BL23SU. Under the high-pressure science, laser-heated diamond anvil cell system was constructed. And in situ observation of diamond formation process and liquid-liquid phase transition have been surveyed. As a result we succeeded in observing the exceedingly rare transition in the pure substance of phosphorus. For the structural physics research pseudomorphic growth of Pd monolayer on Au electrode surface, quadrupolar order in DyB_2O_2 , oxide glasses, crystal structure of Pd-perovskite catalyst in redox fluctuating atmospheres, magnetic properties of perovskite cobalt oxides, nano-structured ferro-electrics, crystal orientation dependence of spin polarization on Cu in single crystal Co/Cu multilayers, and orbital order in lightly doped $\text{La}_{1-x}\text{Sr}_x\text{MnO}_3$ were studied. Under surface chemistry research program, a surface reaction analysis apparatus was constructed, and applied it to the initial oxidation of silicon surface. Desorption of fragment ions caused by inner shell electron excitation were studied, and a core-to-valence resonant excitation in adsorbed molecule was determined as a main trigger to the fragment ion desorption. X-ray absorption near edge structures spectral changes of ribose by irradiation in the energy region around oxygen K-shell absorption edge and orientation-selective surface photochemistry were also studied. For heavy atom research a soft X-ray emission spectrometer was developed using CCD camera. And bulk electronic states of solids were probed by high-resolution photoemission spectroscopy. In the electronic material science photoelectron spectroscopy for strongly correlated electron systems, and synchrotron Mössbauer spectroscopy were studied. For the further development of experimental facilities effect of gas brems-strahlung due to stored electron beam was studied from the viewpoint of radiation measurement together with the development of X-ray beam position monitor for bending magnet beam line.

2. Facilities of Advanced Photon Research Center

The main research subject at the Advanced Photon Research Center (APRC) is the development and application of novel light sources; T-cube lasers and X-ray lasers. The facilities of the APRC were constructed in Kizu-town at Kyoto in 1999 as shown in Figs.1-2. Main facilities consist of four laboratories as shown in Fig. 3.

T-cube lasers are compact lasers emitting coherent light with extremely high intensity in a focusing spot, comparable to that of a solar flare, in an ultra-short duration of a fifty-trillionth of a second. X-ray lasers, which emit highly coherent light of short wavelength in the X-ray region, are developed for practical use in scientific research and industrial applications.

Activities at APRC include development of a tunable wavelength free electron laser, laser particle acceleration which may lead to downsizing conventional electron accelerators by over a factor of one hundred, optics technologies indispensable for development of novel lasers, and computer simulation of various phenomena in the photon-matter interaction, which are difficult to observe experimentally in detail.

By utilizing the novel advanced light sources, APRC challenges development of new frontiers of science and innovative technologies. The ultra-short pulse duration of the T-cube lasers enables us to observe ultra-fast chemical reactions and molecular motions as if their movements are stopped. X-ray lasers allow observation of living cells with high precision. In addition, high intensity lasers can be used to create new matter by controlling nuclear states.

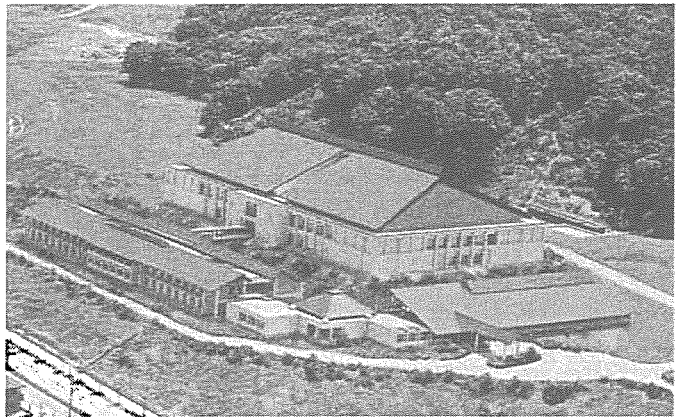


Fig. 1 Bird's eye view of the Advanced Photon Research Center

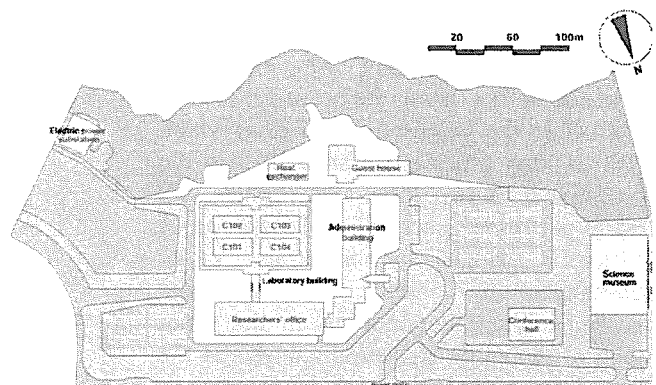


Fig. 2 Facilities of the Advanced Photon Research Center



C102 High repetition T-cube laser laboratory



C103 High peak power T-cube laser laboratory



C101 Laser acceleration laboratory



C104 X-ray laser laboratory

Fig. 3 Four main laboratories of the Advanced Photon Research Center
T-cube laser beams will be transmitted to the X-ray laser and the laser acceleration laboratories.

3. Facilities of Synchrotron Radiation Research Center

SPring-8 shown in Figs. 1-2, a large-scale synchrotron radiation facility Japan Atomic Energy Research Institute (JAERI) has constructed jointly with the Institute of Physical and Chemical Research (RIKEN) in Hyogo prefecture. It has been available to public users since October 1997.

SPring-8 provides synchrotron radiation with the world's highest performance, to users for research in a wide range of fields such as physics, chemistry, biology, medicine, and engineering.

The Synchrotron Radiation Research Center, now having three contract beamlines as shown in Fig. 3 at the SPing-8 facility, develops the application technologies of synchrotron radiation, and carries out research for "observing" what could not be seen before, and "creating" what could not be created before, using the powerful X-rays contained in the synchrotron radiation which is 100 million times more brilliant than the conventional X-ray tube. The center has already performed successful observation of structural change in materials under high-temperature and high-pressure conditions like the condition in the inner region of the earth, structural analysis at the atomic level of biological substances such as small protein crystals and elemental analysis of ultra micro substances which could not be detected by other means before. Furthermore, the center has succeeded in selective breaking of specific chemical bonds of molecules with synchrotron radiation and is continuing the study aiming at creating new materials.

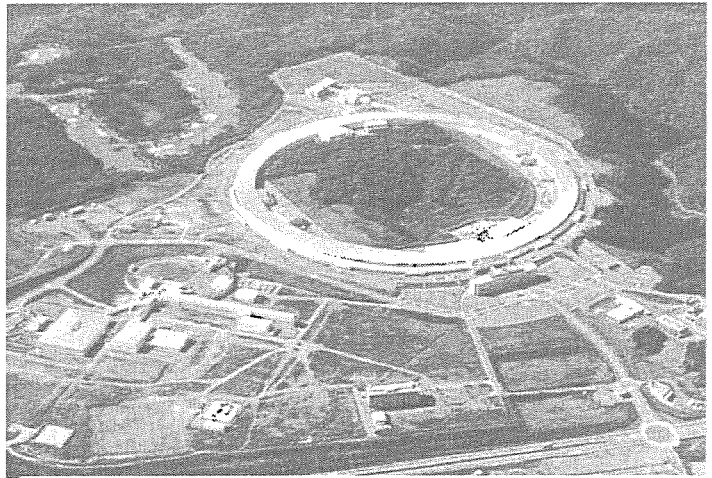


Fig. 1 Bird's eye view of the Synchrotron Radiation Research Center in SPing-8

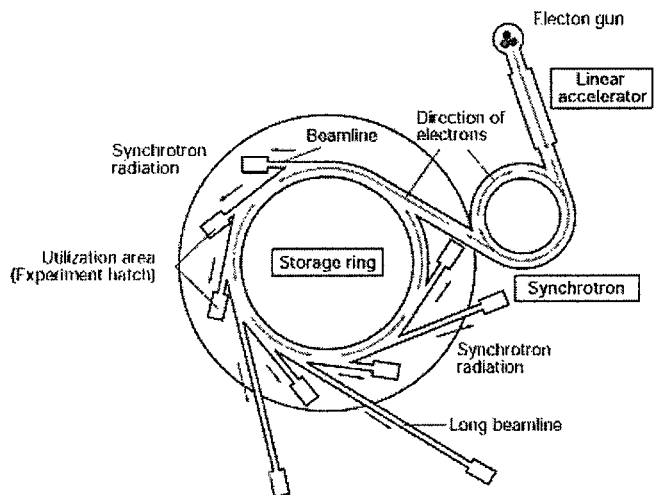
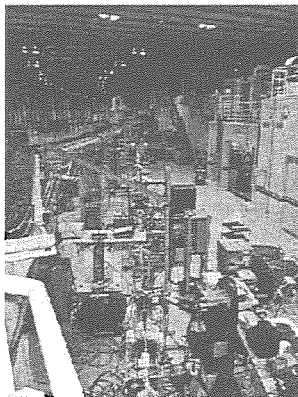
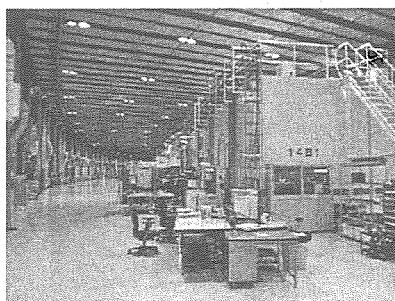


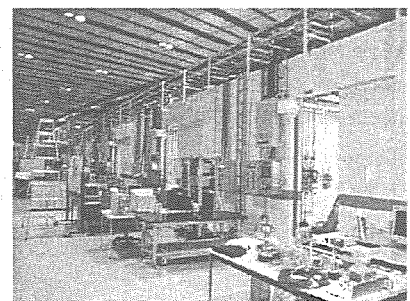
Fig. 2 Schematic diagrams of SPing-8



Beamline BL23SU
Research of biological substances and actinide elements by soft (longer wavelength) X-ray spectroscopy



Beamline BL14B1
Research of the structure and property of materials under the extreme circumstance of high temperature and high pressures and properties of the surface and interface



Beamline BL11XU
Research and development of new optical elements and materials

Fig. 3 The three beamlines (Experimental stations) of JAERI in SPing-8

4. Advanced photon science

This is a blank page.

4.1 High peak power laser development

4.1.1 Development of ultrahigh peak power lasers

Koichi YAMAKAWA, Makoto AOYAMA, Shinichi MATSUOKA,
Yutaka AKAHANE, Fumihiko NAKANO

1. Introduction

The combination of chirped-pulse amplification (CPA) and ultrabroad-band solid-state laser materials has made it possible to produce terawatt and even peta watt femtosecond pulses with enhanced average power^{1,2)}. During the past decade this technique has been extended to produce multiterawatt pulses of less than 20 fs in duration^{3,4)}. Such high peak power with a ultrashort pulse is useful for a variety of high-field applications.

We have developed the techniques for the generation of multiterawatt optical pulses in the 10 fs range based on the Ti:sapphire CPA laser, which has produced sub-20 fs pulses with peak and average powers of 100 TW and 19 W at the 10 Hz repetition rate⁵⁾. We also plan to extend this system to the one with petawatt power level.

2. Design and performance of a 100 TW, sub-20 fs, 10 Hz Ti:sapphire laser system

The 100 TW laser system consists of a Ti:sapphire oscillator, a pulse stretcher, a regenerative amplifier, two multi-pass amplifiers, and a vacuum pulse compressor. The 10 fs seed pulses from a Ti:sapphire oscillator were stretched by more than 100,000 times in a pulse stretcher. The stretched pulse is then first amplified in a regenerative amplifier. The regenerative amplifier uses two etalons with 3 μm thickness as a pulse shaper to encounter gain narrowing³⁻⁵⁾. The 8 mJ output from the regenerative amplifier is then introduced into a 4-pass preamplifier. The output pulse energy from the amplifier was ~ 340 mJ pumped by 700 mJ of 532 nm pump light. The output from the preamplifier is then sent to a 4-pass power amplifier. This amplifier uses a water cooled 40 mm diameter 25 mm long Ti:sapphire crystal and is pumped with a custom built Nd:YAG laser which is capable of producing ~ 7 J of 532 nm radiation at 10 Hz.

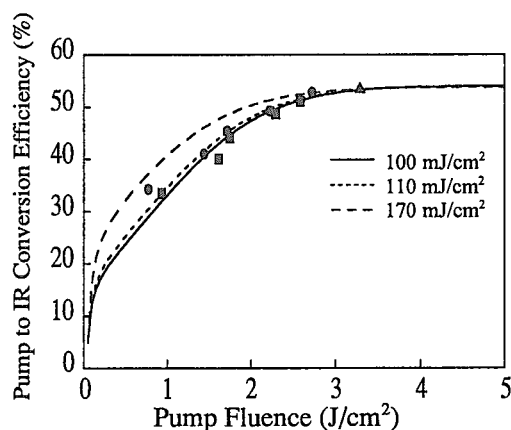


Fig. 1 Saturation characteristics of the 4-pass Ti:sapphire power-amplifier
The three curves show the calculated efficiency for the power amplifier as a function of pump pulse fluence for different input pulses.

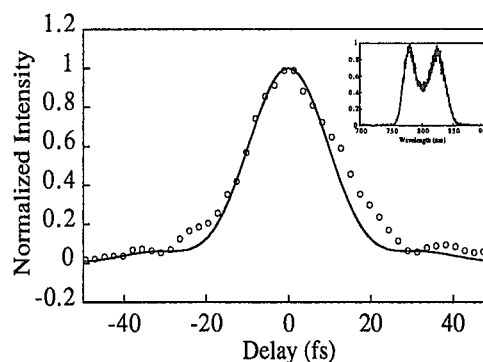


Fig. 2 Measured (circles) and calculated (solid line) autocorrelations for the compressed output
Inset: measured, amplified spectrum after the pulse compressor

The saturation characteristics for the power amplifier are shown in Fig. 1. Squares, circles and a triangle represent the measured efficiencies in the power amplifier. With 6.4 J of pump light incident upon the crystal the amplifier has produced 3.3 J at 800 nm radiation. Under these conditions, this amplifier has reached to the theoretically maximum conversion efficiency for 532 nm pump light to 800 nm radiation. This result agrees well with our model calculation. A typical autocorrelation trace and an amplified

spectrum after the compressor are shown in Fig. 2. The FWHM of the measured pulse duration is 18.7 fs. The transmission of the compressor, including the multilayer dielectric- and gold-coated turning optics, was $\sim 57\%$, yielding a compressed output pulse energy of ~ 1.9 J, which implies a peak power with a laser pulse of 102 TW. The spatial beam quality was about 2 and 2.5 times diffraction limited in vertical- and horizontal-planes, respectively. With an off-axis parabolic mirror with focal length of 150 mm, intensities at the focal spot of $\sim 3 \times 10^{20}$ W/cm² should be possible with this beam quality.

3. Towards a petawatt

To scale the system to peak powers above 100 TW, requires a Ti:sapphire crystal with a large aperture, a higher energy pump laser and larger diameter gratings. We plan to use an 80 mm diameter Ti:sapphire disk as a final booster amplifier. The major problem in constructing a high-energy laser amplifier such as the booster amplifier is parasitic lasing across the large-aperture amplifier disk at high-energy pump. Parasitic lasing is due to the formation of a laser cavity by Fresnel reflections at the material interfaces of

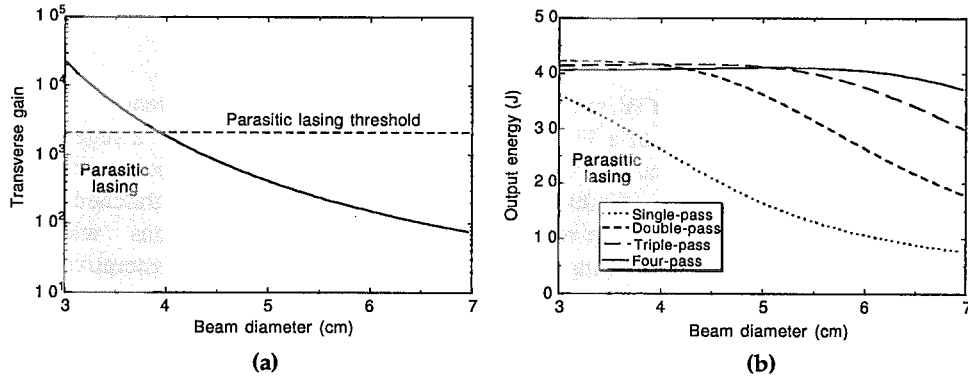


Fig. 3 Calculation results of transverse gain(a) and output energy(b) as a function of the beam diameter for 70-J pump energy

the gain medium. Above parasitic lasing threshold, the gain is clamped, no additional energy can be stored in the amplifier, and the amplifier efficiency is thus reduced. A technique for suppressing these parasitic lasing modes based on index matching the crystal edges with an absorbing doped polymer thermoplastic was developed and demonstrated for large-aperture Ti:sapphire disk amplifiers having significantly higher refractive index ($n = 1.76$)⁶⁾. The thermoplastic has a refractive index of 1.6849 for 800-nm light and the Fresnel reflection at the Ti:sapphire interface is thus estimated to be $\sim 0.048\%$. Therefore, parasitic lasing should not occur across the input face until the transverse gain is reached to $\sim 2,100$. Actually, the transverse gain of the parasitic lasing threshold would be increased by a few times, because the scattering at the frosted disk edge contributes additional transmission loss to the transverse cavity.

Figure 3(a) shows the calculated transverse gain on the disk faces as a function of the beam diameter⁷⁾. The parasitic lasing limit (gain $\sim 2,100$) for the crystal edge with the absorbing doped polymer thermoplastic is also indicated. In order to prevent the parasitic lasing, the beam diameter should be set to be at least ~ 40 mm. At the parasitic lasing threshold the pump fluence is ~ 5.6 J/cm². Figure 3(b) then shows the calculation result of the output energy depending on the beam diameter for single-, double-, triple-, and four-pass configurations. The 800-nm input energy is assumed to be 2.5 J in this calculation. At the diameter of 50-mm, the sufficient amplifier efficiency would be achieved in the triple-pass configuration, where the achievable amplified energy is estimated to be ~ 40 J and at the beam diameter of 50 mm.

We have designed the Offner triplet stretcher⁸⁾ and the Tracy-type compressor⁹⁾ based on the mixed gratings¹⁰⁾ for the petawatt-class laser pulse compression. In order to compensate for the phase distortion of the material in the laser system, we have chosen a 1,200-groove/mm ruled grating in the stretcher and 1,480-groove/mm holographic gratings in the compressor. In the stretcher, the optimized incident angle and perpendicular separation between gratings are 8.5° and 627 mm, respectively. In the compressor, the

incident angle and separation are calculated to be 24.4° and 544 mm, respectively. In this calculation, we assumed that BK7 of 112 cm was used as dispersive materials in the whole laser system. Although the fourth-order dispersion compensation can be accomplished here, the residual fifth-order-limited dispersion would broaden the initial 20-fs pulse to 25-fs duration. The designed stretcher would expand into ~ 800 -ps pulse duration of chirped pulse for spectral width of 70 nm, although the bandpass of the stretcher is approximately 100 nm (centered at 800 nm). The sufficiently long pulse duration of such chirped pulses should ensure the efficient amplification without the optical damage of the materials.

The compressor will consist of four gold coated 1480-groove/mm holographic gratings. A four-grating arrangement is determined by the maximum available size of 1,480-groove/mm gratings and the onset of optical breakdown of the coating material on the last grating. The sizes of the gratings are 220 mm \times 165 mm for the first and last gratings and 420 mm \times 210 mm for the second and third gratings, respectively. The diffraction efficiency of these gratings was expected to be greater than 92% over the 100-nm bandwidth (centered at 800 nm), and thus the overall efficiency should be greater than 70%.

4. Summary

With a compact three-stage Ti:sapphire CPA system, we have produced near diffraction limited and spectrally limited sub-20 fs duration pulses with a peak power in excess of 100 TW. We have designed the petawatt-class Ti:sapphire laser system consisting of the 10-fs oscillator, the four-stage amplifiers, the Offner triplet stretcher, and the Tracy-type compressor. The final large-aperture Ti:sapphire disk amplifier has been designed to achieve efficient energy extraction without the parasitic lasing on the disk faces, and the amplified energy has then been expected to be as much as ~ 40 J for the ~ 70 -J pump. The design of the Offner triplet stretcher and the Tracy-type compressor based on the mixed grating scheme can allow the laser system to generate the compressed pulse of ~ 25 -fs duration. Based on the diffraction efficiency of the grating, the energy of the compressed pulse is estimated to be >28 J. Thus, the peak power for laser pulse is expected to be >1.1 PW.

References

- 1) J. Zhou, C.-P. Huang, M. M. Murnane, H. C. Kapteyn: *Opt. Lett.* **20**, p.64, 1995
- 2) J. P. Chambaret, C. Le Blanc, A. Antonetti, G. Chériaux, P. F. Curley, G. Darpentigny, F. Salin: *Opt. Lett.* **21**, p.1921, 1996
- 3) C. P. J. Barty, T. Guo, C. Le Blanc, F. Raksi, C. Rose-Petruck, J. Squier, K. R. Wilson, V. V. Yakovlev, K. Yamakawa: *Opt. Lett.* **21**, p.668, 1996
- 4) K. Yamakawa, M Aoyama, S. Matsuoka, H. Takuma, C. P. J. Barty, D. Fittinghoff: *Opt. Lett.* **23**, p.525, 1998
- 5) K. Yamakawa, M Aoyama, S. Matsuoka, T. Kase, Y. Akahane, H. Takuma: *Opt. Lett.* **23**, p.1468, 1998
- 6) F. G. Patterson, J. Bonlie, D. Price, B. White: *Opt. Lett.* **24**, p.963, 1999
- 7) S. Matsuoka, K. Yamakawa: to be published.
- 8) G. Chériaux, P. Rousseau, F. Salin, J.P. Chambaret, B. Walker, L.F. Dimauro: *Opt. Lett.* **21**, p.414, 1996
- 9) E. B. Treacy: *IEEE J. Quantum Electron.* **QE-5**, p.454, 1969
- 10) S. Kane, J. Squier: *J. Opt. Soc. Am. B* **14**, p.1237, 1997

4.1.2 High repetition high peak power laser

Yoichiro MARUYAMA, Masaaki KATO, Kazuyoku TEI, Hiromitsu KIRIYAMA,
Fumiaki MATSUOKA, Tohru MATOBA, Takashi ARISAWA

1. Introduction

Ultra short pulse Ti:sapphire laser based on the chirped pulse amplification (CPA) have been developed expecting to drive X-ray lasers, electron acceleration, ion acceleration, micro machining, medical treatment, and so on. Advances in the ultrashort-pulse laser systems with high-repetition-rate and high-average-power are expected to be utilized in many applications, such as high-harmonic generation¹⁻⁴⁾ and material processing⁵⁾, that requires high average photon flux. However, the average power of such systems is still limited to several watts because the high average power caused thermal distortion both in the pump laser and high peak power laser operated at high repetition rate. We have been developing laser-diode-pumped Nd:YAG master oscillator power amplifier (MOPA) system for increasing repetition rates and average power with reduced thermal loads.^{6,7)} The performance of a laser-diode-pumped solid-state laser is superior to that of a lamp-pumped solid-state laser in efficiency, beam quality, output power stability, and compactness because diode lasers emit only suitable wavelength for pump laser or Nd:YAG laser.⁸⁻¹¹⁾ We have first demonstrated 250W average power (1.25 J at 200 Hz) with a Nd:YAG master oscillator power amplifier (MOPA) system.⁶⁾ This system also produced 105 W (0.62 J at 170 Hz) of frequency-doubled average power with a LiB_3O_5 (LBO) crystal. The beam quality was sufficient to pump a Ti:sapphire crystal to produce TW class peak power.⁷⁾

For the generation of high average power laser beams the second harmonic using a large KTP crystal is required with the gray tracking avoided. Although a high quality KTP crystal is able to be grown, its dimension is still small. And so far, a stacked type SHG using 4KTP crystals has been made to produce 5 J green at 33 Hz. For this stacking it is thought that a directly bonding of the crystals is much better to operate at higher repetition rate because higher thermal conductivity is anticipated for the bonded crystal.

Development has been extensively made since 1995, starting from an oscillator and proceeding to the amplifier stage. A wave front correction system both mechanically supported system, and phase conjugate mirror system was constructed and tested aiming at the high quality laser beam.

2. Components development

(1) System description

Figure 1 shows a schematic of an all solid state Nd:YAG laser with MOPA system consisting of an oscillator, a double-side pumped preamplifier (4-pass) and two double-side pumped post-amplifiers. The oscillator is a single-longitudinal-mode Nd:YAG laser. The dimensions of the Nd:YAG slab crystals are (6 x 6 x 82) mm³ for the preamplifier and (6 x 20 x 125) mm³ for the post-amplifiers. The Nd^{3+} concentration of these crystals is at 1%. The total internal reflection surfaces of the slab crystal are cut at the near Brewster's angle to reduce optical losses for the angle-

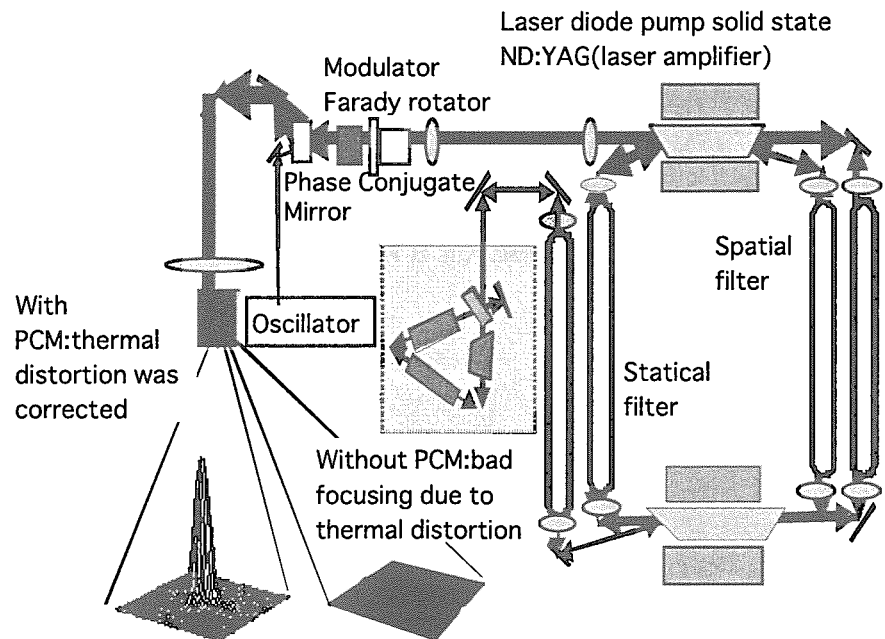


Fig. 1 High repetition all solid pump laser system for high peak power laser with photo-refractive wave front correction system

multiplexed configuration in the multi-pass amplification. These slab crystals are pumped by quasi-cw LDs (Laser Diodes) with a pulse duration of 250 microsecond. A total of 190 LD bars divided into two LD arrays are used for pumping the preamplifier, and 928 LD bars divided into two LD arrays are used in each post-amplifiers. The total stored energy in the post-amplifiers is about 3.5 J at LD drive peak current of 45 A at the repetition rate of 100 Hz. Each LD array is cooled by water to keep the temperature between 25 and 42°C to maximize the stored energy at the repetition rate of 200 Hz by controlling the emission wavelength from the LD array. The measured focal lengths for the both post-amplifiers induced by the thermal lensing effect are infinite (horizontal) and about -6 m (vertical) respectively, which agrees with the thermal analysis calculation.

The seed pulses from the oscillator pass through the preamplifier crystal four times. Two cylindrical telescopes are installed at each end of the preamplifier to enlarge the beam diameter in the preamplifier at the appropriate photon flux. The Faraday isolator is installed between the preamplifier and post-amplifier to prevent the interaction of the laser beams among optics. The laser beam size is adjusted between the preamplifier and the first post-amplifier by the cylindrical telescope. The post-amplifiers are composed of ring-type laser beam chains with a double pass. These two amplifiers are optically connected with each other by three image relay telescopes. The vacuum cells are installed between the telescope lenses to prevent the breakdown of the air by intense laser beams. At each focal point of the telescope between the first and second vacuum cells, pinholes are inserted. The first one acts as a spatial filter, and the second one prevents the laser medium from parasitic oscillations.

(2) All solid state pump laser module

As the laser pulse has to propagate from the oscillator over a long distance through the four-pass amplifier stage, careful adjustments of the cylindrical telescopes are required to avoid the clipping of the laser beam in the amplifier. The single-mode oscillator output amplified in the four-pass amplifier stage is increased by a factor of 100 (to 30 mJ) at 100 Hz. The beam quality described by M_x^2 (horizontal) and M_y^2 (vertical) are 1.0 and 1.1, respectively.

Two post amplifiers with an angle-multiplexed ring-type double-pass configuration, increase the pulse energy to 2.1 J at 100 Hz. This pulse energy corresponds to the energy extraction efficiency of 60% for the stored energy of 3.5 J in the post amplifiers. The average output power changed within a deviation of $\pm 1\%$. The near-field and far-field images of the MOPA output were recorded on a CCD camera. Although three Fresnel fringes are observed in the horizontal near-field image, the laser beam pattern is a near-top-hat profile. The far-field spot is obtained with a tens of 1-m focal length and has a small side lobe, which contains about 30% of the whole pulse energy. The horizontal size corresponds to 2x diffraction limit, which compares to the plane-wave propagation through a hard aperture. The vertical size corresponds to 3x diffraction limit, which compares to the Gaussian beam propagation. The temporal pulse profile of the MOPA output shows the pulse width of 85-ns FWHM and contains modulation which is imposed in the post amplifier chain. The modulation may be caused by the timing overlap between the first and second

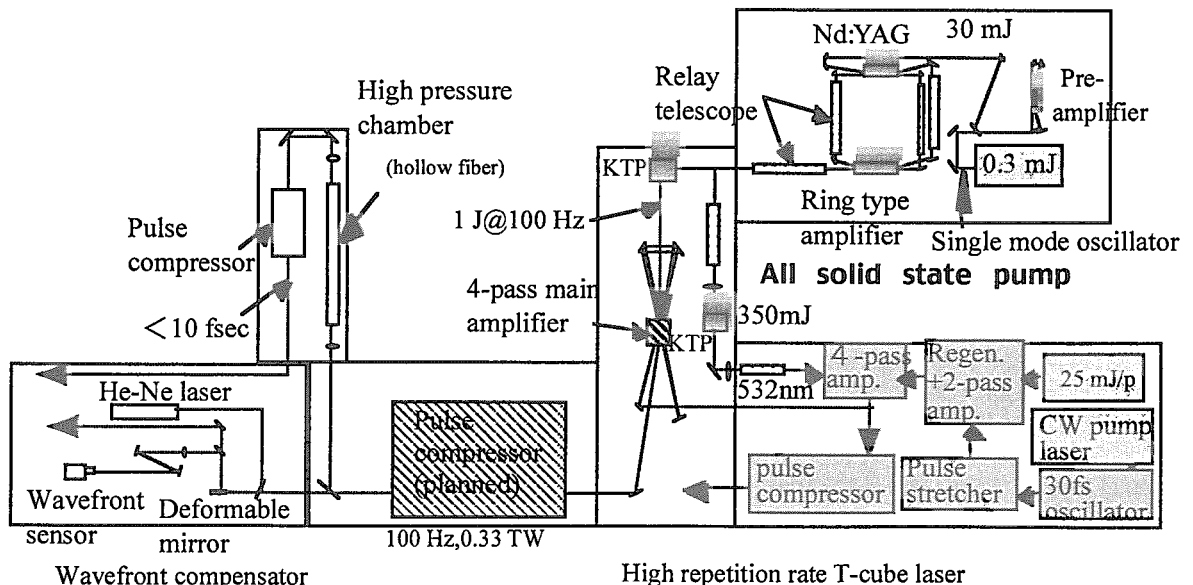


Fig. 2 Experimental setup for high repetition rate T-cube laser

passes.

(3) Second Harmonic Generation and Wave front compensation

The amplified laser pulse is relayed to the wavelength converter by an image relay telescope, which is composed of a directly bonded KTP crystal and a single KTP crystal. For bonding the KTP crystals, two (10 x 10 x 10) mm³ KTP crystals with gray tracking resistance are prepared. Two KTP crystals are contacted optically and pressurized and kept at 800°C to be bonded together. After bonding, the input and output surfaces are polished and AR-coated. Size of the bonded KTP crystal is (8 x 18 x 10) mm³. For the wavelength conversion, the temperature of the crystal is maintained at 70°C. The green laser pulse produced by this bonded crystal is separated by two dichroic mirrors and relayed to the Ti:sapphire post amplifier. Residual fundamental laser pulse is relayed to the single KTP crystal by the different telescope and introduced into a down collimator. The size of the KTP crystal is (10 x 10 x 10) mm³. The green laser pulse is used to pump the Ti:sapphire preamplifier. For the bonded KTP crystal a small phase mismatch around 4mrad between two segments is observed. As the angular acceptance of the KTP is wider than 40 mrad, this amount of phase mismatch does not affect the conversion efficiency. The average power of second harmonic emitted from the bonded KTP increases linearly. The input energy of 1 J in green is produced at the fundamental input energy of 2.1 J with the energy conversion efficiency is 48%. The pulse width of the second harmonic is shortened to around 70 ns from 85 ns for the fundamental process in the SHG process. The stability of average power in green is within $\pm 1\%$. This is due to the sufficient gain saturation in the double pass amplifier. After the bonded KTP, another single KTP is placed and residual fundamental laser pulse is introduced to increase conversion efficiency. With these crystals, the pulse energy of 1.35 J in green is obtained at the pulse repetition rate of 100 Hz.

(4) Ultra short pulse laser

In the preliminary system setup commercially available mode lock oscillator and pulse stretcher/compressor system were used. In order to increase the laser pulse energy two pass amplifier and four pass amplifier were developed, and at the output of the four pass amplifier 0.33 TW was obtained at 100 Hz. However at this moment a part of the pump power is supplied to the Ti:sapphire crystal, because the non-uniform power distribution in the laser beam causes the damage to the laser crystal. Therefore laser beam clean-up technologies development is underway.

3. Summary and outlook

We have developed a laser-diode-pumped zigzag slab Nd:YAG MOPA system that produced 2.1-J pulses at 100 Hz. The beam quantity was 3 times better than the diffraction limit in spite of the employment of phase conjugator. The coolant temperatures of all LD arrays are optimized to maximize the stored energy at the repetition rate of 200Hz. We are certain that an average power above 400 W in the infrared should be achievable with this system at the repetition rate of 200 Hz. In our initial system setup we used a LBO crystal for second harmonic generation (SHG), because damage occurred with the KTiOPO₄ (KTP) crystal. However, the pulse duration (85 ns) of the present system is longer than that of the prior system (20 ns). Hence we could come to use a KTP crystal which has a higher nonlinearity coefficient, and for 1-J SHG beam was achieved while avoiding damage to the crystal.

References

- 1) Q.Fu, F.Seier, S.K.Gayen, R.R.Alfono, *Opt.Lett.* **22**(10), 712-714(1997)
- 2) S.Backus, C.G.Durfee III, G.Mourou, H.C.Kapteyn, M.M.Murnane, *Opt.Lett.* **22**(16), 1256-1258(1997)
- 3) M.Nisoli, S.De Silverstri, O.Svelto, R.Szipocs, K.Frencz, Ch.Spielmann, et al., *Opt.Lett.* **22**(8), 522-524(1997)
- 4) A.Rundquist, C.G.Durfee III, Z.Chang, M.M.Murnane, H.C.Kapteyn, et al., *Science* **280**, 1412-1415(1998)
- 5) B.C.Stuart, M.D.Perry, M.D.Feit, L.B.Da Silba, A.M.Runbenchik, J.Neev, S.Herman, H.Nguyen, P.Armstrong, 1997 CLEO, *CTuR1*, 159-160(1997)
- 6) K.Tei, M.Kato, Y.Niwa, S.Harayama, Y.Maruyama, T.Matoba, and T.Arisawa, *Opt.Lett.* **23**(7), 514-516(1998)
- 7) K.Tei, M.Kato, Y.Niwa, S.Harayama, Y.Maruyama, Y.Matoba, T.Arisawa, *Proc.SPIE* **3265**, 212-218(1998)
- 8) J.J.Kasinski, W.Hughes, D.Dibiase, P.Bournes, R.Burnham, *IEEE J.Quant.Electron.* **28**(4), 977-985(1992)
- 9) L.E.Holder, C.Kennedy, L.Long, and G.Dube, *IEEE J.Quantum Electron.* **28**(4), 986-991(1992)
- 10) H.Injeyan, R.J.StPierre, J.G.Berg, R.C.Hilyard, M.E.Weber, M.Farey, *CLEO Paper CThC1*, p281(1994)
- 11) R.StPierre, G.Holleman, M.Valley, H.Injeyan, J.Berg, G.Harpole, R.Hilyard, M.Mitchell, M.Weber, J.Zamel, T.Engler, D.Hall, *Proc.Adv.Solid-State Lasers*, **10**, 288-291(1997)

4.1.3 Characterization of phase and contrast for high peak power laser with ultrashort pulse width

Akito SAGISAKA, Makoto AOYAMA, Shinichi MATSUOKA, Yutaka AKAHANE,
Fumihiko NAKANO, Koichi YAMAKAWA

1. Introduction

A high-peak power and ultrashort pulse laser system can realize pulses with a peak intensity over 10^{20} W/cm²¹⁾, which are indispensable for the variety of high-field applications such as the generation of ultrafast x-ray radiation²⁾ and high harmonic generation³⁾ from solid targets and photoionization pumped x-ray lasers⁴⁾. However the ultrashort laser pulses may, in general, have pedestals and/or amplified spontaneous emission (ASE) associated with the main laser pulse. In a laser produced plasma experiment, such a pedestal and/or ASE would create a low density plasma in advance of the arrival of the main laser pulse and thus significantly alter the physics of the laser/plasma interaction. It is, therefore, crucial to characterize the phase and contrast of the pulse.

2. Measurements

We used a part of our Ti:sapphire laser system operating at a 10 Hz repetition rate¹⁾. After the compressor, the phase of the compressed pulse was measured by using a second-harmonic generation (SHG) frequency-resolved optical gating (FROG) technique⁵⁾. Figure 1(a) shows the pulse intensity and phase in time retrieved from the SHG FROG trace. The pulse duration is 20 fs full width at half maximum (FWHM) accompanied with pre- and post-pulses. The intensity and phase of the pulse in frequency are also shown in Fig. 1(b). The spectral width is 67 nm FWHM. The measured pulse contains the group delay dispersion of 2.83×10^2 fs², cubic phase of 3.73×10^3 fs³, and quartic phase of 3.80×10^6 fs⁴. Based on these results, we conclude that the predominant phase distortion is quartic.

The contrast of the laser pulse was measured with a high dynamic range third-order cross-correlation technique. The arrangement of the cross-correlator is that of a Type I phase-matched, noncollinear geometry which incorporates SHG and THG nonlinear crystals. The detection limit of this apparatus is approximately 10^{-8} . The measured contrast is of the order of 10^{-6} limited by ASE coming from the amplifiers. ASE can be easily suppressed by two orders of magnitude by using a solid-state saturable absorber with a preamplifier before the pulse expander⁶⁾.

3. Summary

We have fully characterized a high-peak power, ultrashort laser pulse in a Ti:sapphire CPA laser system. The contrast, temporal and spectral phases of the 20 fs pulse are determined by using high dynamic range cross-correlation and SHG FROG techniques simultaneously. The pulse duration is 20 fs FWHM accompanied with pre- and post-pulses resulting from the predominant quartic phase distortion. The measured contrast of the pulse is of the order of 10^{-6} limited by ASE.

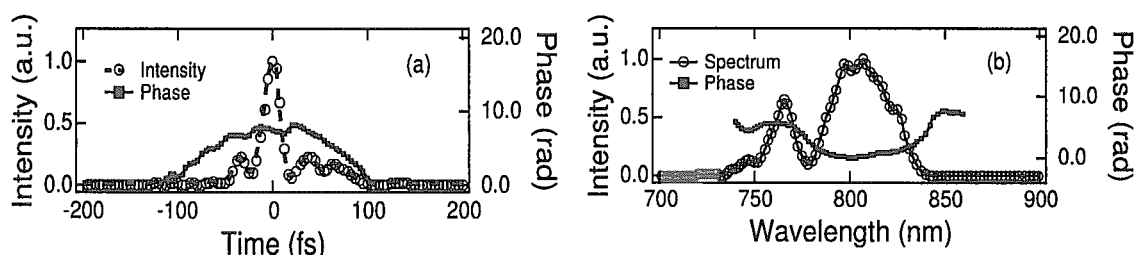


Fig. 1 Retrieved intensities and phases of the SHG FROG trace for the compressed pulse
(a) Pulse intensity and phase in time
(b) Spectral intensity and phase as a function of wavelength

References

- 1) K. Yamakawa, M. Aoyama, S. Matsuoka, T. Kase, Y. Akahane, H. Takuma: Opt. Lett. 23, p.1468, 1998
- 2) T. Guo, C. Rose-Petrucci, R. Jimenez, F. Raksi, J. Squier, B. Walker, K. R. Wilson, C. P. J. Barty: SPIE. 3157, p.84, 1997
- 3) P. Gibbon: IEEE J. Quantum Electron: 33, p.1915, 1997
- 4) H. C. Kapteyn: Appl. Opt. 31, p.4931, 1992
- 5) R. Trebino, K. W. DeLong, D. N. Fittinghoff, J. N. Sweetser, M. A. Krumbugel, B. A. Richman, D. J. Kane: Rev. Sci. Instrum. 68, p.3277, 1997
- 6) J. Itatani, J. Faure, M. Nantel, G. Mourou, S. Watanabe: Opt. Commun. 148, p.70, 1998

4.1.4 Wave front compensation by deformable mirror

Katsuaki AKAOKA, Takashi ARISAWA, Yoichiro MARUYAMA

1. Introduction

A Ti:sapphire laser with ultra short and high peak power suffers from thermal distortion in the laser crystals when pumped by high average power lasers. Through this thermally distorted optics a wave front of the laser beam is deformed which leads to a vague focal point even with focusing optics, which does not realize the ultra high intensity irradiation essentially required to the high peak power laser applications aiming at the ultra high field laser physics. We have succeeded in constructing the system with the combination of a measurement unit with Shack-Hartmann wave front sensor and a wave front correction unit with a deformable mirror. This system was applied to the 100 fs pulse laser and the control of wave front distortion to one tenth of the original value was achieved. ¹⁻⁵⁾

2. Wave front compensation system

Figure 1 shows the incident laser beam is enlarged by a telescope to conform with the effective diameter of the deformable mirror by taking out a part of the laser beam by a beam splitter to measure wavefront by a Shack-Hartman type sensor. A computer calculates out the control parameters in order to achieve a closed loop control by fitting the wave front of the incident laser beam to the final wave form. The Shack-Hartman type sensor uses 32x32 lenslet array, and the inclination of the wave front is measured as a focal position through the lenslet by CCD camera located on the back. Slopes are integrated by the computer to reconstruct the wave front and sent to the computer for control in order to drive 8x8 actuators on the deformable mirror.

3. Experiments

Static performance is characterized by correcting the wave front of a standard He-Ne laser beam, and we verified that 2 or 3 iterations is sufficient to control it at the repetition rate of 8 Hz. When applied to the second harmonics of the Nd:YAG laser pumped by LD, deviation from the flat wave front was improved from 0.96 micrometer to 0.12 micrometer in terms of P-V value. When applied to the Ti:sapphire laser with 100 fs pulse width and 0.25 TW peak power, wave front is corrected from 0.33 micrometer to 0.063 micrometer in RMS basis without changing pulse width.

4. Conclusion

We constructed the wave front correction system composed of wave front sensor and deformable mirror, and correction of one tenth of wavelength is achieved. This technique will be applied not only to the high average power pump laser but also ultra high peak power laser system.

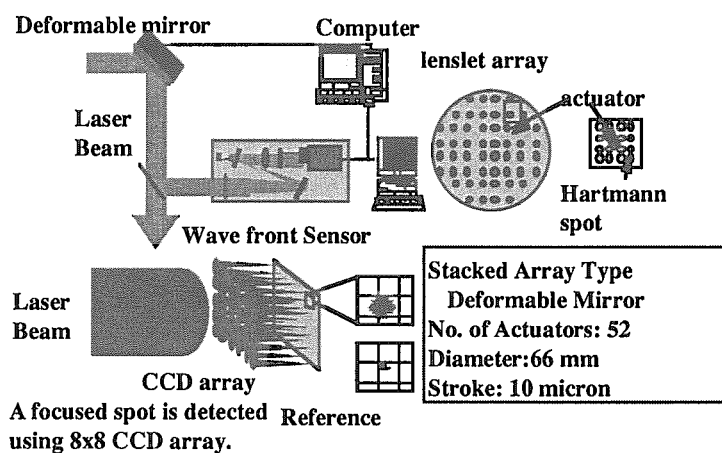


Fig. 1 Wave front correction system for high peak power

References

- 1) Y.Maruyama et al., OSA Topics on Advanced Solid State Lasers, Vol.1, p.369(1966)
- 2) K.Akaoka, Y.Maruyama and T.Arisawa, SPIE Vol.2986, p55(1997)
- 3) K.Akaoka, S.Harayama, K.Tei, Y.Maruyama and T.Arisawa, SPIE Vol.3265, p219(1988)
- 4) K.Akaoka, I.Wakaida and T.Arisawa, SPIE Vol.2375, p72(1995)
- 5) K.Akaoka, Y.Maruyama and T.Arisawa, Patent H10-254926(1998)

4.1.5 Wave-front reconstruction of TW-class ultrashort laser pulses using Fresnel phase retrieval method

Shinichi MATSUOKA, Koichi YAMAKAWA

1. Introduction

We demonstrate single-shot wave-front measurements of high peak power 100-fs laser pulses using Fresnel phase retrieval method. Wave fronts of terawatt-class laser pulses are measured and then compared with the measured far-field intensity distributions. With increasingly sophisticated high power laser applications, the quality and focusability of the laser beam have improved remarkably. The Fresnel phase retrieval method, which is a noninterferometric method, has a relatively simple configuration, and is applied to reconstruct the object image from the Fresnel diffracted image¹⁻²⁾. With this method, wave fronts of the beam are reconstructed from only two measured intensity distributions at two planes along the optical axis.

2. Experiments

We used a part of our Ti:sapphire chirped-pulse-amplifier laser system operating at a 10 Hz repetition rate³⁾. The laser system was operated to generate the laser pulses of 100-fs duration. We have measured the wave fronts of high energy 100-fs pulses at different conditions of the four-pass amplifier. Two intensity distributions of the laser beam passing through the pulse compressor at two planes were measured by two CCD cameras (COHU, 6400), which were placed after reflect-off from two beam-splitters located in the optical axis. The distance between two measured planes was set to be 1.7 m.

3. Results

Figure 1 shows the measurement of two intensity distributions and the reconstructed wave fronts of the 100 fs pulses at different output power levels. Output energies of the four-pass amplifier were controlled by changing the timing of the flash-lamps of the pump laser in the case of Figs. 1(a) and 1(b) and by changing the pump energy in Fig. 1(c). The wave fronts are somewhat deformed with increasing the output energy of the four-pass amplifier mainly due to thermal aberrations in the Ti:sapphire amplifier crystal. The accumulated B-integral through the laser system were also estimated to be 0.07 in Fig. 1(a) and less than 0.01 in Figs. 1(b) and 1(c), respectively. The reconstructed wave front of the 42 mJ output, corresponding to terawatt-level output peak power after compression, was 0.36λ peak-to-valley (PV) and 0.05λ root-mean-square (RMS), respectively. The spot diameter of the measured focused beam of this high peak power pulse was measured to be $\sim 170 \mu\text{m}$, corresponding to a 1.04 and a 1.07 times diffraction limited in vertical- and horizontal-planes, respectively. The measured far-field profiles agreed well with them calculated from the reconstructed wave fronts.

References

- 1) I.Kodama, M.Yamaguchi, N.Ohyama, T.Honda, K.Shinohara, A.Ito, T.Matsumura, K.Kinoshita and K.Yada, Opt. Commun. **125**, 36-42 (1996)
- 2) C.Roddier and F.Roddier, Appl. Opt. **32**, 2992-3008 (1993)
- 3) K.Yamakawa, M.Aoyama, S.Matsuoka, T.Kase, Y.Akahane and H.Takuma, Opt. Lett. **23**, 1468-1470 (1998)

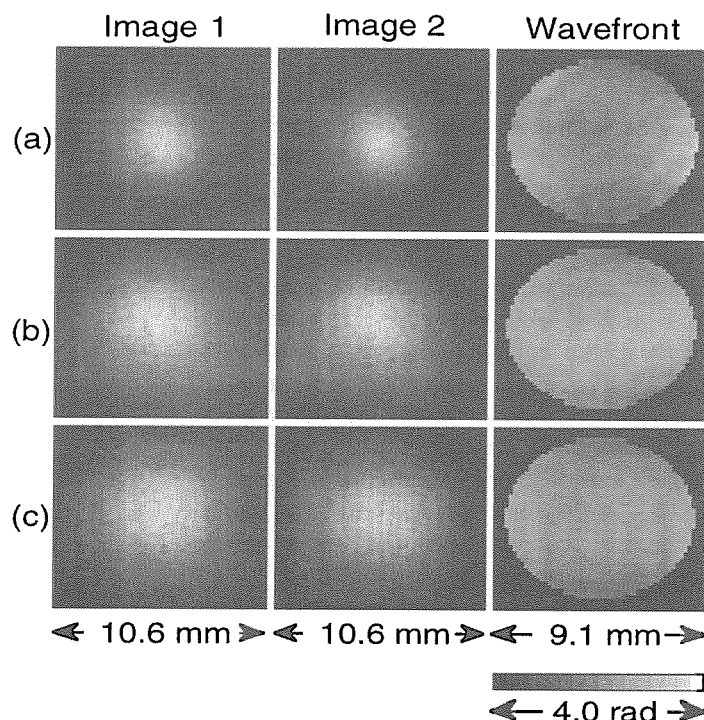


Fig. 1 The measured two intensity distributions (taken at Image 1 and Image 2) and the reconstructed wave fronts of the 100 fs pulses (a) without and (b) with a cylindrical lens with a focal length of 4.6 m

The reconstructed wave fronts were measured to be (a) 0.12λ PV and 0.02λ RMS, and (b) 2.07λ PV and 0.53λ RMS, respectively.

4.1.6 Wave front correction by photorefractive crystal

Fumiaki MATSUOKA, Kazuyoku TEI, Masaaki KATO, Yoichiro MARUYAMA, Takashi ARISAWA

1. Introduction

Recently, solid state phase conjugators in laser systems have been received much attention¹⁾⁻³⁾. However a Brillouin scattering (SBS) in solid state media needs high power over the threshold to generate phase conjugate wave. Laser beam with degraded quality increases this SBS threshold power level, which approaches the damage threshold. Therefore the dynamic range of solid state SBS is limited in a narrow range. Photorefractive(PR) effect, on the other hand, has the advantage of wide dynamic range because the effect has no power threshold. We have developed a Nd:YAG MOPA system with a PR self-pumped phase conjugator⁴⁾ based on the ring geometry.

2. Experimental setup

As shown in Fig. 1⁴⁾, a 45°-cut rhodium-doped (3,200 ppm) BaTiO₃ crystal is used as the phase conjugator to construct gratings in the crystal. To form this external loop arrangement, an image relay telescope is used. The crystal location coincides with the conjugate points of the telescope. This consideration brings about fast response time and great capability of phase compensation in the phase conjugation crystal. Adding to this arrangement, a dove prism is installed in the external loop to rotate the beam cross section by 90° in order to suppress the generation of higher order transverse grating modes in the direction perpendicular to the beam intersection plane. The beams in the external plane are phase-modulated by a mirror attached to a piezo transducer. The phase modulation of feedback beams suppresses the formation of reflection gratings in the crystal. Above considerations bring about a high reflectivity (>60%) and a high power stability (<1% for tens of minutes) while the phase conjugator preserves the capability of phase compensation for highly distorted beams ($M^2 > 100$).

3. Results

Figure 2 shows the far field pattern of MOPA output beam at the focus of the lens. The pattern has side lobes because the near field pattern has a flat-top shape peculiar to the saturation amplification. The radius of the first zero is 1.2 times diffraction limit. The output beam quality is the same with that of the seed beam except for the intensity profiles. This means that the phase conjugator corrects perfectly the phase distortion of the laser beam induced in the crystal.

4. Conclusion

We show that the developed photorefractive phase conjugator can be used in a high power or high energy Nd:YAG MOPA system. The arrangement offers for high power laser systems the high ability of phase correction using photorefractive effect.

Reference

- 1) Brignon, J-P. Huignard, M. H. Garrett and I. Mnushkina, *Opt Lett.* **22**(1997)215
- 2) H. J. Eichler, B. Liu, A. Haase, O. Mehl, A. Dehn, *Proc. of SPIE* **3263**(1998)20
- 3) M. J. Damzen, R. P. M. Green, K. S. Syed, *Opt. Lett.* **20**(1995)1704
- 4) K. Tei, Y. Niwa, M. Kato, Y. Maruyama, T. Arisawa, *Jpn. J. Appl. Phys.* **38**(1999)

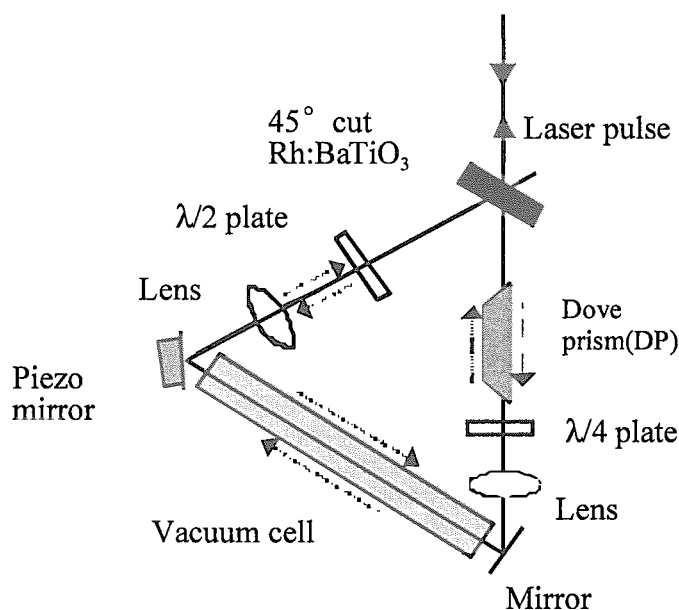


Fig. 1 Arrangement of phase conjugate mirror

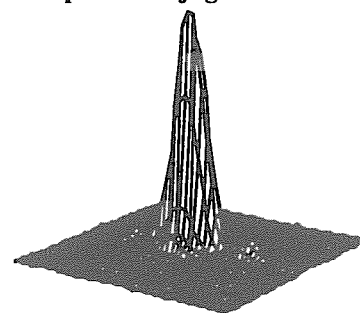


Fig. 2 Far-field profiles of the output beam from a system with the phase conjugate mirror

4.1.7 Second harmonic generation by quadrature configuration

Hiromitsu KIRIYAMA, Shinichi MATSUOKA, Fumihiko NAKANO, Koichi YAMAKAWA

1. Introduction

In order to generate a high energy green output at high efficiency for pumping a high peak power laser system with ultrashort pulse width, a quadrature frequency conversion scheme was proposed, which resulted in a high efficiency of 83% for frequency doubling of a Nd:YAG laser using CsLiB₆O₁₀ crystals. The second-harmonic output of 27.3 W was obtained from 32.7 W of an input fundamental laser at 10 Hz.

2. Experimental setup

The experimental arrangement for the two-pass quadrature frequency conversion scheme is shown in Fig. 1. The laser source used in this experiment was a Q-switched Nd:YAG laser system¹⁾, which is operated at a repetition rate of 10 Hz. The 1,064-nm fundamental beam diameter was 10.9 mm with a pulse duration of 13 ns FWHM. The two type II CsLiB₆O₁₀ (CLBO) crystals were arranged so that the 532-nm second-harmonic beams generated in them are orthogonally polarized²⁾. In this quadrature arrangement, the conversion efficiency is much less sensitive to the laser pulse nonuniformities than in a single crystal method, and the 532-nm second-harmonic beam generated in the first crystal does not interact with the 1,064-nm fundamental beam in the second crystal. The size of the CLBO crystals was 18 mm × 18 mm × 10 mm and had no antireflection coating. The crystals were operated at 160 °C and purged by Ar-gas to avoid the degradation. By using polarization rotation, the 1,064-nm fundamental beam was passed through this quadrature arrangement up to two times.

3. Results

Figure 2 shows the 532-nm second-harmonic conversion efficiency as a function of the input 1,064-nm fundamental laser intensity. As can be seen in this figure, a high conversion efficiency of 83% for second harmonic generation has been achieved with 1,064-nm incident laser intensity of 330 MW/cm². The 532-nm second-harmonic output energy of 2.73 J was obtained with the 1,064 nm incident laser energy of 3.27 J at 10 Hz. This successful operation demonstrates that it is applicable and scalable to the design of a high power laser system with high efficiency.

References

- 1) K.Yamakawa, M.Aoyama, S.Matsuoka, T.Kase, Y.Akahane, H. Takuma, *Opt. lett.* **23**, 1468-1470, 1998
- 2) D. Eimerl : *IEEE J. Quantum Electron.* **23**, 1361-1371, 1987.

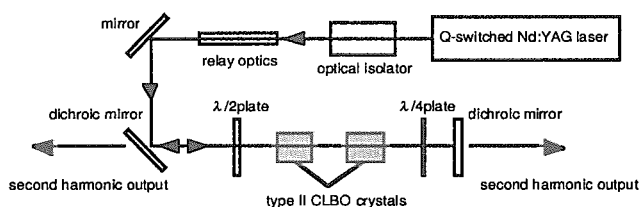


Fig. 1 Experimental arrangement of two pass quadrature frequency conversion scheme

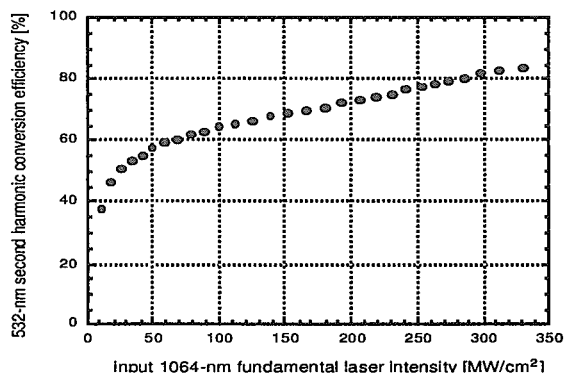


Fig. 2 532-nm second-harmonic conversion efficiency as a function of the input fundamental laser intensity

4.1.8 Efficient noncollinear second harmonic generation with proper frequency chirp and tilted pulse fronts of femtosecond laser pulses

Makoto AOYAMA, Fumihiko NAKANO, Yutaka AKAHANE, Koichi YAMAKAWA

1. Introduction

Since the appearance of the Ti:sapphire crystal, there has been rapid progress in generating femtosecond laser pulses and many studies have been devoted to the study of their frequency conversion. However it is well known that there are difficulties^{1,2)} of the frequency conversion in the nonlinear crystals like a second-harmonic generation (SHG) with femtosecond laser pulses. To overcome these problems, we are studying noncollinear type I second-harmonic generation with tilted pulse fronts of femtosecond pulses which have a proper frequency chirp³⁾. In this report, we mainly describe the compensation of the phase mismatch by controlling the frequency chirp of fundamental pulses and an improvement of the conversion efficiency with our scheme.

2. Experimental setup

A schematic picture is shown in Fig. 1. Two fundamental pulses are incident on gratings and their pulse fronts are tilted at appropriate angles. The two fundamental pulses are incident at the angles upon the nonlinear crystal so that the pulse fronts of the two fundamental pulses may propagate in the nonlinear crystal at angles such that the pulse fronts are normal to the Z-axis. The group-velocities on the Z-axis can be adjusted by the incident angles. SHG occurs on the superposition of the fundamental pulses and the generated SH pulses propagate in the Z direction. It should be noted that the angles of the two fundamental pulses on the crystal are adjusted under the phase-mismatching condition in this experiment. The proper frequency chirp of the fundamental pulses was introduced with the fundamental laser system for verifying compensation of the phase-mismatch.

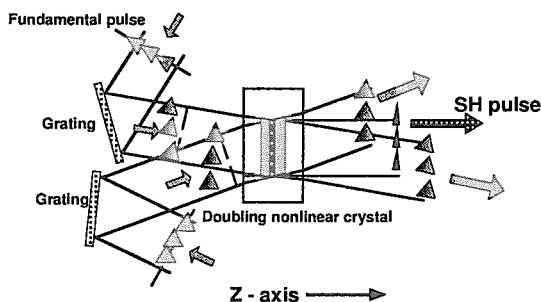


Fig. 1 Schematic diagram of noncollinear Type I SHG

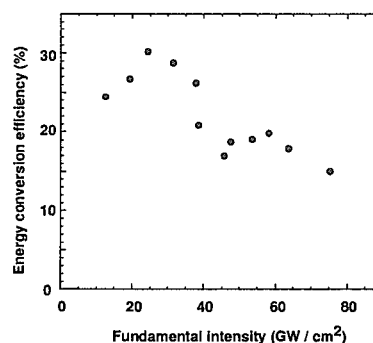


Fig. 2 Energy conversion efficiency of SHG as a function of fundamental intensity

3. Results

Energy conversion efficiencies to fundamental laser intensities from 10 to 75 GW/cm² are shown in Fig. 2. If the fundamental pulses were frequency chirp free, the conversion efficiency had to be numerically less than 0.4%. We experimentally obtained much higher conversion efficiencies by introducing the proper frequency chirp of the fundamental pulses. Maximum conversion efficiency was 30.1% at the intensity of 23.7 GW/cm². This meant that phase-mismatch was compensated by controlling the frequency chirp of the fundamental pulses.

References

- 1) I. V. Tomov, R. Fedosejevs, A. A. Offenberger, IEEE J. Quantum Electron. 18, p.2048, 1982
- 2) R. C. Eckard, J. Reintjes, IEEE J. Quantum Electron. 20, p.1178, 1984
- 3) M. Aoyama, T. Zhang, M. Tsukakoshi, K. Yamakawa, Jpn. J. Appl. Phys. 39, p.3394, 2000

4.1.9 Ti:sapphire free running laser for pumping Yb material

Akira OHZU, Akihiko NISHIMURA, Tsutomu USAMI, Tohru MATOBA

1. Introduction

A flashlamp pumped Ti:sapphire free running laser has been developed for pumping Yb doped solid state materials, which are anticipated as promising laser media for table top compact lasers¹⁾. This laser essentially requires high energy output at 920-975 nm with longer pulse duration for the efficient pumping. The fundamental parametric dependence and operating conditions useful for designing the high power pumping laser were surveyed.

2. Experimental setup

As shown in Fig. 1, a Ti:sapphire rod (length 190 mm, diameter 8 mm, 0.1 wt%) parallel to a xenon flashlamp is installed in a single elliptical reflector made of ceramics provided as a laser head. A cerium-doped quartz plate and a plastic filter were placed between the flashlamp and the Ti:sapphire rod. With the cerium-doped plate and glass tube of the lamp, UV emission of below 400 nm from the flashlamp, which induces solarization in the rod, is firstly converted to visible light above 400 nm useful for Ti:sapphire pumping²⁾. The remaining UV emission below 400 nm is rejected with the plastic filter. A pulsed power discharge circuit with the storage capacitor of 130 μ F, which uses an ignitron switch and is capable of continuously pulsed discharge at 0.5 Hz is terminated to the flashlamp in the head.

3. Results

A maximum output energy of 6.8 J with an electrical efficiency of 0.7% and a pulse width of 140 μ s has been obtained at 800 nm. An output energy of 2 J sufficient for high energy pumping to a Yb glass was achieved at 920 nm. Furthermore, the other lasing performance indispensable for a pumping laser source, such as output energy stability of $\pm 5\%$, polarization over 0.96, and spatial pointing stability over 95 % in 5 mrad at the maximum output energy, were also obtained. Near top-hat spatial profile in the laser intensity was observed. Laser action was obtained in the range from 720 to 950 nm. It was found that an input power above 600 J caused a thermal distortion of the rod, which strongly influences on the spatial profile.

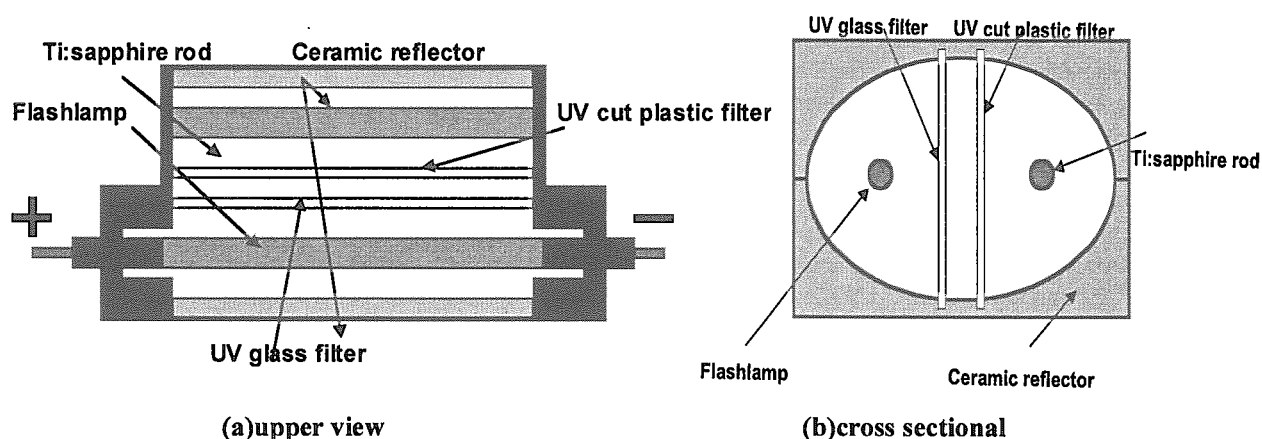


Fig. 1 A schematic diagram of Ti:sapphire free running laser

References

- 1) S. Biswal, J. Nees, A. Nishimura, H. Takuma, G. Mourou : Opt. Commun., **160**, 92-97, 1999
- 2) A. Hoffstädt : IEEE J. Quantum Electronics, **33**, 1850-1863, 1997

4.1.10 Measurement of thermal lens effects on highly pumped ytterbium glass

Akihiko NISHIMURA, Katsuaki AKAOKA, Akira SUGIYAMA, Akira OHZU, Tsutomu USAMI

1. Introduction

Coherent X-ray generation driven by a CPA laser has been involved in advanced photon research. Since the demonstration of CPA, 15 years have been passed. Nowadays, Ti:sapphire and Nd:glass are used for commercially available high peak power CPA lasers in the world ¹⁾. In principle, tunable solid state gain materials can be candidates for CPA. All of them are four-level materials. Practically, the style of CPA laser system is strongly dependent on the gain materials and pumping methods.

On the other hands, quasi-three level of ytterbium doped materials show very low quantum defect and are expected to be available for the LD direct pumping, which provides the possibility to make CPA laser systems more compact and efficient. A flashlamp pump Ti:sapphire laser was developed for a high energy pumping source. Thermal lens effects should be suppressed to avoid the unstable condition of a regenerative amplifier cavity. In order to measure the time constant of thermal lens, we have applied Shack-Hartmann wavefront sensor. The pumping intensity on the Yb:glass exceeded 800 kW/cm^2 , which is several times higher than laser diode pumping intensity. In the above mentioned CPA laser development history, high intensity pumping experiments for Yb:glass CPA has been proceeded in JAERI. The features of ytterbium materials will provide the possibility to make CPA laser systems more compact and efficient than the conventional Ti:sapphire system, which can lead to the compact drivers for X-ray lasers in the future.

2. Experimental setup

The experimental setup consists of a wavefront monitor, a flashlamp pumped Ti:sapphire laser, and a Yb:glass oscillator ²⁾. In the Shack-Hartmann sensor the each focal position focused by a lenslet array directly indicates the slope of the local wavefront so that it has the great advantage of responsibility in time-resolve measurements in comparison with other interference type sensor. A stabilized He-Ne laser was used as a reference source. An IR cut filter was inserted to protect a CCD camera from the Yb:glass laser output pulses. The wavefront of the laser beam from the Yb:glass oscillator was imaged on the CCD camera through the lenslet. Wavefront is divided by a 32×32 lenslet array and focused on a CCD camera with 256×256 array. A centroid of each focal point on the CCD array was calculated based on the signal intensity distribution of the 8×8 CCD arrays, which increased the accuracy of the position of the focal points. Data was sampled at 100 Hz repetition. The reconstruction of the wavefront and the expansion to Zernike coefficients were carried out. The 19 wt% Yb doped phosphate glass was used. The pumping wavelength was 915 nm. The absorption cross section of the Yb:glass was $0.15 \times 10^{-20} \text{ cm}^2$ at 915 nm. The size of the Yb:glass was $15 \times 14 \times 8.7$ mm. The pump pulse was focused on the surface with the area of 15×14 mm by a 25 cm focal length spherical lens. The pumping intensity was reached to 800 kW/cm^2 from 1 J/pulse pump laser. The Yb:glass was set in a plane-concave cavity with the length of 37 cm at room temperature. The output coupler was 10% transmission at 1,030 nm.

3. Results

We measured the thermal lens effects on a strongly pumped Yb:glass oscillator pumped by a flashlamp pumped free running Ti:sapphire laser by a Shack-Hartmann sensor, which was developed and improved. The pumping intensity of 800 kW/cm^2 was realized on the focal plane on the Yb phosphate glass surface. The pulse energy of 330 mJ from Yb:glass was obtained with 53% slope efficiency with 0.5 Hz repetition rate. The absorbed pump pulse energy inside Yb:glass caused strong thermal lens effects. The focus coefficient and the astigmatism coefficients completely disappeared after 300 ms from the laser oscillation. These basic thermal data were employed for the proper design of CPA laser system with Yb-glass laser materials. And this experimental apparatus can be used for the characterization of various types of Yb-doped materials and is being improved year by year keeping with the upgrade of operation software.

Information exchange for Yb:glass CPA laser has been held under the international collaboration with Univ. of Michigan, Center for Ultrafast Optical Science since 1999.

Reference

- 1) "Present and Future Prospects of Advanced Photon Research", Organized by Atomic Energy Bureau in Science Technology Agency, Edited by Advisory Committee on the Advanced Photon Researches, Published by The Japan Foundation of Public Communication on Science and Technology, Nov. 1996
- 2) A. Nishimura, et al., Proc. SPIE, 3889, pp. 414-419

4.1.11 Laser oscillation with cooled Yb:YLF

Junji KAWANAKA, Koichi YAMAKAWA, Hajime NISHIOKA^{a)}, Kenichi UEDA^{a)}

a) Institute for Laser Science, University of Electro-Communications

1. Introduction

High-peak power lasers with compactness, free-maintenance and high output power stability are in high demand for many application fields such as material processing and high field science. Directly diode-pumped solid-state lasers are one of practical candidates which will enable such easy operation. Yb:YLF has an absorption spectral range centered at 940 nm, which is matched to the emission wavelength of high power laser diodes, and a wide emission spectrum width of 35 nm, which can generate a short pulse with 40 fs duration. The energy extraction efficiency, however, of Yb:YLF is too low for diode-pumping at room temperature, because there are much re-absorption of the lower level population in the laser transition which is necessarily found in quasi-three-level laser system. We demonstrate an efficient diode-pumped laser oscillator with a cooled Yb:YLF crystal for the first time. ¹⁾ An active population control of cooling an Yb:YLF crystal was used to increase the energy extraction efficiency by suppressing the re-absorption.

2. Experimental setup

Figure 1 shows a schematic diagram of diode-pumped laser oscillator with a cooled Yb:YLF crystal. Two high-brightness single-emitter laser diodes were used as a pump source. Each laser beam was tightly focussed on a laser crystal using two lenses and a telescope using a cylindrical lens pair. Pump intensity could thus be changed up to 100 kW/cm². We used a thin Yb:YLF crystal with a thickness of 0.3 mm. The Yb:YLF thin plate was set on the sample stage of a cryostat and the crystal temperature was controlled between 8 K and 300 K. The x-type cavity configuration consisted of a flat high reflector, a flat output coupler, and two dichroic concave mirrors. The laser output power was measured as a function of a crystal temperature.

3. Results

Figure 2 shows the output power as the Yb:YLF crystal was cooled. The output power and power conversion efficiency at 50 K was increased to 30% which was 1-order larger than that at room temperature. Cooling the Yb:YLF crystal is an effective method to increase the power conversion efficiency when laser diodes are used for pumping with a lower intensity comparably to other solid-state laser source.

References

- 1) J. Kawanaka, H. Nishioka, K. Ueda, CLEO 2000 Technical Digest CWC3, 250-251 (2000)

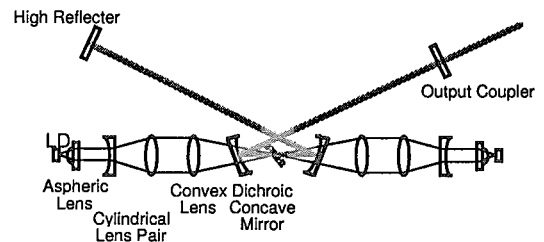


Fig. 1 Schematic diagram of diode-pumped laser oscillator with cooled Yb:YLF

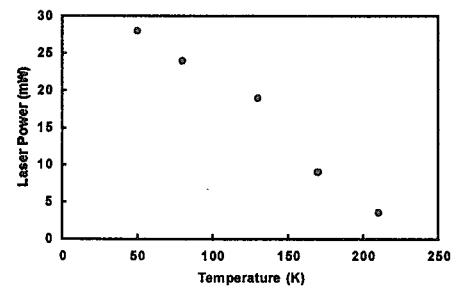


Fig. 2 Laser output power as the crystal temperature was decreasing.

4.1.12 Dynamic imaging using a laser pumped soft X-ray source

Yoji SUZUKI, Takashi ARISAWA, Akira OHZU, Yoichiro MARUYAMA

1. Introduction

An ultra short pulse with high peak power laser is an appropriate light source for generating short pulse X-ray available for the dynamic biological imaging. There are two methods of generation, one of which is a laser induced plasma X-ray and the other one is the higher harmonics generation by the irradiation of ultra short laser pulses. In the first step plasma X-ray was produced using a solid target to find out an optimum configuration of the optics for reducing debris. Dynamic measurement was developed using the combination of Schwarzschild type collimator with CCD camera. A 200 nm spatial resolution was obtained by a single shot images with 20 frames per second. A laser plasma source at 20 nm wavelength is used for the preliminary studies. This wavelength will be shorten down to the "water window" region between oxygen absorption edge of 2.3 nm and carbon edge of 4.3 nm which is suitable for observing biological objects.

2. Experimental setup

A soft X-ray monochromator is used for taking spectroscopy from the plasma in the range of the wavelengths between 0.5 nm to 30 nm. An X-ray is collimated onto a gold coated toroidal mirror and dispersed by a flat field type grating enabling the flat image for the streak camera without degrading wavelength resolution. The soft X-ray camera is equipped with palyren film as a window, and thin gold film on the photoelectron surface. Temporal resolution was 2 ps for pulsed X-ray from the laser plasma. A PMMA resist extractor can be used both for forming a PMMA film on a Si substrate, and for reading out the images on the X-ray exposed film by AFM. For imaging by a soft X-ray camera the a light type CCD with a 0.5 mm thick phosphor converter is coupled with an image intensifier, which is connected to the bundle type fiber optics equipped with a 200 ns gating for taking account of the imaging with trace amount of photon irradiation to the living cell with a single shot of laser pulse. For the stable and reliable operation of the laser induced plasma X-ray source the debris from the ablated surface is controlled by considering the angular distribution of X-ray. A tungsten and aluminum are selected as a target material to measure the angular distribution of X-ray emission as well as ablated particles. The second harmonic of Nd:YAG laser with 9 kW/cm² intensity with a 40 micrometer beam diameter was focused down to the target and quartz thickness meter was used for the measurement of ablated particles. About 10,000 shots are available before the reduction of X-ray light to the 30% of the initial intensity. Measurement of angular distribution of X-ray from laser induced plasma was made by focusing a second harmonic on the target surface through 200 mm focal length on the Si photo detector filtered by aluminum 100 nm thin foil to cut visible wavelength. Although this thin foil gives losses to the photons around 120 eV, soft X-ray spectroscopy was taken by the soft X-ray streak camera, and broad band spectroscopy was obtained in the wavelength region between 5 nm to 30 nm. As a result soft X-ray is distributed by cosine distribution law. Based on the above results an imaging was tested by the 2,000 lines/inch copper mesh (wire width 2.5 micrometer, wire spacing 12.7 micrometer), which resulted in the spatial resolution of 200 nm.

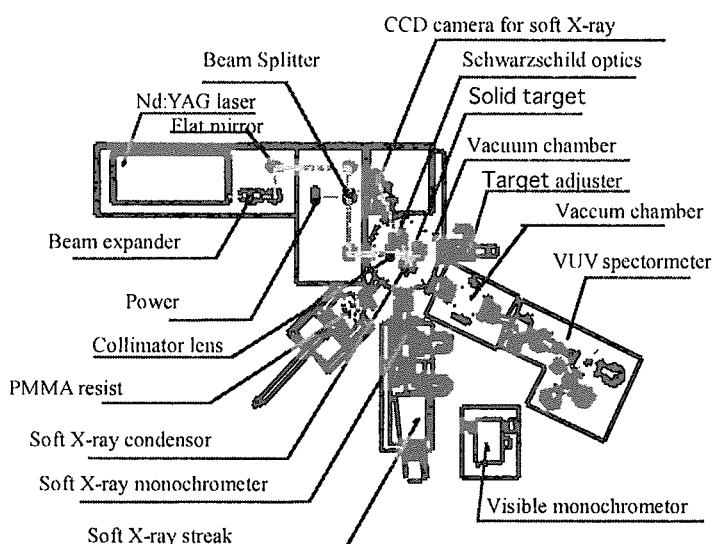


Fig. 1 Experimental set-up for imaging by laser plasma x-ray source

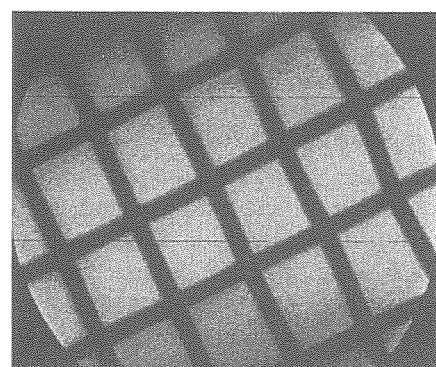


Fig. 2 Mesh test for X-ray

4.1.13 Generation of short pulse hard X-ray by a laser assisted discharge

Akira OHZU, Kazunori ITO

1. Introduction

X-ray sources employing short pulse discharge techniques are compact and capable of operating at high repetition rates with higher electric efficiency than conventional sources¹⁾. In particular a vacuum spark discharge is potentially attractive as an efficient x-ray source with wide photon energy range from a few to above a few hundreds keV²⁾. Hard x-ray emission from the anode surface on which a laser pulse is focused to provide a pre-ionization plasma, is expected to be available for generating a short x-ray pulse. We have therefore developed the hard x-ray source using optically driven Marx generator and investigated the x-ray output characteristics.

2. Experimental setup

The x-ray source consists of a small Marx generator, a Nd:YAG laser device and a cylindrical stainless tube equipped with the Marx generator. Hard x-ray is emitted from a pin anode electrodes (2 mm ϕ , 10 mm) in the tube as shown in Fig. 1. The laser pulse is focused onto the tip surface of the anode, and produces a laser-induced plasma on it as a pre-ionizing source at the gap (10 mm) of pin electrodes. On using the plasma, a vacuum spark discharge is driven by the generator. High energy electron beams in the discharge interact with the anode and an intense hard x-ray pulse thus emits around the surface of the electrode.

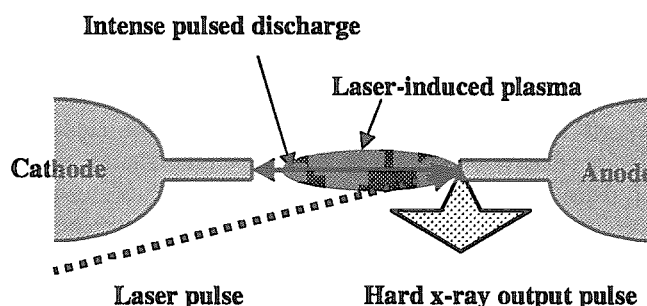


Fig. 1 Schematic diagram of a laser assisted vacuum discharge

3. Results

Figure 2 shows the typical wave forms of the incident laser pulse, the discharge voltage and current, and x-ray output pulses when a vacuum spark discharge (voltage (b), current (c)) starts simultaneously with the laser irradiation (a). Under this drive condition, intense x-ray output pulse was emitted from the onset of the discharge as shown in Fig. 2(d). The x-ray exposure was about 10 mR per pulse. The x-ray pulse included a spike pulse as shown in Fig. 2(e) in the front part of the pulse. The pulse duration is similar to that of the laser pulse. And, its effective photon energy of 150 keV corresponded to the charging voltage of the Marx generator. It has been observed that the x-ray output characteristics strongly depends on the laser pulse energy and time delay between the laser irradiation and the pulse discharge.

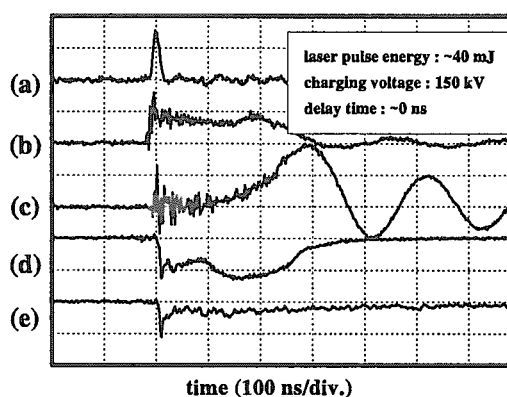


Fig. 2 Pulse wave forms of the generated X-ray pulses

References

- 1) C. L'abbé, R. Coussement, J. Odeurs, E. E. Apl, W. Sturhahn, *et al.*: Phys. Rev. E **61**, p.4181, 2000
- 2) H. Chuaqui, M. Favre, R. Saavedra, E. Wyndham, P. Choi, *et al.*: Phys. Plasmas **4**, p.3696, 1997

4.2 X-ray laser development

4.2.1 The outline of X-ray laser research in APRC

Akira NAGASHIMA, Keisuke NAGASHIMA, Masataka KADO, Tetsuya KAWACHI,
Noboru HASEGAWA, Momoko TANAKA, Kouta SUKEGAWA, Peixiang LU,
Akito SAGISAKA, Tomonao HOSOKAI, Kenjiro TAKAHASHI, Yoshiaki KATO

1. Introduction

Since the first demonstration of X-ray laser which was driven by a giant laser system of inertial fusion research facility on 1984¹⁾, the X-ray laser research has been intensively progressed because of its attractive application possibility such as microscopic use for biology, micro-processing by short wavelength, plasma diagnostics with high cut off density, nonlinear optic research in X-ray with coherent high brightness, etc.. These application are based on the excellent property of X-ray laser such as high brightness, high coherence, short wavelength, short pulse, etc..

The X-ray laser research group in APRC has started on April 1998. The main purpose of the group is to develop compact high performance X-ray laser system regarding to the short wavelength X-ray generation up to or beyond the region of the water window (2-4 nm), enhancement of coherence more than ASE feature and demonstration of attractive application of the high quality X-ray. The main activity in FY1998 was devoted to the development of a ultra short pulse laser driver system for the X-ray laser research including CPA configuration which can be used for many different experiments. In 1999, the total system was installed in the newly constructed APRC KIZU site X-ray laser laboratory. All the capability has been examined to give the results as expected including the function of a new development such as a double pulse generator which produces coaxial 2 pulses for ionization and excitation, focusing optics with no aberration, CPA optics such as stretcher and compressor, etc.. The first detection of X-ray lasing with the scheme of transient collisional excitation (TCE) was observed by using Ti target as Ne-like ion lasing system at 32.6 nm in December 1999. The generation of the shorter wavelength laser has been progressed very rapidly down to 12 nm of Ni-like Sn until March 2000 which is the shortest wavelength with a 10 J class driver²⁾. The further progress would be expected in the next year.

2. X-ray laser research

The investigation of coherent X-ray generation by a highly ionized plasma has been progressing with the experiment system of Fig. 1. Two folds of CPA driver laser beam-line are prepared for multipurpose usage including a pump and probe application for a very short interval dynamics.

Many schemes to demonstrate X-ray laser are being investigated such as (1) transient collisional excitation, (2) recombination, (3) optical field ionization, etc.. The activities of these researches are explained in the following sections with the explanation of the experimental system development. The first result is shown in Fig. 2 for Ne-like Ti ion.

3. High energy X-ray generation

The research and development of laser assisted high brightness and high energy compact X-ray source is the another issue of the research group. The possibility of MeV X-ray generation has been investigated utilizing the Compton scattering with high energy electrons produced by an ultra high peak power laser.

Reference

- 1) D.L. Matthews, et al., Phys. Rev. Lett. 54, p110, 1985
- 2) M.Kado, et al., 7th Int. Conf. On X-Ray Laser Proceeding, Malo, France, 18-25 June (2000)

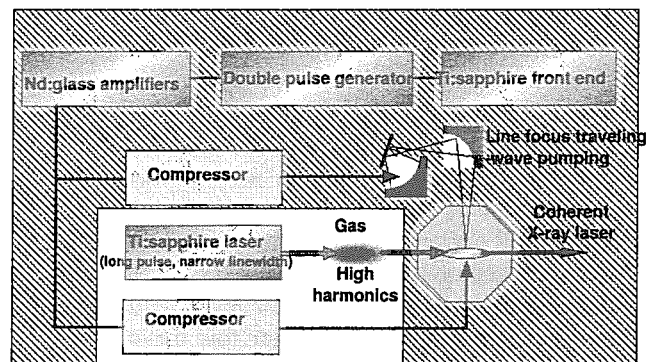


Fig. 1 X-ray laser experiment system with Nd:glass CPA laser

The X-ray coherence will be increased by using high harmonic seeder. The gray area shows the present configuration of the system.

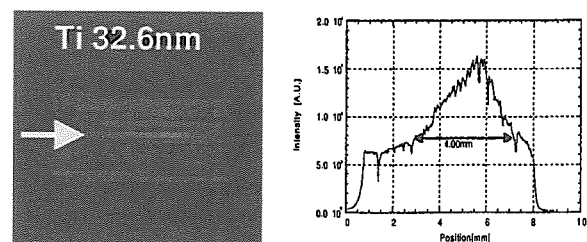


Fig. 2 First X-ray laser at APRC with TCE scheme

The laser line of Ne-like Ti, the wavelength is 32.6nm. Beam divergence 4mm corresponds to 3.2mrad.

4.2.2 X-ray laser generation with transient collisional excitation scheme

Masataka KADO, Tetsuya KAWACHI, Noboru HASEGAWA, Momoko TANAKA, Kouta SUKEGAWA,
Keisuke NAGASHIMA, Akira NAGASHIMA, Yoshiaki KATO

1. Introduction

The transient collisional excitation¹⁻⁴⁾ (TCE) scheme uses a long pulse (\sim ns) to generate plasmas and a short pulse (\sim ps) to excite electrons. The electrons are excited from the ground state faster than the electron relaxation time. This scheme produces larger x-ray laser gain than the gain produced with ordinary collisional excitation scheme and pumping laser energy required to generate x-ray lasers of 10 nm in wavelength is only 10 J. A new TCE scheme is also proposed⁵⁾ to reduce the laser energy furthermore, which uses short laser pulse (\sim ps) to generate plasmas instead of long laser pulse. Using short laser pulse for generating plasmas high electron temperature and high electron density are obtained at same time and create high collisional ionization rate.

Hybrid laser system with Ti:sapphire front end and Nd:glass amplifiers has been developed. This laser system has been designed and optimized for the TCE x-ray laser experiments. The x-ray laser experiments with TCE scheme and new TCE scheme have been conducted with this laser system.

2. Experiments

In our experiments two sets of pre-pulse and main pulse combination were selected. One was 1.5 ps pre-pulse and 1.5ps main pulse combination and the other was 600 ps pre-pulse and 1.5 ps main pulse. Pulse separations of the both cases were 1.2 ns. The energy ratio of the pre-pulse and the main pulse was 1:5 for the 1.5 ps - 1.5 ps combination and 1:2 for the 600 ps - 1.5 ps combination. The pulse separation was monitored with a S-20 type streak camera. Target surface was monitored with two sets of long distance microscope with magnification of 25x.

The primary diagnostics along the target surface was a flat-field grazing incidence x-ray spectrometer with a 1,200 lines/mm aperiodically ruled grating. The spectrometer was coupled with a back illuminated CCD camera. The spectral range of the spectrometer was 10 to 40 nm. Al and Si_3N_4 filters were used to provide variable attenuation for different x-ray laser wavelengths. The time and spatial resolved scattered light from the x-ray laser plasma was measured with the S-20 type streak camera to monitor the laser plasma interaction such as the filamentation instability. Filters were used to cut the laser fundamental and second harmonics scattered light and detected mostly 700 nm wavelength, which is mainly scattered from the quarter critical density region and is sensitive to the laser filamentation instabilities.

3. Results

Time integrated axial spectra were shown in Figs. 1(a) and 1(b). Figures 1(a) and 1(b) are the spectra of the x-ray from Ag and Sn targets, respectively. The output from Ag target is completely dominated by the Ni-like Ag $J=0-1$ laser transition at 13.9 nm. The intensity of the laser line was attenuated by a 20 nm thick Si_3N_4 filter to 15% to avoid saturation of the

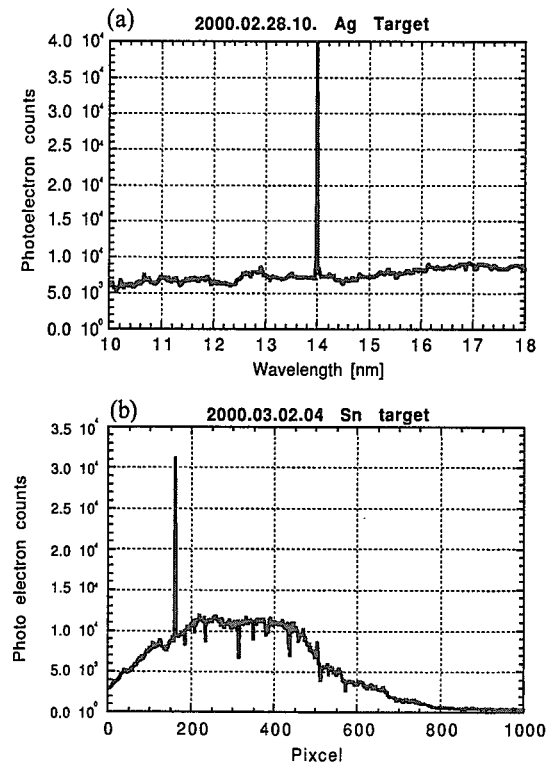


Fig. 1 Time integrated axial spectra
The (a) and (b) are the spectra of the x-ray from Ag and Sn targets, respectively.

CCD detector. The output energy was estimated to be 4 μJ . For the case of Sn target the laser line was not strong enough to dominate the x-ray spectrum.

The output intensities of the Ag and Sn laser were plotted in Fig. 2 against plasma length. The plasma length was controlled with changing target length. The increase of the output intensity of the laser line is a simple exponential form with the plasma length less than 4 mm for Ag and 6 mm for Sn. The gain coefficients were determined by fitting the Linford formula to those data in the exponential region, to be 23 cm^{-1} for Ag and 14 cm^{-1} for Sn.

Shown in Figs. 3(a) and 3(b) are temporal profiles of the plasma image measured with the filtered visible streak camera. The target for the both data are titanium slabs. The pulse durations of the prepulse are 1.5 ps and 600 ps for Figs. 3(a) and 3(b), respectively. The image showed evidence of filamentation instabilities for the data with 600 ps pre-pulse.

4. Summary

In conclusion, we have generated x-ray lasers from Ni-like Ag and Ni-like Sn with the TCE scheme (600 ps prepulse and 1.5 ps main pulse combination) and also the new TCE scheme (1.5 ps prepulse and 1.5 ps main pulse combination). Gain coefficient 14 cm^{-1} for Ni-like Sn laser line with 10 J laser energy was obtained. The temporal image of plasma showed the evidence of filamentation instabilities with the 600 ps pre-pulse case.

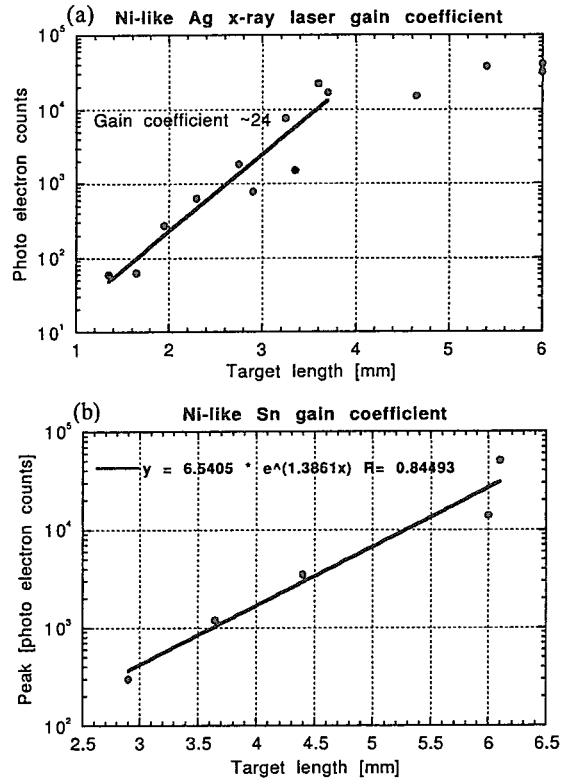


Fig. 2 Output intensity of x-ray lasers vs. target length

The gain coefficients were determined by fitting the Linford formula to those data in the exponential region, to be 23 cm^{-1} for Ag (a) and 14 cm^{-1} for Sn (b).

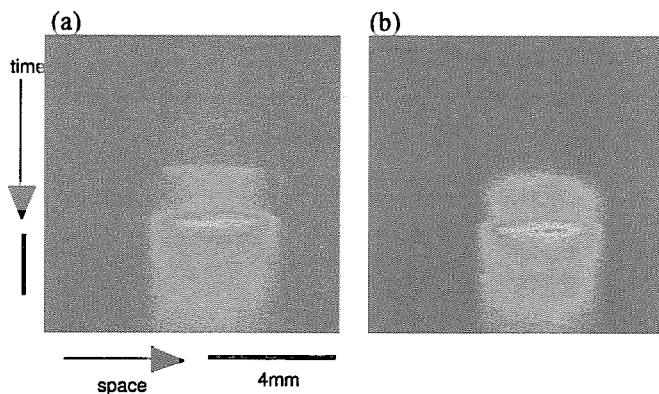


Fig. 3 Temporal image of x-ray laser plasmas

The (a) and (b) are the data with 1.5 ps pre-pulse and 600 ps pre-pulse with titanium targets. The (b) shows the evidence of nonlinear scattering from a quarter critical density and self-focusing.

References

- 1) P. V. Nickles, V. N. Shlyaptsev, M. Kalachnikov, M. Schnurer, I. Will and W. Sandner, Phys. Rev. Lett. 78, p. 2748 (1997)
- 2) J. Zhang, A. G. MacPhee, J. Nilsen, J. Lin, T. W. Barbee, Jr., C. Danson, M. H. Key, C. L. S. Lewis, D. Neely and R. M. N. O'Rourke, Phys. Rev. Lett. 78, p. 3856 (1997)
- 3) J. Dunn, A. L. Osterheld, R. Shepherd, W. E. White, V. N. Shlyaptsev and R. E. Stewart, Phys. Rev. Lett. 80, p. 2825 (1998)
- 4) J. Dunn, J. Nilsen, A. L. Osterheld, Y. Li and V. N. Shlyaptsev, Opt. Lett. 24, p. 101 (1999)
- 5) M. Kado, A. Nagashima, K. Nagashima, T. Kawachi, N. Hasegawa, M. Tanaka, T. Hosokai, K. Suegawa, A. Sasaki and Y. Kato, SPIE Proc. 3776, p. 242 (1997)

4. 2. 3 Calculation of populations of the lithiumlike and berylliumlike ions in low temperature dense recombining plasma

Tetsuya KAWACHI

1. Introduction

Recent advent of high-intensity laser made it possible for us to generate highly charged ions in high density plasma. In such a high density plasma, ions may be in their multiply-excited levels, *e.g.*, doubly excited levels. The spectroscopic characterization of such ions, and the clarification of the production mechanism of doubly excited ions under a given plasma condition is one of the objectives of the plasma spectroscopy, and is necessary for the development of high-brightness x-ray sources and x-ray lasers. Recently several experimental and theoretical studies relevant to doubly and triply excited ions in plasmas are published¹⁾, in which atomic processes involving multiply-excited levels such as resonance excitation (RE) and dielectronic recombination (DR) from excited levels are well-investigated.

A couple of years ago, the author showed theoretically¹⁾ and experimentally²⁾ that another process played a decisive role in low temperature dense plasmas. An excited lithiumlike ion, *i*, may capture a continuum electron by 3-body (3B) or radiative recombination (RR) to be a doubly excited berylliumlike ion, and due to the following collisional excitation and deexcitation substantial populations are made in the doubly excited levels. In low temperature dense plasmas, the populations of the doubly excited levels, (*i*, *j*) with *j* > *p*_{LTE} may be described by local thermodynamics equilibrium (LTE) with respect to the population of the lithiumlike excited level *i* and the continuum electron density, where *p*_{LTE} indicates the lower bound of the LTE region. The populations of the doubly excited ions may autoionize into the lithiumlike ions, or the captured electron may deexcite by the collisional-radiative processes from the LTE region into the lower-lying levels. Since the lower-lying levels are not in LTE but in the ladderlike deexcitation region, the captured electron autoionizes into the lower-lying lithiumlike ions or deexcites by collisional and radiative process into the non-autoionizing levels. As a result, these processes effectively enhance the depopulation of the lithiumlike excited ions.

In our previous work, however, several points should be clarified. First, we did not clarify the population flow from the doubly excited levels in ladder-like deexcitation region. If the collisional-radiative deexcitation is dominant, these doubly excited levels may contribute to production of ground-state beryllium-like ions, and if the autoionization is dominant, the production of the ground-state lithium-like ions may be enhanced. Because this may strongly affect on the ion abundances in plasmas, it is important for the recombination x-ray laser research. Secondly, we should investigate critical time in which the LTE populations are established in doubly excited levels in low temperature dense recombining plasma. The temporal behaviour of populations of singly excited level has been well investigated however, the similar estimation for the doubly excited levels is to the author's knowledge new. In order to clarify these points we construct a collisional-radiative (CR) model involving singly excited lithiumlike ions and singly and doubly excited berylliumlike ions. In this report the details of the CR-model and the calculated result are shown.

2. CR-model

Temporal development of population *n*(*p*) of the level *p* of ions in plasma can be expressed by following differential equation,

$$\begin{aligned} \frac{dn(p)}{dt} = & \sum C(q, p)n_e n(q) - \left[\sum_{q < p} F(p, q) + \sum_{q > p} C(p, q) \right] n_e + \sum_{q < p} \{A(p, q) + A_e(p, q)\} n(p) \\ & + \sum [F(q, p)n_e + A(q, p) + A_e(q, p)] n(q) - S(p)n_e n(p) + [\alpha(p)n_e + \beta(p) + \gamma(p)] n_e n_{He}. \end{aligned} \quad (1)$$

which is coupled with similar equations for other levels, where *p* and *q* represent singly excited level of the lithiumlike ions or singly or doubly excited levels of the berylliumlike ions. *n*_{He} and *n*_e are helium-like ion density and electron density, respectively. $\alpha(p)$, $\beta(p)$, $\gamma(p)$ are three-body (3B) recombination, radiative recombination (RR) and dielectronic recombination (DR) rate coefficients from the helium-like ground state ion to singly excited level *p* of the lithiumlike ion, respectively. In the case that both level *p* and *q* are lithiumlike ions, or berylliumlike ions, *A*(*p*, *q*), *C*(*p*, *q*), *F*(*p*, *q*) represent Einstein's A coefficient, collisional excitation rate coefficients, collisional deexcitation rate coefficients from level *p* to level *q*, respectively. In the case that level *p* is doubly excited berylliumlike ion and level *q* is singly excited lithiumlike ion, *A*(*p*, *q*),

$C(p, q)$ and $F(q, p)$ represent autoionization probability from level q to level p , collisional ionization from level q to level p , and sum of the recombination processes (3B and RR and DR) from level q to level p .

We solved the coupled differential equations and derived excited level populations of the singly excited lithiumlike ions and the singly and doubly excited beryllium-like ions.

3. Calculated result

Figures 1(a), 1(b) and 1(c) show calculated populations of the ground state and the excited levels in Boltzmann plot at $t = 200$ fs, 1 ps and 10 ps, respectively, where t is the time measured from the start of the recombination. T_e and n_e are assumed to be 8 eV and $1 \times 10^{20} \text{ cm}^{-3}$, respectively. Configuration of each level is indicated by arrows. Hatched vertical line is the ionization potential energy of the ground state lithiumlike aluminum ions, *i.e.*, the doubly excited levels in the right hand side are autoionizing levels, and those in the left-hand side are non-autoionizing levels. At $t = 200$ fs, almost all the level populations are small, however the high-lying levels of the lithiumlike ions with $n \geq 8$ and the doubly excited levels hanging below these levels are already in LTE values. Thus, it can be concluded that the critical time in which the populations of the doubly excited levels reach the LTE value is almost equal to that for the singly excited levels. At $t = 1$ ps, the excited levels of the lithiumlike ions with $n \geq 5$ and the doubly excited levels of the beryllium-like ions with (n, n') ($n \geq 5$ and $n' > 5$) reach their equilibrium values. At $t = 10$ ps, all the excited levels reach their equilibrium values. In Figs. 1 (b) and 1(c), the populations of the $(3l, n)$ levels are small compared with the populations of the $(2s, n)$ and $(2p, n)$ levels. This is because that the $(3l, n)$ levels may autoionize into the lower lying levels, whereas since the $(2p, n)$ with $n \leq 9$ and $(2s, n)$ levels are non-autoionizing levels. This means that the autoionization is still dominant depopulation process for (n, n') levels with $n \geq 3$ under this electron density, *i.e.*, the populations of the (n, n') levels with $n \geq 3$ mainly contribute to production of the lithiumlike ground state ions. Whereas, the dominant depopulation from the $(2p, n)$ is collisional or radiative processes into the low-lying berylliumlike ions, and the populations of the $(2p, n)$ levels mainly contribute to production of the berylliumlike ground state ions.

In conclusion, the populations of the doubly excited levels of the berylliumlike ions in low temperature dense recombining plasma are calculated. The critical time in which LTE is established in the doubly excited levels is almost equal to that of the singly excited levels. The population flow through the $(2p, n)$ levels may affect the ion abundance of the lithium- and berylliumlike ions and the gain coefficient of the lithiumlike recombining plasma laser. The investigation of this effect on the gain will be an important subject in near future.

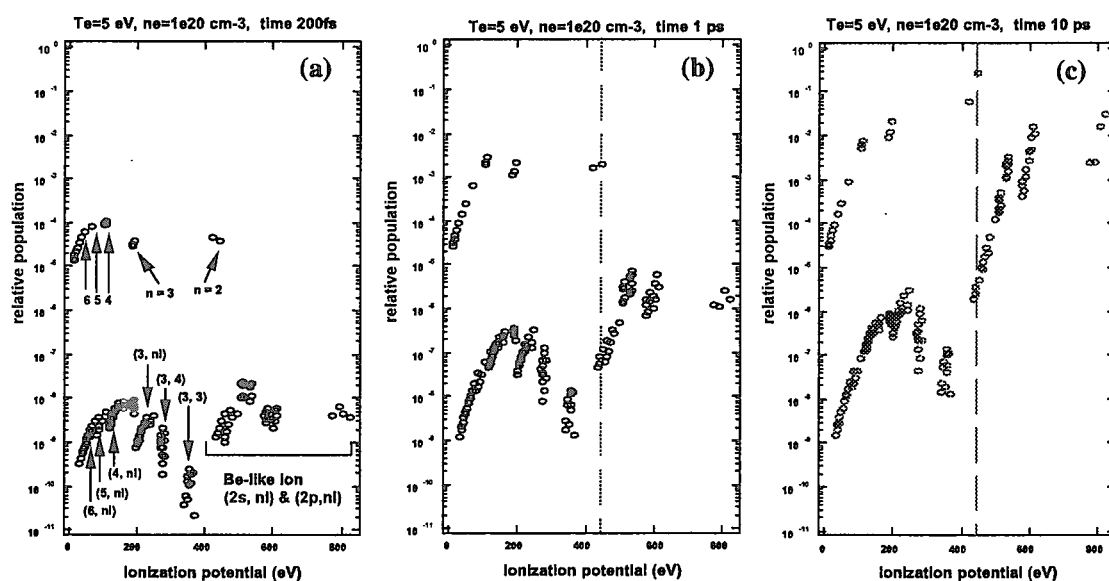


Fig. 1 Temporal evolution of excited level populations of the lithiumlike ions in Boltzmann plot at 200 fs (a); 1 ps (b); and 10 ps (c)

We assume electron temperature and electron density to be 8 eV and 10^{20} cm^{-3} , respectively.

References

- 1) Many papers related with multiple-excited ions can be seen in "journal of quantitative spectroscopy and radiation transfer", 51,1994
- 2) T. Kawachi and T. Fujimoto, Phys. Rev. E53, p.1836, 1997
- 3) T. Kawachi *et al.*, J. Phys. B33, p.156, 1999

4.2.4 Development of CPA glass laser system

Kouta SUKEGAWA, Masataka KADO, Tetsuya KAWACHI, Noboru HASEGAWA, Momoko TANAKA, Keisuke NAGASHIMA, Akira NAGASHIMA, Yoshiaki KATO

1. Introduction

An ultra-large size glass laser system was required to generate X-ray laser before chirped pulse amplification (CPA) technique had been invented. The CPA laser system can produce high peak intensity with a compact system. The development of CPA glass laser system was mainly focused on the research of transient collisional excitation (TCE) scheme X-ray laser. TCE scheme requires a long pre-pulse (~1 ns) of 10^{12} W/cm² to generate plasma of suitable ionization state and an ultra-short laser pulse (~1 ps) of 10^{15} W/cm² to produce high gains instantly. Requirements for the TCE scheme are the following ; (a) 1 ns pre-pulse and 1 ps main pulse, (b) the control capability of pulse duration and interval, (c) uniform beam profile, (d) high contrast for satellite pulse.

2. Explanation of Nd:glass laser system

The laser system consists of CPA Ti:sapphire front end which works with the wavelength of 1 μm and includes 1 ns pulse stretcher, and Nd:glass main amplifiers (CPA hybrid laser system). Shown in Fig. 1 is the schematic view of the laser system. The front end system consists of a Tsunami oscillator pumped by a Millenia-X, a pulse stretcher, regenerative amplifier and newly developed double pulse generator. The output energy from the front end system is 4 mJ and the beam diameter is 5 mm. The uniform image by a serrated aperture is successively relayed on the target surface with vacuum spatial filters.

The main amplifiers consists of two 9 mmφ rod amplifiers, a 25 mmφ double path rod amplifier, and three 50 mmφ rod amplifiers (50 mmφ beam is divided into 2 after the first) and total gain is over 6×10^5 . The system has two beam lines and each beam line is designed to produces 20 J pre pulse and 20J main pulse. The pulse duration of the output pulses and time separation is controllable.

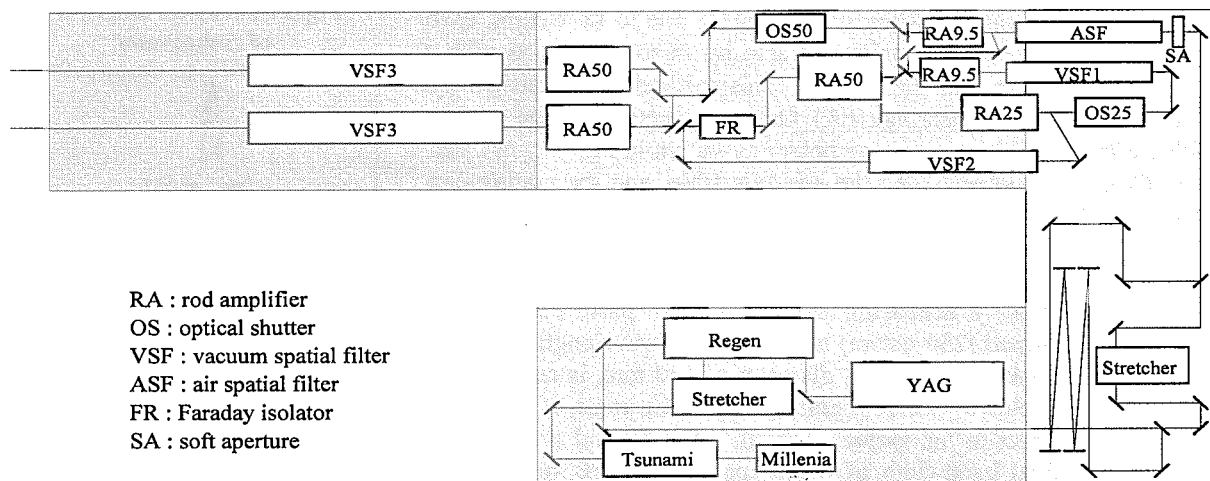


Fig. 1 The schematic view of glass laser system

3. Results

The laser system has been built and the performance was tested and measured. The specifications and the examined results are shown in Table 1.

Table 1 Designed specifications of glass laser system and measured results

	design	result
energy	20 J	~30 J
pulse duration	500 fs	pre pulse 600 ps or 1.3 ps/main pulse 1.3 ps
focusing capability	20 μm	<17 μm
bandwidth	3.0 nm	2.5 nm

4. 2. 5 Design of pulse compressor of CPA glass laser system for x-ray laser research

Tetsuya KAWACHI, Masataka KADO, Kouta SUKEGAWA, Noboru HASEGAWA, Momoko TANAKA, Keisuke NAGASHIMA, Akira NAGASHIMA, Yoshiaki KATO

1. Introduction

Since the first demonstration of amplification of the 32.4 nm line of neonlike titanium ions driven by ps laser pulse¹⁾, transient collisional excitation scheme has been intensively studied because of its possibility to generate high gain coefficient, and the importance of CPA glass laser system as driver laser of x-ray laser has been recognized. Pulse compressor is one of the most important parts in the CPA laser, and the performance of the compressor may exert influence on the pulse duration, the width of the line focus, and the output laser energy. In this report, we will show the details of the design and the performance of the pulse compressor of our CPA glass laser system.

2. Pulse compressor and its performance

In order to generate x-ray lasers at wavelengths of around 10 nm, in typical cases, 1 ps, 10 J heating laser pulse is needed. This together with the damage threshold of gratings (~ 250 mJ/cm²) and the capability to cover the spectral bandwidth of the laser light (~ 4 nm) leads to large-size grating, *i.e.*, the diameter of several hundred millimeters. We used circular-shaped holographic gratings made by Jobin Yvon with 1,740 grooves/mm, diameter of 420 mm, thickness of 70 mm and $\lambda/8$ ($\lambda = 1$ μ m) surface quality. The diffraction efficiency was measured for 33 points on each grating using 1,064 nm light under Littrow condition, and it was better than 95.1% for all the points. For avoiding buckling of the grating due to its weight, each grating was fixed to an aluminum frame by injecting silicon rubber between the grating and the frame. This method is established by Institute of Laser Engineering (ILE), Osaka university²⁾. The grating with the frame is set on a grating holder as shown in Fig. 1. We can slide the grating holder along the one-axis table, and the grating can be rotated around z- and y-axis, and can be slanted on the y-z plane. The accuracy of the one-axis table is better than 50 μ m, and the accuracy of the angle of rotation, tilt and slant was better than 0.05°.

Figure 2 shows a schematic diagram of our pulse compressor. The incident chirped (250 ps/nm) laser light at a wavelength of 1,053 nm with 2.5 nm-width (FWHM), diameter of 130 mm, is reflected by M1 and is diffracted by the first grating G1. The angle of incidence is 61° with respect to the surface normal. The second grating, G2, cover the spectral bandwidth of 6 nm for all the parts of the laser light: At the edge of right or left hand side of the incident laser light, the blue- or red-wing of the spectrum may be cut at the 3 nm from the central wavelength, respectively, however fourier transform calculation shows that no serious problem is caused under the present situation.

After the diffraction by G2, laser light is reflected by M2, changes the height in the elevation mirrors M3, goes to M2 \rightarrow G2 \rightarrow G1 \rightarrow M1 \rightarrow M4, and finally reaches a line focusing system. The details of the line focusing system is described in another report.

The efficiency of the compressor was derived by comparing the laser energy before the compressor to that after the compressor, and it was 70%. This value was higher than the values of similar compressors in other laboratories. It may be due to the high efficiency of the grating. Pulse duration was measured to be 1.3 ps (See Fig. 3) by use of single shot auto-correlator. Since the spectral bandwidth of our glass laser system was 2.5 nm (FWHM), this pulse duration was reasonable and sufficient for x-ray laser research.

Reference

- 1) P. Nickles et al., Phys. Rev. Lett. 78, p.2748, 1997
- 2) H. Kitamura, private communication

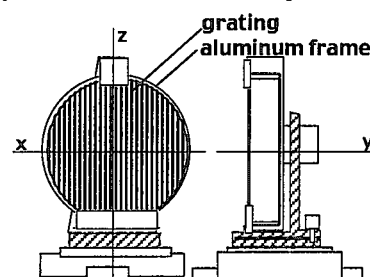


Fig. 1 Grating holder

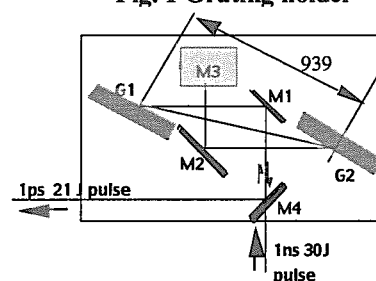


Fig. 2 Schematic diagram of compressor

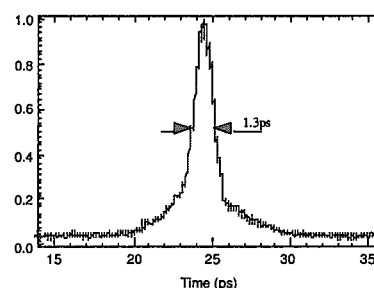


Fig. 3 Single shot auto-correlator signal of the laser pulse after the compressor
Pulse duration is 1.3 ps (FWHM).

4.2.6 Line focusing system for the transient x-ray laser

Noboru HASEGAWA, Tetsuya KAWACHI, Masataka KADO, Momoko TANAKA,
Kouta SUKEGAWA, Akira NAGASHIMA, Yoshiaki KATO

1. Introduction

The x-ray laser using a transient collisional excitation (TCE) pumping scheme^{1), 2)} is expected for high efficiency and practical use. This scheme is required a rapid excitation of the ion comparing with radiative decay. A laser system with high peak intensity and short pulse duration such as CPA (Chirped Pulse Amplifier) laser, is suitable for the pumping source of this scheme. Since the CPA laser has large bandwidth, an ordinary focusing system using transmission optics is not suitable. We have the line focusing system with all reflective optics.

2. Line focusing system

We have generated TCE x-ray lasers with a CPA hybrid (Ti:Sapphire front end and Nd:Glass main amplifiers) laser system (30 J, 1.3 ps, 130 mm ϕ)³⁾. The requirements for the focusing system for this experiment are following, A tight, long and homogeneous focusing, a large distance (~ 1 m) from final mirror to target surface for keeping away from the target debris, the incident angle to the target surface must be normal to target and laser light need to reach at the same time (arriving time difference < 100 fs) in the focusing area. For example, TCE of Ni-like Silver ion, the length of x-ray laser medium enough to saturate lasing is about 6.0 mm. Under this condition, focusing width enough to pumping this ion is 30 μm . The line focusing scheme is shown in Fig. 1. In this design, the line focusing is produced by making the astigmatism on the sagittal (horizontal) plane⁴⁾, focusing width is decided from the primary focal point diameter focused by off axis parabolic mirror. The distance from spherical mirror to the target surface is almost equal to the spherical mirror radius. General design was decided by the optical design software OPTICA, and each parameter calculated by the ray tracing program. From the result of calculation of line focus length(L), the difference of laser light arriving on target surface(dt) and beam size on the spherical mirror(R) as a function of the off axis incident angle to spherical mirror(θ), spherical mirror radius(r), the distance from spherical mirror to the target surface(D), each parameter is decided, $\theta = 8.3$ deg., $r = 1,000$ mm, $D = 988$ mm, $L = 6.1$ mm, $dt = 53$ fs, $R = 171$ mm.

3. Result

Shown in Fig. 1 is the measured focusing pattern on the Titanium target. Good line focusing (6.1 mm x 20 μm) is obtained. This result bring to generating the saturated Ne-like Titanium ($\lambda = 32.6$ nm) and Ni-like Silver ($\lambda = 13.9$ nm) x-ray laser. In addition, we success Ni-like Tin ($\lambda = 11.9$ nm) x-ray laser generation.

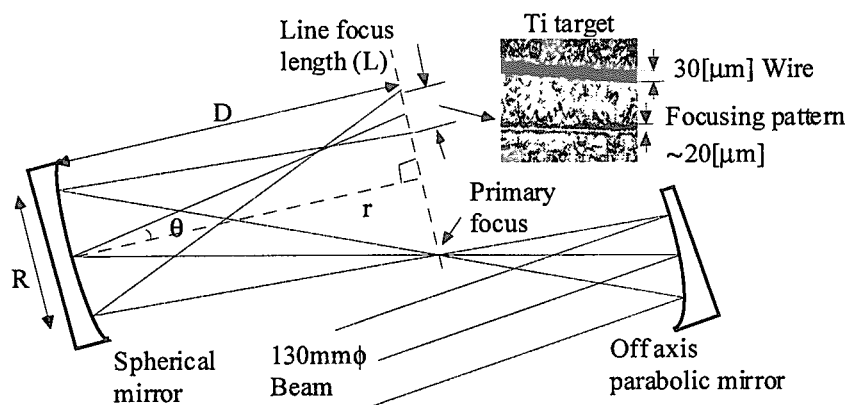


Fig. 1 Line focusing system geometry

Reference

- 1) P. V. Nickles, V. N. Shlyaptsev, M. Kalachnikov, M. Schnurer, I. Will, and W. Sandner, Phys. Rev. Lett. **78**, p.2748, 1997
- 2) J. Dunn, A.L.Osterheld, R. Shepherd, W. E. White, V. N. Shlyaptsev, and R. E. Stewart, Phys. Rev. Lett. **80**, p.2825, 1998
- 3) M. Kado, A. Nagashima, K. Nagashima, T. Kawachi, N. Hasegawa, M. Tanaka, T. Hosokai, K. Sukegawa, A. Sasaki, and Y. Kato, Proc. of SPIE **3776**, p.242, 1999
- 4) I. N. Ross, J. Boon, R. Corbett, A. Damerell, P. Gottfeldt, C. Hooker, M. H. Key, G. Kiehn, C. Lewis, and O. Willi, Applied optics, vol.26, No.9, p.1584, 1 May 1987

4.2.7 Near field pattern of transient collisional excitation x-ray laser

Momoko TANAKA, Tetsuya KAWACHI, Masataka KADO, Noboru HASEGAWA, Kouta SUKEGAWA,
Akira NAGASHIMA, Yoshiaki KATO, Hisataka TAKENAKA^{a)}

a) NTT Advanced Technology Co.

1. Introduction

Since the first demonstration of x-ray lasers¹⁾, compact and applicable x-ray laser systems have been intensively studied²⁾. In order to use x-ray lasers for various applications, e.g., laser microscope and laser processing, it is indispensable to characterize the x-ray lasers in terms of the spatial gain profile, output energy, and the near field pattern.

We have been successful to generate x-ray lasers such as the Ne-like titanium, Ni-like silver, and Ni-like tin in transient collisional excitation scheme using picosecond CPA glass laser system with pre-pulse technique. We report the spatial profile of the Ni-like silver laser ($\lambda = 13.9$ nm).

2. Experimental

Measuring the spatial profile of the x-ray laser, we used a near field imaging system composed of a concave mirror, a planar mirror, and a soft x-ray CCD camera. The mirrors are coated with molybdenum/silicon multilayers for 13.9 nm x-ray at reflection angle 8° by NTT Advanced Technology. The x-ray laser light is reflected by the 25 mm planar mirror, then focused to the CCD camera by the concave mirror with curvature 1,020 mm and diameter 25 mm. The magnification of the imaging system is 10.

3. Results

Shown in Fig. 1 are the results of near field imaging. Silver target was on left hand side of the images and pumping laser incidented from right hand side. Although the observed images seems too large in size compared to those of the gain region due to outfocusing of the imaging system, they show some characteristics of the x-ray laser gain region. The gain region was separated in vertical direction (Fig. 1(a)), since the x-ray laser was refracted in the plasma due to the plasma density gradient. We see some evidence of localizing high gain area and hot spot from Fig. 1(b). The hot spot in the plasmas was also observed with the time resolved visible imaging system. It is arisen from self focusing or filamentation. The x-ray laser refracted at the target edge showed interference pattern and indicated high spatial coherence although further detailed analysis is needed.

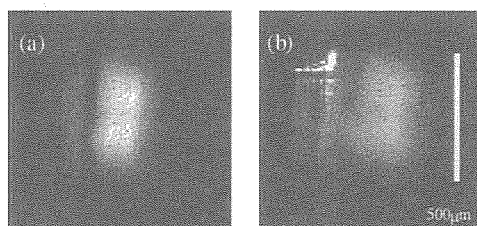


Fig. 1 Far field pattern of Ni-like Ag x-ray laser
(a) target 3.5 mm, filter Y 0.3 mm, input energy 600 ps, 2.6 J + 1.5 ps, 5.2 J
(b) target 5 mm, filter Al 0.1 mm, input energy 600 ps, 3.8 J + 1.5 ps, 7.6 J

References

- 1) D.L. Matthews et al., PRL **54**, p.110, 1985
- 2) D. Korobkin, A. Goltsov, A. Morozov and S. Suckewer, PRL **81**, p.1607, 1998

4.2.8 Cold-electron production for optical-field ionization x-ray lasers using mixed gases

Keisuke NAGASHIMA, Tohru MATOBA, Hiroshi TAKUMA

1. Introduction

Recent advances in ultra-short pulse (<100 fs) and high-intensity ($>10^{17}$ W/cm²) lasers have made it possible to develop new types of x-ray lasers using the optical-field ionization (OFI) process. Here, we propose a new recombination type scheme for x-ray lasers using hydrogen to supply cold electrons¹⁾. The working atoms are mixed with hydrogen of much higher density and a high-intensity ultra-short pulse laser is focused with a long focal length.

2. Numerical calculation

Since low energy electrons are needed for the recombination x-ray laser, a laser with shorter wavelength and linear polarization is required in order to generate cold electrons from optical field ionization. The residual energy and small-signal gain for neon/hydrogen mixed gas were calculated using a laser wavelength of 400 nm, a peak intensity of 4×10^{17} W/cm² and a pulse length of 50 fs. The maximum value of the small-signal gain was 19 cm⁻¹, which was obtained at a neon density of 9×10^{17} cm⁻³ and a mixing ratio of about 60. The FWHM duration of the gain was 1.4 ps. Since the gain-length product at saturation intensity is about $GL \approx 15$ ²⁾, the saturation length was estimated to be $L \approx 0.8$ cm. The saturation intensity was evaluated to be 1×10^9 W/cm² and the energy efficiency was 10^{-7} . This efficiency is about a factor of 10 less than conventional x-ray lasers.

3. Conclusion

The use of mixed gases of working atoms with a much higher density of hydrogen has been proposed in recombination type x-ray lasers excited by high-intensity ultra-short pulse lasers. Hydrogen was chosen as the most suitable material to supply low energy electrons in the optical-field ionization. Numerical analysis shows that a maximum gain can be expected for lithium-like neon at a relatively low neon density of 9×10^{17} cm⁻³ with 60 times higher hydrogen density.

References

- 1) K. Nagashima, T. Matoba, and H. Takuma, Phys. Rev. A 56, p.5183, 1997
- 2) D. C. Eder, P. Amendt and S. C. Wilks, Phys. Rev. A 45, p.6761, 1992

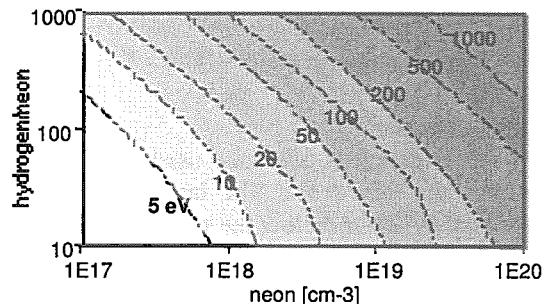


Fig. 1 Residual energy for hydrogen using a mixed gas with hydrogen and neon
The laser parameters are a wavelength of 400 nm, a peak intensity of 4×10^{17} W/cm² and a pulse length of 50 fs.

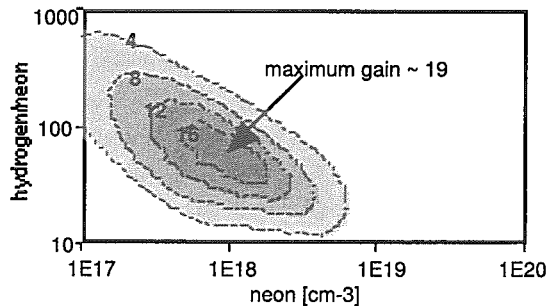


Fig. 2 Small-signal gain using a mixed gas with hydrogen and neon
The laser parameters are the same as those in Fig. 1.

4.2.9 Observation of x-ray spectra from nitrogen clusters irradiated with high-intensity ultrashort laser pulses

Akito SAGISAKA, Hiroshi HONDA^{a)}, Kiminori KONDO^{a)}, Hajime SUZUKI^{a)}, Keisuke NAGASHIMA, Tetsuya KAWACHI, Akira NAGASHIMA, Yoshiaki KATO, Hiroshi TAKUMA
 a) Center for Tsukuba Advanced Research Alliance (TARA), University of Tsukuba

1. Introduction

Recently, there has been significant interest in intense ultrashort pulse laser interaction with atomic clusters. Generation of highly charged ions and intense x-rays have been observed with rare-gas clusters^{1,2)}. Reduction of the ionizing intensity is also desirable in the case of optical-field ionized (OFI) recombination type x-ray lasers, where an intensity over 10^{18} W/cm² is required for the lasing wavelength to reach the water window³⁾. In the case of nitrogen (N), where Lyman- α wavelength is 2.48 nm, the required intensity for fully stripped ions corresponds to 2×10^{19} W/cm².

2. Experiments

In this experiment, we have used a Ti: sapphire laser, producing 60 mJ, 100 fs pulses at 800 nm at a repetition rate of 10 Hz. The laser beam was focused by an off-axis parabolic mirror ($f=165$ mm) approximately 2 mm below the nozzle orifice. X-ray emission from the laser-driven plasma in the direction perpendicular to the laser propagation and parallel to the laser polarization was collected with a flat crystal spectrometer, where a KAP crystal with a working area of 55 mm \times 9 mm was used. The spectra were recorded with an x-ray film (Kodak DEF). The wavelength range and spectral resolution of the spectrometer were 19 - 25 Å and $\Delta\lambda/\lambda \sim 10^{-3}$, respectively. For this experiment the spectra were recorded with an integration over typically 72,000 shots and were corrected for the film sensitivity, crystal diffraction efficiency, and filter transmission.

3. Results

Figure 1 shows the time-integrated x-ray spectra of nitrogen at a laser irradiance of 7×10^{17} W/cm² with backing pressures of 12.5 atm. The gas density and the mean cluster size correspond to 8.5×10^{18} cm⁻³ and 7.7×10^3 , respectively. The dashed line and $n = \infty$ represent a Maxwellian distribution with an electron temperature of 19 eV and the ionization limit of N⁵⁺. Line emissions due to H-like (N⁶⁺) and He-like (N⁵⁺) nitrogen ions have been observed, although tunneling theory predicts that the maximum charge state will be N⁵⁺ at a laser intensity of 7×10^{17} W/cm². Numerical calculations for the optical-field and collisional ionizations in the laser field show that N⁶⁺ and N⁷⁺ will be produced due to collisional ionization in the clusters. We have observed bright emission of the He- δ line, which we have ascribed to the charge exchange between N⁶⁺ and nitrogen molecules to populate the $n = 5$ state of N⁵⁺. The population inversion inferred from the observed spectra shows the possibility for a charge exchange x-ray laser.

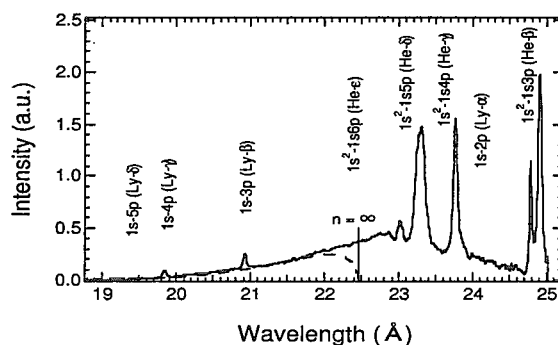


Fig. 1 The x-ray emission spectra of nitrogen at a backing pressure of 12.5 atm

References

- 1) A. McPherson et al.: Phys. Rev. Lett. **72**, 1810 (1994)
- 2) T. Ditmire et al.: Phys. Rev. A **53**, 3379 (1996)
- 3) N. H. Burnett, P. B. Corkum: J. Opt. Soc. Am. B **6** 1195 (1989)

4.2.10 Collisional effects on population inversion in optical-field-ionized plasmas

Akito SAGISAKA, Keisuke NAGASHIMA, Mitsuru YAMAGIWA, Tohru MATOBA, Hiroshi TAKUMA

1. Introduction

Optical field-induced ionization (OFI) provides a mechanism for an efficient production of cold electrons that are necessary for realization of recombination type x-ray lasers. In the previous works the population inversion of hydrogen-like ions and small-signal gain for x-ray lasers were calculated by assuming Maxwellian distribution of electrons at various temperatures¹⁻³). However, since the electron energy distribution is far away from a Maxwellian in an actual OFI plasmas, it is necessary to calculate the atomic process for a realistic distribution including the heating and relaxation processes.

2. Electron Energy Distribution

The electron energy distribution at the end of an ultra-short high intensity laser irradiation is determined by above-threshold ionization (ATI) and collisional heating (inverse bremsstrahlung) using the binary collisional model^{4,5}). The time dependent electron energy distribution after the laser irradiation is determined from the Fokker-Planck calculation⁶). Figure 1 shows the time-dependence of the electron energy distributions at the ion density of $5 \times 10^{17} \text{ cm}^{-3}$ during the relaxation process after the laser pulse. The energy relaxation caused by electron-electron collision reduces the cold component of the electron energy distribution.

3. Results

The collisional relaxation reduces the cold component of the electron energy distribution which is non-Maxwellian at the end of the laser pulse. In the ion density regime where ATI is dominant, we find that the population inversion density is significantly higher than that for the Maxwellian distribution with the same average electron energy, showing the importance of the calculation with the non-Maxwellian distribution. Dependence of the gain on the ion density and laser pulse width has been calculated for hydrogen-like helium using a time dependent electron energy distribution. In the low density regime it was found that the relaxation processes are very important in the analysis of recombination type x-ray lasers pumped by ultra-short pulse high intensity lasers. The maximum gain is significantly higher when a short laser pulse ($\leq 30\text{fs}$) of 400 nm wavelength is used.

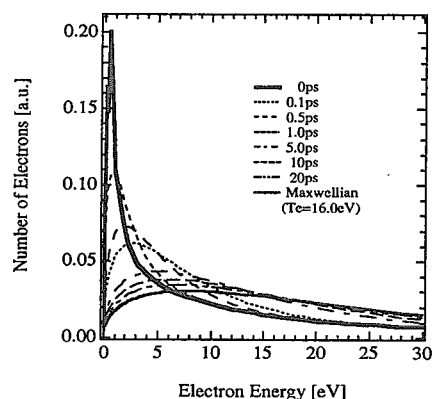


Fig. 1 Time dependent electron energy distribution during the relaxation process

References

- 1) N .H. Burnett et al.: IEEE J, Quantum Electron. **26**, p.1797, 1990
- 2) P. Pulsifer et al.: Phys. Rev. A **49**, p.3958, 1994
- 3) T. D. Donnelly et al.: Phys. Rev. A **51**, R2691, 1995
- 4) T. Takizuka et al.: J. Comput. Phys. **25**, p.205, 1977
- 5) K. Nagashima et al.: Phys. Rev. A **56**, p.5183, 1997
- 6) M. G. McCoy et al.: Comput. Phys. **24**, p.37, 1981
- 7) T. Ditmire et al.: Phys. Rev. E **54**, p.6735, 1990

4.2.11 Short pulse x-ray source by inverse-Compton scattering

Kenjiro TAKAHASHI, Masataka KADO, Akira NAGASHIMA, Yoshiaki KATO

1. Introduction

The recent progress of high intensity short pulse laser is opening up a new field of laser science. One of the most important features of the high intensity laser plasma interaction is production of high energy electrons. The energetic electrons produced by high intensity short pulse laser have a high current density and a short pulse duration, because the energetic electrons are accelerated in short time depending on the laser-pulse duration.

An interaction of the short pulse laser to the short pulse electrons has a potential to emit the short pulse and bright x-ray. The x-ray emissions, which is caused by inverse-Compton scattering between the short pulse laser and the energetic electrons by a use of 10 TW laser and 1 PW laser, have been calculated.

2. Scheme

Shown in Fig. 1 is the schematic of the interaction of energetic electrons and the short pulse laser. The laser light is split to two beams. One is focused on the solid target and accelerates electrons, and another interacts the energetic electrons.

3. Results

The x-ray emission by using 10 TW laser has continuum spectra below a few keV in the energy region. The photon emission between 0.1 - 3.0 keV is estimated to be 5.9 MW, and the energy 5.9 μ J. The brilliance of 1 keV photon is 10^{16} photons/sec/mrad²/mm²/0.1% relative bandwidth.

The x-ray emission by using 1 PW laser has continuum spectra below a few hundred keV. The photon emission between 0.1 - 200 keV is estimated to be 4.7 GW, and the energy 47 μ J. The brilliance of 100 keV photon is 10^{16} photons/sec/mrad²/mm²/0.1% relative bandwidth.

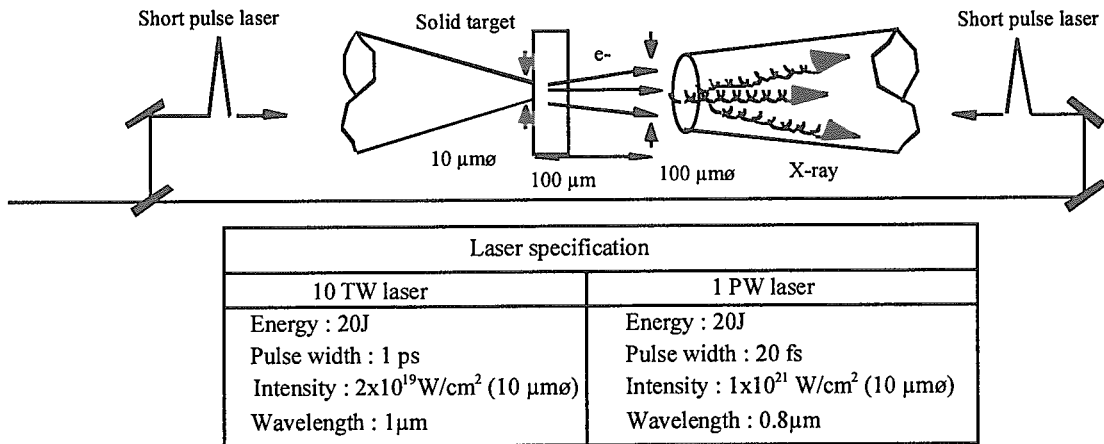


Fig. 1 The schematic of the interaction of energetic electrons and the short pulse laser

References

- 1) D. Strickland and G. Mourou, Opt. Commun. **56**, p.219, 1985
- 2) M. Kado et al., Proc. SPIE, Vol. **3886**, pp.278-284, November 1999
- 3) J. D. Kmetec et al., Phys. Rev. Lett. **68**, p.1527, 1992
- 4) K. W. D. Ledingham et al., Phys. Rev. Lett. **84**, p.899, 2000
- 5) M. Tabak et al., Phys. Plasmas. **1**, 1626 (1994).
- 6) R. Wagner et al., Phys. Rev. Lett. **78**, p.3125, 1997
- 7) G. Malka et al., Phys. Rev. Lett. **79**, p.2053, 1997
- 8) C. Bamber et al., Phys. Rev. Lett. **76**, p.3116, 1996

4.3 Free Electron Laser development

4.3.1 The JAERI industrial 1.3 micron 40 kw highly-efficient FEL driven by the superconducting rf linac

Eisuke MINEHARA, Toshihiko YAMAUCHI, Masayoshi SUGIMOTO, Masaru SAWAMURA,
Ryoichi HAJIMA, Ryoji NAGAI, Nobuhiro KIKUZAWA,
Nobuyuki NISHIMORI, Toshiyuki SHIZUMA

1. Introduction

In a conventional laser device, there are commonly three major components of the driver like a flash lamp, the gain medium like a crystal, and the optical resonator like a pair of mirrors. In the conventional laser system, heat losses and damages in the components give the serious limitations to the applications and intrinsic performances since the invention in 1960. In a free-electron laser (FEL) system unlike the conventional, the losses in the gain medium will be quickly removed from the inside because the medium consists of an undulator generating an alternating magnetic field and a highly energetic electron beam. Resultantly, no deterioration is observed in the optical quality of the gain media during the high power operation. However, a normal conducting rf linac as the FEL driver produces a large amount of heat, and is very inefficient like the lamp. In order to improve drastically the efficiency and power output, and to realize very small errors of the amplitude and phase in acceleration, we have to introduce a superconducting rf linac because of a negligibly small heat loss inside the cavities.

We summarize our results in three steps of the JAERI superconducting rf linac based FEL program¹⁻⁴⁾. Final goal of the program is a demonstration of the high power and highly efficient continuous wave (CW) FEL lasing using the JAERI superconducting rf linac driver with a full energy recovery scheme. After a successful ending of the program, the wall-plug efficiency will be expected to be very high. First, we spent about 7 years to build a prototype of the driver¹⁾. We could operate the driver with a nearly 100% conversion efficiency from the rf power to the electron beam one optimizing the adjustable coupler. Second, we spent another 4 years to demonstrate 2.3 kW FEL power averaged in a qCW operation with the world-highest extraction efficiency of 4.6%. To realize twice or more of a 1 kW FEL output, we have improved the electron gun⁴⁾, rf phase and amplitude controls, resonator opticals and injection system. Third, beam energy recovery will be demonstrated by adding another electron beam re-circulation half loop in the existing FEL facility within a few years^{2,3)}. Especially, conceptual design and considerations are discussed about a 40 kW CW 1.3 micron industrial FEL as shown in Fig. 1.

2. Design considerations

In order to apply the superconducting rf linac based high power FELs to many fields, we have to demonstrate its superiority with all other light sources in many itemized features and performances, i.e., high power capability, high wallplug-efficiency, low weight, small volume, tunability, low toxicity, no harmful by-products, little radiation hazard, low running cost, low capital cost, easy operation, maintenance free and so on. In a shipbuilding yard, high speed welding and cutting machines being free from post and pre-processing's have been needed to develop a 1.3 micron 40 kW Iodine chemical laser welder. The Iodine laser is coupled with a small diameter of 0.8 - 1.2 mm and a few hundreds meter long transmission fiber in order to realize the high speed welding of thick steel plates. Instead of the Iodine chemical laser, we plan to do a conceptual design work of a 1.3 micron 40 kW superconducting rf linac based high power FEL, and to do some developmental works of the components in the FEL facility at Tokai, JAERI. As dispersion-free is observed to be 1.3 micrometer, and the minimum loss 1.6 micrometer in a telecommunication textbooks, we plan to shorten the wavelength and to tune to be 1.3 micrometer for the industrial FEL machine in the design.

Requirements to such a high power industrial FEL machine are already itemized above. An FEL device of the industrial is rather conventional except for the huge heat load of the laser light. We need some cooling devices and their interlocks to remove the huge heat concentration in the mirrors, windows and outcouplers. Electron beam power also become huge, but interruption of the beam means a sudden beam stop, and no damage in the driver like a storage ring because the rf power is planned to recycle inside the superconducting rf linac's cavities.

Basic design options for the JAERI industrial FEL are as follows.

- (1) A 180 degrees reflected or half-turn geometry of the re-circulated energy recovery scheme shall be

used instead of the 360 degrees full-turn one to improve the recovery efficiency of the superconducting cavities up to 100% in low energy.

- (2) A coupling coefficient of the main rf coupler shall be very small for each superconducting cavity to minimize losses in the rf system. Resultantly, very low powered simple main coupler and low rf power supply are enough to excite the cavity.
- (3) Low cost sputter-coated Nb cavities without higher mode couplers shall be used in order to minimize the capital cost of the machine.
- (4) A laser illuminated photocathode cw electron gun at a very high working voltage up to 0.5 - 2 MV, or the existing thermionic high-current and high-charge cw electron gun at 0.25 - 0.5 MV shall be used.
- (5) An energy recovering DC decelerator coupled with the electron gun shall be used to maximize the wall-plug efficiency, and to minimize the radiation hazards.
- (6) Other options of the machine shall be the same or the similar with the existing facility.

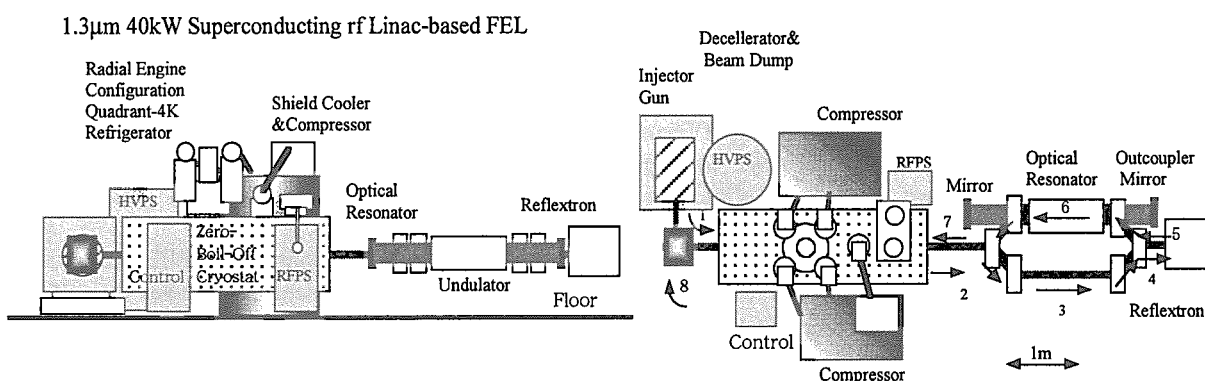


Fig. 1 A layout of 40 kW CW 1.3 micron industrial FEL

Usually, we have to pay about 30% of the total capital cost for the superconducting rf linac modules, the 20% for the rf system, the 20% for the refrigerators, the 20% for the electron gun, injection and transport system, and the 10% for the FEL related. We can cut about 70% or more of the superconducting cavity modules and 90% - 99% of the rf system by developing above items. Electricity of the system is mainly consumed in the refrigerators, electron gun and decelerator. The industrial FEL machine has about several tens mA of electron beam current, 40 kW of FEL power, and several MW of beam power.

References

- 1) E.J.Minehara et al., pp159-161, in the proceedings of Particle Accelerator Conference, 1995, Dallas.
- 2) T.Shizuma, et al., "Injector Design for the JAERI-FEL Energy Recovery Transport", to be published in the EPAC2000 proceedings.
- 3) R.Hajima, T.Shizuma, and E.J.Minehara, "Study on Emittance dilution in the JAERI-FEL Energy -Recovery Transport", to be published in the EPAC2000 proceedings.
- 4) N.Nishimori, et al., "A Thermionic Electron Gun System for the JAERI Superconducting FEL", to be published in the EPAC2000 proceedings.

4.3.2 Optimization of an optical resonator with insertable scraper output coupler for the JAERI far-infrared free-electron laser

Ryoji NAGAI, Ryoichi HAJIMA, Nobuyuki NISHIMORI, Masaru SAWAMURA,
Nobuhiro KIKUZAWA, Toshiyuki SHIZUMA, Eisuke MINEHARA

1. Introduction

To realize a high-power and high-efficient FEL system, optimization of the high-efficient output coupler of the optical resonator is indispensable and is an important factor of the over 1 kW lasing of the JAERI-FEL. The insertable scraper output coupler was chosen for the JAERI-FEL. The coupler allows easy adjustment of the output coupling for optimization of the efficiency of the optical resonator.

2. Evaluations and results

Performance of the optical resonator with the output coupler was investigated at optical wavelength of 22 μm by using an optical mode calculation code. Efficiency factor of the optical resonator was introduced for the evaluation of the optical resonator performance. If the FEL is spiking-mode lasing, the efficiency factor is represented by the following equation and gauges the optical resonator performance,

$$\eta_{opt} = \frac{\alpha_{out}}{\alpha_{loss}^{3/2}}. \quad (1)$$

The efficiency factor of the optical resonator for the center-hole coupler and insertable scraper couplers are shown as a function of the total loss in Fig. 1 with the maximum around 4% of the total loss. The insertable scraper coupler, which is inserting in parallel to the wiggling plane of the electron beam, is most efficient output coupler as shown in Fig. 1. Comparison between the measured and calculated factors indicates that there is another loss related to the optical resonator, which is due to its misalignment. The measured efficiency factor of the resonator is degraded due to the increase of the optical resonator loss. The measured efficiency factors decrease rapidly for the large total loss, since lasing mode shifts spiking-mode to normal-mode. The spiking-mode needs very large net gain, so the lasing mode shifts to normal-mode for the large total loss.

3. Conclusion

The output coupler for the optical resonator of the JAERI far-infrared free-electron laser was optimized to achieve over 1 kW lasing. The insertable scraper coupler allows easy adjustment of the output coupling for optimization of the efficiency of the optical resonator, and enables the wide broadband operation. As a result of the evaluation, it was found that the insertable scraper coupler was the most suitable to far-infrared free-electron laser.

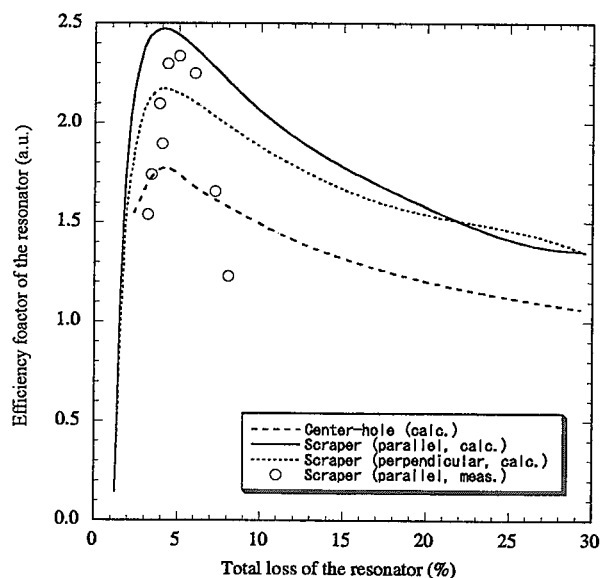


Fig. 1 Efficiency factors of the optical resonator for the JAERI-FEL are shown as a function of the total loss.

4.3.3 Decomposition experiment of Dioxins by IR laser irradiation

Toshihiko YAMAUCHI, Eisuke MINEHARA, Nobuhiro KIKUZAWA, Takehito HAYAKAWA, Masaru SAWAMURA, Ryoji NAGAI, Nobuyuki NISHIMORI, Ryoichi HAJIMA, Toshiyuki SHIZUMA, Yasutaka KAMEI^{a)}, Hisato IKAI^{a)}, Shinichi ITOH^{a)}, Yukio FURUKAWA^{b)}

a) Kyoto Biseibutu Kenkyusho b) Waseda University

1. Introduction

The generation of dioxin becomes large problem as a hostile environment material. Measurement and decomposition for controlling the generation of this dioxin become an important research theme.

It is studied to find the condition of compatibility of the decomposition by the wide infrared wavelength range of JAERI FEL. To begin with, before starting the examination of decomposition by the FEL, the possibility of the photolysis using the wavelength 10.6 μm of CO_2 laser, or the decomposition by the laser absorption are studied.

Here, not only the FEL (22 μm and 25 μm are chosen) being available to change the wavelength in the infrared region as a preliminary examination but also CO_2 laser to which the dioxin shows the absorption were used¹⁾. And, OCDD (octachloro dibenzo-para-dioxin) and OCDF (octachlorodibenzofuran) in which toxicity equivalency quantity (TEQ) is the lowest are chosen²⁾.

2. Experimental arrangement

The laser beam was focused on the dioxin sample by the lens and the focusing radius was $\sim 50 \mu\text{m}$. The FEL laser of 600 μs pulse duration (macropulse) with the repetition frequency 10 Hz is composed of the pulse train of 1 \sim 40 ps (micropulse) with the repetition rate 10.4 MHz. The laser power of the macropulse was ~ 0.1 kW, and the power of the micropulse was 1 \sim 10 MW. The CO_2 laser power was 10 W, the pulse width could be varied from milli-second to continuous.

3. Experimental result

The strong absorption spectra of dioxin OCDD lie at wavenumbers 999 cm^{-1} and 1425 cm^{-1} from the Fourier transform infrared (FTIR) absorption spectrum³⁾. Three samples (first one was left in the chemical laboratory, second was irradiated and third was not irradiated) were made using the liquid of dioxin dissolved in toluene.

The experimental result of which degradation rate (dioxin quantity of (without - with irradiation) \times 100/dioxin without irradiation) over 90% was obtained as described in the following. In the first place, the octachloride dioxin was irradiated with the wavelength 10.6 μm (pulse width: 80 μs , laser power: 4 W, 50 minutes' irradiation), and the high degradation rate was measured by the gaschromatograph. Next, the same octachloride dioxin was irradiated with wavelengths 22 μm and 25 μm , and the decomposition could not be clearly observed. The experimental result of the decomposed dioxin quantity on laser wavelength is represented in Fig. 1.

4. Summary

The decomposition experiment of the dioxin was studied using three infrared wavelengths. As the result, the decomposition successfully completed by irradiating with the infrared laser. The followings were clarified by the experiment.

- (1) By irradiating with the wavelength 10.6 μm which is approximate to the peak of infrared absorption spectrum, the decomposition of dioxin was observed.
- (2) At the wavelengths 22 μm and 25 μm , the effective decomposition could not be observed.
- (3) The resolved dioxin did not become the 4 \sim 7 chloride dioxin, or it was decomposed into other chemical substances or the 1 \sim 3 chloride dioxin, and the noxious dioxin disappeared.

Hereafter, it is considered to raise the decomposition efficiency by irradiating with the FEL adjusted to the strong absorption lines 7.0 μm (OCDD) and 6.5 μm (OCDF).

References

- 1) N. Kikuzawa et al. : Nucl. Inst. and Meth. , Vol.A331, p.276-281, 1993
- 2) edited by J. Kanei : "Daiokisinrui Sokutei Manyuaru", Kougaitaisaku Gijyutu Doyukai, Vol.33, p.77, 1997
- 3) S. Sommer et al. : Analy. Chem. , Vol.69, p.1113-1118, 1997

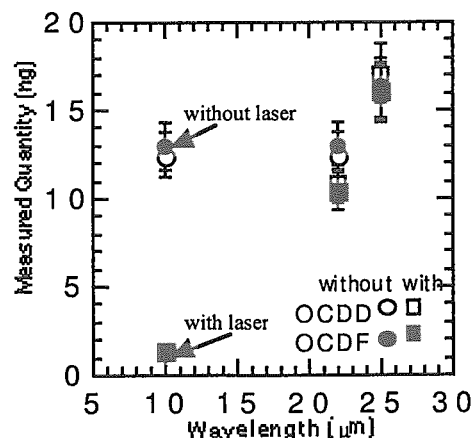


Fig. 1 OCDD and OCDF decomposition quantity dependent on incident laser wavelength

4.3.4 Second harmonic generation in CdTe plate by free electron laser

Toshihiko YAMAUCHI, Nobuhiro KIKUZAWA, Eisuke MINEHARA, Ryoji NAGAI, Nobuyuki NISHIMORI, Masaru SAWAMURA, Ryoichi HAJIMA, Toshiyuki SHIZUMA, Takehito HAYAKAWA

1. Introduction

The second harmonic generation (SHG) technique is used to measure the ultrashort pulse width of a titanium sapphire femtosecond laser, whose instrument is called as an autocorrelator. The typical crystal for SHG is β -BaB₂O₄ (BBO). This system is applicable for the visible and near-infrared ranges. However, the study using the SHG technique has not been intensive in the mid- and far-infrared ranges, except for the single wavelength of CO₂ laser experiments, because ultrashort pulse lasers were rare. Each SHG study has consequently been performed using the Q-switched CO₂ laser¹⁻³). It was found in those studies that cadmium telluride (CdTe) has a high conversion efficiency and an easy tunability. The characteristics of CdTe, the coherence length, the reflective index and nonlinear coefficient, depend on the wavelength.

Since the FEL has been oscillated in the range of 15 to 28 μ m (fundamental wavelength), the authors performed an SHG experiment in CdTe using the FEL fundamental wavelength of 22 μ m for the first time.

2. Experimental setup

A sample of CdTe which was 9 mm x 28 mm, with edge angles of 5° and a maximum thickness of 0.98 mm was installed in front of the MCT detector. The FEL was oscillated in the range of 15 to 28 μ m at a maximum macropulse power of ~2 kW (pulse width 400-600 μ s) composed of micropulse power of 5 ~ 200 MW (electron beam pulse width 1 - 40 ps). The electric field vector of the laser beam was almost parallel to the [1 1 1] direction inside the CdTe. The coherent length l_c is estimated to be 119 μ m at the wavelength of 22 μ m. The thickness at the center of the input surface is 595 μ m which corresponds to five coherence lengths. The input laser power was controlled by the aperture and the KRS-5 plate, and the macropulse power was 12 W. The micropulse power was 240 kW and the laser intensity was 120 MW/cm² (Pulse width is assumed to be 5 ps). The CdTe plate was installed 3.5 mm beyond the focal length $f = 35$ mm to avoid damage. The second harmonic signal was measured using a liquid-nitrogen-cooled MCT detector.

3. Experimental result

The optical path of the laser beam was set normal to the (-1 1 0) surface and the linear polarization was almost parallel to the [1 1 1] direction in order to generate the maximum second harmonic output. The quantity of the absolute conversion efficiency was experimentally determined using the measured signals. The ratio of the SHG signal to the fundamental signal, which is equal to the product of the signal without the CdTe plate and the transmittance $T_1(\omega)$, is nearly 1.4. The conversion efficiency α is approximately estimated by $P(2\omega) \sqrt{\{T_1(\omega)T_1(2\omega)\} \alpha T_2(2\omega) \eta(2\omega)} / P(\omega) T_1(\omega) (1-\alpha) T_2(\omega) \eta(\omega) = 1.4$ ---(1), then $\alpha = 3 \times 10^{-3} \%$ ---(2), where $P(\omega)$ is the input power, T_1 is the transmittance of the CdTe crystal, T_2 is the transmittance of the ZnSe optical filter and η is the quantum efficiency of the MCT detector, and ω and 2ω are the fundamental angular frequency (wavelength 22 μ m) and the second harmonic angular frequency (11 μ m), respectively. As the micropulse power is ~120 MW/cm², the conversion efficiency is $\gamma = 3 \times 10^{-5} \%$ /(MWcm⁻²) ---(3). The measured thickness of CdTe on the incident area was nearly five coherence lengths.

By adding a ZnSe optical filter, no significant reduction of SHG signal was observed; this is different from the fundamental signal. Therefore, it is understood that a clear SHG signal is produced when using the CdTe plate.

4. Discussion and summary

The second harmonic intensity is given by¹⁾ $I(2\omega) = 21.2 d_{14}^2 l_c^2 I(\omega)^2 / n(\omega)^2 n(2\omega) \lambda(\omega)^2$ ---(4), where d_{14} is the relevant effective nonlinear coefficient (cm/statV), l_c is the coherence length $\lambda(\omega)/4(n(2\omega)-n(\omega))$, $I(\omega)$ is the fundamental laser intensity (W/cm²), $n(\omega)$ and $n(2\omega)$ are the refractive indexes at the frequencies ω and 2ω , respectively and $\lambda(\omega)$ is the wavelength. The main second harmonic conversion efficiency parallel to the [1 1 1] direction is $\gamma = 2 \times 10^{-5} \%$ /(MWcm⁻²) ---(5), which is nearly equal to the experimental value of eq. (3). The SH signal generated from the input wavelength of 22 μ m of a FEL was observed using a non-birefringent CdTe plate. The conversion efficiency is experimentally obtained to be ~3 x 10⁻⁵ %/(MWcm⁻²) which is almost equal to the calculated value.

References

- 1) M.S. Piltch, C.D. Cantrell and R.C. Sze: J. Appl. Phys., 47, p.35143517, 1976
- 2) C.K.N. Patel: Phys. Rev. Lett., 16, p.613-616, 1966
- 3) J.J. Wynne and N. Bloembergen: Phys. Rev., 188, p.1211-1220, 1969

4.3.5 Study on recirculating beam transport and RF instability for the energy-recovery experiment at JAERI-FEL

Ryoichi HAJIMA, Toshiyuki SHIZUMA, Eisuke MINEHARA

1. Introduction

FEL lasing over 2 kW in average power has been obtained at JAERI-FEL. For the further increasing of the FEL power, we plan to add an energy-recovery system to the existing machine. The recirculating beam transport in the energy-recovery system must be designed to meet the requirements: isochronicity, achromaticity, large energy acceptance, small second-order aberrations, path-length controllability and RF stability.

2. Design of recirculating beam transport

We chose a configuration with triple-bend isochronous arcs for the recirculation, which is a natural extension of the existing beam transport. The designed recirculating beam transport completely fulfils the above requirements. It is found that the RF instability can be suppressed by a simple feedback loop of RF amplitude and phase¹⁻²⁾.

Emittance dilution, through the recirculation, caused by space-charge force, higher-order aberrations and coherent synchrotron radiation force has been also studied³⁾. Numerical simulations with several kind of accelerator simulation codes shows that the emittance dilution is due mainly to higher-order aberrations in the vertical plane and CSR force in the horizontal plane. The amount of emittance dilution for the both planes is found to be much smaller than the critical value which degrades the FEL performance.

See the listed references for the detail discussions.

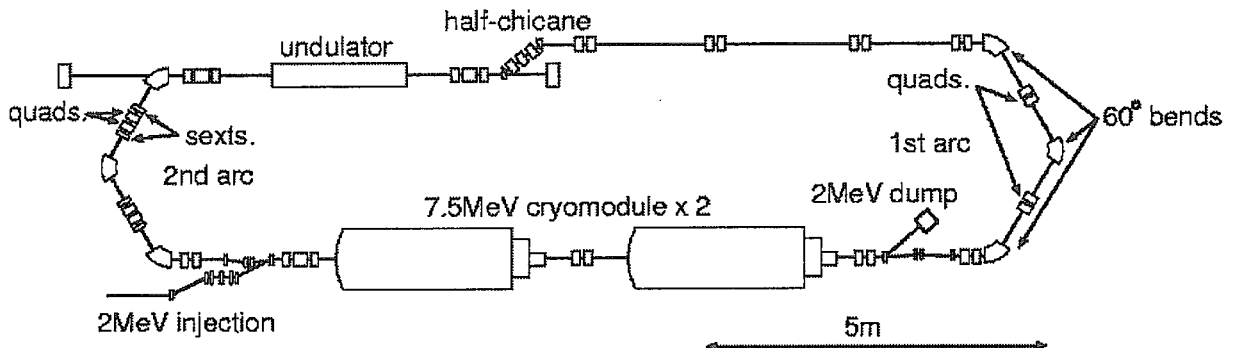


Fig. 1 Recirculating beam transport for the energy-recovery experiment at JAERI-FEL

References

- 1) R.Hajima et al., Nucl. Inst. Meth. A445 (2000) 384-388
- 2) R.Hajima et al., Proc. 12th Symposium on Accelerator Sci. and Tech. (1999) 42-44
- 3) R.Hajima et al., Proc. European Particle Acc. Conf. (2000)

4.3.6 Development of SHG autocorrelator for far infrared JAERI FEL

Nobuhiro KIKUZAWA, Toshihiko YAMAUCHI, Ryoji NAGAI, Eisuke MINEHARA

1. Introduction

Second harmonic generation (SHG) technique is used to measure the ultrashort pulse width of the femtosecond laser, whose instrument is called as an autocorrelator. However, the autocorrelator is not commercially available for a free electron laser (FEL) of far infrared (FIR) wavelength range, because a few SHG crystals are not fixed yet. Since the study for SHG has been performed using Q-switched CO₂ laser with a wavelength 10.6 μm and a pulse width ~200 ns, it was understood that cadmium telluride (CdTe) has a high transmittance, high conversion efficiencies and an easy tunability. For the JAERI FEL oscillated in the range of 15 to 28 μm, the FIR autocorrelation system has been developed by using a sample of CdTe as a SHG crystal to measure the short pulse width of picosecond FEL in FIR wavelength range.

2. SHG autocorrelator setup

The configuration of the FIR autocorrelator with the noncollinear (background-free) SHG method is shown in Fig. 1. As shown in Fig. 1, the FEL beam passes through an aperture and is reflected by a mirror to scrape off a half of the beam. A ratio of the two beams can be adjusted to 1:1 by changing the mirror position. This method of the beam splitting alleviates the problems connected with a dielectric foil's beam splitter, namely low reflectance and difficulties to adjust of ratio of desired splitting. Then, the two beams go to retroreflectors. Delay time between the two pulses is changed by means of the retroreflector (M2) moved linearly by a stepping motor. The pulses are focused in a CdTe crystal by a focusing mirror (M3). The size of CdTe crystal is 7 mm x 15 mm, the edge angle 5° and the maximum thickness 0.78 mm. SHG signal from the CdTe crystal is detected by a liquid-nitrogen-cooled MCT detector.

Alignment of the optical path is performed previously by using a HeNe laser, and therefore the FEL beam is overlapped on this line.

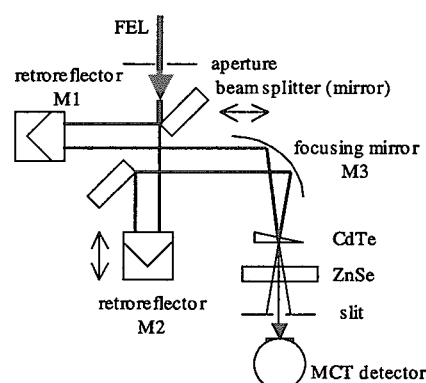


Fig. 1 Layout of the SHG autocorrelator

3. Experimental results

The values of the absolute conversion efficiencies were experimentally¹⁾ and theoretically²⁾ estimated, which were 3 and $2 \times 10^{-5} \%$ /(MWcm⁻²), respectively.

As the signal level was very low, many parameters were searched, such as the diameter of FEL beam, the focus point, the slit width, the number of ZnSe plates and the position of the MCT detector. Then, the weak signal of the SHG was observed as shown in Fig. 2. However, as it is not easy to decide the pulse width using the obtained data by changing the position of M2, the additional improvement of the system will be tried, such as the replace of another CdTe crystal or new Te crystal.

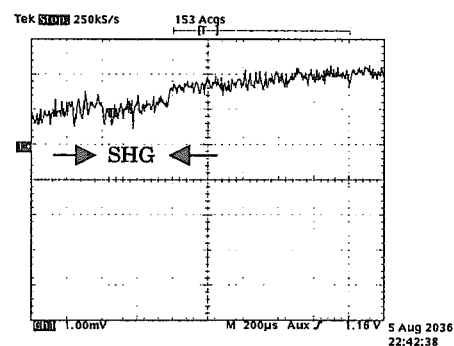


Fig. 2 Example of the SHG signal detected by the MCT detector

References

- 1) T. Yamauchi, et al., to be published in Jpn. J. Appl. Phys. (2000)
- 2) M.S.Plitch, C.D.Cantrell and R.C.Size: J. Appl. Phys., 47, p3514 (1976)

4.3.7 Injector design for the energy-recovery transport at JAERI-FEL

Toshiyuki SHIZUMA, Ryoichi HAJIMA, Nobuyuki NISHIMORI, Ryoji NAGAI, Eisuke MINEHARA

1. Introduction

At the JAERI-FEL facility, the energy-recovery experiments are planned for increasing an average FEL power. In order to merge the injected and recirculated beams, a magnetic buncher is necessary before the main-accelerator. In this report, we describe the current design of the injection buncher.

2. Design study

In order to inject high quality electron beam to the main cryomodule, the injection buncher should meet several requirements as; (1) The magnetic lattice should be achromatic to avoid beam degradation at the exit; (2) The lattice geometry should be symmetric or anti-symmetric; (3) The bending angle should be small as possible. Satisfying the last two requirements would contribute to construct a compact achromatic array, and therefore to prevent a transversal emittance growth due to space charge effects. After several types of achromatic buncher were investigated^{1,2)}, we chose a staircase buncher with all the above requirements being fulfilled (Fig. 1).

The staircase buncher consists of four rectangle dipoles with bending angle of 22.5° . Achromatic condition is kept by properly adjusting strength of two quadrupole singlets beside the second and third dipoles. One quadrupole singlet at the center is used to optimize beam envelope functions at the buncher exit. The staircase buncher is achromatic without space charges. In this case the emittance growth is negligible to the first order. With space charges, both the electron beam energy and radial velocities are modified from magnet to magnet that cause a horizontal emittance growth³⁾. The effect can be minimized when the beam enters with a waist to the buncher entrance in the bending plane. The normalized rms emittances are calculated with PARMELA⁴⁾ including space charges as $\epsilon_x = \epsilon_y = 20\pi$ mm-mrad at the entrance and $\epsilon_x = 38\pi$ and $\epsilon_y = 25\pi$ mm-mrad at the exit of the staircase.

The longitudinal motion was also studied with PARMELA, and the beam parameters of rms bunch length of 9 ps, rms energy spread of 0.9% at 2.6 MeV was obtained at the entrance to the main-accelerator.

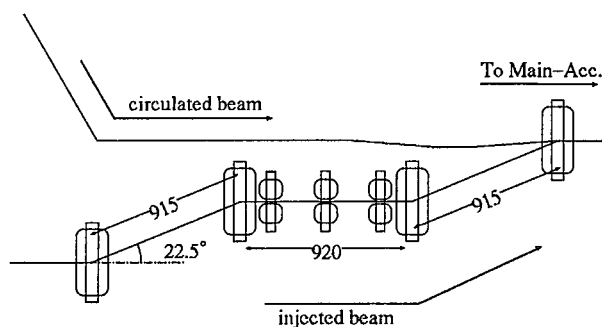


Fig. 1 Layout of the staircase buncher

References

- 1) T.Shizuma et al., JAERI-Conf 2000-006, p230
- 2) T.Shizuma et al., Proc. of EPAC2000, Vienna
- 3) B.E.Carlsten and T.O.Raubenheimer, Phys.Rev.E51(1995)1453
- 4) L.M.Young, LA-UR-96-1835

4.3.8 Simulated performance for the present JAERI-FEL injection system

Toshiyuki SHIZUMA, Ryoichi HAJIMA, Nobuyuki NISHIMORI, Ryoji NAGAI, Eisuke MINEHARA

1. Introduction

So far, no realistic simulation with space charge included has been made for the present JAERI-FEL injection system. We therefore performed a numerical calculation by using the simulation code PARMELA¹⁾. Results fairly produce the measured values of the transversal emittance and the axial bunch length. We also investigated possibility of shortening the bunch length.

2. Simulation and results

The JAERI-FEL injector consists of a 230 kV electron gun and an 83.3 MHz sub harmonic buncher (SHB) followed by two units of a 499.8 MHz super conducting rf cryomodule. The beam parameters at the electron gun exit are electron energy 230 keV, bunch charge 0.5 nC, rms pulse width 0.34 ns, rms beam radius 1.6 mm, and normalized rms emittance 14π mm-mrad. Although the high voltage of 230 kV is applied, the linear space charge force is expected to cause a large emittance growth for such a low energy electron bunch²⁾. We therefore estimated its effects by PARMELA including space charge. As a result, it is found that the transversal emittance increases to 20π mm-mrad at the pre-accelerator exit. The value is comparable with the measured vertical rms emittance of $\epsilon_y = 22\pi$ mm-mrad³⁾. (The measured horizontal emittance is $\epsilon_x = 40\pi$ mm-mrad. This would be due to the misalignment of the beam line.)

The axial motion with space charge included was also simulated using PARMELA. Optimal bunching is obtained as rms bunch length of 2.6 ps (Fig. 1(a)) at the entrance to the main-cryomodule. The value reproduces the measured value of 2.5 ps³⁾.

When the path length between the pre- and main-accelerators is shorten to a half of the current one, the calculation shows that the electron bunch length becomes 1.3 ps (Fig. 1(b)), due to less effect from the space charge force. The energy spread, however, increases to about twice.

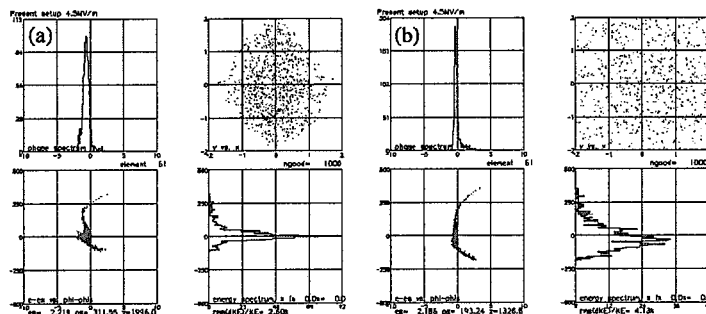


Fig. 1 Various distributions of the axial phase space at the entrance to the main cryomodule for the present geometry (a), and for the geometry in case that the path length between the pre- and main-accelerators is shorten to one half (b).

References

- 1) L.M.Young, LA-UR-96-1835
- 2) B.E.Carlsten and T.O.Raubenheimer, Pys.Rev.E51(1995)153
- 3) N.Nishimori et al., Proc. of the 25th Linear Acc. Meeting, Himeji, 2000, p.5

4.3.9 Interband E1 transitions of ^{157}Gd

Takehito HAYAKAWA, Yosuke TOH, Masumi OSHIMA, Yuichi HATSUKAWA, Makoto MATSUDA,
Nobuo SHINOHARA, Hideki IIMURA, Yu Hu ZHANG^{a)}, Hideshige KUSAKARI^{b)}

a) Institute of Modern Physics, Chinese Academy of Science, Lanzhou 730000, P.R.China

b) Chiba University, Inage, Chiba 263-8522, Japan

1. Introduction

Nuclei in a mass ~ 150 region were understood by interplay of collective motions and single-particle excitations. A neutron of odd-A nuclei can occupy the $h_{9/2}$, $h_{11/2}$ and $i_{13/2}$ orbitals, which have large angular momentum, near the Fermi surface in the single-particle states. The ^{157}Gd ($N = 93$) nucleus is located in rare-earth region, and show typical rotational bands.

In the previous Coulomb excitation experiments of ^{155}Gd ($N = 91$)^{1,2)}, the high-spin states of the $i_{13/2}$ band, which has an opposite parity against the ground-state, have not been strongly excited. However, in our recent investigation using the multiple Coulomb excitation with a heavy Zr ion beam³⁾, a strong enhancement of the $i_{13/2}$ band has been observed, and this excitation mechanism has been still an open problem. It is important to study the high-spin states of the $i_{13/2}$ configuration in neighboring nuclei. In order to investigate the high-spin states of ^{157}Gd , a gamma-gamma measurement by the multiple Coulomb excitation was carried out.

2. Experiment

Nucleus ^{157}Gd ($N = 93$) was excited with multiple Coulomb excitation using a ^{136}Xe heavy ion. The ^{136}Xe beam with 516 MeV energy provided by an ECR ion source and accelerated by the tandem accelerator with linac post accelerator at Japan Atomic Energy Research Institute (JAERI). The target was a self-supporting metallic foil enriched to 96.1% with a thickness of 21 mg/cm². Gamma-rays from excited states populated after the reaction were detected with an array of 10 HPGe detectors with BGO Compton suppressors. The HPGe detectors were placed at angles of 32, 58, 90, 122 and 148° with respect to the beam direction. The energy resolutions of HPGe detectors were 2.0 - 2.3 keV at 1.3 MeV. The efficiencies of HPGe detectors were about 40 - 70% relative to 3" x 3" NaI detector. The experimental data were recorded on magnetic tapes event by event when two or more HPGe detectors were fired. The double or higher fold gamma-gamma coincidence events were sorted to E-E matrices. Approximately 1×10^7 gamma-gamma coincidence events were collected. The gated spectra were constructed from the 4,096 x 4,096 matrices. Relative intensities were derived from singles and gated spectra. The spin assignment was made from a DCO ratio of 32 and 90°. The DCO ratios of the pure dipole (E1) transitions were clearly separated from ones of quadrupole transitions.

3. Results

In previous work, the ground band was measured up to $25/2^-$ using the Coulomb excitation. The low-spin states and gamma-transitions of the $i_{13/2}$ band below $11/2^-$ were studied by the beta-gamma spectroscopic method and the $11/2^-$ and $13/2^-$ states were measured using one-nucleon transfer reactions. In this experiment, the ground-state band and the $i_{13/2}$ band were extended up to $29/2^-$ and $29/2^+$, respectively. New nine E1 interband transitions from the ground-state band to yrast band were also observed. The interband transitions decay from the favored (unfavored) band of the ground-state band to the favored (unfavored) band of the yrast band. The $B(E1)$ values of the interband transitions in the ^{157}Gd were derived by the branching ratio and the mean lifetime which had been measured using the recoil-distance method¹⁾. The $B(E1)$ values are $1.6 \times 10^{-5} \sim 1.2 \times 10^{-6}$ [e²b] and become larger with increasing excitation energy.

References

- 1) H. Kusakari, *et al.*, Phys. Rev. C **46**, 1257, 1992
- 2) A. E. Stuchbery, *et al.*, Nucl. Phys. A **642**, 361, 1998
- 3) M. Kidera, *et al.*, J. of Phys. Soc. of Japan, **66**, 285, 1997

4.3.10 Temperature characteristics of RF control system for the JAERI FEL

Masaru SAWAMURA, Ryoji NAGAI, Nobuhiro KIKUZAWA

1. Introduction

The operation parameters of the RF system of the JAERI FEL superconducting linac drift with time. This phenomenon appeared saliently at the beginning of operation of the linac. As the temperature drift of the RF control system caused this phenomenon, we tried to stabilize the RF control system by controlling the temperature with Peltier elements. This is expected to stabilize the wavelength and the output power of the FEL.

2. Experiments

The RF system mainly consists of a standard signal generator, a phase-shifter-attenuator unit (A- ϕ unit), an amplitude control unit (A-ctrl unit), a phase control unit (ϕ -ctrl unit), and an RF amplifier. The RF power is driven from the RF amplifier to the accelerator cavities and the pick-up signals of the field in the cavities are used as feedback signals. The feedback system of A- ϕ unit, A-ctrl unit and ϕ -ctrl unit controls the amplitude and phase of the RF amplifier. To measure the temperature characteristics of the RF system, the RF amplifier and the cavities were removed and the output signal from the A- ϕ unit was used as the pick-up signal for the feedback.

First the control signals from the A-ctrl unit and the ϕ -ctrl unit were measured under no temperature control. Secondly the Peltier elements were installed to the A- ϕ unit, A-ctrl unit, and ϕ -ctrl unit. The cooling power of the Peltier elements was about 35 W. The Peltier elements were attached to the circuit boxes in each unit and the temperature of the circuit boxes was control with a digital thermo-controller by switching the current to the Peltier element. The same signals were measured under the temperature control.

3. Results

The temperature of the A-ctrl unit changed according to the room temperature drift and the fluctuation of the control signals followed to the change of the temperature. The correlate coefficients between the temperature and the fluctuation of the control signal were 0.7%/K for the A-ctrl unit and 0.5%/K for ϕ -ctrl unit (Fig. 1). After controlling the RF system the temperature change and the fluctuation of the control signal reduced below 0.2 K and 0.2% respectively (Fig. 2).

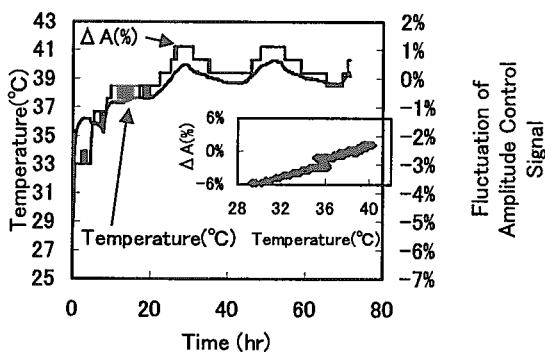


Fig. 1 Temperature change and fluctuation of the control signal in the amplitude control unit with no temperature control

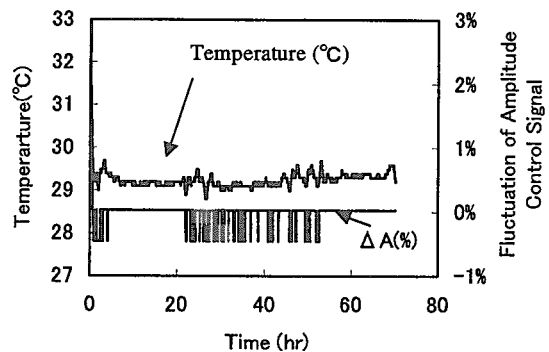


Fig. 2 Temperature change and fluctuation of the control signal in the amplitude control unit with temperature control

4.3.11 A stable and bright DC electron gun system with a thermionic cathode for the JAERI far-infrared free-electron laser

Nobuyuki NISHIMORI, Ryoji NAGAI, Ryoichi HAJIMA, Toshiyuki SHIZUMA, Eisuke MINEHARA

1. Introduction

A highly stable and bright electron beam source was developed at the JAERI Free Electron Laser (FEL) facility. Though the electron beam source is a traditional DC electron gun with a thermionic cathode driven by a grid pulser, improvement of the gun greatly contributed to recent high brightness electron beam production at the JAERI FEL.

2. Evaluations and results

A unique feature of our electron gun is the high voltage (230 kV) of the accelerator tube. The high voltage gun is very useful to prevent the influence of space charge effects in the low energy region and also to produce the electron beam with low longitudinal and transversal emittances. In spite of the above advantage, the high voltage gun has a restriction that the accelerator tube must be installed in a chamber filled with the highly pressured SF₆ gas to avoid the discharge. The input reference signal from the master oscillator to the grid pulser is converted to the optical signal and fed to the high voltage deck through the optical fiber. If the gun is operated in the air, the optical fiber can be directly linked to the high voltage deck. In our case, though, the optical signal is attenuated too much at the optical connector attached to the SF₆ gas chamber, and the input signal for the GP circuit becomes very small. Therefore our GP circuit is very sensitive to the floating capacitance or other electrical error sources and we must assemble the GP circuit and mount it inside the accelerator tube very carefully. The Details of how to reduce the time jitter and produce the high brightness electron beam is described elsewhere¹⁾. We show the achieved performance of our gun in Table 1.

3. Conclusion

The JAERI FEL thermionic electron gun was improved to produce 230 keV electron beam with peak current of 630 mA and pulse width of 0.81 ns. The amplitude fluctuation and rms timing jitter were reduced less than 1% and 23 ps, respectively. Especially the small timing jitter significantly contributed to recent achievement of the high extraction FEL efficiency near perfect synchronism of the optical cavity in our laboratory.

Table 1 Achieved performance of JAERI FEL thermionic electron gun

Bunch Charge	0.51 nC
Peak Current	630 mA
Pulse Width	0.81 ns
Norm. rms Emittance	13 mm-mrad
Time Jitter	23ps
Amplitude Fluctuation	< 1%
Operational High Vol.	230 kV
Micropulse Repetition	10.4125MHz
Macropulse Duration	Up to 1ms
Macropulse Repetition	10 Hz
Thermionic Cathode	Y646B
Cathode size	4 mm radius
Grid Pulser	Koontz type
SF ₆ Gas Abs. Pressure	2.5 atm

References

1) N. Nishimori et al., Proc. of EPAC2000, to be published.

4.4 Optics research and development

4.4.1 Optics development

Masato KOIKE

1. Introduction

Development of advanced lasers such as the T-cube laser and soft X-ray laser requires novel optics including laser crystals, multi-layered mirrors, and diffraction gratings in addition to development of laser oscillation technology. The efforts of the Novel optics research group are devoted to the research and development on optical components, optical systems, and basic technologies for development and application of the advanced lasers and other soft X-ray state-of-arts sources.

2. Achievements

An apparatus for the direct bonding of Ti: sapphire crystals was designed and manufactured to prepare large, high-quality crystals needed for the development of high-power T-cube lasers. Our bonding technique did not require any adhesives and high pressure that may cause optical damage and distortion in crystals. The bonded crystal was mechanically strong and showed the same optical characteristics as that of a single crystal. (Fig. 1)

Mo/Si multilayers are expected as a soft X-ray mirror because of its high reflectivity at around $\lambda = 13$ nm. We are characterizing the structure of Mo/Si multilayers by X-ray diffraction and transmission electron microscopy (TEM) for the purpose to improve the quality of the multilayer. From the TEM image (Fig. 2), inter mixing layers can be seen between Mo (black) and Si (white) layers.

For development of the diffraction gratings for X-ray laser research, laminar type holographic gratings were fabricated by optimizing the varied line space and the shape of rectangular groove. The newly fabricated gratings showed high diffraction efficiency at much lower the higher-orders and stray lights compared to those with conventional ruled gratings (Fig. 3).

3. Future direction

Soft X-ray light having an energy from a few hundreds to three thousands electron volt is very important to explore the structure of the very familiar materials, for example, carbon, aluminum, and silicon. Recently high-brightness soft X-ray sources, such as soft X-ray lasers, laser-generated plasmas, and low-emittance synchrotron radiation sources, have been developed. On the course of these trends one of future directions of our group will be focused on the development of high resolution and high efficiency spectroscopic instruments matching to the new high-brightness sources. Already a theoretical investigation has been made and, based on this, a proto-type machine has been fabricated and under testing.

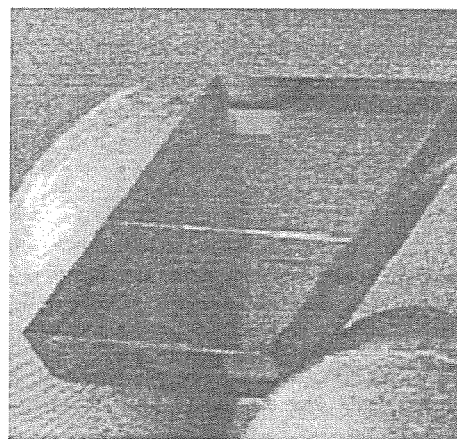


Fig. 1 Direct-bonded Ti: sapphire crystal

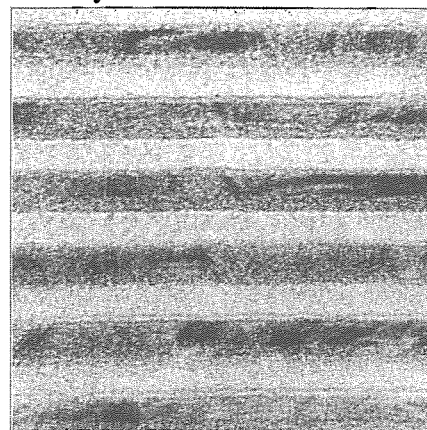


Fig. 2 TEM image of Mo/Si multilayer

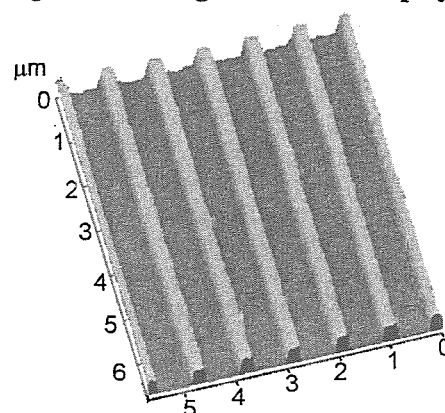


Fig. 3 AFM(atomic force microscope) image of laminar-type holographic grating

4.4.2 Development of high quality large laser crystals for a CPA laser system

Akira SUGIYAMA

1. Introduction

The ultra-short pulse and ultra-high peak power lasers have brought a new field called "super strong field science" which can be studied from sites of large laser facilities to normal size laboratories. Such a progress has been realized by a new technique called CPA (Chirped Pulse Amplification), supported by a solid laser system using neodymium doped YAG and titanium doped sapphire crystals. The demand of high intensity laser system is getting ever higher. It is quite difficult to grow large laser crystals by conventional methods often being accompanied with defect and inhomogeneity of doped ions in crystals. Therefore, we have studied possibility to solve these problems by two different methods.

2. Experimental results

One of the methods was a development of Czochralski crystal growth method for neodymium doped YAG crystals using a double crucible and continuous materials charging techniques¹⁾. The most significant problem in the development was a thermal shielding effect by an inside wall of the crucible. It forced to reduce temperature gradient of 30 K/cm at growth part. As a result from optimization of insulator installed in a furnace, the gradient reached to 70 K/cm and a neodymium doped YAG crystal of 110 mm was achieved. The fluctuation of doped ion concentration along the growth direction was less than 4%, nearly 1/4 of the crystal grown by a conventional method³⁾ (Fig. 1).

The other method was based on a direct bonding technique of commercially available small crystals with high quality²⁾ to obtain large laser crystals. We applied this method to bond titanium doped sapphire crystals with a bonding surface of 12 mm x 6 mm. The polished surfaces were treated with chemical treatments to clean up and to form a hydrophilic layer for creating hydrogen bonding in an atmospheric furnace. Successive heat treatment at 1,373 K in a vacuum furnace transformed the hydrogen bonding into the oxygen-bridged direct bonding. Fracture and inspection by a transmission electron microscope showed that the bonded crystal has a quality as high as the original crystal at the atomic level (Fig. 2). It was also shown that an oscillator signal had no differences in output power and spatial profile when a normal crystal was replaced with the bonded one³⁾.

To evaluate mutual effects of doped ions and host crystals, we also performed spectroscopic measurements of samarium ions doped with fluoride crystals by a laser site selective excitation method^{4),5)}. With a regular manner, most of the samarium ions entered a crystal of YLF in the trivalent state. On the other hand, vast majority of samarium ions entered a crystal of KYF in the divalent. This result suggests that the difference can be attributed to the presence of fluorine ions vacancies during the crystal growth.

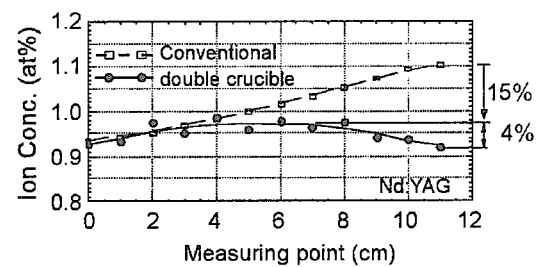


Fig. 1 Fluctuation of doped ion concentration

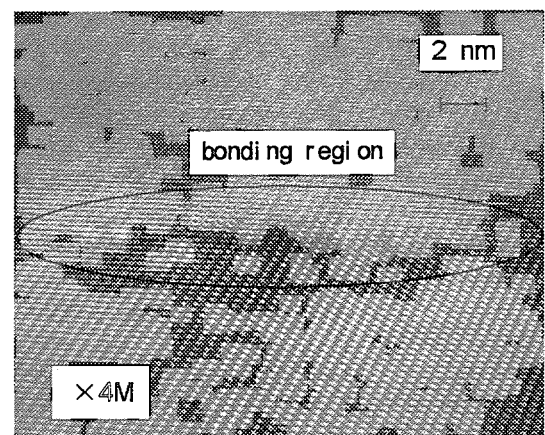


Fig. 2 Magnified image of the bonded region

References

- 1) A. Sugiyama, Y. Anzai, M. Katsurayama, T. Yamaguchi, K. Yamagishi, T. Sasuga, T. Arisawa and H. Takuma, JAERI-Tech. 97-049, 1997
- 2) A. Sugiyama, H. Fukuyama, T. Sasuga, T. Arisawa and H. Takuma, Appl. Opt. 37, p.2407-2410, 1998
- 3) A. Sugiyama, H. Fukuyama, M. Katsurayama, Y. Anzai, S. Nagai, JAERI-conf 2000-006, p.71-74, 2000
- 4) J. P. R. Wells, A. Sugiyama, T. P. J. Han and H. G. Gallagher, J. of Luminescence 85, p.91-102, 1999
- 5) J. P. R. Wells, A. Sugiyama, T. P. J. Han and H. G. Gallagher, J. of Luminescence 87-89, p.1029-1031, 2000

4.4.3 Development of multilayer mirrors for soft x-rays

Osamu YODA, Masahiko ISHINO

1. Introduction

The work concerned with the multilayer mirrors for soft X-ray optics started actually in the fiscal year 1997. In this year we designed a fabrication apparatus for multilayer mirrors, which was equipped with an ion beam gun for sputter deposition of the multilayer. Some of the advantageous features of the ion beam sputtering method are a low working pressure in the deposition chamber and the flexibility in design for the introduction of an in-situ monitor to evaluate the quality of multilayers. The fabrication system was accomplished at the end of the fiscal year 1997.

2. Performance of the fabrication system of the multilayers

Because multilayers composed of Mo and Si have been known to have an extraordinarily high reflectivity for soft X-rays at a wavelength of 13.2 nm and hence studied quite extensively, we have tried to fabricate Mo/Si multilayers to examine the performance of our apparatus. The configurations of the deposition system have been first optimized to make the thickness of multilayers uniform enough on two 2 in. flat substrates; they are (a) relative positions of the ion gun, the target and the substrate, (b) angles of the target and the substrate with respect to the sputtering ion beam and the target normal, respectively, and (c) the speed of substrate rotation. An in-plane uniformity better than 1% has been attained for 30-bilayer Mo/Si multilayers of about 10 nm periodic thickness.

3. Characterization of the substrate and multilayers

We have used two kinds of substrates to fabricate multilayers: One is commercially available silicon wafer, and the other is polished, partially crystallized ceramic glass with very small thermal expansion coefficients (CLEARCERAM-Z[®]). By specular reflectivity measurements using CuK α_1 X-rays, the root-mean-square (rms) surface roughness was estimated to be 0.28 nm and 0.91 nm for Si wafer and ceramic glass, respectively. Figure 1 shows specular reflectivity curves obtained with CuK α_1 X-rays for Mo/Si multilayers prepared on Si wafer (a) and on ceramic glass (b). The composition, i.e. the thickness of each layer, has been designed optimally as a mirror for X-rays of $\lambda=13.2$ nm with an angle of incidence of 45 degree. A large number of superlattice peaks in the reflectivity curve of Fig. 1(a) is indicative of abrupt interfaces within the multilayer deposited on the surface of small rms roughness, while imperfect layer boundaries of the sample prepared on the rough surface cause preferential attenuation of higher order superlattice reflections (Fig. 1(b)). From Fig. 1(a), it is seen that the reflectivity of the first Bragg peak of the Mo/Si multilayer on Si wafer reaches as high as 95% of the calculated ideal reflectivity¹⁾. A more detailed characterization of the multilayer structure is under way.

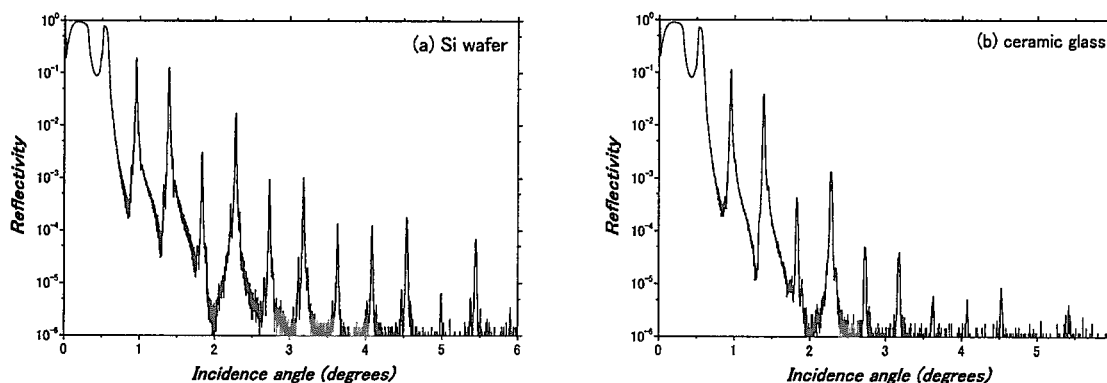


Fig. 1 Specular reflectivity of Mo/Si multilayers prepared on Si wafer (a) and on ceramic glass (b)

Reference

- 1) M. Ishino, M. Nishii, and O. Yoda, *JAERI-Conf. 2000-06*, 270-272, 2000

4.4.4 Evaluation of a laminar-type holographic grating for the soft X-ray flat-field spectrograph

Masato KOIKE, Yoshihisa HARADA^{a)}, Eric GULLIKSON^{b)}, Kazuo SANO^{a)}, Sadayuki ISHIKAWA^{c)}, Takashi IMAZONO^{c)}, Stanley MROWKA^{b)}, Mihiro YANAGIHARA^{c)}, James. H. UNDERWOOD^{b)}, Osamu YODA, Siro NAGAI, Takeshi NAMIOKA^{c)}

a) Production Research Center, Shimadzu Corporation

b) Center for X-Ray Optics, Lawrence Berkeley National Laboratory

c) Research Institute for Scientific Measurements, Tohoku University

1. Introduction

Soft X-ray flat field grazing spectrographs are widely applied for plasma diagnostics. With the advent of the modern numerical-controlled ruling engine it became possible to fabricate a wide variety of varied-line-spacing (VLS) gratings. Taking advantage of this, Nakano et al.¹⁾ developed a compact flat-field grazing incidence soft X-ray spectrograph working in the 0.5 - 40 nm region. In this spectrograph, the focal plane is almost perpendicular to the diffracted rays, an advantage for the use of 2-D detectors.

Recently laminar-type holographic gratings have been revived in the soft X-ray region. The advantages of laminar-type holographic gratings over mechanically ruled gratings are: (1) the suppression of overlapping higher orders; (2) reduction of scattered or stray-light; (3) durability to higher heat loads. The purpose of this note is to present measurements of the diffraction efficiency and resolution of a laminar-type holographic grating recorded by aspheric wave-fronts²⁾ and a blazed-type ruled VLS grating.¹⁾

2. Experimental results

Figure 1 shows the absolute efficiency of both the holographic and the ruled VLS gratings, in which m is the spectral order. The measurements were performed at a fixed incident angle $\alpha = 87^\circ$ just as the gratings are used in the spectrograph.

Figure 2 shows the spectral resolution for the 4.36-nm C-K spectrum measured using a spectrograph¹⁾ with a laboratory X-ray source. The intensity was normalized to the intensity of the respective first diffraction order.

3. Conclusion

We have experimentally examined the performance of the fabricated laminar-type holographic grating in comparison with that of the ruled VLS grating, both in the standard spectrograph configuration. The following results were obtained. (1) The first-order efficiency of the holographic grating was $\sim 10\%$ for wavelengths of 4.5 - 12 nm and was higher (or lower) than that of the ruled VLS grating for soft X-rays of 6.5 nm and shorter (or longer). (2) The laminar-type holographic grating was much more effective than the ruled VLS grating in suppressing the higher orders and stray-light level. (3) The holographic grating showed a comparable spectral resolution to the ruled VLS grating.

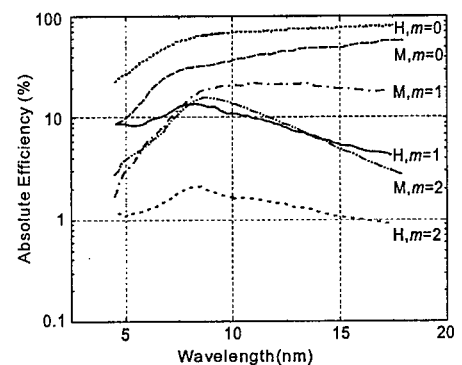


Fig. 1 Absolute efficiencies of the laminar-type holographic grating, H, and the ruled VLS grating, M, measured at a fixed incident angle of 87° , m being the spectral order

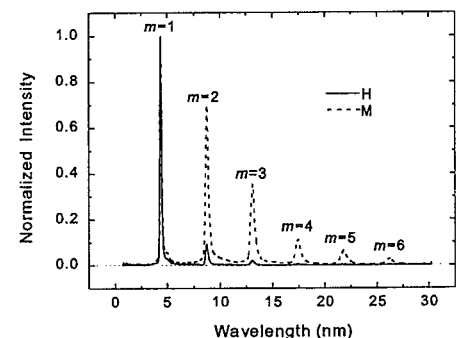


Fig. 2 The 4.36-nm C-K spectrum taken with the holographic grating, H, (solid line) and the ruled VLS grating, M, (dotted line) both mounted in the standard spectrograph

The intensity is normalized with respect to the first-order peak intensity.

References

- 1) N. Nakano, H. Kuroda, T. Kita, T. Harada, *Appl. Opt.* **23**, 2386-2392 (1984)
- 2) M. Koike, T. Yamazaki, Y. Harada, *J. Electron Spectroscopy and Related Phenomena* **101-103**, 913 (1999)

4.4.5 Femtosecond time-resolved fluorescence spectra of a coumarin dye in glass-forming liquids

Hiroshi MURAKAMI

1. Introduction

The structural dynamics of complex systems, such as liquids, polymers and biomolecules, is currently a topic of interest. Extensive experimental studies have clarified the existence of several universal features in the structural dynamics of complex systems, while various theories for interpreting them are under lively discussion ¹⁾. Most of the experimental studies have been performed in the frequency domain, e.g., by dielectric relaxation, neutron and light scattering. A method to study the structural dynamics of complex systems in the time domain is to employ a dye molecule as a probe, i.e., to measure the time-resolved fluorescence (TRF) spectrum of a dye molecule in complex systems. After light irradiation, various relaxation processes occur in the surroundings of the dye molecule in the electronic excited state. If the time scales of such relaxation processes are within the lifetime of the electronic excited states of the dye molecule, the processes are reflected in the TRF spectrum. Thus, we have constructed an experimental system for the femtosecond TRF spectroscopy and have measured the TRF spectra of a coumarin dye in glycerol (CG) and in propylene glycol (CPG) up to 1 ns at room temperature ²⁾.

2. Experimental procedure

A sum frequency generation technique was employed for FTRF spectroscopy by the combination of a mode-locked Ti : Sapphire laser pumped by a CW, multiline argon ion laser and a nonlinear crystal of β -barium borate. The instrumental response function to the laser pulse in the experimental system, i.e., the autocorrelation, was ~ 120 fs (full width at the half-maximum). The samples were excited by the second harmonic (410 nm) of the laser pulse.

3. Experimental results and discussion

The FTRF spectrum of CG shows a time-dependent red shift up to 1 ns, while the time-dependent shift of the spectrum of CPG is completed at ~ 300 ps. It has been found that the time evolution of the peak wavelength of the spectrum of CPG can be expressed by a sum of three exponential functions with time constants of 0.19, 2.9 and 66 ps. On the other hand, a good agreement between the experimental result and the curve calculated from a sum of three exponential functions was not attained in the case of CG. A sum of two exponential functions with time constants of 0.13 and 1.9 ps and a stretched exponential function with a time constant of 460 ps and a stretching exponent of 0.38 reproduces the time-evolution of the peak wavelength of the FTRF spectrum. The stretched exponential time behavior has been observed in the structural dynamics of glycerol by dielectric relaxation and neutron scattering measurements at room temperature. It is considered that the fastest component is due to the vibrational relaxation of the matrices, and other fast and slow components reflect the so-called fast β -process and α -relaxation of the matrices, respectively, which have been observed in various complex systems.

References

- 1) H. Murakami, T. Kushida, H. Tashiro: *Journal of Chemical Physics*, 108, p.10309-10318, 1998, and references therein.
- 2) H. Murakami: submitted to *Journal of Molecular Liquids*.

4.4.7 UV photochemical oxygenation and cross-linking of thin polymer film

Nobuyuki ICHINOSE, Shunichi KAWANISHI, Toshiyuki TAMAI^{a)}, Kazuhiko MIZUNO^{b)}

a) Osaka Municipal Technical Research Institute b) Osaka Prefecture University

1. Introduction

Fundamental aspects of UV-irradiation effects toward polymer surfaces are important for understanding the mechanism of polymer photo-degradation. In contrast, photo-degradation would be useful in the design of photo-degradable polymer as an environment-friendly polymer material. The UV-irradiation is also applied to control the polymer surface properties such as hydrophilicity or acidity.¹⁻³⁾ We have studied UV-laser irradiation effects of polymer surfaces involving oxidative degradation to control their surface properties.

2. Experimental

Poly(4-trimethylsilylmethylstyrene) (PTMSMS, $M_w = 77,000$, $M_n = 34,000$) was prepared by the radical polymerization of 4-trimethylsilylmethylstyrene (TMSMS). Poly(4-methylstyrene) (P4MS, $M_w = 72,000$), polystyrene (PS, $M_w = 43,000$), Rhodamine 6G and other chemicals were used without further purification. Thin films of these polymers were prepared by spin-coating on quartz plates from their toluene solutions. The polymer films were irradiated in air incontact with or without a photomask by use of an excimer laser operated with a KrF gas mixture (248 nm, 15 mJ/cm²/pulse) at 10 Hz through a beam homogenizer. The polymer films were also irradiated in air at 254 nm with a 60 W low-pressure Hg lamp through a water filter to eliminate the 185 nm line. Contact angle of the film with water droplet was measured with Kyowa Kaimen CA-A, and standard buffer solutions of specific pH to detect surface acidic functionalities. Surface composition of the polymer films was analyzed by measuring atomic ratios and C1s X-ray photoelectron spectra with a spectrometer. PTMSMS films irradiated through a photomask were stained with an aqueous solution of Rh6G for 5 min, washed with water, and observed by a fluorescence microscope. Irradiated polymer films were also developed with ethanol- benzene (6:1) for 5 min and were observed by contact mode atomic force microscopy.

3. Results

The irradiation of P4MS and PS films, on the other hand, induced oxidative degradation of the polymer main chain. Selective cleavage of the benzylic C-Si bond of PTMSMS gives benzyl-type radicals, which react with oxygen, leading to the formation of carboxylic acid groups at the surface, or couple with each other, giving the cross-linked structure inside the film. Cleavage of the C-H bond of the main chain in P4MS and PS would be involved in the oxidative degradation of the polymer main chain. Since the cross-linking is an apparent two-photon reaction and requires the closely formed radicals, efficiency of the C-Si bond cleavage and the following radical formation at the 4-position of the benzene ring also must play a crucial role in the cross-linking ability.

References

- 1) Uchida, T.; Sugimura, H.; Kemnitz, K.; Shimo, N.; Masuhara, H. *Appl. Phys. Lett.*, **59**, 3189, 1991
- 2) Niino, H.; Yabe, A. *Appl. Phys. Lett.*, **60**, 2697, 1992
- 3) Ichinose, N.; Kawanishi, S. *Macromolecules*, **29**, 4155, 1996; *Langmuir*, **13**, 5805, 1997

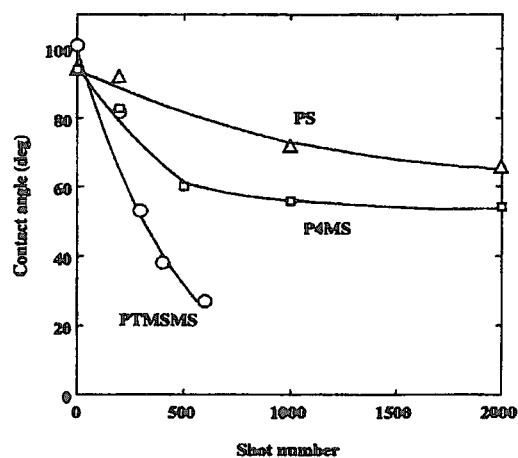


Fig. 1 Plot of shot number vs. contact angle of the irradiated films with the water droplet for PTMSMS, P4MS, and PS

4.4.8 Energy transfer quenching of a fluorescent excited radical cation

Nobuyuki ICHINOSE, Tomoko TANAKA, Shunichi KAWANISHI, Tetsuro MAJIMA^{a)}

a) The Institute for Scientific and Industrial Research, Osaka University

1. Introduction

Recent advances in time-resolved laser spectroscopy, such as femto- to nanosecond laser flash photolysis or fluorescence measurements, have revealed the details in photoinduced electron transfer mechanisms for these two decades¹⁾. On the basis of the spectroscopic data, distance between donor and acceptor molecules R in photo-induced electron transfer process as shown in Scheme^{1,2)} such as exciplex, contact and solvent separated radical ion pairs, and free ions has been discussed extensively as well as the degree of their solvation because it is a critical factor in back electron transfer rates at each stage²⁾. Charge separation from solvent separated ion pair to free radical ions overcoming the back electron transfer is also an important process in photo-induced electron transfer reactions²⁻⁶⁾. We report the dissipation of radical ions generated by photo-induced electron transfer from the estimation of the Forster-type ET quenching of the fluorescence of TMB^{•+}.

2. Experimental

Acetonitrile Dojindo, spectrograde, 1,3,5-tri-methoxybenzene Aldrich and other chemicals were used as received. The measurement of the fluorescence from TM^{•+} has been performed with a monochromatic ns transient absorption measurement or a gated multi-channel detector system. The sample was excited with a XeCl excimer laser and a YAG laser¹⁰⁾ operated with a temporal control by a delay generator unit. Fluorescence intensity was measured as a function of the delay time of γ 100 to 2,000 ns. The absorption spectrum of DCN[•] was measured by the laser flash photolysis of a Nitrogen purged acetonitrile solution containing DCN, biphenyl, and benzyl-trimethyl-silane which was used as a radical cation scavenger.

3. Results

Fluorescence intensity observed as a function of the delay time of the excitation pulse relative to generation pulse for TMB^{•+} indicated the quenching by DCN[•] at 220ns was related to the fluorescence behavior by the Forster-type energy transfer theory. The distance between TMB^{•+} and DCN[•] during their dissipation after the initial photoinduced electron transfer was estimated as a function of time.

References

- 1) G.J. Karvarnos, Fundamentals of Photoinduced Electron Transfer, Wiley VCH, New York, 1993
- 2) I.R. Gould, S. Farid, Acc. Chem. Res. **29**, 522, 1996
- 3) H. Beens, H. Knibbe, A. Weller, J. Chem. Phys. **47**, 1183, 1967
- 4) D. Rehm, A. Weller, Isr. J. Chem. **8**, 259, 1970
- 5) I.R. Gould, D. Ege, J.E. Moser, S. Farid, J. Am. Chem. Soc. **112**, 4290, 1990
- 6) H. Knibbe, D. Rehm, A. Weller, Ber. Bunsenges. Phys. Chem. **72**, 257, 1968

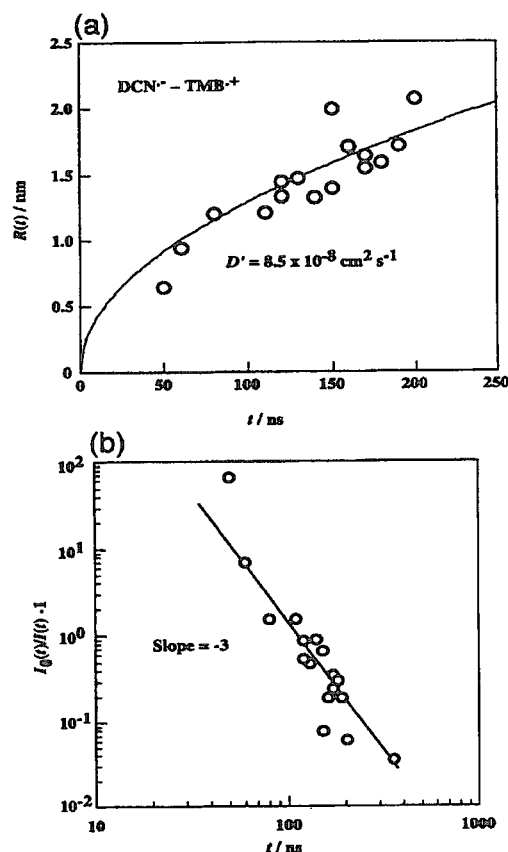


Fig. 1 A plot of the time dependence of the TMB-DCN distance
The solid line represents the best fit of the simple diffusion equation.

4.4.9 Development of debris-free target for laser-plasma x-ray source

Norio OGIWARA, Kazuaki SUGANUMA, Yoji SUZUKI

1. Introduction

Laser-plasma driven by high peak power lasers with ultra short pulse width is an attractive source for generating x-ray for the application to the microscopy, diffractometer and even lithographer. However, conventional laser plasma x-ray sources with solid targets produce debris, which may destroy or coat fragile and sensitive x-ray optical components. In order to solve the problem, we are now developing two types of targets (cryo-target of rare gases and liquid-jet) for laser plasma aiming at continuous operation.

2. Rare gas cryo-target

As a first step solid targets are prepared with rare gases such as Ar, Kr, and Xe which are condensed on a cryopanel made of Cu. These condensed gases are packed tightly by means of heating and pressing. Finally the surface of the solidified gases is mechanically polished by rotating a Teflon plate. Heat caused by the friction between Teflon and target surface makes the surface of the cryo-target flat with the roughness less than 0.1 mm.

These cryo-targets have been tested by irradiating with Nd:YAG laser. The pulsed laser beam with the energy up to 0.3 J in 3 ns was focused onto the targets. The targets have been found to be stable for the laser heat flux as high as ~ 10 W average power. (See Fig. 1) Thus we can operate the x-ray source with Ar, Kr, and Xe targets continuously for more than 2 or 3 hours without any debris. In addition, these sources can be run in vacuum at the pressure level lower than 10^{-3} Torr without any supplementary evacuation.

3. Liquid-jet target

Development of the liquid-jet target is also now in progress to realize a high repetition x-ray source by removing heat generated by the laser irradiation. We have succeeded to form a stable liquid jet with ethanol by forcing the liquid at the pressure level of ~ 10 bar through an ~ 50 μm diameter orifice. Figure 2 shows the image of a stable liquid-ethanol jet.

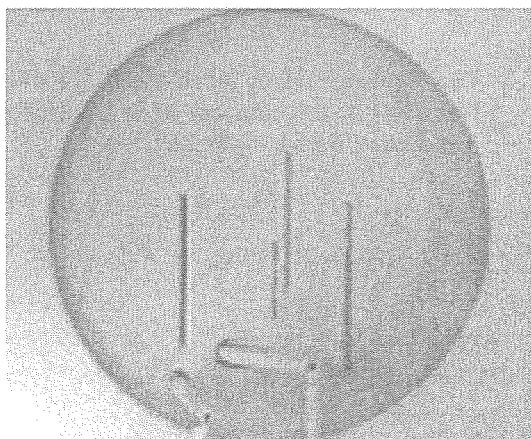


Fig. 1 Traces after the laser beam irradiated on the polished Ar surface

Four vertical traces are clearly seen. The width of each trace is dependent on pulse energy of laser.

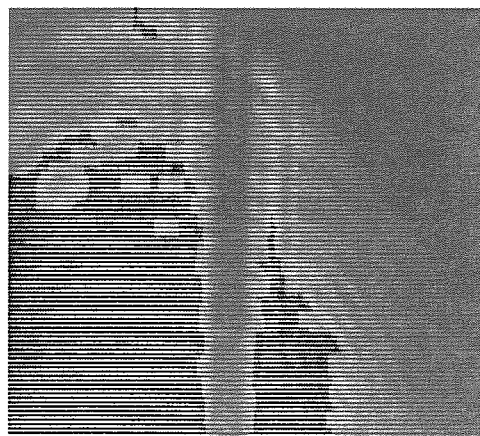


Fig. 2 The image of a stable liquid-ethanol jet in a vacuum

The shadow of the jet is vertically shown in the center. The diameter of the jet is estimated to be ~ 65 μm .

4.4.10 Application to chiral chemistry

Yuichi SHIMIZU

1. Introduction

Application of brilliant short wavelength laser to organic chemical reactions is promising for both direct and selective synthesis of valuable compounds. The study of chiral chemistry concerned with optically active compounds such as α -amino acids is one of the most striking subjects in modern chemistry. Since α -amino acids are chiral biomolecules and usually comprise only one enantiomer in life, an efficient asymmetric synthesis is essential for their preparation. We therefore have attempted to achieve an efficient synthesis of the enantiomer from α -amino acid racemates using the circularly polarized light (CPL) from a XeF (351 nm) excimer laser¹⁾. Furthermore, it can be considered that the study of the initial process using short-pulsed laser through this stereoselective enantiodifferentiation is useful for understanding the mechanism of the transmission of the photonic information of visual substance such as rhodopsin protein.

2. Results and conclusion

As shown in Fig. 1, although the concentration of D-methionine decreased with increasing absorbed energy, that of L-methionine did not decrease and was almost constant throughout the irradiation. Thus, it was clearly revealed that L-form can be enriched from the racemate by irradiation with a right CPL from the laser. In sharp contrast, D-form also could be enriched by irradiation with a left CPL. Consequently, it can be concluded that the irradiation of CPL from laser can induce the enantiodifferentiating reaction of racemic methionine by switching the sense of the CPL (Scheme 1). Although similar results were also obtained for threonine, it was newly revealed that these reactions are largely affected by the chemical structure, especially the functional groups, of α -amino acids. Furthermore, it was shown for the first time that the irradiation of a proline-valine mixture with the CPL induces their enantioselective reactions simultaneously through the photodecomposition, suggesting the occurrence of intermolecular interaction between proline and valine.

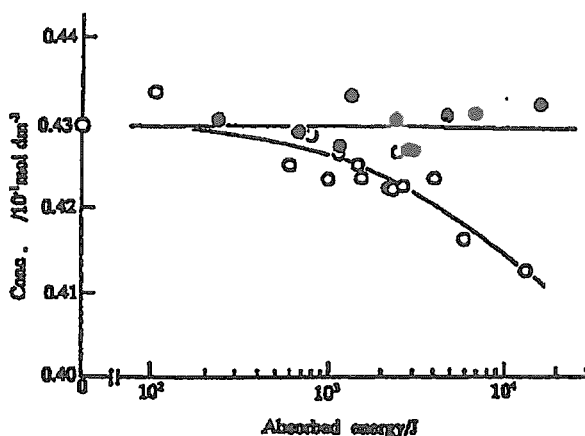
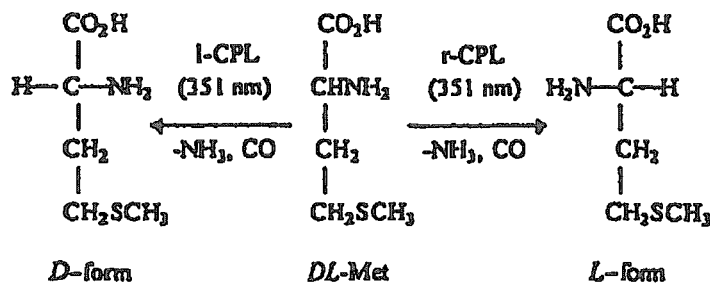


Fig. 1 The concentrations of D-form(○) and L-form(●) in the solution of D L-methionine irradiation with a right CPL



Scheme 1

Reference

1) Y. Shimizu, *Laser Chem.*, **18**, 143-154, 1999

4.5 Laser driven particle acceleration development

4.5.1 Laser driven particle acceleration research

Kazuhiisa NAKAJIMA^{a)}, Tomonao HOSOKAI, Shuhei KANAZAWA, Masaki KANDO, Shuji KONDO, Hideyuki KOTAKI, Takashi YOKOYAMA

a) JAERI Kansai and High Energy Accelerator Research Organization

1. Introduction

Recently, there has been a great interest in ultrahigh field particle acceleration driven by ultra-intense laser pulses in plasmas since a laser-plasma accelerator concept was proposed by Tajima and Dawson¹⁾. In particular, advance in generation of ultra-intense short pulse lasers has brought about tremendous progress in laser wakefield accelerators (LWFA), which have been first demonstrated by Nakajima et al.²⁾. Recent world-wide experiments have resulted in 100 MeV electron acceleration and several 10's MeV ion acceleration with ultrahigh gradient of ~ 100 GeV/m, which is more than 3 orders higher gradient than that of conventional RF accelerators. Therefore laser driven particle accelerators can be expected to provide a promising breakthrough for next generation particle accelerators.

Since 1996 we have started "GeV laser wakefield acceleration project" to achieve more than 1 GeV energy gain with high quality beam owing to the LWFA mechanism. The first observation of high energy electron acceleration exceeding 100 MeV has been shown by LWFA experiments in 1996. The beam test of the photocathode RF gun started in 1997 to develop a high quality electron beam injector. The 2 cm optical guiding of 2 TW, 90 fs laser pulse has been demonstrated by using a fast Z-pinch capillary discharge plasma channel in 1999.

2. High energy gain LWFA experiments using a T³ laser

We have carried out the acceleration experiments using a table-top terawatt laser (T³) to demonstrate the electron acceleration by laser wakefields as shown in Fig. 1³⁾. The laser pulses with duration of 90 fs and the peak power of 2 TW produced by the Ti-Sapphire table-top laser system at 790 nm wavelength were focused by a f/10 off-axis parabolic mirror. The measured focal spot radius was 13 μm . A single bunch electron beam with the energy of 17 MeV and the FWHM bunch duration of 10 ps from the RF linac at 10 Hz repetition rate is brought to a focus with the FWHM beam size of 0.8 mm. An electron pulse was synchronized to the laser pulses within the rms jitter of 3.7 ps. The energy gain spectra of accelerated electrons were measured for various He gas pressures and the laser peak powers as shown in Fig. 2. The maximum energy gain up to 300 MeV was observed for the peak power of 1.8 TW at 20 Torr.

The wakefield excitation has been confirmed by direct measurements of the plasma wave oscillation with the frequency domain interferometer as shown in Fig. 3. Figure 3(a) shows 1-D plasma oscillation, while Fig. 3(b) shows 2-D plasma oscillation contours. The measured density perturbation has shown the longitudinal wakefields of the order of ~ 10 GeV/m in good agreement with the accelerating wakefields expected theoretically. Measurements of the Thomson scattering image of the 1.8 TW pump laser in He gas plasma at 20 Torr have indicated that the strong self-guiding of the laser beam occurs over 2 cm in a plasma as shown in Fig. 4. We have also observed a jet-like

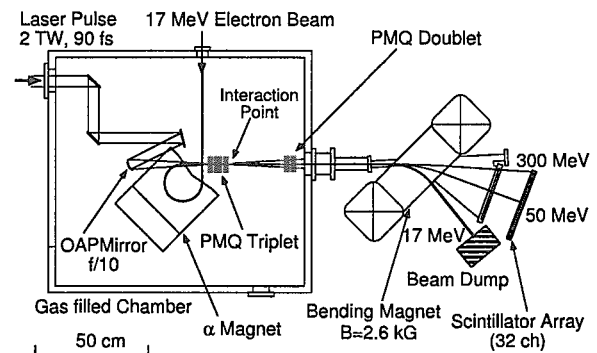


Fig. 1 Schematic of the experimental setup for the laser wakefield acceleration

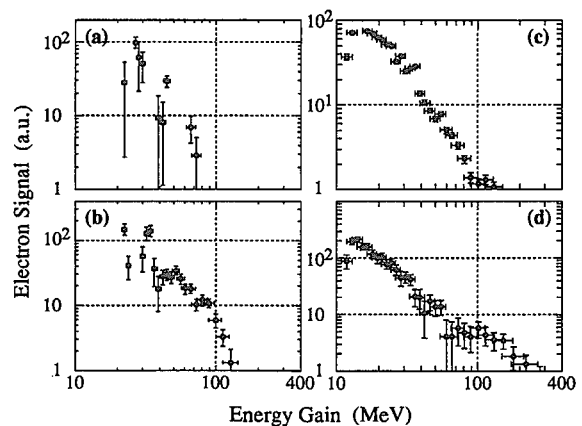


Fig. 2 Measured energy gain spectra of accelerated electrons for (a) 3.4 Torr, $P=0.9$ TW, (b) 20 Torr, $P=0.9$ TW, (c) 2 Torr, $P=1.8$ TW, and (d) 20 Torr, $P=1.8$ TW

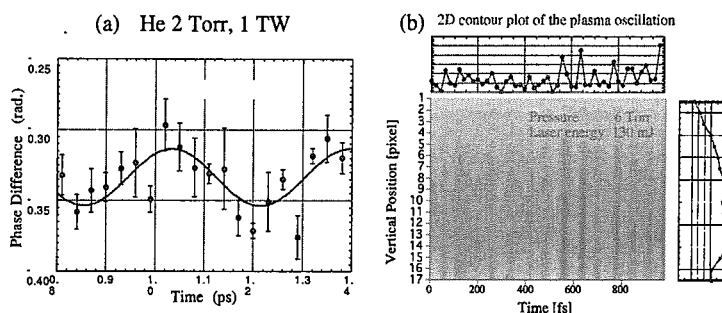


Fig. 3 The frequency domain interferometry measurements of the plasma density oscillation

formation generated with numerous energetic electrons transversely ejected from the central region of plasmas. The detail measurements have shown that an electron jet produced an outward electron flux with the maximum energy higher than 140 keV in a cylindrically homogeneous distribution around the laser propagation axis. This implies that energetic electrons are accelerated by the transverse wakefields higher than 140 MeV/cm, assuming a transverse acceleration length of 10 μm . Since the longitudinal wakefield is higher than the transverse wakefield for the laser focusing parameters, it is inferred that the maximum energy gain exceeds 280 MeV, which indicates a good consistency with the acceleration measurements.

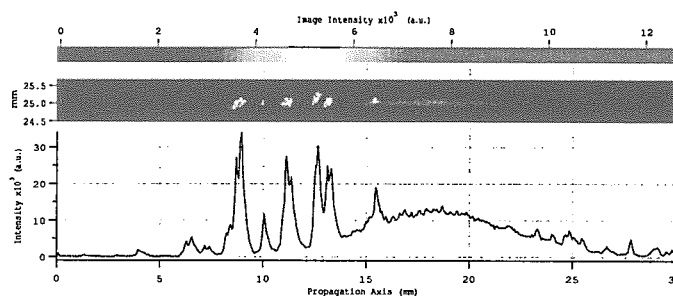


Fig. 4 A lineout of Thomson side scattering image for $P=1.8$ TW at 20 Torr He gas

3. GeV LWFA experiments using a 100 TW laser

In the next step of LWFA research, two major problems must be overcome to accomplish so called controlled acceleration. The one is the injection matched to wakefields in their phase space to accelerate a high quality beam with a low emittance and a small energy spread. The other is the optical guiding to achieve high energy gains exceeding 1 GeV. In order to achieve the acceleration energy gains of higher than 1 GeV in a single stage, it is necessary to extend the acceleration length limited by diffraction effects of laser beams. We propose the plasma channel-guided laser wakefield accelerators in which both the driving laser pulses and particle beams can be guided through Z-pinch capillary discharge plasmas of cm-scale. The design research of GeV range LWFA indicates that the energy gain of 1 GeV will be accomplished by means of the channel-guided scheme over 1.5 cm pumped by 50 TW, 40 fs laser pulses.

From these points of view, our researches have concentrated on developments of the high quality beam injector and the plasma waveguides. We have developed the compact microtron with the photocathode RF gun as a high quality beam injector for the laser wakefield acceleration experiments. Recently commissioning of the injector system has been successfully conducted to produce a 150 MeV beam with a single bunch of 100 pC electrons at 10 Hz. The optical guiding development have resulted in a cm-scale plasma waveguide using the fast Z-pinch capillary discharge. We have succeeded in demonstrating propagation of 2 TW, 90 fs laser pulses over 2 cm in the plasma waveguide using a fast Z-pinch capillary discharge plasma channel. In addition to these experimental achievements, we will construct the femtosecond bunch slicing stage as a part of the laser acceleration test facility to generate a femtosecond electron pulse injected into laser wakefields with femtosecond accuracy. Finally the facility including the 100 TW laser system constructed at JAERI-APR will enable us to conduct the laser wakefield acceleration experiments achieving high energy gains more than 1 GeV as well as high quality beam acceleration.

References

- 1) T.Tajima and J.M.Dawson : *Phy. Rev. Lett.* **43**(267), 1979
- 2) K.Nakajima et al. : *Rhy. Rev. Lett.* **74**(4428), 1995
- 3) H.Dewa et al. : *Nucl. Instr. and Meth. in Phys. Res.* **A410**(357), 1998; M. Kando et al.: *Jpn. J. Appl. Phys.* **38**(L967), 1999
- 4) T. Hosokai et al. : *Optics Letters*, **25**, 10-12, 2000

4.5.2 First commissioning of 150 MeV microtron injected by photocathode RF gun

Masaki KANDO, Hideyuki KOTAKI, Shuji KONDO, Tomonao HOSOKAI, Takashi YOKOYAMA, Shuhei KANAZAWA, Tohru MATOBA, Kazuhisa NAKAJIMA^{a)}

a) JAERI Kansai and High Energy Accelerator Research Organization (KEK)

1. Introduction

We are preparing the 2nd generation laser wakefield electron acceleration experiments, which will achieve an improved energy spectrum of accelerated electrons and a higher energy gain of 1 GeV over diffraction length. For the purpose, the initial electron beam should be injected to match the acceptance of the laser wakefield properly. The pump laser is focused to tens of microns and the pulse length is an order of hundred femtoseconds, therefore the acceptance requires very high quality electron injection. We decided to use a photocathode RF gun as a high quality electron source and a racetrack microtron as a compact energy booster, which is commercially available. The transverse beam matching is relatively easy because its acceptance is an order of 10π mm-mrad, while the longitudinal acceptance is very difficult to achieve by conventional accelerator techniques. However, in case that only the transverse matching is achieved, the energy spectra of the accelerated electrons will be improved. For the perfect beam matching, we try to apply bunch slicing technique which can produce a femtosecond bunch from inverse free-electron (IFEL) mechanism. In this report, we describe the installation and the first commissioning results of the high quality electron injector system constructed at the facility at Kizu in Kyoto.

2. Overview of the high quality electron beam injector

The high quality electron injector at JAERI-Kansai consists of a photocathode RF gun and a racetrack microtron (RTM). The layout of the accelerator system is depicted in Fig. 1. The photocathode RF gun is the improved BNL-type (GUN-IV)¹⁾ of which specification is summarized in Table 1. The gun cavity has 1.6 cells and π -mode resonance frequency at 2,856 MHz and a maximum electric field of 100 MV/m at the cathode surface. We had over two-year operation experience in the same type gun at Nuclear Engineering Research Laboratory, The University of Tokyo. The detailed explanation is found in this report.²⁾ The drive laser is a frequency quadrupled Nd:YLF laser which has a wavelength of 263 nm, a pulse length of 6 ps, and a pulse energy of 160 μ J. Most remarkable feature of the laser system is rms energy stability which is less than 0.5%.

The original RTM is produced by Sumitomo Heavy Industries (SHI) with a thermionic electron gun. It has two major dipole magnets with a typical magnetic field of 1.23 T and an accelerating structure (we call linac), placed between the magnets. The injected electrons go through the linac and then turn back to the linac. This twice-acceleration at the first stage is to accelerate injected low energy electron beam (100 keV) to a moderate energy in order to avoid beam loss resulting from small turn separation when the thermionic gun is used. In our situation, this twice-acceleration scheme at the injection is not necessarily required, we adopt the same injection scheme because the least modification is required to achieve this. We optimized parameters of the RTM using a computer code MIC, which tracks a single particle orbit in the RTM. We also designed the injection beam transport by transfer matrix method, TRACE-3D code, and PARMELA code. Extraction beam transport was designed to be doubly-achromatic because the extraction magnet in the

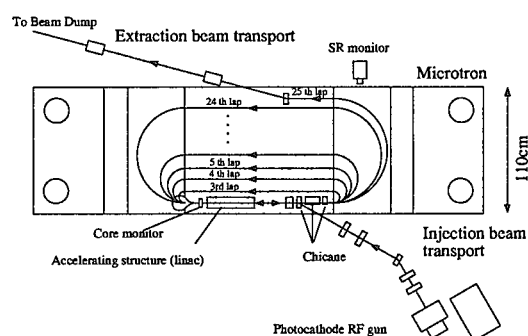


Fig. 1 Layout of the high quality electron beam injector : photocathode RF gun and racetrack microtron

Table 1 Specification of the photocathode RF gun

Input RF power	6 MW (10 MW max)
Acceleration Gradient	100 MeV/m
Shunt impedance	57 M Ω /m
Energy	3.5 MeV
Charge	< 3 nC
Emittance	1 ~10 π mm-mrad
Pulse length	< 10 ps
Quantum efficiency	1.4×10^{-4}

RTM was settled on the dispersive straight section.³⁾ As a result, a horizontal emittance of $10 \pi \text{mm-mrad}$, a pulse length of 5 ps (FWHM), a charge of 280 pC was expected to be accelerated in the RTM, when a charge of 1 nC was injected to the RTM.

3. Chronological report of installation and commissioning

The day, August 20, 1999, when the main body of the RTM was brought to the facility at Kizu, was the beginning of the installation of the system. Figure 2 shows the system which was under construction. The total system was successfully installed until December. RF conditioning of the RF gun and the linac was started in late December. We suffered from the arc discharges in waveguides, especially power variators, during the conditioning. After some improvements, we started beam commissioning of the microtron on March 9, 2000. The 150 MeV electron beam was successfully accelerated and brought to the beam dump on March for the first time. Figure 3 shows a typical output of a synchrotron radiation (SR) monitor, which measures SR from bent electrons in the RTM main magnet. The SR monitor was very useful at the first stage of the commissioning, because we could see beam position in the RTM and on which lap the electron beam was lost. The maximum output charge from the RTM is 91 pC at an injection charge of 350 pC, that corresponds to a transmission efficiency of 26%. The maximum transmission efficiency observed to date is 42%. The beam transmission efficiency can be roughly obtained by a core monitor placed before the linac (Fig. 4). The short-term stability of the output beam is 3.6% (rms) and this is mainly due to the stability of the extracted beam stability of the rf gun. The long-term stability of the beam is 10 - 20% (rms) and is now under improvement.

Our facility passed the inspection for the radiation facility on June 16. We plan to measure beam characteristics this fiscal year.

4. Achievements

We have constructed a photocathode RF gun injected microtron and succeeded in acceleration of 150 MeV, 91 pC electron beam. The short-term stability of charge is 3.6% (rms) and the long-term stability of charge is an order of 10% (rms).

5. Acknowledgements

We would like to thank T. Ishizuka, F. Sakai, K. Aoki, K. Kawamura, H. Morimoto, and T. Hori of SHI for their contributions during the installation and the commissioning. We also wish to thank peoples in Kansai Research Establishment, JAERI, especially, Y. Kato, T. Arisawa, and T. Watanabe of APR for their encouragement and supports.

References

- 1) X. J. Wang et al. : Nuclear Instruments and Methods A 375, p.82, 1996
- 2) H. Kotaki et al. : in this report
- 3) M. Kando et al. : Proceedings of 1999 Particle Accelerator Conference, pp. 3702-3704, 2000

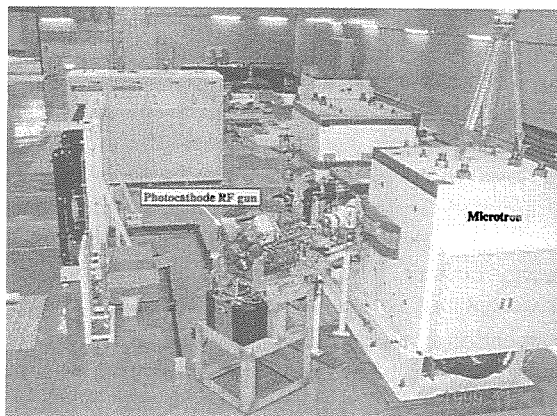


Fig. 2 Photograph of the acceleration system which was under construction



Fig. 3 Synchrotron radiation from the bent electrons in the RTM

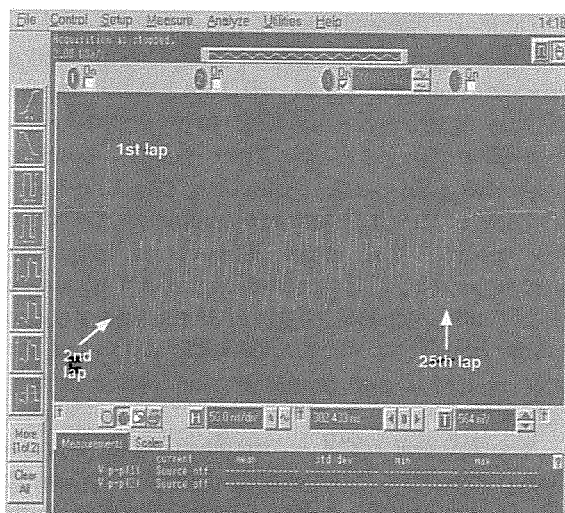


Fig. 4 Core monitor output. Electron signals at each lap can be clearly observed.

4.5.3 Experimental characterization of photocathode RF gun

Hideyuki KOTAKI, Masaki KANDO, Shuji KONDO, Hideki DEWA*, Shuhei KANAZAWA,
Takashi YOKOYAMA, Tomonao HOSOKAI, Fumio SAKAI†, Kazuhisa NAKAJIMA^{a)}

a) JAERI Kansai and High Energy Accelerator Research Organization (KEK)

1. Introduction

Recently, a photocathode RF gun has been studied widely in the world because it has potential to generate a high quality (low emittance, short pulse length) electron beam, that will be used for short pulse X-ray generation¹⁾, laser particle accelerators²⁾, and pulse radiolysis. We adopted a photocathode RF gun for a high quality injector oriented for 2nd generation laser wakefield acceleration experiments planned at JAERI Kansai. The photocathode RF-gun we use is based on GUN-IV, which was originally developed by a collaboration between Brookhaven National Laboratory (BNL), University of California at Los Angeles (UCLA) and Stanford Linear Accelerator Center (SLAC), and improved to work at high duty operation (~50 Hz).³⁾ This RF gun can produce an emittance of 1π mm-mrad owing to a solenoid magnet that compensates emittance growth by linear space-charge effects. We started the RF gun tests at the University of Tokyo since 1997. The results were briefly summarized in Sect. 2.⁴⁾ In June 1999, our new facility was completed at Kizu in Kyoto and we started to construct the high quality electron accelerator since August. The accelerator consists of the similar photocathode RF gun and a microtron.⁵⁾ The detailed description of the system is found in this report. In Sect. 3, we present status of RF conditioning and operation of the gun at Kizu.

2. Summary of photocathode RF gun tests at The University of Tokyo

The photocathode RF gun was installed into the 17 MeV linear accelerator at Nuclear Engineering Research Laboratory, the University of Tokyo (UTNL), replacing the thermionic electron gun and the subharmonic buncher. The drive laser for the photocathode is a frequency quadrupled Nd:YLF laser. The oscillator has a repetition rate of 79.3 MHz, that is 36th subharmonic of master oscillator. A series of laser pulses is amplified to ~2 mJ in the regenerative amplifier and converted to 4th harmonic in nonlinear crystals. The FWHM pulse width of the UV laser is 5 ps FWHM, and the wavelength is 264 nm, of which photon energy corresponds to 4.7 eV (close to copper work function, 4.65 eV). The most remarkable feature of the laser is its energy stability of 0.5% (rms). The incident angle to the cathode is 68 degrees. The maximum pulse energy is 100 μ J on the cathode surface.

The photocathode RF gun has been tested for two years. Quantum efficiency (QE) of the copper photocathode was 1.4×10^{-4} at an applied electric field of 100 MV/m. It varied from 1×10^{-6} to 1.4×10^{-4} by conditioning status.^{4, 6)} It is useful to maintain high QE to keep high vacuum in the gun. A maximum charge of 2.7 nC was obtained when a laser pulse of 91 μ J was irradiated on the cathode. We succeeded in generation of electron beams with a transverse emittance of less than 10π mm-mrad, a pulse length of less than 7 ps, an energy of 3.5 MeV and a charge of 100 pC.

3. Photocathode RF gun tests at JAERI-Kansai

Figure 1 shows the photocathode RF gun installed in the new facility at Kizu in Kyoto.⁷⁾ The gun is the same type described in the previous section and the drive laser, that is located next to the gun, is just same one described in Sect. 2. The RF power fed to the RF cavity is 6 MW for the present, and the pulse width of the RF is 6 μ s. The repetition rate of the RF is variable up to 60 Hz. There is a solenoid magnet after the photocathode RF gun to focus the electron beam from the photocathode. The charge from the photocathode is measured by Faraday cup located just after the RF gun.

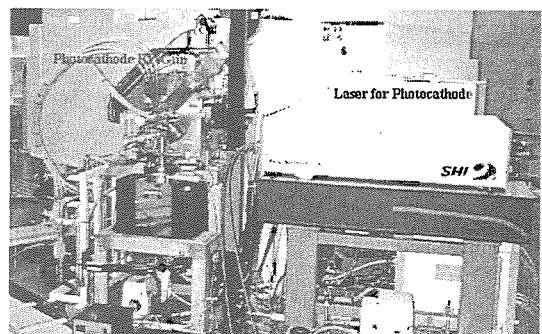


Fig. 1 Photocathode RF gun installed at JAERI-Kansai

* Present address: Japan Synchrotron Radiation Research Institute (JASRI)

† Present address: Sumitomo Heavy Industries, Ltd.

There are two types of currents from photocathode: one is photo emission current and the other is field emission current called dark current. Photo emission charges are due to photoelectric effect induced by the irradiated laser pulse. The photo current depends on the electric field as $Q \propto (h\nu - W + \text{const.} \cdot \sqrt{\beta E})^2$, where Q is photo emission charge, $h\nu$ is photon energy, W is work function of the cathode, β is dimensionless field enhancement factor, and E is electric field. The 3rd term generates enhancement of charge known as Schottky effect, as shown in Figure 2(a). Figure 2(b) shows the phase dependence of the QE. It also shows the Schottky effect because the electric field on the cathode varies as a function of laser injection phase against the RF. It is important to select an appropriate laser-injection phase to operate the photocathode RF gun.

A dark current also depends on the electric field such as $I \propto E^{2.5} \exp(-\text{const.}/E)$. Figure 3 shows the dark currents as a function of RF power in various dates. At the beginning of RF conditioning (indicated as 4/24), the dark current was high, and it gradually reduced to 5 nC/pulse at 6 MW after continuous conditioning.

4. Conclusion

We have tested BNL-type photocathode RF gun at the University of Tokyo. The beam measurements resulted in a transverse emittance of less than 10π mm-mrad, a pulse length of less than 7 ps, an energy of 3.5 MeV and a charge of 100 pC. The QE was improved from 1×10^{-6} to 1.4×10^{-4} and it has been found that high vacuum condition is required to maintain a high QE.

The photocathode RF gun was installed at Kizu facility of JAERI as a high quality electron beam injector. At present the QE is 1.8×10^{-5} and the dark charge is 5 nC. Further studies on increasing QE and reduction of dark current will be progressed.

5. Acknowledgements

We would like to thank M. Uesaka, T. Watanabe, T. Ueda, and K. Yoshii for their collaboration during the experiments at UTNL.

References

- 1) H. Kotaki, et al. : Proc. of SPIE, **3935**, p.149, 2000
- 2) T. Tajima and J. M. Dawson : Phys. Rev. Lett., **43**, p.267, 1979
- 3) X. J. Wang, et al., NIM A **375**, p.82, 1996
- 4) M. Kando, et al., Proc. of the 24th Linear Accelerator Meeting in Japan, pp. 128-130, 1999
- 5) M. Kando et al., in this report.
- 6) T. Ueda et al., Proc. of the 24th Linear Accelerator Meeting in Japan, pp. 139-141, 1999
- 7) H. Kotaki et al., Proc. of the 25th Linear Accelerator Meeting in Japan, pp. 147-149, 1999

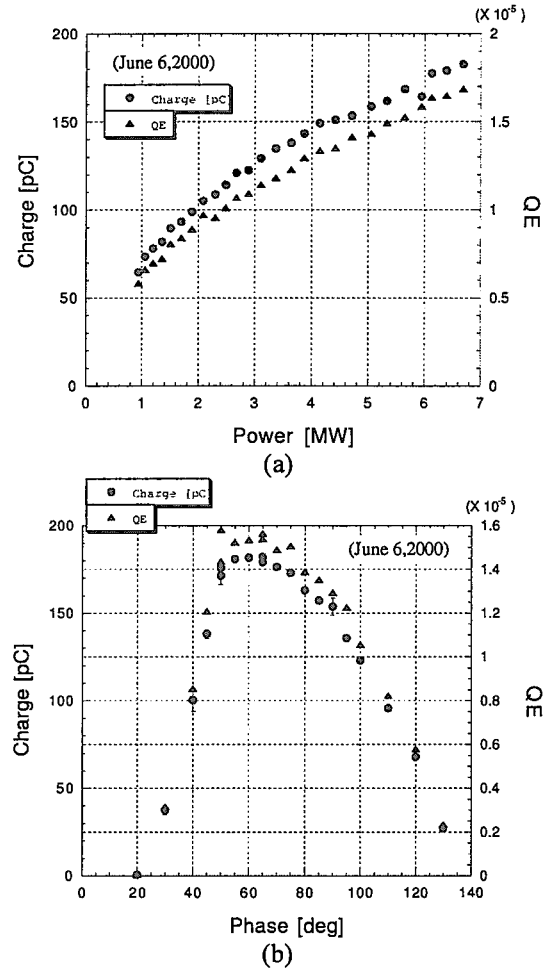


Fig. 2 Schottky effect on the surface of the photocathode (a) the rf dependence, (b) the phase dependence

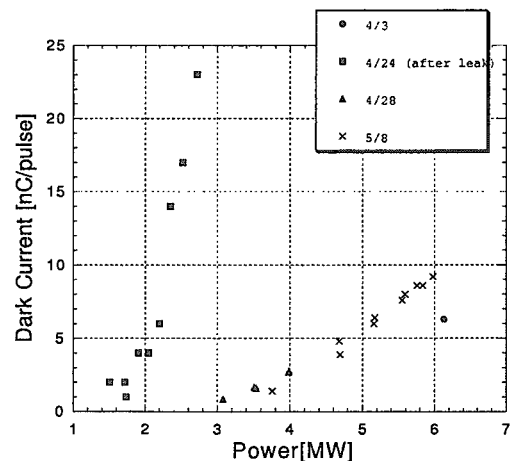


Fig. 3 The dark current vs. RF power

4.5.4 Optical guiding of terrawatt laser pulses by fast Z-pinch

Tomonao HOSOKAI, Masaki KANDO, Hideki DEWA*, Hideyuki KOTAKI, Shuji KONDO,
Kazuhiko HORIOKA^{a)}, Kazuhisa NAKAJIMA^{b)}

a) Department of Energy Sciences, Tokyo Institute of Technology

b) JAERI Kansai and High Energy Accelerator Research Organization (KEK)

1. Introduction

First-generation experiments of laser wakefield acceleration (LWFA) have successfully shown that the laser-plasma interaction can produce ultra-high accelerating gradients higher than 10 GeV/m and relativistic electron acceleration up to more than 100 MeV.¹⁾²⁾ The second-generation experiments should be aimed at a high-energy gain of more than 1 GeV. However several effects limit the energy gain in LWFA. The most critical limitation in increasing acceleration energy is diffraction effect of the laser pulses.³⁾ The diffraction of the laser pulses limits the laser-plasma interaction length to the extent of the vacuum diffraction length. Therefore it is essential to extend interaction length of a laser pulse with a plasma to increase the energy gain in the acceleration. In order to overcome the limit of the acceleration length restricted by diffraction, optical guiding channel has been proposed as a promising way of propagating a high-intensity laser pulses over many Rayleigh lengths in plasma. It is predicted that the electron acceleration of GeV energies by laser wakefield will be achieved using cm-scale optical guiding in plasma. For the optical guiding of laser pulses, the electron density profile in the channel must be symmetric in the radial direction and have a minimum on the axis, causing the wavefront to curve inward and the laser beam to converge.

We have presented a new method of optical guiding of high intensity laser pulses using the implosion phase of fast Z-pinch and experimentally demonstrated the guiding over 2 cm.⁴⁾ A high current fast Z-pinch discharge generates strong azimuthal magnetic field, which contracts the plasma radially inward down to $\sim 100 \mu\text{m}$ in diameter. The imploding current sheet drives the converging shock wave ahead of it, producing a concave electron density profile in the radial direction just before the stagnation phase. The concave profile is approximately parabolic to out a radius of $\sim 50 \mu\text{m}$, beyond which the density falls off. The concave profile in the core of the plasma column plays an important role of the optical guiding channel.

2. Experiment

The typical experimental setup is shown in Fig. 1. We used a capillary with an inner diameter of 1 mm and a length of up to 2 cm. With this configuration, the discharge current generated a peak of 4.8 kA with a rise time of about 15 ns and a duration of 70 ns (FWMH). The capillary was filled with helium, under differential pumping at an initial pressure which was varied from 0.5 to 5 Torr. A DC discharge circuit was used to form an uniformly preionized helium gas. A high intensity Ti:Sapphire laser pulse (2.2 TW, $\lambda = 790 \text{ nm}$, 90 fs, $1 \times 10^{17} \text{ W/cm}^2$) was focused on the front edge of the capillary to a spot size of $40 \mu\text{m}$ in diameter. The transmitted laser beam profile at the exit of the capillary was observed through a band pass filter ($\Delta\lambda = 10 \text{ nm}$) with a CCD camera.

3. Results

Figure 2 shows typical CCD images of the transmitted high intensity Ti:sapphire laser pulse profile through the capillary discharge plasma. These show clearly that a high intensity laser pulse

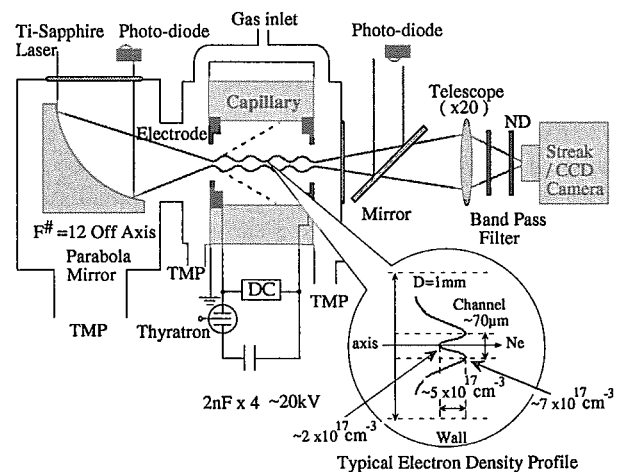


Fig. 1 Experimental setup of fast Z-pinch discharge for optical guiding

A typical electron-density profile of the implosion phase of the discharge in the radial direction is illustrated in the inset.

* Present address: Japan Synchrotron Radiation Research Institute (JASRI)

could be guided through the channel over a distance of 2 cm corresponding to $12.5 Z_{R0}$, where $Z_{R0} = 1.6$ mm is the Rayleigh length of the laser beam. The laser energy transmission through the capillary without discharge was 30% ; however, it increased to 64% through the channel. The electron density profile in the channel was estimated by corroborating the experimental results with the results of a 1D-MHD simulation. The electron density in the fully ionized channel was estimated to be $2.0 \times 10^{17} \text{ cm}^{-3}$ on the axis and $7.0 \times 10^{17} \text{ cm}^{-3}$ on the peaks of the channel edge with a diameter of $70 \mu\text{m}$. We assumed that the incident laser had a radial Gaussian profile, the channel was uniform over the channel length and the channel radius r_{ch} was $35 \mu\text{m}$ according to the observed value. Under these assumptions, the matched beam radius r_m was given by $r_m = [r_{ch}^2/\pi r_e \Delta n]^{1/4}$, where Δn was the channel depth and $r_e = e^2/m_{ec}^2$ was the classical electron radius.⁵⁾ With $r_{ch} = 35 \mu\text{m}$ and $\Delta n \sim 5.0 \times 10^{17} \text{ cm}^{-3}$, the matched beam radius is $r_m = 23 \mu\text{m}$. The observed spot radius of $20 \mu\text{m}$ was consistent with this value.

4. Next step of the study

At present we have demonstrated the feasibility of optical guiding of high intensity laser pulses by fast Z-pinch. The guiding channel with an optimum depth, width and shape could be obtained using properly controlled implosion plasma in wide density range. In our experiment, the channel was operated in the density range of $10^{16} - 10^{18} \text{ cm}^{-3}$ with an implosion velocity in the order of 10^7 cm/s . Faster implosion schemes can drive more intense shock waves, so that it will be able to produce higher densities with a larger density gradient channel as long as it has sufficient margin of stability.

As a next step of the study, we started the development of new Z-pinch devices to extend obtained techniques to higher density and longer optical guiding channel formation. Figure 3 shows a photograph of a cutaway view of the fast Z-pinch plasma waveguide generator which is under construction. It consists of a marx generator and a water capacitor, which is designed to drive the discharge current of several tens ampere within several nano seconds. We expect that the new Z-pinch device can produce optical guiding plasma channel with density of more than 10^{19} cm^{-3} and length of over 10 cm.

Rererences

- 1) H.Dewa *et al.* : Nucl. Instr. and Meth. **410(357)**, 1998
- 2) M.Kando *et al.* : Jpn.J.Appl.Phys.**38(967)**, 1999
- 3) K.Nakajima *et al.* : Phys Plasmas. **3(2169)**, 1996
- 4) T.Hosokai *et al.* : Opt.Lett. **25(10)**, 2000
- 5) P. Sprangle, E. Esarey, J. Krall, and G. Joyce : Phys. Rev. Lett. **69(2200)**, 1992

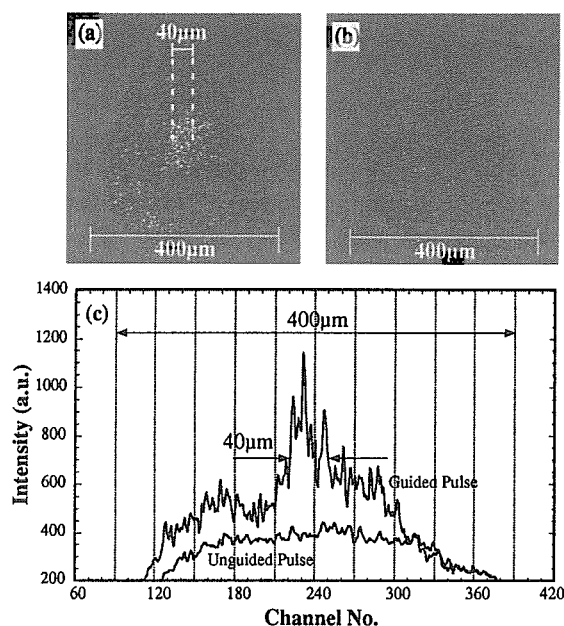


Fig. 2 Typical CCD images of the transmitted high intensity Ti:sapphire laser pulse through the capillary at an initial pressure of 0.9 Torr of He: (a) $t = 8.5 \text{ ns}$, (b) no discharge, (c) intensity profiles in the radial direction

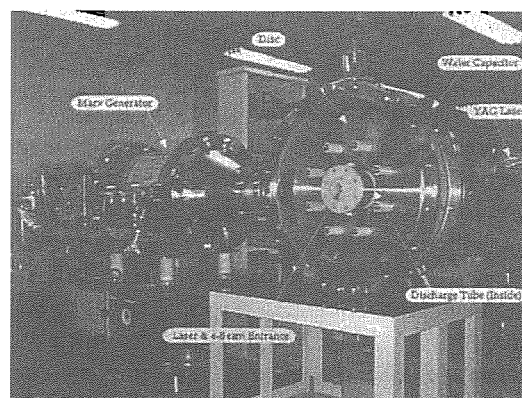


Fig. 3 Photograph of a cutaway view of the fast Z-pinch plasma waveguide generator which is under construction

4.6 Advanced photon simulation research

The simulation group for advanced photon science*
(by Mitsuru YAMAGIWA)

*Toshiki TAJIMA^{a)}, Hitoshi IHARA, Mitsuru YAMAGIWA, Akira SASAKI, James KOGA, Kengo MORIBAYASHI, Yutaka UESHIMA, Ichirou FUKUMOTO, Alexei ZHIDKOV, Levan N. TSINTSADZE, Junzo CHIHARA, Takayuki UTSUMI, Takuya ARAKAWA, Keisuke NAKAGAWA, Toshizo SHIRAI, Yasuaki KISHIMOTO, Kentaro SUZUYA, Hiroo TOTSUJI^{b)}

a) Univ. Texas and Lawrence Livermore National Laboratory

b) Okayama University

Computational science is a science that involves analysis, construction of new theories, or the discovery or clarification of phenomena. Typically this type of analysis is carried out on research objects which are difficult to do experimentally and/or observe, and problems which are theoretically difficult to analyze, by combining and building up many known principles. In recent years, due to the rapid development of supercomputers more complex models closer to reality have become treatable.

The missions of the simulation group for advanced photon science are: (i) to theoretically and computationally study the laser-matter interaction processes, particularly those relevant to laser acceleration and X-ray lasers, two of the main topics of the Advanced Photon Research Center; (ii) to promote the research techniques and tools to carry out the above investigations, particularly the simulation techniques in a state-of-the-art parallel computer environment; (iii) to predict and proact on research opportunities of high field science by exploring frontier topics. Some of us work on material properties of dense plasma/atoms generated from the laser irradiation on a solid. Some of us work on accelerator physics problems of laser driven accelerators. Some of us work on novel methods of laser cooling of atoms and molecules. Some of us work on X-ray laser processes resulting from the laser irradiation of matter. Some of us work on ultrabright X-ray sources based on the ultrafast laser irradiation. Some of us build state-of-the-art computer simulation codes in novel algorithms and novel software paradigms. Some of us invent new ways to apply intense and ultrafast lasers to carry out new avenues of energy research. Some of us venture into the frontier of atomic physics and plasma physics in their unprecedented physical parameters. Throughout these investigations novel pieces of information on laser-matter (atom and plasma) interactions have been added to our knowledge.

We have proceeded with the development of basic codes for laser acceleration as well as X-ray laser simulation. From numerical simulations utilizing these codes, we have made contributions to advanced photon experimental research such as experimental equipment design and preliminary experimental data analysis. Furthermore, as a part of High Field Science Research, we have developed a two-dimensional “giga” particle simulation code, which can treat one billion particles. Using the massively parallel Paragon computer (Paragon XP/S 75MP834), we have implemented a simulation with a performance above 30% of the catalog specifications. As a result of this, we have accomplished results exceeding expectations such as guiding experimental research and quantitatively evaluating physical phenomena occurring in the interaction of high intensity lasers with various materials such as the generation of high-energy photons and electrons, ion acceleration, and plasma X-ray sources.

In addition, we have introduced and maintained the basic atomic process code HULLAC as well as the detailed code Grasp92 which are invaluable for Advanced Photon Research. We have preformed theoretical calculations of the energy level, transition probability, collisional cross-sections for multi-charged ions, and have investigated the code’s characteristics and applications.

In the following, we report some recent research activities of our group.

4.6.1 Development of hydrodynamic code for the simulation of the laser-matter interaction

Takayuki UTSUMI

1. Introduction

In the development of the X-ray laser and incoherent X-ray sources, it is essential to improve our understanding of complicated physical processes in high temperature high-density plasmas from both the point of views of experiments and simulation. In transient collisional X-ray lasers using the prepulse technique, which is one X-ray laser scheme, the condition of the laser plasma produced by irradiation of a solid target by the first laser pulse must be thoroughly investigated. When the first laser pulse strikes a solid target, the target melts and evaporates. Resultingly, hot and dense plasmas in an extreme state of high-energy concentration are produced. These complicated processes can be investigated hydrodynamically assuming the system is composed of continuum media or multi-phase/multi-component fluids. In order to simulate these phenomena, it is necessary that the sharp interface discontinuity in the density and pressure must be traced accurately in the solid, liquid and gas phases, i.e. compressible and incompressible fluids must be treated simultaneously.

2. Numerical methods

Recently, Cubic Interpolated Propagation (CIP) and CIP-Combined Unified Procedure (C-CUP) were introduced by Yabe *et al.*¹⁾. These schemes are a low diffusion and stable algorithm for solving general hyperbolic equations, and have been successfully applied to many complex flow problems. They serve to be very useful tools for solving hydrodynamic phenomena including the solid, liquid and gas phases. We have extended these methods and developed a hydrodynamic code²⁾ to apply to the simulation of the laser-matter interaction. In the code, the energy equation is converted to the Poisson equation adopting the same technique as that for the equation of a one-component ideal gas, and numerically solved with the Modified Incomplete Cholesky Decomposition Conjugate Gradient (MICCG) method. The equation of radiation transfer is also written in the finite-difference form, and solved with the Successive Over-Relaxation (SOR) method.

3. Results

We carried out a numerical simulation with the condition of a laser pulse incident on a solid slab Aluminum target at normal incidence. The results are shown in the following Fig. 1. The size of the analysis system is $1.6 \mu\text{m} \times 2.4 \mu\text{m}$, and number of meshes is 80×120 . The 10^{12} W/cm^2 laser pulse is irradiated downward from the upper center onto the Al target and the exposure time is 20 psec with a rectangle time profile. We assumed the targets are surrounded with transparent ideal air, and the initial pressure and temperature of the system are 0.01 MPa (0.1 atm) and 300 K, respectively. The computational time step is 25 fsec. The formation and propagation of laser-produced plasmas are obtained with good numerical stability.

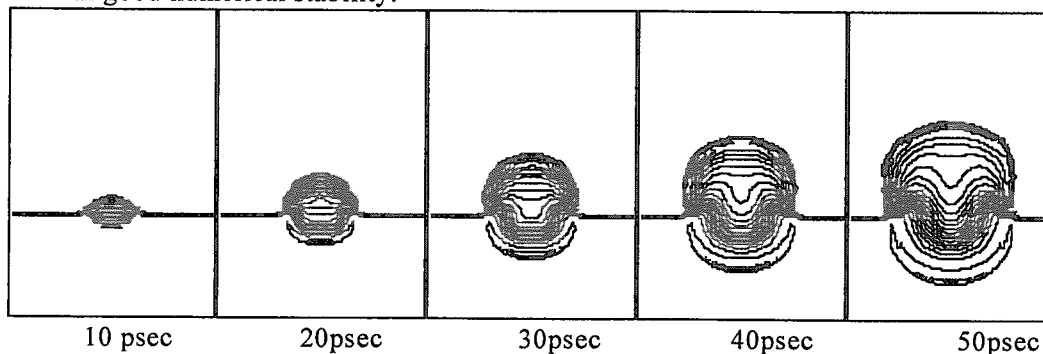


Fig. 1 Temporal changes of density distribution in the case of Al slab target irradiation
The unit is $\log_{10}(\text{kg/m}^3)$ and the interval of contour is 0.1.

References

- 1) T. Yabe, T. Aoki, *Comput. Phys. Commun.* **66**, p. 219, 1999
- 2) T. Utsumi, A. Sasaki, T. Kunugi, S. Fujii, M. Akamatsu, *CFD Journal* **8**, p. 128, 1999

4.6.2 Plasma simulation with the differential algebraic cubic interpolated propagation scheme

Takayuki UTSUMI

1. Introduction

In the analysis of nonlinear oscillations and instabilities of plasmas, numerical calculation plays an important role. Many numerical techniques have been proposed in recent years such as particle simulation, Fourier-Hermite transform, Fourier-Fourier transform, finite element, and splitting methods. For the elucidation of nonlinear plasma phenomenon in super strong electromagnetic fields generated by ultra high peak and ultra short pulse lasers, the development of high-precision and efficient numerical techniques have been continually desired.

2. Method of calculations

A computer code based on the Differential Algebraic Cubic Interpolated Propagation scheme has been developed for the numerical solution of the Boltzmann equation for a one-dimensional plasma with immobile ions. The scheme advects the distribution function and its first derivatives in the phase space for one time step by using a numerical integration method for ordinary differential equations, and reconstructs the profile in phase space by using a cubic polynomial within a grid cell. The method gives stable and accurate results, and is efficient. It is successfully applied to a number of equations; the Vlasov equation, the Boltzmann equation with the Fokker-Planck or the Bhatnagar-Gross-Krook (BGK) collision term and the relativistic Vlasov equation. The method can be generalized in a straightforward way to treat cases such as problems with nonperiodic boundary conditions and higher dimensional problems.

3. Results

Typical numerical results for the collisionless plasma simulation are described to demonstrate the accuracy and efficiency of the DA-CIP scheme. The physics of the collisionless plasma is described by the Vlasov-Poisson equation without the collision term and the results are shown elsewhere¹⁾ for well-understood problems; the recurrence effect for a free streaming distribution, linear Landau damping, strong nonlinear Landau damping, the two-stream instability, and the bump-on-tail instability.

Here we only show the case for the evolution of a two-stream plasma to Bernstein-Greene-Kruskal (BGK) equilibria. Figure 1 shows that at first the two-hole structure appears at time=60, then two holes start to coalescence due to the perturbation term, and finally one-hole BGK structure appears and persists from $t = 240$.

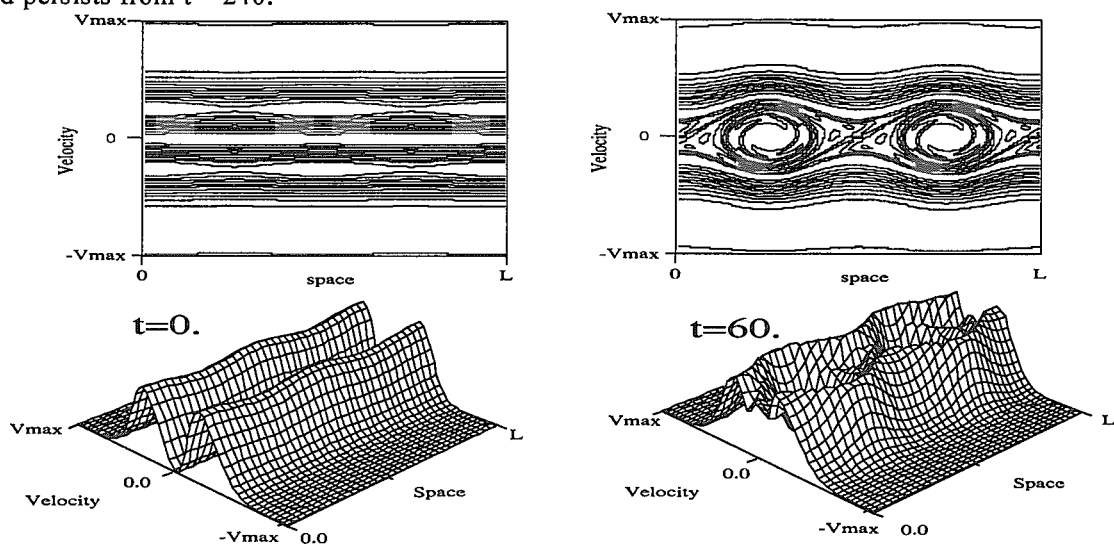


Fig. 1 The contour and over-view of the distribution function showing the appearance of two-hole structure

Reference

- 1) T. Utsumi, T. Kunugi, J. Koga, *Comput. Phys. Commun.* **108**, p. 159, 1998

4.6.3 Molecular dynamics simulation on laser ablation due to ultra-short pulse laser irradiation

Ichirou FUKUMOTO, Etsuji OHMURA^{a)}

a) Osaka University

1. Introduction

Laser materials processing has been used industrially in various fields such as drilling, cutting, and welding. It is known that ultra-fine particles or plasma are produced in the vaporizing process due to laser irradiation¹⁾. In order to clarify microscopically fusing and vaporizing phenomena of a material with laser irradiation, the material must be regarded as an aggregate of atoms or molecules, not as a continuum. In this study, laser materials processing of metals is simulated by the molecular dynamics method. Vaporization processes and temperature distributions are analyzed.

2. Simulation methods

Monocrystalline Aluminum, which can be applied with a pair potential between two atoms, is chosen as the subject of simulation. The (1 1 1) plane in the cubic lattice is analyzed. 1.6×10^4 atoms are arranged in 400 atoms per layer in the direction of the surface and there are 400 layers in the direction of depth. In this simulation, we use the modified molecular dynamics method which corrects thermal conductivity caused by free electrons²⁾.

3. Results

When aluminum is irradiated during 10 ps with a laser of 5 GW/cm^2 , examples of ablation process are shown in Fig. 1. In Fig. 1(a), the regions from the surface to depths of about 15 nm fused. In Fig. 1(b), the vicinity of the surface of Al bounds out forming into relatively large lumps.

Figure 2 shows the temperature distribution of Fig. 1. The temperature of the regions from surface to depths of about 15 nm is higher than the melting point in Fig. 2(a). But, vaporization does not occur yet. Figure 2(b) shows that the area, which has a higher temperature than the melt point, is deeper than the actual melting area. However, the boiling point of the simulation and reality are well in agreement.

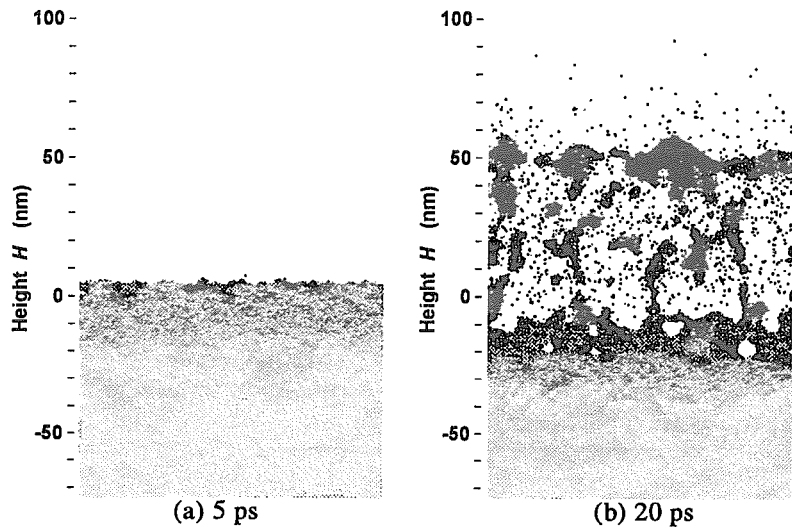


Fig. 1 Ablation process of Al

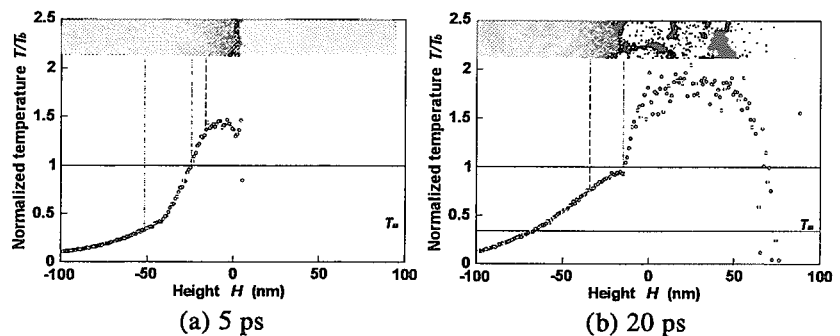


Fig. 2 Temperature distribution in Fig. 1

References

- 1) H. van Brug, K. Murakami, F. Bijkerk, M. J. van der Wiel, J. Appl. Phys. **60**, p. 3438, 1986
- 2) E. Ohmura, I. Fukumoto, Int. J. Japan Society for Precision Engineering **31**, p. 206, 1997

4.6.4 Laser acceleration and laser propagation

James KOGA, Susumu KATO^{a)}, Levan N. TSINTSADZE, Yasuaki KISHIMOTO

a) Electrotechnical Laboratory

1. Introduction

In recent years with the development of high intensity short pulse lasers through the use of Chirped Pulse Amplification (CPA) laser wakefield acceleration of charged particles has become realizable. In order to achieve this the propagation characteristics of an intense laser pulse propagating in plasmas and gases need to be determined. The propagation characteristics determine not only the distance and strength of the wakefield occurring behind the laser pulse, but also determine the quality of the wakefield.

2. Self-focusing of an intense laser pulse

In experiments where a high intensity short pulse laser propagates for long distances in a neutral gas the modulation of the pulse by the gas can become significant. In order to study these effects a simulation model including nonlinear polarization of a background neutral gas on the propagation of intense short pulse lasers is developed. Since the time duration of short laser pulses is becoming comparable to the response time of the gases, the model includes the finite response time of the gas by using a soft-core Coulombic potential for the bound electrons. A test problem for self-focusing of an intense laser pulse in a gas with a finite-response-time nonlinear polarization included is shown¹⁾. Figure 1 shows contours of the electric field of a laser pulse after it has propagated past the self-focus point which can be seen on the left side of the figure. After the focus point, the part of the pulse which propagates behind is disrupted. This may be attributed to the high density of the gas and the resulting strong polarization current which exists there. This focus point produces a large current which is large enough to produce an emitting radiation signal. It can be seen that the center of the laser pulse is chaotic. Only the very front of the pulse maintains the original laser wave structure. Trailing behind the very front of the pulse there is a thin neck. This structure has been predicted theoretically and observed experimentally. It has been found to exist over long propagation distances.

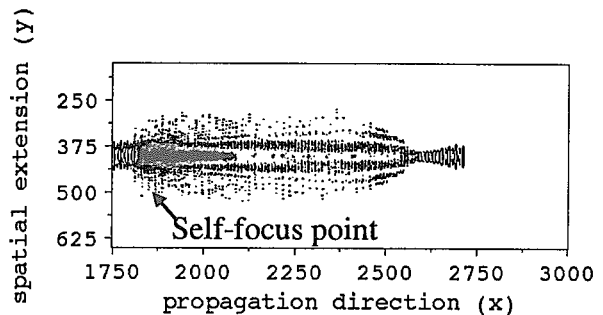


Fig. 1 Electric field of a laser pulse after propagating past the self-focus point

3. Wakefield excitation by an ionization front

In addition to the neutral gas effects on the laser pulse, ionization of the gas by the pulse can significantly alter the laser pulse. A one-dimensional particle-in-cell (PIC) simulation code including the effect of optical field ionization has shown that the ionizing plasma induces significant modulation. Even in the regime where the matching condition between laser pulse length and plasma wavelength is not satisfied, strong wake fields are excited and amplified due to the modulation of an intense laser pulse²⁾. The modulation is characterized by a gradual steepening of the pulse front where there is a copropagating density gradient, which is due to the rapid plasma formation from ionization there. Accordingly, the wake field is convectively amplified to a significant level. This amplification of plasma waves always occurs, more or less, for laser propagation in ionizing plasmas.

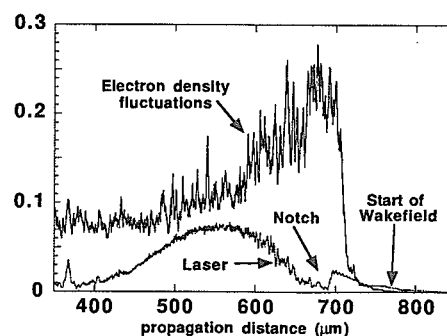


Fig. 2 PIC simulation result showing start of wakefield at the front of the laser pulse

In recent experiments involving high intensity short pulse lasers propagating in ionizing gases, large

wakefields have been observed to occur even when the pulse is much longer than the length necessary to generate wakefields. It was observed in the experiments that the plasma wave starts near the position of the ionization front. The whole process of wake amplification from optical field ionization to Raman scattering is investigated by using this PIC simulation code. It is found that a large wakefield with wavelength comparable to the plasma wavelength is generated at the position of the ionization front. Figure 2 shows that the modification of the pulse front acts as both a plasma wave starting near the position of the ionization front and a noise source for forward Raman scattering which generates the wake field³.

4. Self-organized critical model for laser pulse propagation

Recent experiments of short pulse lasers propagating in air have shown that these laser pulses can propagate and generate plasma over very long distances. Here we present a model of this propagation using a modified version of the self-organized criticality (SOC) model developed for sandpiles by Bak, Tang, and Weisenfeld⁴. The model includes the formation of plasma by ionization which acts as a diffusion term and self-focusing by the nonlinear index of refraction of the gas which is similar to gravitational attraction. Results of this simple model in Figure 3 show that an initial gaussian pulse filaments and spreads. The time variation of the number of ionizations induced by the pulse under conditions of strong focusing shows SOC behavior.

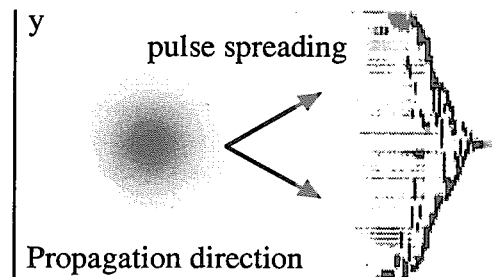


Fig. 3 Initial gaussian pulse (left) and filamented pulse after propagating some distance (right)

5. Low frequency electromagnetic wave generation

As the intensity of the short laser pulse increases relativistic effects take on great importance. In order to describe the propagation of a relativistically intense short laser pulse in an isotropic plasma new analytical methods are developed. Under the condition that the relativistically intense laser pulse have a wide spectrum, a new mechanism for the emission of low-frequency electromagnetic waves, including the generation of a quasistatic magnetic field is found. The emission is due to a modulational and filamentational instabilities of the photon gas in a plasma. The generation of the magnetic field is associated with a significant change in the laser pulse shape during the propagation. This process is identified in our 2D PIC simulations with a high intensity laser pulse⁵ (see Fig. 4).

A kinetic equation for the spectral function of the electromagnetic waves is derived for an arbitrary amplitude pump wave, where the fully relativistic case is considered. The resulting kinetic equation of the spectral function is used along with the set of equations of the plasma to derive a general dispersion relation, where relativistic effects play an important role. In the case of a superstrong short laser pulse, Langmuir waves, with phase velocities larger than the speed of light, and waves of ion-sound type, which are damped only on ions, are found. In addition, for the case when the plasma density along with the mass of the electrons satisfies the “frozen-in” condition, stationary nonlinear new types of ion-sound waves are found⁶.

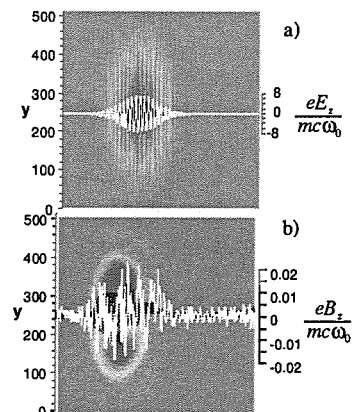


Fig. 4 Plots of laser field (a) and magnetic field (b)

References

- 1) J. Koga, Optics Letters 24, p. 408, 1999
- 2) S. Kato, Y. Kishimoto, J. Koga, Physics of Plasmas 5, p. 292, 1998
- 3) J. Koga, S. Kato, Y. Kishimoto, S.P. LeBlanc, M.C. Downer, Nucl. Instr. Meth. Phys. Res. A 410, p. 499, 1998
- 4) J. Koga, IPSJ Symposium Series 2000, p. 109, 2000
- 5) L. N. Tsintsadze, T. Tajima, K. Nishikawa, J.K. Koga, K. Nakagawa, Y. Kishimoto, Physica Scripta T84, p. 94, 2000
- 6) L.N. Tsintsadze, K. Nishikawa, T. Tajima, J.T. Mendonca, Physical Review E 60, p. 7435, 1999

4.6.5 Calculation of the high gain of the transient collisional X-ray laser using a thin foil target

Akira SASAKI, Takayuki UTSUMI, Kengo MORIBAYASHI

1. Introduction

We have developed a system of simulation codes which can guide the experimental investigation of the transient collisional excited (TCE) X-ray lasers. The soft X-ray gain is calculated by a collisional radiative model based on the atomic data calculated by the HULLAC code¹⁾, using the temporal evolution of the temperature and density of the short pulse laser produced plasma calculated by a 1D hydrodynamics code²⁾. The calculated result shows that the system can be applicable to a short wavelength soft X-ray laser below 130 Å by using a thin foil target pumped by short (ps) intense laser pulses.

2. Calculation

Figure 1 shows the electron temperature and density, and soft X-ray gain coefficient of the 4d-4p transition of Ni-like Silver. The calculation is carried out for a solid target irradiated by a weak prepulse (4×10^{12} W/cm²) and main pulse (8×10^{13} W/cm²) laser, separated by 3 ns. It is found that the underdense region of the low temperature preplasma, where the ion density is approximately 10^{19} cm⁻³, is heated up to 1 keV to ionize and excite the plasma to produce soft X-ray gain. The gain at the plateau region (≈ 30 cm⁻¹), and its location are found to agree qualitatively with the experiment³⁾.

3. Discussion

We expected that a new scheme which uses a thin foil target irradiated by two ps laser pulses has advantages over the conventional method, because the plasma temperature can become higher without the loss of energy through the heat conduction into the solid target⁴⁾. Higher temperature is essential for fast ionization and excitation. We found a peak gain of 600 cm⁻¹ in a silver plasma produced from a 0.1 μm thick foil irradiated by two, 10^{15} W/cm², 2 ps laser pulses (interval = 100 ps). Calculations will be carried out to maximize the gain as well as to minimize the plasma density gradient to reduce the refraction along with verification of the code through comparison with the spectroscopic measurements.

References

- 1) M. Klapisch, A. Bar-Shalom, J. Quant. Spectrosc. Radiat. Transf. **58**, p. 687, 1997
- 2) J.T. Larsen, S.M. Lane, J. Quant. Spectrosc. Radiat. Transf. **51**, p. 179, 1994
- 3) S. Sebban, H. Daido, N. Sakaya, Y. Kato, K. Murai, H. Tang, Y. Gu, G. Huang, S. Wang, A. Klisnick, Ph. Zeitoun, F. Koike, H. Takenaka, Phys. Rev. **A61**, p. 4381, 2000
- 4) A. Sasaki, T. Utsumi, K. Miribayashi, T. Tajima, H. Takuma, Rev. Laser. Eng. **27**, p. 185, 1999 (in Japanese)

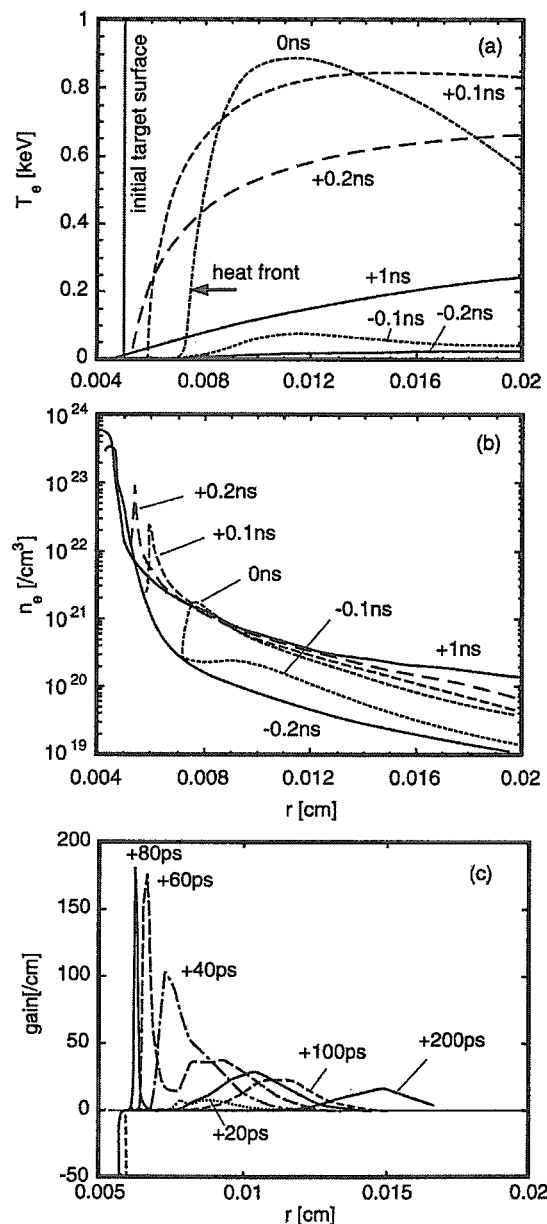


Fig. 1 Profile of the electron temperature (a) and electron density (b) calculated by 1D hydrodynamics code, and for gain (c) of a silver plasma irradiated by two 100ps laser pulses

0 ns corresponds to the peak of the main pulse.

4.6.6 Inner-shell ionization and hollow atom X-ray lasers

Kengo MORIBAYASHI, Akira SASAKI, Yutaka UESHIMA, Toshiki TAJIMA^{a)}

a) Lawrence Livermore National Laboratory

1. Introduction

Recent progress in intense pulsed lasers allows us a new source of high brightness X-rays. Larmor X-rays due to the acceleration of electrons in the laser-magnetic field¹⁾ are suitable for an X-ray pumping source because they have high brightness and short pulse. An X-ray pumped inner-shell ionization laser has been thought to be a useful method for the X-ray laser²⁻⁵⁾. Here we have been studying atomic processes in inner-shell ionization and hollow atom X-ray lasers for the purpose of searching for advantageous target materials and models. We have also suggested an experimental class of an inner-shell ionization X-ray laser.

2. Inner-shell ionization X-ray laser

We adopt vapor of Na, Mg or Al as a target material in order to avoid fast atomic processes except for the inner-shell ionization processes⁴⁾. Figure 1 shows an example of the detailed requirement for an experiment. As soon as the high intensity (10^{20} W/cm²) short-pulse laser irradiates a plasma with electron density of $n_e = 3 \times 10^{19}$ cm⁻³, high brightness X-rays (10^{13} W/cm²) are emitted¹⁾. By using these X-rays as a pumping source and Mg vapor with a density of 10^{17} cm⁻³ as a target, the inner-shell ionization X-ray laser with the gain of 10 cm⁻¹ may be realized.

3. Hollow atom X-ray laser

For a high brightness X-ray source, which makes inner-shell ionization processes much faster than any other atomic processes, the successive inner-shell photoionization of an inner-shell ionized ion takes place until all electrons in the shell are removed to produce hollow atoms. Figure 2 illustrates atomic processes in a hollow atom X-ray laser of Mg. A hollow atom X-ray laser has the clear advantages of shorter wavelength and longer duration time over the conventional inner-shell ionization X-ray laser³⁾. For a Mg vapor target with a density of 10^{17} cm⁻³, we estimate 10^{14} W/cm² for necessary intensities of the X-ray source.

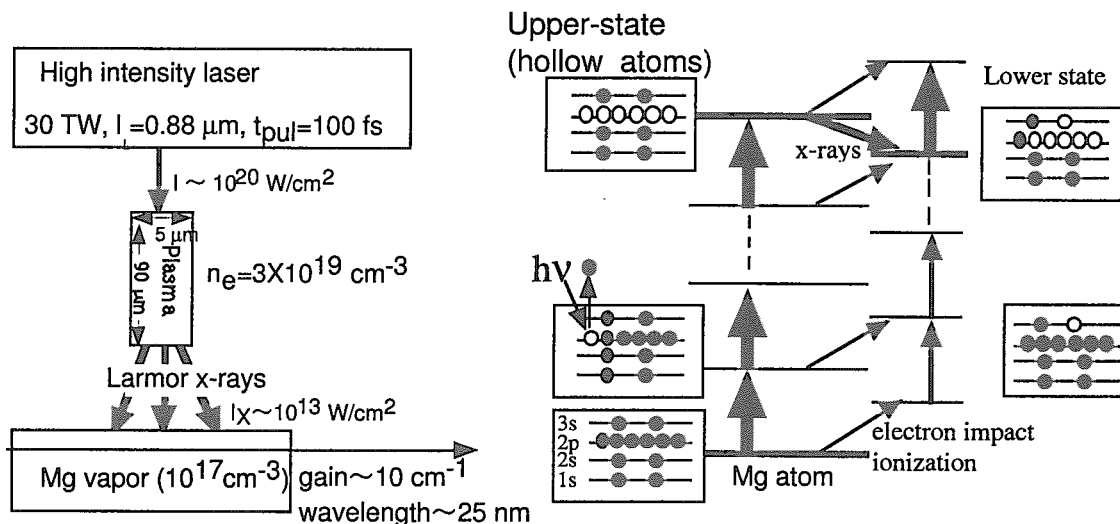


Fig. 1 An example of the detailed requirement for an experiment in the inner-shell ionization X-ray laser

Fig. 2 Atomic processes in a hollow atom x-ray laser of magnesium

References

- 1) Y. Ueshima, Y. Kishimoto, A. Sasaki, T. Tajima, *Laser and Particle Beam* **17**, p. 45, 1999
- 2) S.J. Moon, D.C. Eder, *Phys.Rev.A* **57**, p.1391, 1998
- 3) K. Moribayashi, A. Sasaki, T. Tajima, *Phys.Rev.A* **58**, p.2007, 1998
- 4) K. Moribayashi, A. Sasaki, T. Tajima, *Phys.Rev.A* **59**, p.2732, 1999
- 5) K. Moribayashi, A. Sasaki, Y. Ueshima, *SPIE* **3886**, p.634, 2000

4.6.8 Calculations of the wavelengths of Ni-like 4d to 4p X-ray laser lines

Takayuki UTSUMI

1. Introduction

Many of the Ni-like lasers are designed and carried out to lase on the $3d^9 4d-3d^9 4p$ transition in Ni-like ions of various elements (the ground state of Ni-I is $3d^{10}$), with wavelengths in the range of about 900 to 30 Å. The Ni-like 4p-4d lines lase by having strong collisional excitation from the ground state, which populates the upper metastable 4d levels, while the lower 4p levels are rapidly depopulated by radiative decay to the ground state. In the course of the development of x-ray lasers and their applications, precise values of the lasing wavelengths are required, particularly since, for collisionally pumped x-ray lasers, highly charged Ni-like ions, which have a complex atomic structure, are used as a lasing medium. Since the plasma parameter range for amplification is sensitive to the atomic data, it is important to understand the complex level structure through the comparison of experimental and calculated wavelengths.

2. Method of calculations

We use the GRASP92¹⁾ code to calculate energy levels. Here, we designate the upper 4d levels of Ni-like ions in the jj-coupling scheme, $3d_{3/2} 4d_{3/2} J=0$, $3d_{5/2} 4d_{5/2} J=1$, $3d_{5/2} 4d_{5/2} J=2$, as shown in Fig. 1.

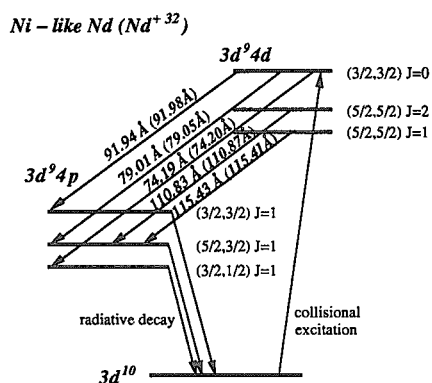


Fig. 1 Simplified level diagram and the designations for the Ni-like 4d to 4p x-ray lasing lines

The figure also illustrates the calculated wavelengths of Nd. The values in ref. 2) are shown in the parenthesis. Lasing is driven by strong collisional excitation from the $3p^6 3d^{10} \ ^1S_0$ ground state populating the upper 4d levels. The lower 4p levels rapidly decay back to the ground state.

3. Results

The present calculations give good agreement with recent measurements for Pd ($Z=46$), Ag ($Z=47$), Cd ($Z=48$), Sn ($Z=50$), and Xe ($Z=54$), which are calculated to be at 146.92, 139.12, 131.94, 119.48, 99.90 Å, while measured at 146.79 ± 0.15 , 138.92 ± 0.15 , 131.66 ± 0.15 , 119.3 ± 0.1 , and 100 Å. Furthermore, the transition B for Nd ($Z=60$) which was measured at 79.06 Å is in good agreement with our calculation to within 0.02 Å. For Yb, the lines A, B, D, and E were measured at 50.23, 56.11, 81.07, and 84.41 ± 0.02 Å, respectively. For Ta, these lines were 44.83, 50.97, 74.42, and 77.47 ± 0.02 Å, respectively. For W, the lines A, D, and E were measured at 43.19, 72.40, and 75.35 ± 0.01 Å, respectively. For Au, the line A was measured at 35.60 ± 0.02 Å.

Recent measurements³⁾ of the transition B for Nd, Sm, Gd, Dy, and Ho ($Z=60, 62, 64, 66, 67$) were at 79.2, 73.6, 68.6, 64.1, and 62.0 Å with a measurement error ± 0.2 Å, while calculated at 79.04, 73.54, 68.58, 64.05, 61.94 Å. In that experiment the transition A for Sm, Gd, Dy, Ho, Yb, Hf, and Ta ($Z=62, 64, 66, 67, 70, 72, 73$) were measured at 68.5, 63.3, 58.5, 56.3, 50.3, 46.5, and 44.6 Å, while calculated to be at 68.49, 63.30, 58.56, 56.34, 50.22, 46.53, 44.80 Å. Our calculations show close agreement with measurements within experimental uncertainties for these elements.

References

- 1) F.A. Parpia, C. F. Fischer, I.P. Grant, Comput. Phys. Commun. **94**, p. 249, 1996
- 2) J.H. Scofield, B.J. MacGowan, Phys. Sci. **46**, p. 361, 1992
- 3) H. Daido, S. Ninomiya, M. Takagi, Y. Kato, F. Koike, J. Opt. Soc. Am. B **16**, p. 296, 1999

4.6.9 Generation of high energy photons, electrons, and ions by short-pulse laser

Mitsuru YAMAGIWA, Yutaka UESHIMA, Alexei ZHIDKOV, James KOGA, Akira SASAKI, Levan N. TSINTSADZE, Takuya ARAKAWA, Keisuke NAKAGAWA, Yasuaki KISHIMOTO, Toshiki TAJIMA^{a)}

a) Lawrence Livermore National Laboratory

1. Generation of ultra-short pulse hard X-rays with an ultra-short pulse intense laser

A relativistically intense ultra-short pulse (around 10 femto seconds) laser can produce a large flux of X-rays through the interaction with electrons that are driven by its intense electromagnetic fields. In the case of high-Z matter irradiation by an intense laser, X-rays with a long tail are generated through complex processes, such as polarization and atomic processes, although two main fast processes, Larmor radiation and Bremsstrahlung, are among the most significant mechanisms for X-ray emission from short pulse laser irradiation of low-Z matter in the relativistic intensity regime. We have evaluated the power, energy spectrum, brilliance, polarization, and time structure of these ultra-short X-rays. We suggest a few methods that significantly enhance the power of Larmor X-rays. Because of the peakedness of the energy spectrum, Larmor X-rays have important applications, such as a light source of the hollow atom X-ray Laser and ultra-fast spectroscopy¹⁾.

2. Higher harmonics generation from a solid thin film irradiated by an intense laser

We have completed the massive parallelization of a 2-dimensional giga-particle code and have achieved a 530-fold acceleration rate with 512 processing elements (PE's). Using this we have implemented a simulation of the interaction of a solid thin film and a high intensity laser and have discovered a phenomenon in which high quality short pulses from the far ultraviolet to soft X-rays are generated at the back surface of the thin layer. When a laser is irradiated onto a solid thin film, the laser is reflected from the surface. However, in the case of an ultrahigh peak power laser, a part is transmitted through the thin film. Furthermore, in a subject of great interest, we have found that this transmitted light is composed of more fine intervals, and powerful short wavelength coherent light below 1/10 of the laser wavelength (far ultraviolet or soft X-rays) is emitted as shown in Fig. 1²⁾.

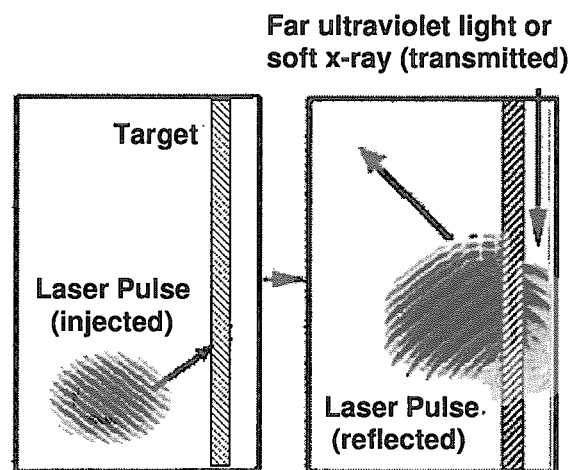


Fig. 1 Injected, reflected, and transmitted laser light in an ultrahigh peak power laser-solid thin film (hatched) interaction

3. Hot electron generation and ion acceleration

Ion acceleration and expansion in the interaction of a relativistically intense short-pulse laser with an underdense plasma layer has been investigated. Ion and electron dynamics have been studied by using a two-dimensional PIC simulation code with a real mass ratio. Figure 2 shows the time evolution of the electron density contour. Just after the laser injection, electrons are pushed in the propagation direction of the laser. The electron density rises at the front of the laser pulse. A local condensation or evacuation of electrons leads to a dip or cavity formation in the electron density. The cavity region continues to proceed together with the laser propagation. At the time of 90, which is normalized by the electron plasma frequency, electrons go across the original right boundary, when the laser has crossed the entire plasma layer (Fig. 2(d)). Thus, some of the electrons are completely swept up from the main plasma region. At the time of 150, electrons have moved further forward, as shown in Fig. 3(a). Electron acceleration continues until when the electrons are overtaken by the peak point of the laser intensity. Ion acceleration and expansion near the original plasma boundary are also clearly seen, as shown in Fig. 3(b) the ion energy spectrum ($E_{\max} < \sim 5$ MeV) and (c) the ion density contour, respectively. Figure 3(d) shows a contour of the ion

distribution in the x - P_x plane, where P_x is the ion momentum in the x -direction, indicating that ions are accelerated in the x direction near the original plasma boundary. In this way, it is after the laser completely passes through the plasma layer that the ion acceleration starts to be significant ³⁾.

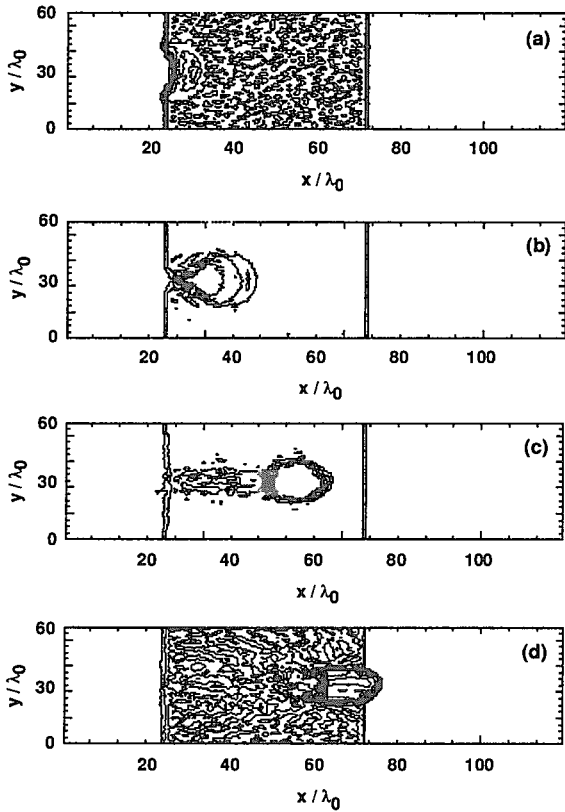


Fig. 2 Time evolution of the electron density contour
 λ_0 is the laser wavelength. $\omega_{p0}t = 20$ (a), 40(b), 70(c), and 90(d).

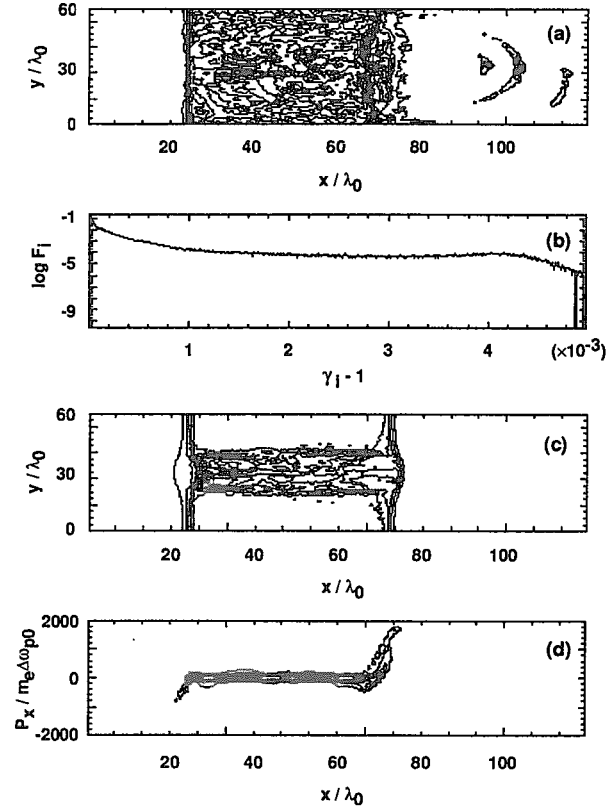


Fig. 3 (a) the electron density contour, (b) the ion energy spectrum, (c) the ion density contour, and (d) the contour of the ion distribution in the x - P_x plane for $\omega_{p0}t = 150$

A new method has also been proposed for producing ^{18}F , a positron emitter, via $^{18}\text{O}(p,n)^{18}\text{F}$ reactions with fast protons from the interaction of a relativistically-intense short-pulse laser with an underdense plasma layer. The instantaneous production rate of ^{18}F has been found to be two orders of magnitude larger than by the standard method using a cyclotron ⁴⁾.

From a full kinetic PIC simulation including elastic collisions and collisional and field ionization, we have found that emission of MeV multiple-charged ions from a non-low-Z matter foil irradiated by a short laser pulse sensitively depends on the ion charge distribution. In spite of strong elastic collisions, the anisotropy of the hot electron velocity distribution enhances the ion energy and improves the emittance. With up to 10% conversion of the laser energy, Al^{+6} - Al^{+7} ions over MeV energy are produced from a $0.125 \mu\text{m}$ foil with an obliquely incident (45°) p-polarized laser pulse of 1 ps duration in the range of intensity $10^{16-17} \text{ W/cm}^2$ ⁵⁾.

References

- 1) Y. Ueshima, Y. Kishimoto, A. Sasaki, T. Tajima, Laser and Particle Beam 17, p. 45, 1999
- 2) Y. Ueshima, T. Arakawa, Y. Kishimoto, A. Sasaki, T. Tajima, Inst. Phys. Conf. Ser., No. 159, p. 325, 1999
- 3) M. Yamagiwa, J. Koga, L.N. Tsintsadze, Y. Ueshima, Y. Kishimoto, Phys. Rev. E 60, p. 5987, 1999
- 4) M. Yamagiwa, J. Koga, J. Phys. D: Appl. Phys. 32, p. 2526, 1999
- 5) A. Zhidkov, A. Sasaki, T. Tajima, Phys. Rev. E 61, R2224, 2000

4.6.10 Short-laser-pulse driven emission of energetic ions into a solid target from a surface layer spalled by a laser prepulse

Alexei ZHIDKOV, L.V. ZHIGILEI^{a)}, Akira SASAKI, Toshiki TAJIMA^{b)}

a) University of Virginia, USA

b) Lawrence Livermore National Laboratory

1. Introduction

An efficient emission of energetic protons and carbon ions from a thin layer spalled from a solid by a laser prepulse is demonstrated numerically. We combine the molecular dynamics technique and multi-component collisional particle-in-cell method with plasma ionization to simulate the laser spallation and ejection of a thin (~20 - 30 nm) solid layer from an organic target and its further interaction with an intense femtosecond laser pulse. In spite of small thickness, a layer produced by laser spallation efficiently absorbs ultra-short laser pulses with the generation of hot electrons that convert their energy to ion energy. The efficiency of the conversion of the laser energy to ions can be as high as 20%, and 10% to MeV ions^{1,2)}. A transient electrostatic field created between the layer and surface of the target is up to 10 GV/cm.

2. Results

The results of the present computational study demonstrate the feasibility of the proposed method for an efficient generation of energetic ions near a target sample. We have showed that the direct irradiation of a bulk organic sample by a laser pre-pulse performed in the regime of stress confinement^{3,4)} can lead to the ejection of a layer of relatively intact material with thickness determined by the laser penetration depth and fluence. The further irradiation of the spalled layer by an obliquely incident *p*-polarized, second harmonics laser pulse leads to an efficient emission of carbon ions with energies over 1 MeV and protons with energy up to 1 MeV even at a modest intensity of 10^{17} W/cm². The distance between the spalled layer and the target is controlled by the delay between the first and the second pulses and can be optimized for the maximum intensity of the ion beam. A transient electrostatic field generated between the layer and the surface of the target can be up to 10 GV/cm and the efficiency of the conversion of the laser energy to the energy of the ions can be as high as 20% for all ions and 10% for ions with energy above 1 MeV.

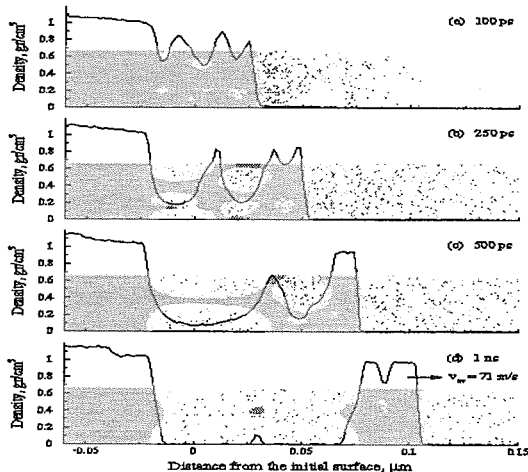


Fig. 1 Density profiles near the surface of an irradiated sample for a simulation with a 15 ps laser pulse and fluence of 34 J/m^2

Corresponding snapshots from the simulation are shown in the background of the density plots.

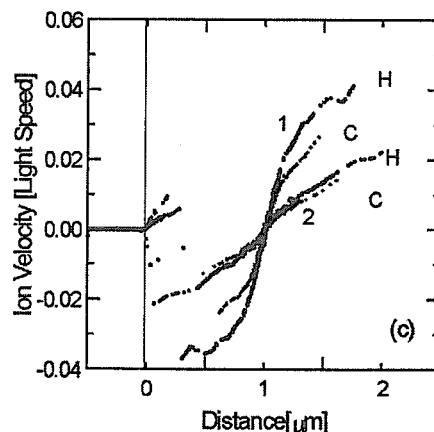


Fig. 2 Spatial distribution of the velocities of carbon ions and protons just after the end of the laser pulse

Data is given for $\lambda=400 \text{ nm}$ and intensities (1) $I=10^{17} \text{ W/cm}^2$ and (2) $I=10^{18} \text{ W/cm}^2$.

References

- 1) A. Zhidkov, A. Sasaki, T. Tajima, Rev. Sci. Instrument 71, p. 931, 2000
- 2) A. Zhidkov, S. Sasaki, T. Tajima, Phys. Rev. E 61, R2224, 2000
- 3) L. V. Zhigilei, B. J. Garrison, Appl. Phys. Lett. 74, p. 1341, 1999
- 4) L.V. Zhigilei, P. B. S. Kodali, B. J. Garrison, J. Phys. Chem. B 101, p. 2028, 1997

4.6.11 Energy distribution of particles accelerated during the interaction of intense femtosecond laser pulses with solids

T. AUGUSTE^{a)}, P. D'OLIVERA^{a)}, S. HULIN^{a)}, P. MONOT^{a)}, Alexei ZHIDKOV, Akira SASAKI, Toshiki TAJIMA^{c)}, Ya. FAENOV^{b)}, T.A. PIKUZ^{b)}, I.Yu. SKOBELEV^{b)}

a) Commissariat a l'Energie Atomique-Centre D'Etudes de Saclay, France

b) Multicharged Ions Spectra Data Center of VNIIFTRI, Russia

c) Lawrence Livermore National Laboratory

1. Introduction

The energy distribution of hot electrons produced by a very short, intense laser pulse ($I = 2/4 \times 10^{18} \text{ W/cm}^2$, 60 fs, $\lambda = 800 \text{ nm}$, obliquely incident p -polarized) has an energy cut-off. We observe the distribution of hot electrons near the energy cut-off via direct measurement and particle-in-cell simulation. The energy distribution of energetic multiple-charged ions of fluorine is studied via spectroscopy measurement of the blue wing of He_{ω} , He_{β} and Ly_{α} lines along with particle modeling. We find He - and H -like ions of fluorine with energy over 1 MeV produced via the optical field ionization dominated by the hot electron driven acceleration.

2. Experiments

The experiments were performed with the UHI10 laser which was designed to generate 10-TW ultrashort pulses (60-fs) at 10-Hz. The pulse energy is about 1.8 J after four stages of amplification. Spatially resolved x-ray spectra of fluorine in the 13.7 - 17.2 Å spectral range were obtained using the Focusing Spectrometer with Spatial Resolution (FSSR-2D). Two large aperture (15 x 50 mm) spherically bent mica (2d in the first order of reflection is about 19.91 Å) crystals with a 150 mm radius of curvature were placed in different experiments at distance 250 - 290 mm from the plasma. They covered Bragg angles that allowed reception of spectra of He -like ions of $F VIII$ and Ly_{α} of H -like FLX . The electron spectrometer (Fig. 1) is composed of two parallel rectangular magnetic deflectors shielded by an iron box. Electrons entering through a 1 mm aperture follow a hemispheric trajectory before being detected by a 40-mm diameter MCP chevron assembly coupled to a phosphor screen. The rear side is imaged then by a CCD camera via a 45° incidence mirror. The 0.18 Tesla magnetic field allows recording of electron spectra from 100 keV to 2.2 MeV in a single shot. The solid target to spectrometer distance is 1 m. This spectrometer was tested on the LSI* Van de Graaff source from 600 keV to 2.2 MeV. The energy distribution bandwidth of the source remains below 15 keV in this range. The dispersion is found to correspond to the one predicted within the spectrometer accuracy. The MCP response is found to be flat in this range.

3. Results

We have demonstrated, via direct spectroscopic measurement and PIC simulation, ion acceleration over MeV energies by an intense femtosecond p -polarized pulse laser. We have found that the ion acceleration is dominated by hot electrons, which have a transient energy distribution, see Fig. 2. This distribution cannot be characterized by only temperature, especially in the MeV region. The method used for hot electron measurement along with the PIC calculation is useful for study of the transient process of hot electron relaxation in plasmas irradiated by very short laser pulses and consequent emission of energetic ions.

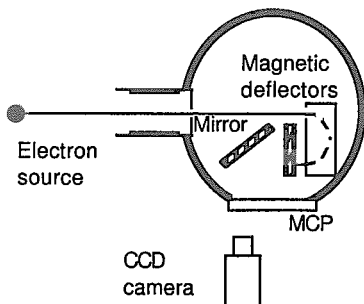


Fig. 1 The set-up for the magnetic deflectors measurements

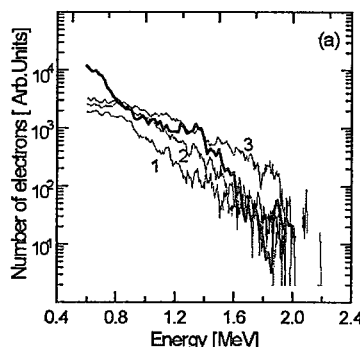


Fig. 2 The hot electron distribution in MeV region; thin lines – experimental, (1) $I = 1.3 \times 10^{18}$, (2) 2.6×10^{18} , (3) $4 \times 10^{18} \text{ W/cm}^2$; the thick line – the calculated, $I = 4 \times 10^{18} \text{ W/cm}^2$

4.6.12 Effect of amplified spontaneous emission on the interaction of intense femtosecond laser pulses with high-Z solids

Alexei ZHIDKOV, Akira SASAKI, Takayuki UTSUMI, Ichirou FUKUMOTO, Toshiki TAJIMA^{a)},
F. SAITO^{b)}, Y. HIRONAKA^{b)}, K. G. NAKAMURA^{b)}, K. KONDO^{b)}, M. YOSHIDA^{c)}

a) Lawrence Livermore National Laboratory

b) Tokyo Institute of Technology

c) National Institute of Material and Chemical Research

1. Introduction

$K\alpha$ emission of high-Z solid targets irradiated by an intense, short (<100 fs) laser pulse in the 10 keV region is shown to be sensitive to the electron energy cut-off which is strongly dependent on the density gradient of the plasma corona formed by the amplified spontaneous radiation. The absorption rate of short laser pulses, the hot electron distribution, and X-ray emission from a Cu slab target are studied via a hybrid model, which combines hydrodynamics, collisional particle-in-cell, and Monte-Carlo simulation techniques, and via direct spectroscopic measurement. A new absorption mechanism originating from the interaction of the laser pulse with plasma waves is found to increase the absorption rate over 30% even for a very short, s -polarized laser pulse. Calculated and measured X-ray spectra are in good agreement, proving the electron energy cut-off

2. Experiments

A table top terawatt laser system, which consists of a Ti-sapphire laser (Coherent Mira 900) and a chirped pulse amplification system, operating at 10 Hz is used to initiate X-ray emission from a Cu disk (with 70 mm diameter and 5 mm thickness) with a polished surface. The amplified laser beam has a pulse width of 300 ps, a diameter of 50 mm, and maximum pulse energy of 400 mJ at wavelength of $\lambda = 785$ nm. The laser beam is compressed to a pulse with duration of 42 fs. The laser intensity is estimated to be about 10^{17} W/cm². The X-ray spectra with energy below 30 keV is measured with a direct-detection X-ray CCD camera. The integrated intensity of the X-rays is also measured with an X-ray silicon photodiode XPD. The XPD is sensitive to X-rays with energy between 4 keV and 30 keV. Higher energy X-rays (<100 keV) are measured with a semiconductor detector. The detector is sensitive to X-rays with energy from 5 keV to 100 keV.

3. Results

We have found a clear ‘energy cut-off’ in the distribution of hot electrons produced during the interaction of a short laser pulse of moderate intensity with solids targets. This energy cut-off is about $2T_h$ and strongly depends on the contrast ratio of the ASE pulse and the main laser pulse. We showed via PIC simulation that, due to the effective coupling of the plasma with both the incoming and the outgoing (reflected) laser pulses in the vicinity of the critical density, the maximal absorption rate exceeds 60%, while the overall absorption efficiency is about 25%. The most energetic hot electrons are produced at the time of the intense interaction of the plasma with both laser pulses. For a laser intensity of 10^{17} W/cm² and pulse duration of about 40 fs, the $K\alpha$ emission efficiency is about $(1 - 2) \times 10^{-4}$ and the pulse duration is shorter than 7 ps. The X-ray properties, i.e. the small energy cut-off, $E_{\text{cut}} < 100$ keV, the high efficiency, and the short pulse duration of Cu $K\alpha$ emission at 8 keV make such a table-top laser X-ray source safe and practical in various applications.

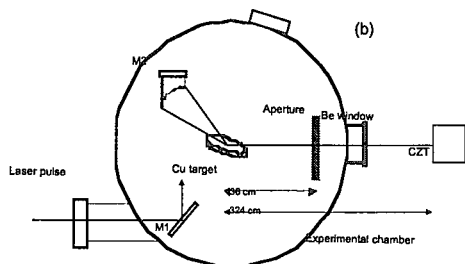


Fig. 1 The scheme of the experimental set-up for the CZT detector

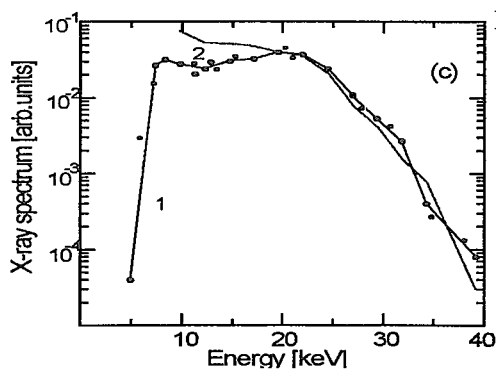


Fig. 2 The intensity of X-ray emission from the Cu plasma, measured spectrum (line with dots), line-the spectrum calculated with sampled distribution (solid line)

This is a blank page.

5. Synchrotron radiation science

This is a blank page.

5.1 Beamline

5.1.1 Construction of JAERI beamline III (BL11XU) at SPring-8

Hideaki SHIWAKU

1. Introduction

The third beamline of JAERI, BL11XU, is for material sciences using synchrotron radiation from an insertion device. BL11XU conforms to a standard undulator beamline at SPring-8. The insertion device is a standard in-vacuum type linear undulator with source characteristics of $\lambda = 32$ mm, $N = 140$ periods, tunable energy range about 5 ~ 70 keV using first, third and fifth harmonics x-ray, and linear polarization. The front-end components are in accordance with other beamlines, but a novel x-ray beam position monitor is installed in front of the Fast Closing Shutter (FCS) for one of the R&D projects.

This beamline consists of one optics hutch and three experimental hutches. The length of the beamline at the experimental hall is 37 m, and the total length of the beamline (from the x-ray source point to the end of the experimental hutch 3) amounts to 70 m. We have mainly developed four experimental plans for this beamline. Details have been reported elsewhere^{1,2)}.

2. Beamline Construction

Planning of BL11XU construction began in 1996. The front-end was designed and produced in the same year. In 1997, the insertion device was designed and produced, and the front-end was installed and adjusted. The next year the insertion device was installed and adjusted. At the same time, a transport channel, interlock system and beamline control system were designed, produced and installed. Then the beamline was constructed at the end of October in 1998.

This is the first case of beamline construction in user experimental time. Therefore, we took special care to guard against shock and vibration. Furthermore, we made other modifications to the beamline, for example, we made use of metallic materials instead of plastic and resinous materials to protect against radiation damage. Characteristically, there are two "multipurpose spaces" for installing mirrors, differential pumping systems, and other experimental apparatuses for use in future developments.

3. Beamline commissioning

The commissioning of BL11XU began in October 1998 and was finished by December of the same year. We performed the test running and the fine-tuning of the inclined double crystal monochromator. The optical alignments were accomplished by the same method as the preceding beamline commissioning group. In the off-line alignment, the simple double-L-Shaped tools and only a few levels were used without x-ray. These tools were used to find the zero angle and to determine the origin or the center of each stage. Before the application experiments were started, the beamline was investigated for its performance. The flux, which was measured at a sample position by a PIN photo diode, was 1.6×10^{13} cps at $I_b = 69$ mA, ID gap = 20.1 mm, and $E = 14.4$ keV (first harmonics of the undulator). This value was the same order intensity as used with the other standard undulator beamlines of SPring-8. FWHM of experimental results are 1.4 ~ 3.4 times larger than that of the theoretical value. In contrast to the theoretical values, FWHM values increased with an increase in photon energy. This might be the result of a distortion in the 1st Si crystal caused by the direct water-cooling system.

4. Conclusions

This beamline is designed for the various kinds of studies on Mössbauer spectroscopy, high-pressure science, inelastic x-ray spectroscopy, surface science, and other sciences. Scientific programs with commissioning of experimental equipment began from 1999.

References

- 1) H. Shiwaku et al., SPring-8 Annual Report 1997, p.111 (1998)
- 2) H. Shiwaku et al., SPring-8 Information, Vol.3 No.6, p.29 (1998), and Vol.4 No.5, p.4 (1999)

5.1.2 Bending magnet beamline BL14B1 at SPring-8

Yasuo NISHIHATA, Hiroyuki KONISHI, Jun'ichiro MIZUKI

1. Introduction

The beamline BL14B1 for Japan Atomic Energy Research Institute was constructed at a bending magnet source with high brilliance, low emittance and high photon flux at SPring-8. It is designed for various kinds of experiments on diffraction and XAFS spectroscopy in a wide energy range 5 - 110 keV for monochromatized beams and 5 - 150 keV for white beams.

2. Beamline

The source is the bending magnet of type B1: $\sigma_x = 0.182$ mm, $\sigma_y = 0.058$ mm, $\sigma'_y = 0.065$ mrad (@10 keV). The critical energy is 28.9 keV. The main optics refers to the standard SPring-8 bending magnet system, which consists mainly of a fixed-exit double crystal monochromator, two mirrors, 4D-slits, and γ -ray stopper¹⁾. The adjustable inclined double-crystal monochromator can provide the wide energy range by inclining a single pair of Si (311) crystals in-situ in the vacuum²⁾. It is estimated that the photon flux at the sample position is 10^{10} - 10^{12} photons/sec with energy resolution $\Delta E/E = 10^{-4}$. A second crystal to focus the beam by sagittal bending is under development. The mirrors are rhodium coated and are used for higher order harmonics elimination below 40 keV, while detuning of the double crystal monochromator is performed for it above the energy. These mirrors are bent by the cramp rotation bending mechanics³⁾. The first mirror collimates the incident x-ray vertically to improve energy resolution of the monochromatized x-ray. The second mirror focuses the x-ray beam vertically to achieve the beam size as small as 0.1 mm at the sample position. These optical components can be removed from the optical axis for the experiment with white beams. This beamline has two experimental hutch: white x-ray hutch and monochromatic x-ray hutch. Figure 1 shows several beam arrangements for experiments. Some kinds of detectors are available: gas-flow type ionization chamber, scintillation counter, Lytle detector, SSD, PSPC.

3. Areas of research

A multi-anvil high-pressure apparatus is installed in the white x-ray hutch. X-ray diffraction and XAFS techniques are employed under high pressure up to 20 GPa and high temperature up to 2,000 °C for high-pressure science and phase transition under extremely condition.

A κ -type multi-axis diffractometer is available in the monochromatic x-ray hutch. It has two extra axes useful for surface and interface structural studies such as surface reaction in electrochemistry and multilayered materials. It is also dedicated to the study on single crystals, powder samples, medium-range order of glass using high-energy x-ray, and DAFS. The diffractometer is equipped with a closed-cycle He gas refrigerator or an electric furnace to control the sample temperature from 10 to 1,000 K.

References

- 1) S. Goto, M. Yabashi, H. Ohashi, H. Kimura, K. Takeshita, T. Uruga, T. Mochizuki, Y. Kohmura, M. Kuroda, M. Yamamoto, Y. Furukawa, N. Kamiya, T. Ishikawa: *J. Synchrotron Rad.* **5**, 1202-1205, 1998
- 2) T. Uruga, H. Kimura, Y. Kohmura, M. Kuroda, H. Nagasawa, K. Ohtomo, H. Yamaoka, T. Ishikawa, T. Ueki, H. Iwasaki, S. Hashimoto, Y. Kashihara, K. Okui: *Rev. Sci. Instrum.* **66**, 2254-2256, 1995
- 3) J. Tanase, K. Endo: *JPSE Proceedings of the second U.S. - Japan workshop on soft x-ray optics*, 479-482, 1997

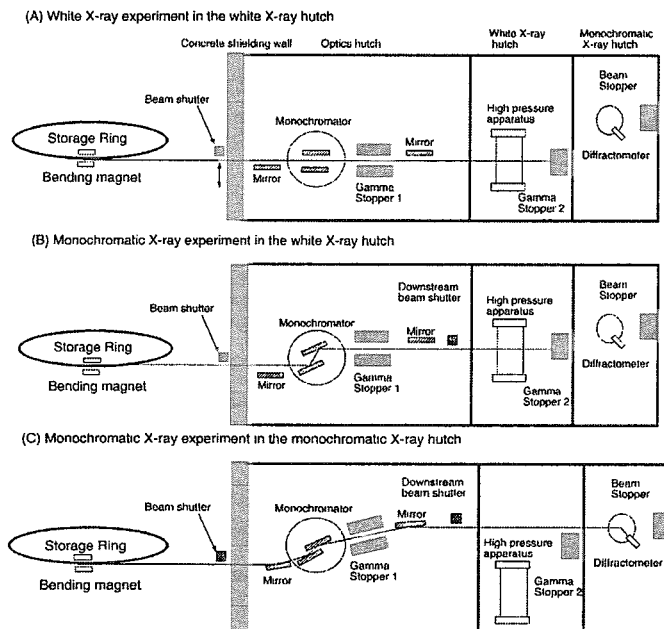


Fig. 1 Schematic drawing of beam arrangements in the white x-ray hutch and the monochromatic x-ray hutch of the BL14B1 beamline

5.1.3 Soft X-ray beamline -BL23SU- at the SPring-8

Akane AGUI, Akitaka YOSHIGOE, Yuji SAITOH, Yuden TERAOKA, Akinari YOKOYA

This report introduces an undulator beamline, BL23SU, which has been constructed for soft x-ray spectroscopy studies in a wide variety of applications at the SPring-8. Figure 1 shows the layout of the beamline system¹⁾.

An insertion device (ID23) has been installed (in 1997) in the storage ring of SPring-8 at BL23IN as a light source that is a double-array variable undulator of APPLE-2 (advanced planar polarized light emitter) type which produces both linearly and circularly polarized soft x-rays²⁾. The energy range of soft x-rays from 0.5 and 1.5 keV in the circular polarization mode is covered by the first harmonic.

Below front-end components, we have been constructing a varied line-space (VLS) plane grating monochromator since 1998³⁾. This consists of an entrance slit, spherical mirrors, varied-line-spacing gratings, an exit slit, a post-focusing mirror, and refocusing toroidal mirrors. The beamline is partly specialized for studies of actinides and radioactive materials. The experimental stations for actinide samples will be placed in hot sample area that is separated from common experimental hall. The x-rays are guided over a very long distance across the two areas and the last force-point is guided at over 125 m from the undulator.

The beamline has four experimental stations in a tandem fashion: a surface chemistry station (installed in 1999)⁴⁾, an electron paramagnetic resonance on biological molecule station (installed in 1999), a photoelectron spectroscopy station, and a magnetic circular dichroism station (tested in 1999 in the common experimental hall).

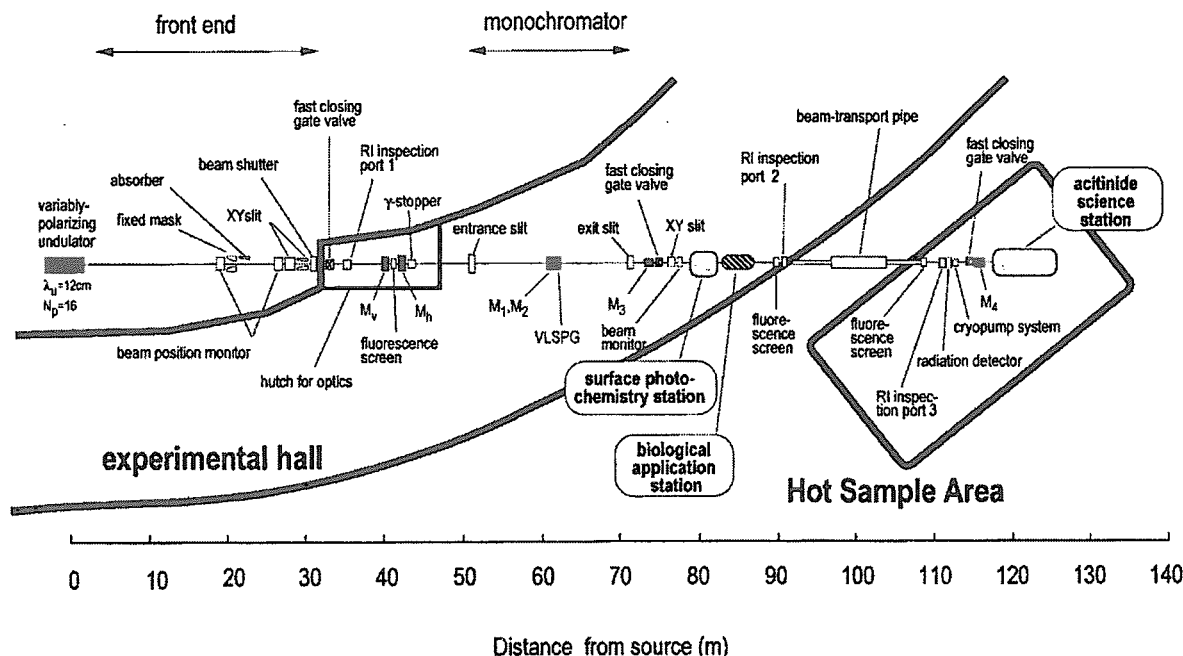


Fig. 1 Schematic illustration of the beamline components of BL23SU

References

- 1) A. Yokoya *et al.* : J. Synchrotron Rad. **5**, 10, 1998
- 2) S. Sasaki *et al.* : Nucl. Instrum. Method, **A347**, 83, 1994
- 3) Y. Saitoh *et al.* : Nucl. Instrum. Method to be published
- 4) Y. Teraoka and A. Yoshigoe : Jpn. J. Appl. Phys. **38**, Suppl. 38-1, 642, 1999

5.1.4 Construction of public beamlines in SPring-8

Hiroyuki KONISHI

1. Introduction

The JAERI-RIKEN project team completed the first-phase ten public beamlines in SPring-8 before the operation for public use started in the beginning of October 1997. Some R&D works concerning important problems on beamlines had carried out before the starting of the beamline constructions. Basic specifications and standard design concepts of SPring-8 beamline had been almost established through the designing and the construction of these beamlines. After the project team was dissolved in 1998, each of JAERI and RIKEN continue to construct new public beamlines in collaboration of JASRI.

At present, public beamlines constructed by JAERI's budget contain five bending-magnet beamlines, six X-ray undulator beamlines, two soft X-ray undulator beamlines and one wiggler beamline as shown in Table 1.

2. First Public Beamlines

On the construction of the first phase beamlines, we had to guide the vendors in order to let them reflect correctly results of our R&D to realized facilities. So JAERI and RIKEN had divided some construction works into each of facilities included in beamlines. Then JAERI had mainly contributed to the following items on budgetary points.

- Insertion devices (two standard in-vacuum X-ray undulators and one elliptical wiggler)
- Front ends (for seven beamlines)
- High heat load components of front-end: slits, masks and absorbers (for five X-ray insertion device beamlines)
- Beamline interlock systems (for all beamlines)
- Radiation shielding hutches (for all beamlines)
- Standard double crystal monochromators (for two beamlines)
- Some experimental facilities: especially, including some kinds of diffractometer

3. Additional Bending Magnet Beamlines

JAERI and RIKEN divide the construction works of additional beamlines into each beamline.

BL02B2 and BL28B2 were completed in the end of FY1998 by a revised budget of this fiscal year. Their beamline optics follows the SPring-8 standard such as BL02B1 and BL04B1, respectively. So the construction had been finished in a short term comparatively.

BL02B2 is especially oriented to powder diffraction study. A bending flat mirror system is installed to exit a parallel beam for highly angular resolution.

BL28B2 has no monochromators or mirrors in its optics hutch. White radiation is utilized for topography experiments.

4. Additional Insertion Device Beamlines

The construction of BL35XU, an X-ray inelastic scattering beamline, started in FY1998. To observe the dispersion of phonon in materials, high energy and high angular resolution was strongly required in the X-ray optics. Therefore, back scattering optics is adopted in monochromator and analyzer systems. The spherical crystal analyzer was machined by NEC. To optimize the optics, the beamline hutches have become very long, very large.

The construction of BL13XU was authorized in a revised budget of FY1999. This beamline follows the insertion device beamline standard of SPring-8 fundamentally. The facilities of experimental stations will be specialized for surface/interface structural studies. It is under construction to be completed in the end of FY2000.

Table 1 List of Public Beamlines in SPring-8 constructed by JAERI's Budget

	Scientific Subject	Light Source	Optics
● First Ten Public Beamlines			
BL01B1	XAFS	Bending Magnet	Standard double crystal monochromator, Collimating/focusing mirrors
BL02B1	Crystal Structure Analysis	Bending Magnet	Standard double crystal monochromator, Collimating/focusing mirrors
BL04B1	High Temperature and High Pressure Research	Bending Magnet	No monochromators or mirrors
BL08W	Compton Scattering Spectroscopy	Elliptical Wiggler	Asymmetric Johann monochromator, Doubly bent monochromator
BL09XU	Nuclear Resonant Scattering	Standard In-Vac XU	Standard double crystal monochromator
BL10XU	High Pressure Cell Experiments and High Brilliance XAFS	Standard In-Vac XU	Standard double crystal monochromator, Double-flat mirror system
BL25SU	Soft-X-ray Spectroscopy of Solid	Helical SU	Varied-space plane gratings, Cylindrical or spherical mirrors
BL27SU	Soft X-ray Photochemistry	Figure-8 SU	Grating monochromator et al. Branching to three lines.
BL39XU	X-ray Magnetic Research and X-ray Micro-Spectrochemical Analysis	Standard In-Vac XU	Standard double crystal monochromator, Plane mirror
BL41XU	Bio-Crystallography	Standard In-Vac XU	Standard double crystal monochromator, Vertical/horizontal focusing mirrors
● Bending-Magnet Beamlines completed in FY1998			
BL02B2	Powder Diffraction	Bending Magnet	Standard double crystal monochromator, Collimating mirror
BL28B2	White Radiation Topography	Bending Magnet	No monochromators or mirrors
● ID Beamline under Construction, to be completed to the autumn of 2000			
BL35XU	High Resolution Inelastic Scattering	Standard In-Vac XU	Back Scattering Optics for High Energy Resolution
● ID Beamline to be completed to the End of FY2000			
BL13XU	Surface/Interface Structural Study	Standard In-Vac XU	Standard double crystal monochromator, Collimating/focusing mirrors

XU: X-ray Undulator

SU: Soft X-ray Undulator

5.1.5 Present status of BL-27 at the Photon Factory of KEK and recent highlights

Yuji BABA, Tetsuhiro SEKIGUCHI, Iwao SHIMOYAMA, Hiroyuki YAMAMOTO^{a)},
Hideo OHTSUKA^{a)}, Yoshihiro OKAMOTO^{a)}, Tsuyoshi YAITA^{a)}, Haruhiko MOTOHASHI^{b)}

a) Department of Materials Science

b) SPring-8 Service Co.

1. Present status of BL-27

The BL-27 at the Photon Factory of High Energy Accelerator Research Organization (KEK-PF) was constructed in 1992 in cooperation with KEK. The main purpose of the beamline is to study samples containing radioactive materials including actinide elements. The beamline is composed of two branch lines: one is soft X-ray beamline (BL-27A) covering the photon energy range from 1.8 to 6 keV, and the other is hard X-ray beamline (BL-27B) ranging from 4 to 15 keV. In the BL-27A, the studies on surface chemistry and radiation biology are conducted. In the BL-27B, XAFS and X-ray diffraction as well as radiation biology are studied. The detailed performance of the beamline has been described elsewhere.¹⁾

About half of the users time of the BL-27 is allocated to the research groups of JAERI in various departments, such as Synchrotron Radiation Research Center, Department of Materials Science, Department of Environmental Science, and Advanced Science Research Center. Also the BL-27 is now open to the users from not only JAERI and KEK but also the other institutes or universities under the approval of the Photon Factory Program Advisory Committee.

2. Research topics at BL-27

The research topics being available in 2000, which have been proposed by the staff of JAERI, are summarized in Table 1.

Table 1 Research titles for BL-27 being available in 2000, proposed by the staff of JAERI

Spokesperson	Department	Research Title
Y. Baba	Synchrotron Radiation Research Center	Photo-fragmentation of adsorbed silicon alkoxide by inner-shell electron excitation
Y. Baba H. Yamamoto	Synchrotron Radiation Research Center Department of Materials Science	In-situ observation on the formation of carbon nitride thin films Non-destructive depth profile analysis by X-ray absorption near-edge structure and photoelectron spectroscopy
T. Yaita T. Ohonuki	Department of Materials Science Department of Environmental Science	XAFS analysis of f element complex for advanced separation systems Research on fixation mechanism of elements to minerals and bacteria by XANES and EXAFS with synchrotron X-ray radiation
Y. Okamoto M. Akabori A. Iwase	Department of Materials Science Department of Materials Science Department of Materials Science	Structural analysis of high-temperature actinide melts by EXAFS X-ray absorption spectroscopy studies of actinide compounds Research on X-ray induced atomic displacements in solids

3. Recent highlights at BL-27A

In the BL-27A, the mechanism of surface chemical reaction induced by inner-shell electron excitation has been investigated. Due to the localized nature of the inner-shell electron, we can excite a specific element or specific site in a molecule by tuning the photon energy. Our concern is whether or not a specific chemical reaction happens in adsorbed layer or condensed phase following the core-to-valence resonant photoexcitation. One of the clear examples has been found in adsorbed silane derivatives.²⁾ Here trimethylfluorosilane ($\text{Si}(\text{CH}_3)_3\text{F}$) molecules adsorbed on Cu(111) surface are excited by X-rays corresponding to the resonant excitation from Si 1s to unoccupied σ^* orbitals localized at the Si-F bond. As a result, we found that only F^+ ions are desorbed from the surface, which is quite different from the results for electron impact. These results show the potentiality of monochromatized synchrotron beam to use as "chemical scissors", by which we can cut a specific chemical bond in a molecule.

References

- 1) H. Konishi et al. Nucl. Instrum. Methods Phys. Res. A **372**, 322 (1996)
- 2) T. Sekiguchi and Y. Baba, Surf. Sci. **433-435**, 849 (1999)

5.2 High pressure science

5.2.1 *In situ* observation of diamond formation process under high pressures and high temperatures

Wataru UTSUMI, Takashi TANIGUCHI^{a)}, Kenichi FUNAKOSHI^{b)}, Osamu SHIMOMURA

a) National Institute for Research in Inorganic Materials

b) Japan Synchrotron Radiation Research Institute

1. Introduction

Diamond formation under high-pressure and high-temperature has been extensively studied, resulting in large-scale synthesis of diamonds using industrial high-pressure technology. However, most of the previous studies were based upon information obtained at ambient conditions from recovered specimens, and very few *in situ* experiments have been reported. Such experiments would be indispensable for the direct study of the diamond formation process. A combination of a large volume press and synchrotron-derived x-ray radiation have made it possible to carry out real-time *in situ* observation of the catalytic graphite-diamond conversion process at high-pressure and high-temperature.

2. Experimental

Experiments were performed using a large-volume multi-anvil high pressure apparatus, SPEED1500, installed at BL04B1 beamline. As a catalyst, $K_2Mg(CO_3)_2$ (potassium magnesium carbonate) was used in the present study. This carbonate material has interested many geoscientists in relation to the diamond formation in the earth's interior. Powder x-ray diffraction profiles of the specimen were obtained under each pressure-temperature condition by the energy dispersive method using the white synchrotron radiation beam from a bending magnet.

3. Results

Figure 1 shows the variation of x-ray diffraction profiles of the sample with increasing temperature at 9.3 GPa. At low temperature, sharp diffraction peaks of graphite and catalyst in solid state were clearly observed. When temperature was increased to 1400 °C, several diffraction peaks of catalyst became very strong owing to its grain growth. These strong peaks suddenly disappeared at 1450 °C so that the catalyst melted completely. In spite of the melting of catalyst, all the graphite peaks still survived and no obvious cubic diamond peaks appeared at this temperature. Instead, a broad hexagonal diamond 002 peak was observed between 100 and 101 peaks of graphite. It is known that hexagonal diamond is a meta-stable phase and is produced even at room temperature compression without catalysts. Hence, this hexagonal diamond peak did exist before the catalyst melting but had been hidden by the peak of solid catalyst. Cubic diamond peaks began to appear when temperature was further increased up to 1600°C. The peaks of hexagonal 002 and cubic 111 were clearly distinguished; clear shift in peak position and sudden decrease in peak width were observed when cubic diamond began to form. The formation of cubic diamond could be confirmed also by the appearance of other cubic diamond peaks (220, 311). This *in situ* observation demonstrates that the melting of the catalyst is not a sufficient condition to form cubic diamonds; in order to synthesize diamond using $K_2Mg(CO_3)_2$ at this pressure, higher temperature than its melting point is needed. This result is contrast to the fact that when metal catalysts such as nickel and cobalt are used, diamond always begins to form at their melting temperatures.

Our present study demonstrates that *in situ* x-ray diffraction under high pressures-temperatures combined with a large volume press is a powerful tool for the diamond research. This technique will be further developed and be applied to many research topics of diamond both in the academic science.

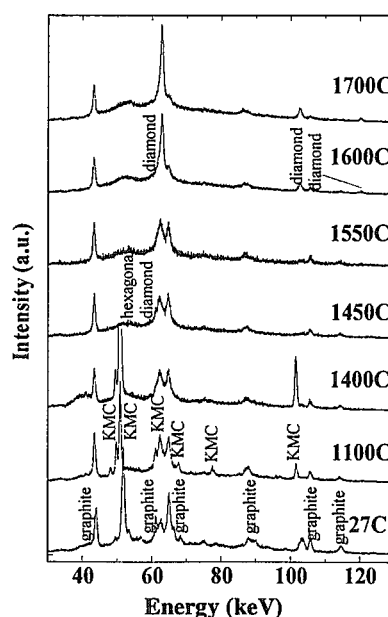


Fig. 1 Variation of x-ray diffraction profiles of the sample with increasing temperature at 9.3 GPa

5.2.2 Construction of the laser-heated diamond anvil cell system

Tetsu WATANUKI, Takehiko YAGI^{a)}, Tadashi KONDO^{b)}, Osamu SHIMOMURA

a) Institute for Solid State Physics, University of Tokyo

b) Department of Science, Tohoku University

1. Introduction

One of the experimental stations at BL10 is dedicated to the study of high-pressure x-ray diffraction using a diamond anvil cell (DAC) which can generate the high pressure, and the diffraction from the sample is detected by the Imaging Plate system. The systems for the experiments at room temperature and at low temperature are already available.

We also constructed the high temperature DAC system by a laser-heating method, which is designed for the investigation of the x-ray diffraction study in the temperature region up to 3,000 K and also in the pressure region up to 100 GPa. The laser heating method has the following advantages in contrast to the method of heating DAC directly; (1) high temperature more than 1,000 K can be much more easily obtained, (2) pressure shift during heating is much smaller, and (3) conventional DAC's are available.

2. Experimental facilities

This system consists of a laser source, a focusing unit, and an optical unit (Fig. 1). We use Nd:YAG laser (LEE LASER) as a multi mode continuous wave source. The wave length is 1,064 nm and the maximum power is 100 W. The beam power is controlled by the Q-switch. The laser beam is guided to the sample by the focusing unit. In order to heat the sample homogeneously, the laser beam is split into two paths and irradiate the sample through the both side of the DAC. The beams are focused down 0.1 mm in diameter at the sample position by lenses. Both sides of the sample can be monitored by CCD cameras through the reverse laser path. The optical unit is used as a microscope for the sample, and is also designed for the sample pressure measurement with use of the ruby luminescence and also the temperature measurement by analyzing the radiation spectra from the sample. The laser beam power control, positioning and focusing can be operated from the outside of the experimental hutch with the remote controller with monitoring the sample.

We carried out the experiment to test the system, and could obtain the powder diffraction pattern of γ -Fe at 21 GPa and at more than 1,200 K.

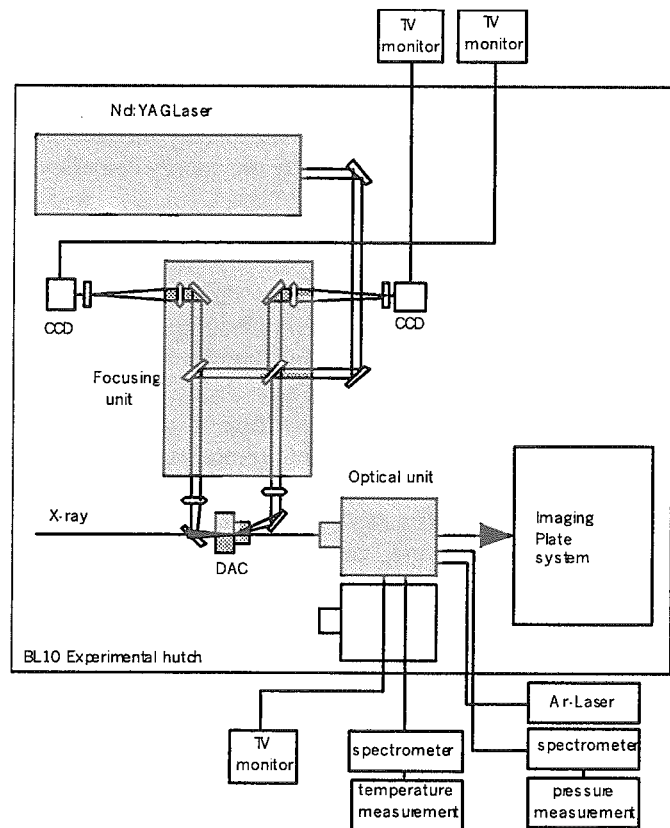


Fig. 1 Double-sided laser heating system for diamond anvil cell

5.2.3 A first-order liquid-liquid phase transition in phosphorus

Yoshinori KATAYAMA, Takeshi MIZUTANI, Wataru UTSUMI, Osamu SHIMOMURA,
Masaaki YAMAKATA^{a)}, Kenichi FUNAKOSHI^{a)}
a) Japan Synchrotron Radiation Research Institute

1. Introduction

Although first-order structural phase transitions are common in crystalline solids, first-order liquid-liquid phase transitions are exceedingly rare in pure substances. Recently, possibility of such transitions has been proposed for several materials but their observations by structural methods have not been reported yet¹⁾. Phosphorus is one of the candidates that exhibit liquid-liquid transition. We have studied structure of liquid phosphorus under high-temperature high-pressure conditions²⁾.

2. Experimental

Experiments were performed using a large-volume multi-anvil high-pressure apparatus, SMAP180, installed at BL14B1 beamline. X-ray diffraction profiles were obtained by the energy-dispersive method using the white synchrotron radiation beam from a bending magnet.

3. Results

In addition to a known form of liquid P - a molecular liquid comprising tetrahedral P₄ molecules - we have found a polymeric form at pressures above 1 GPa. Figure 1 shows the structure factor, $S(Q)$, as a function of wave number Q , obtained from X-ray diffraction data. There is a large difference between $S(Q)$ below and above 1 GPa. A prominent first peak around 1.4 Å⁻¹ disappears at high pressures. A new maximum around 2.45 Å⁻¹ appears above 1 GPa. On the other hand, $S(Q)$ at 0.77 GPa is almost identical to that at 0.96 GPa and $S(Q)$ at 1.01 GPa is similar to that at 1.38 GPa. These results indicate that there are two distinct forms of liquid P.

The low- and high-pressure forms are obtained by melting black P below and above 1.0 GPa, respectively. In addition, the high-pressure form can be directly obtained from the low-pressure form and *vice versa* by a change in pressure. Figure 2 shows the diffraction patterns taken at a diffraction angle of 6.0° across the transformation. A broad peak around a photon energy of 25 keV in pattern (a) corresponds to the first maximum of $S(Q)$ for the low-pressure form. The pressure was increased at the rate of about 0.01 GPa/min. During compression, the peak around 25 keV abruptly decreased. Pattern (b) was taken during the transformation. After 15 min, the diffraction pattern did not show any further change (pattern (c)). An increase in pressure by about 0.02 GPa results in a completely different diffraction pattern.

The features of the transformation strongly support the view that it is a first-order liquid-liquid phase transition.

References

- 1) P. H. Poole, et al.: Science 275, 322 (1997), V. V. Brazhkin, et al.: High Pressure Res. 15, 267 (1997), O. Mishima, H. E. Stanley: Nature 396, 329 (1998)
- 2) Y. Katayama, T. Mizutani, W. Utsumi, M. Yamakata, K. Funakoshi: Nature 403, 170 (2000)

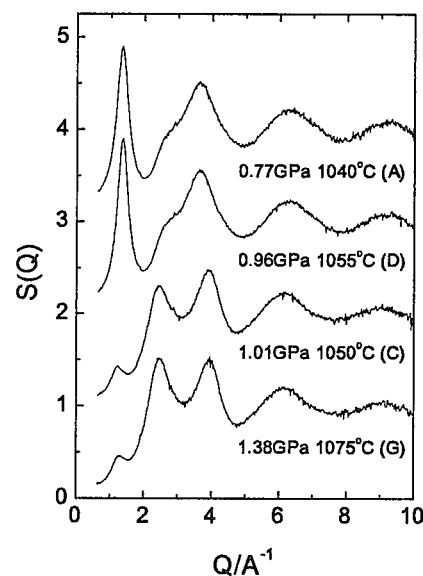


Fig. 1 Structure factor $S(Q)$ of liquid phosphorus at different pressures

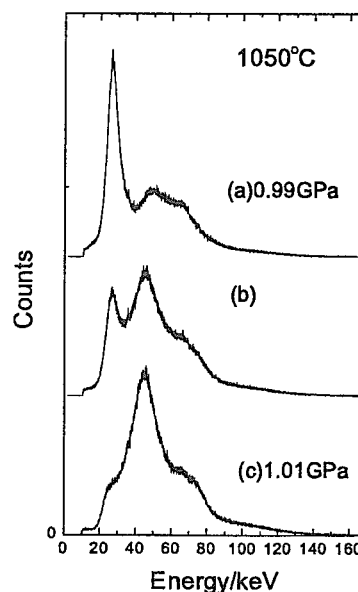


Fig. 2 X-ray diffraction pattern that show transformation from low-pressure form to high-pressure form

5.3 Structural physics research

5.3.1 Pseudomorphic growth of Pd monolayer on Au(111) electrode surface

Masamitsu TAKAHASHI, Yukio HAYASHI, Junichiro MIZUKI, Kazuhisa TAMURA^{a)},
Toshihiro KONDO^{a)}, Hideo NAOHARA^{a)}, Kohei UOSAKI^{a)}

a) Division of Chemistry, Graduate School of Science, Hokkaido University

For the studies on electrode-electrolyte interfaces, surface X-ray diffraction (SXD) is a unique technique because it is not much influenced by the solution encapsulating the sample surface. Also, the penetrating feature of X-rays allows the determination of crystallographic relationship between the overlayer and the substrate. Thus, SXD is complementary to electrochemical scanning probe microscopy which is sensitive only to the outermost layer.

The surface structure of a Pd monolayer electrochemically deposited onto Au(111) has been studied by SXD¹⁾. The specular rod profile is shown in Fig. 1(a). Following convention, we use the hexagonal coordinates with $a = [1/2, 0, 1/2]_{\text{bulk}}$, $b = [-1/2, 1/2, 0]_{\text{bulk}}$ and $c = [1, 1, 1]_{\text{bulk}}$. Compared with the profile for the ideally terminated Au(111) surface (a dotted line), the observed intensity decreases remarkably between neighboring bulk Bragg peaks. This destructive interference effect results from a uniform Pd monolayer formed on Au(111). The least squares fitting gives the calculated curve (a solid line) corresponding to the Pd-Au interlayer spacing, 2.27 Å. The lateral adsorption site of Pd is ascertained by the measurement of the (0 1) rod shown in Fig. 1(b). The observed profile agrees well with the adsorption to the cubic closest packing site (a solid line). Other adsorption sites, such as the hexagonal closest packing site (a dashed line) and the atop site (a dot-dashed line), fail to reproduce the observation. The Pd-Au bond length is calculated as 2.82 Å, which is close to the sum of the atomic radii of Pd and Au in each bulk.

It is noteworthy that such a pseudomorphic smooth Pd layer as obtained by the electrochemical method is not available in vacuum. The formation of the stable Pd layer in electrolyte is ascribable to the lifting of the $23 \times \sqrt{3}$ surface reconstruction of the Au substrate.

References

- 1) M. Takahashi, Y. Hayashi, J. Mizuki, K. Tamura, T. Kondo, H. Naohara and K. Uosaki, *Surf. Sci.*, **461**(2000) 213

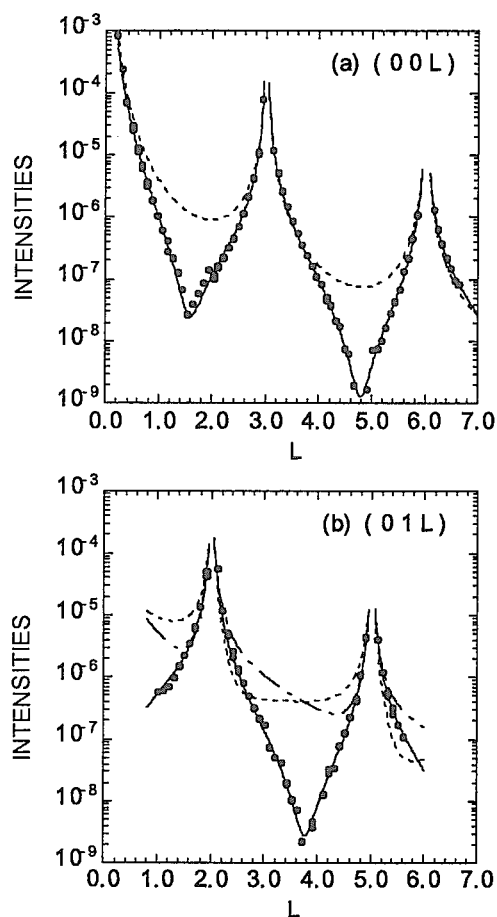


Fig. 1 Specular (a) and non-specular (b) rod profiles for 1ML-Pd on Au(111) electrode surface

5.3.2 X-ray diffraction study on quadrupolar order in DyB₂C₂

Toshiya INAMI, Yoshikazu TANAKA^{a)}, Tetsuya NAKAMURA^{a)}, Hiroki YAMAUCHI^{b)},
Hideya ONODERA^{b)}, Kenji OHOYAMA^{b)}, Yasuo YAMAGUCHI^{b)}

a) Institute of Physical and Chemical Research (RIKEN)

b) Institute for Materials Research, Tohoku University

Under highly symmetric crystalline field, orbital degeneracy usually remains in the ground state multiplet of a rare-earth ion. As a result, a phase transition which lifts the degeneracy may occur in rare-earth compounds at low temperatures. This is the so-called quadrupolar order. Recently, Yamauchi *et al.* have found that DyB₂C₂ undergoes an antiferroquadrupolar (AFQ) order at $T_Q=24.7$ K¹⁾. In order to clarify the nature of the AFQ transition, we have carried out resonant and non-resonant X-ray diffraction measurements²⁾.

The experiments were performed at the beamline 4C in Photon Factory, KEK. The incident energy was the vicinity of Dy L_{III} absorption edge ($E = 7.789$ keV). A single crystal of DyB₂C₂, of which dimensions are about $1 \times 3 \times 0.5$ mm³, grown by a Czochralski method was mounted in a closed-circle ⁴He refrigerator on a six-axis diffractometer.

Two superlattice reflections $00\frac{3}{2}$ and $01\frac{1}{2}$ were measured. Below T_Q , the $00\frac{3}{2}$ reflection shows huge resonance enhancement in intensity, and is essentially observed only near the Dy L_{III} absorption edge. In addition, $00\frac{3}{2}$ reflection shows oscillation in intensity as a function of azimuthal angle (the sample rotation around the scattering vector). These two observations are known as specific features of the anisotropy of the tensor of susceptibility (ATS) scattering³⁾. Since the ATS scattering is a sensitive technique on the symmetry of the atom in question, combined with the temperature dependence measurement, which shows the $00\frac{3}{2}$ reflection arises below T_Q , these results unambiguously indicate that the site symmetry of the Dy³⁺ ion changes to the lower one at T_Q . This is a clear evidence of the AFQ transition at T_Q .

On the other hand, the $01\frac{1}{2}$ reflection also appears only below T_Q . In contrast to the $00\frac{3}{2}$ reflection, the $01\frac{1}{2}$ reflection does not show resonance enhancement. Thus it stems from the lattice distortion accompanied by the AFQ transition. The space group analysis suggests that the structural change is described by the displacement of the B and C atoms, as shown in Fig.1. Above T_Q , DyB₂C₂ has the tetragonal LaB₂C₂-type structure, in which Dy and B-C layers stacks along the c axis. Below T_Q , a pair of the B (C) atoms in the $z' = 1/4$ plane move upward and the other pair move downward along the c axis. In the $z' = 3/4$ plane, the B (C) atoms move to the opposite direction of those in the $z' = 1/4$ plane. According to the site symmetry of Dy³⁺, we present the principal axes (ξ , η , ζ) of the crystalline field of Dy³⁺ in Fig.1. The ζ axis is parallel to the c axis. Since the principal axes of the quadrupole moment are parallel to those of the crystalline field, this is a model of the AFQ order. In the AFQ ordered phase, one of the principal axes of the quadrupole moments orders as shown by thick lines in Fig.1. The azimuthal-angle dependence of the intensity of the $00\frac{3}{2}$ reflection calculated using the above AFQ structure model agrees well with the experimental result.

In summary, we have performed resonant X-ray diffraction on DyB₂C₂ and found that the symmetry of the Dy ion changes to lower one. This strongly suggests the AFQ order at T_Q . We also present a structural model for the AFQ order deduced from lattice distortion pattern.

References

- 1) H. Yamauchi *et al.*, J. Phys. Soc. Jpn. **68** (1999) 2057
- 2) Y. Tanaka *et al.*, J. Phys.: Condens. Matter **11** (1999) L505
- 3) D. H. Templeton and L. K. Templeton, Acta. Crystallogr. Sect. A **42** (1986) 478

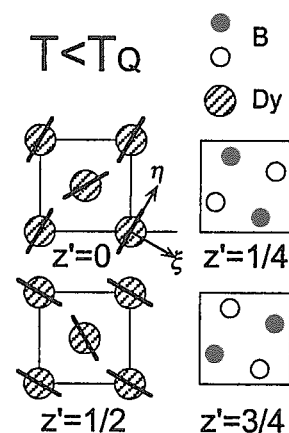


Fig. 1
Structure model of DyB₂C₂ in the AFQ phase. The C atoms are omitted for simplicity. The B atoms of closed circle locate slightly downwards along the c axis and ones at open circle sites locate slightly upwards. The thick lines on Dy atoms represent one of the principal axes of the quadrupolar moment.

5.3.3 High real-space resolution structure of oxide glasses by high-energy X-ray diffraction

Kentaro SUZUYA, Yasuhiro YONEDA, Norimasa MATSUMOTO, Shinji KOHARA^{a)}

a) Japan Synchrotron Radiation Research Institute (JASRI)

1. Introduction

The most interest in the description of the structure of the oxide glasses is commonly directed to knowledge about the basic structural units of the glass-forming oxide and the links, which these units form in the network. The modifier cations Me^{V+} occupy less defined sites preferably in the vicinity of the terminal oxygen atoms. It is expected that the coordination states of the modifier cations do not vary. The asymmetry of their coordination polyhedra may, however, show some changes. The capabilities of high-energy X-ray ($E > 30$ keV) diffraction (HEXRD) in SPring-8 can help to clarify these small changes because the real-space resolution depends on effects of Fourier transformation with upper limit, Q_{max} ($Q = 4\pi\sin\theta/\lambda$, scattering angle 2θ , wavelength λ). The advantage of such experiments is the high-resolution power in real-space due to the high- Q diffraction data and the improved accuracy in the quality of the diffraction data (small corrections due to low absorption, no fluorescence, and small scattering angles). Because of the small X-ray scattering cross-section at higher Q , high counting rates are necessary for such measurements. The instrument with a sagittal focusing bender in double-crystal monochromator at BL14B1 of the SPring-8 allows to obtain scattering data in a range up to $Q \sim 30 \text{ \AA}^{-1}$. In the present report selected examples of such high-resolution structural analysis of oxide glasses are presented.

2. Experiments

The X-ray diffraction measurements were carried out using a six-circle diffractometer at the BL14B1 bending magnet beamline of SPring-8. A double-crystal monochromator was used. The first element is an indirectly water-cooled Si(311) flat crystal and the second is a ribbed Si(311) crystal mounted on a sagittal focus bending device. With the bent crystal set for an incident energy 41 keV, the X-ray focused on the sample with a beam size 5 mm width \times 1 mm height. The photon flux incident on the sample is about $5 \times 10^{11} \text{ s}^{-1}$. Diffraction data were obtained with a NaI scintillation detector, scanned through a scattering angle 2θ in transmission geometry. The angular scans covered an extended region in Q space, from 0.5 \AA^{-1} to 25.0 \AA^{-1} with constant $\Delta Q = 0.05 \text{ \AA}^{-1}$.

3. Results

The normalized X-ray diffraction data, structure factors $S(Q)$, for three metaphosphate glasses are shown in Fig. 1. As can be seen from Fig. 1, $S(Q)$ exhibits significant oscillations up to the maximum Q value of about 24 \AA^{-1} . Figure 2 shows the total correlation functions $T(r)$ of MgP_2O_6 glass obtained by Fourier-transformation of the $S(Q)$ truncated at various values of Q_{max} . P-O, Mg-O, O-O, P-P and Mg-P correlation peaks in the $T(r)$ with $Q_{max} = 24 \text{ \AA}^{-1}$ are clearly distinguished each other because of the high real-space resolution. In particular, it is found that Mg ions form highly distorted MgO_6 octahedra from the asymmetric Mg-O peak in the $T(r)$. HEXRD is very powerful tool to determine the detailed structure of non-crystalline materials. Local structures of many interesting non-crystalline and disordered-crystalline materials are under investigation by HEXRD in BL14B1.

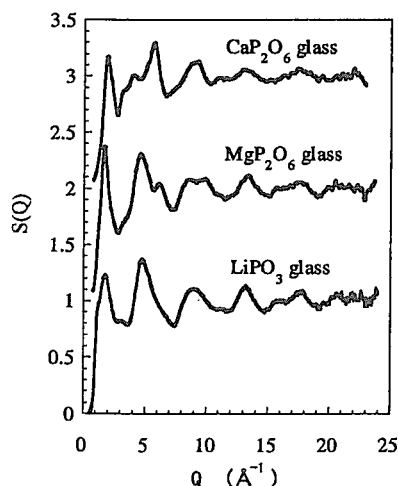


Fig. 1
 $S(Q)$ of
metaphosphate
glasses

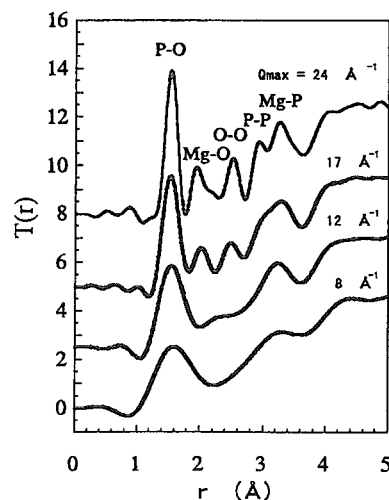


Fig. 2
 $T(r)$ of MgP_2O_6
glass with
various Q_{max}

5.3.4 XAFS in the high-energy region

Yasuo NISHIHATA, Junichiro MIZUKI

1. Introduction

The EXAFS (Extended X-ray Absorption Fine Structure) spectrum with K absorption edge is expected to improve the accuracy of local structure parameters for the elements such as lanthanoids, whose energy range just above the L_{III} edge is restricted owing to the following L_{II} edge. It is known, however, that the finite lifetime of a core hole smears out the EXAFS oscillation, and that this effect becomes more serious for heavier elements. The utility to K edge EXAFS measurement was shown by analyzing the EXAFS spectra systematically for some K edges (Ce, Dy, Ta and Pt) in the energy region from 40 to 80 keV^{1,2)}. The local structure parameters estimated from EXAFS spectra above the K edges were in good agreement with those estimated from EXAFS spectra above the L_{III} edges with the exception of the mean-free-path term for the photoelectron.

2. Experiments

X-ray absorption spectra near K edges of Pt (78.4 keV) and Pb (88.0 keV) for the foils were measured at bending-magnet beamline BL01B1 at SPring-8. Measurements were carried out at room temperature and 12 K in transmission mode with Si (511) planes of the adjustable inclined double-crystal monochromator, which is the standard at SPring-8. The incident and transmitted x-ray intensities were monitored with a flowing Kr gas ionization chambers of 17 cm and 31 cm in length, respectively. The energy resolution at the Pt and Pb K edges were estimated to be as good as 7 and 8 eV, respectively.

3. Results

It was found that the amplitude of the EXAFS oscillation of the Pt foil at 12 K considerably increased in comparison with that at room temperature, indicating that the amplitude is very sensitive to the Debye-Waller factor especially at high-k values. It was qualitative EXAFS signal for an anharmonic analysis. Figure 1(a) shows the first observation for the EXAFS spectrum above the Pb-K edge at 12 K, while it was not observed at room temperature. The inset gives the extracted EXAFS function $\chi(k)$, which is defined well up to high-k values. Figure 1(b) shows the radial structure function around the Pb atom obtained by Fourier transform of k^3 -weighted EXAFS function $\chi(k)$. The interatomic distance from the central atom to the first nearest neighbour was close to the value evaluated by x-ray diffraction in literature. On the other hand, a remarkable reduction of the mean-free-path for the photoelectron was found depending on the short lifetime of the Pb-K hole.

In conclusion, the EXAFS signal can be observed even in the high-energy region when it is measured carefully. The remarkable increase of the EXAFS signal at low temperature indicates that EXAFS signal at high-k values is very sensitive to temperatures. This property seems to be useful for the study concerning lattice vibration or interatomic potential.

References

- 1) Y. Nishihata, O. Kamishima, Y. Kubozono, H. Maeda, S. Emura: *J. Synchrotron Rad.*, **5**, 1007-1009, 1998
- 2) Y. Nishihata, S. Emura, H. Maeda, Y. Kubozono, M. Harada, T. Uruga, H. Tanida, Y. Yoneda, J. Mizuki, T. Emoto: *J. Synchrotron Rad.*, **6**, 149-151, 1999

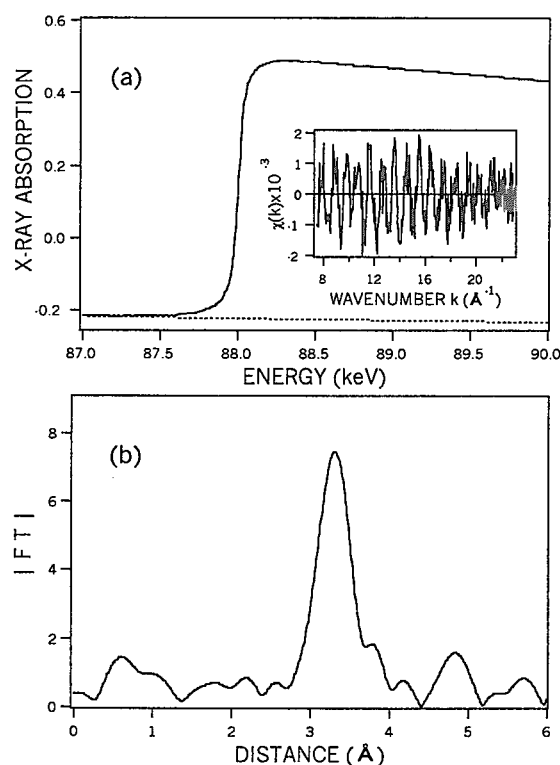


Fig. 1 (a) XAFS spectrum near the Pb-K edge for a Pb-foil at 12 K, (b) Magnitude of the Fourier transform of $k^3\chi(k)$

5.3.5 Crystal structure of Pd-perovskite catalyst in redox fluctuating atmospheres

Yasuo NISHIHATA, Junichiro MIZUKI, Takahiro AKAO, Hirohisa TANAKA^{a)}, Mari UENISHI^{a)},
Mareo KIMURA^{b)}, Tokuhiko OKAMOTO^{b)}

a) Materials R&D Dept., Technical Center, Daihatsu Motor Co., Ltd.

b) Materials Analysis & Evaluation Div., Toyota Central R&D Labs., Inc.

1. Introduction

In conventional catalysts for an automotive engine exhaust gas, precious metals initially having dispersions of nanometer order work well, but the catalytic activity reduces owing to the particle growth of the metals in operation. Perovskite crystals including the precious metal such as palladium, $\text{LaM}_{1-x}\text{Pd}_x\text{O}_3$ ($M = \text{Fe}, \text{Co}, \text{Fe}_{0.6}\text{Co}_{0.4}$), are expected to provide a function for self-regeneration of the metals in a usage ambience without auxiliary treatment. It is important to investigate the electronic state of the Pd and the local structure in the Pd-perovskite catalysts under the condition of reduction-oxidation fluctuating atmospheres in order not only to elucidate the mechanism of self-regeneration of the metal, but also to develop better catalysts. The purpose of this study is to clarify the mechanism to maintain high catalytic activity and to suppress the particle growth of the precious metals.

2. Experiments

Pd-containing perovskite catalysts were prepared by the alkoxide method. The powdered catalyst, $\text{LaFe}_{0.57}\text{Co}_{0.38}\text{Pd}_{0.05}\text{O}_3$, was subjected to thermal aging under oxidation, reduction, oxidation atmospheres in due order at 800 °C for 1 hour on each aging stage. XAFS spectra were measured near the Pd-K edge in transmission mode using Si(311) double crystal monochromator at bending-magnet beamline BL14B1 at SPring-8.

3. Results

Figure 1 shows XANES spectra for the three samples together with a Pd-foil and PdO as standard materials. The chemical shift is observed in the edge position for PdO and the two oxidized samples, indicating that the Pd in the oxidized catalysts is trivalent or tetravalent state. The edge position for the reduced sample is identical to that for the Pd foil. Radial structure functions were calculated by Fourier transform of the k^3 -weighted EXAFS function $\chi(k)$ and were shown for each sample together with that for the Pd-foil in Fig. 2. The local structure parameters were evaluated by non-linear least-squares fitting concerning the first nearest neighbour for the Pd. We conclude that the Pd occupies the B-site in the oxidized sample. For the reduced sample, we failed in fitting calculation as a single Pd-shell, while the fitting calculation converged as a single O-shell. Moreover, the fitting was much improved by considering 2 shells: Pd-O and Pd-Pd shells. About 80% of the Pd occupies the A-site and about 20% of the Pd exists as metallic particles. The local structure for the reoxidized sample is substantially the same as that for the oxidized one.

In conclusion, the Pd occupies the B-site with trivalence or tetravalence state in the oxidation atmosphere, while most of the Pd occupies the A-site with oxidation number as low as the metallic Pd and some of the Pd segregates out from the perovskite crystal as metallic particles in the reduction atmosphere. After the atmosphere changes to air again, the Pd occupies the B-site. This structure change repeats thoroughly in the reduction-oxidation fluctuating atmospheres. The perovskite crystal has an ability to accommodate the precious metal with different radius in the redox fluctuating atmospheres for the suppression of the particle growth of metal.

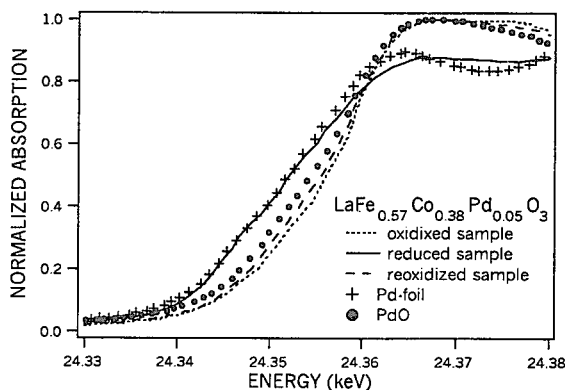


Fig. 1 XANES spectra near the Pd-K edge

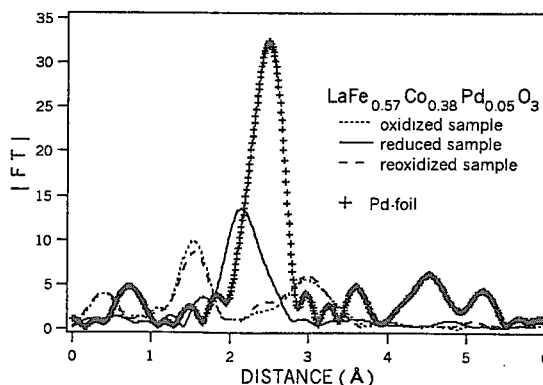


Fig. 2 Radial structure functions around the Pd

5.3.6 Magnetic properties of some perovskite cobalt oxides

Kenji YOSHII, Masaichiro MIZUMAKI^{a)}, Yuji SAITOH, Takayuki MURO^{a)}, Akio NAKAMURA^{b)}

a) Japan Synchrotron Radiation Research Institute (JASRI), Mikazuki, Hyogo 679-5198, Japan

b) Japan Atomic Energy Research Institute (JAERI), Tokai-mura, Ibaraki 319-1195, Japan

Recently, much attention has been paid to perovskite cobalt oxides $Ln_{1-x}A_xCoO_3$ (Ln : rare earth metals, A : alkaline earth metals) because of their unusual physical properties¹⁾. While the end compounds $LnCoO_3$ show no magnetic order, these systems evolve into ferromagnets with Curie temperatures of $< \sim 250$ K as x is increased. Detailed magnetic and transport properties have been investigated mainly for $La_{1-x}Sr_xCoO_3$ containing the nonmagnetic Ln^{3+} ion, La^{3+} . In this work, magnetic properties were studied for some of the other such systems.

The samples were prepared in air by the solid-state reaction method. From powder X-ray diffraction measurements, the crystal structures were found to be of an orthorhombic perovskite type. Magnetization measurements were performed with a SQUID magnetometer between 4.5 and 300 K. To reveal the electronic structures of ferromagnetic phases, magnetic circular dichroism (MCD) spectra were measured at BL25SU of SPring-8²⁾.

Figure 1 shows magnetic susceptibility-temperature (χ - T) curves for $Eu_{0.5}Sr_{0.5}CoO_3$ (EuSr) and $Eu_{0.5}Ba_{0.5}CoO_3$ (EuBa) measured in a field-cooled mode with an applied field of 20 Oe. Ferromagnetic transitions are observed at ~ 170 K for $Eu_{0.5}Sr_{0.5}CoO_3$ and ~ 260 K for $Eu_{0.5}Ba_{0.5}CoO_3$. The curve for $Eu_{0.5}Sr_{0.5}CoO_3$ exhibits typical behavior of ferromagnets. For $Eu_{0.5}Ba_{0.5}CoO_3$, the shape of the curve is similar to that reported previously, which was measured with the field of 200 Oe³⁾. The drop of the susceptibility around 200 - 240 K was attributed to an antiferromagnetic transition³⁾.

Figure 2 shows a XANES (X-ray absorption near edge structure) and an MCD spectra for $Eu_{0.5}Sr_{0.5}CoO_3$ at 50 K. The latter spectrum has apparent MCD effects at the $Co2p_{3/2,1/2}$ edges, which are brought about by the ferromagnetic order of $Co3d$ spin moments. The intensity difference between the two MCD peaks is due to the order of $Co3d$ orbital moments. Based on the sum rules⁴⁾, the ordered spin and orbital moments were calculated to be $\sim 0.35 \mu_B/Co$ and $\sim 0.12 \mu_B/Co$, respectively. No obvious MCD effect has been observed for $Eu_{0.5}Ba_{0.5}CoO_3$ at 50 K. This result is consistent with the appearance of the antiferromagnetic order noted above. Investigations on the other systems such as $Nd_{0.5}Sr_{0.5}CoO_3$ are now in progress, and their results will be published in the near future.

References

- 1) M. R. Ibarra *et al* : Phys. Rev. B 57, R3217-3220, 1998
- 2) Y. Saitoh *et al* : J. Synchrotron Rad., 5, 542-544, 1998
- 3) I. O. Troyanchuk *et al* : Phys. Rev. B 58, 2418-2421, 1998
- 4) For example, J. Stöhr : J. Electron Spectrosc. Relat. Phenom., 75, 253-272, 1995

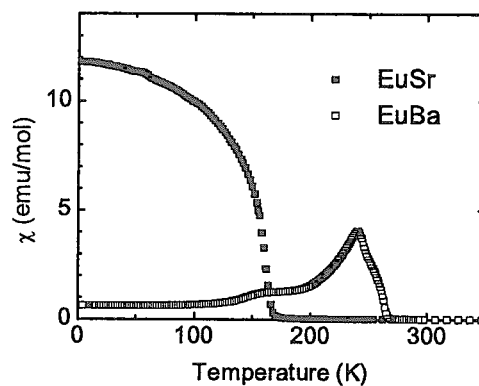


Fig. 1 χ - T curves for $Eu_{0.5}Sr_{0.5}CoO_3$ (EuSr) and $Eu_{0.5}Ba_{0.5}CoO_3$ (EuBa)

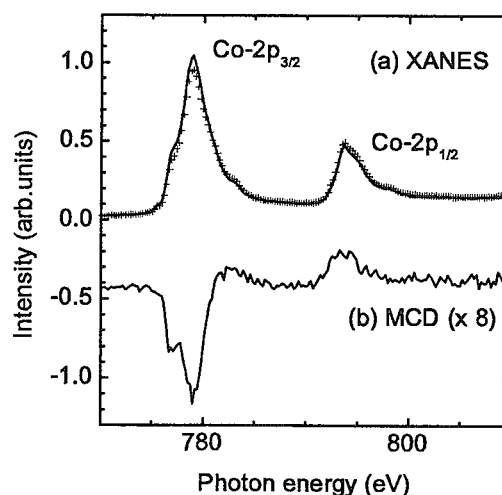


Fig. 2 (a) XANES and (b) MCD spectra for $Eu_{0.5}Sr_{0.5}CoO_3$ measured at 50 K. The MCD spectrum was obtained by subtracting the solid line from the cross markers shown in (a).

5.3.7 Dielectric investigation of nanostructured ferroelectrics

Yasuhiro YONEDA, Hikaru TERAUCHI^{a)}
a) Kwansei-Gakuin University

1. Introduction

Ferroelectric thin films have experienced tremendous development in recent years due to the advance of sophisticated film-synthesis techniques and an increase in the understanding of the related materials science and integration of films into various novel devices.

Ferroelectric materials can be applied to ohmic, voltage-dependent, and thermally sensitive resistors; fast ion conductors; and humidity and gas sensors. With development in field of ferroelectric thin film devices, surface and size effects on ferroelectricity have aroused great interest.

To solve the degradation problem of ferroelectric thin films and to apply to temperature gradient sensor, we prepared barium titanate (BaTiO_3) thin films with nano-order film thickness and investigated them by dielectric measurements.

2. Sample preparation

BaTiO_3 films and multilayer films were prepared by the molecular beam epitaxy (MBE) method.^{1,2)} The phase, crystallographic orientation, film thickness, and crystalline quality of the BaTiO_3 films were analyzed by X-ray diffraction. The spontaneous polarization was measured using a laboratory-build Sawyer-Tower circuit and the capacitance was measured using an LCR meter.

3. Results

The dielectric properties of the BaTiO_3 thin film are sensitive to temperature. Although the dielectric measurement was performed in an air-conditioned laboratory, the capacitance of the BaTiO_3 thin film was fluctuated with temperature. Figure 1 shows the time dependence of the capacitance of a $[(\text{SrTiO}_3)_6(\text{BaTiO}_3)_6]_2$ multilayer film. The measured frequency was 50 kHz. The thickness of the film was 9.6 nm. The fluctuation of the capacitance was never observed in bulk BaTiO_3 crystals.

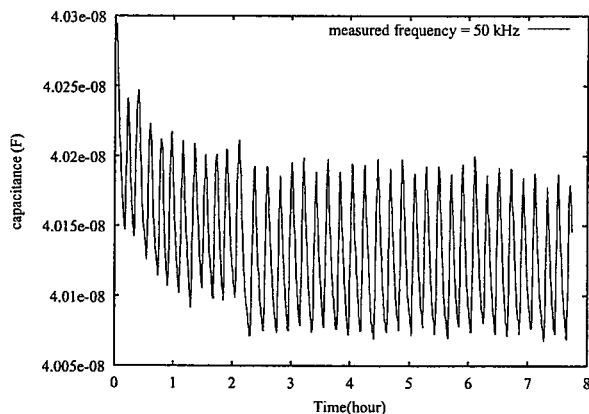


Fig. 1 Time dependence of the capacitance in the $[(\text{SrTiO}_3)_6(\text{BaTiO}_3)_6]_2$ multilayer film.

Ferroelectrics have different polarization stabilize system depending on their thickness. In bulk ferroelectrics, the surface polarization played a depolarization field to stabilize the polarized ferroelectric state. In ferroelectric thin films, the local field at the surface is smaller than in the bulk. A second possible depolarization mechanism is trapping of carriers to space charges in ferroelectrics. The amount of space charge affects the depolarization strongly, as the film thickness decreased. Thus, the ferroelectric films show various dielectric properties depends on their film thickness.

We expected that the dielectric properties of ferroelectric thin film can be modified by controlling the film thickness. There is much

possibilities to develop novel temperature sensors by using nanostructured ferroelctrics.

References

- 1) Y. Yoneda, T. Okabe, K. Sakaue, H. Kasatani, K. Deguchi, H. Terauchi: J. Appl. Phys., **83**, p.2458-2461, 1998
- 2) Y. Yoneda, T. Okabe, K. Sakaue, H. Terauchi: Surf. Sci., **410**, p.62-69, 1998

5.3.8 Crystal orientation dependence of spin polarization on Cu in single crystal Co/Cu multilayers by MCD method

Junichiro MIZUKI, Tatsuo FUKUDA, Hideaki YAMAMOTO^{a)}, Atsushi KAMIJO^{a)}, Motohiro SUZUKI^{b)}, Naomi KAWAMURA^{c)}, Masaichiro MIZUMAKI^{b)}, Shunji GOTO^{b)}
 a) NEC Corp. b) JASRI c) SPring-8, RIKEN

1. Introduction

The discovery of “giant” magnetoresistance (GMR) in a variety of metallic multilayers comprised of alternating layers of magnetic and nonmagnetic layers has generated widespread interest¹⁾. This GMR has been discovered to be related to an oscillatory exchange coupling between successive ferromagnetic layers. The precise nature of the coupling, however, remains controversial. In order to clarify these phenomena the electronic states of the nonmagnetic spacer metal which mediate the magnetic coupling should be identified. The present experiment aims to investigate the effect of the Fermi surface of the spacer layer on the polarization of the spacer layer in multilayers by *K*-edge X-ray Magnetic Circular Dichroism (XMCD) technique with use of single crystals Co/Cu (111) and (001). The main advantages of *K*-edge XMCD are its bulk sensitivity and the possibility to probe directly the conduction electrons, which are expected to mediate the magnetic interactions.

2. Experiments

The sample we have studied were [Co(1.5 nm)/Cu(*t* nm)(111)]₁₂₀, [Co(1.5 nm)/Cu(*t* nm)(001)]₁₂₀, *t* = 0.5, 1.0, 1.5, 2.0, grown by MBE technique. The XMCD was measured by the technique invented by M. Suzuki et al.²⁾ with a fluorescence detection mode at BL-35XU of SPring-8. The sample was magnetized with a magnetic field of 1 T, and the field direction was fixed at 45° away from the incident beam direction.

3. Results

Figure 1 shows the results of the XMCD spectra of the (111) and (001) grown samples with three kinds of thickness in each orientation mentioned above taken at the Cu *K*-edge. The magnitude of the XMCD spectra was normalized to the height of the absorption edge step. These results indicate that the 4*p* band of Cu is magnetically polarized. The shape of the XMCD spectra is expected theoretically different between the two, however, the observed data seem not to be much different among the samples than expected. On the other hand, the thickness dependence of the XMCD spectra on the Co *K*-edge between the (111) and (001) orientation shown in Fig. 2 seems to be different. The detailed analysis together with theoretical calculation based on band theory is under development.

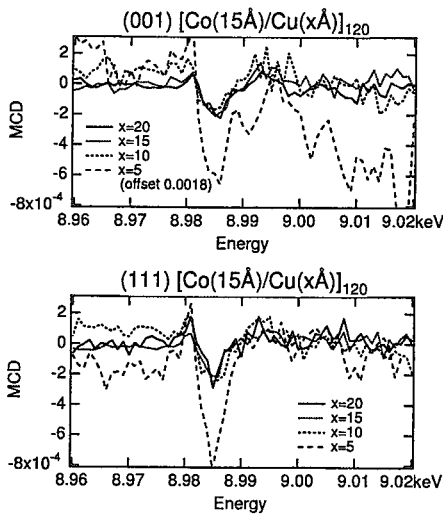


Fig. 1 XMCD spectra of the (001) and (111) grown samples taken at the Cu *K*-edge

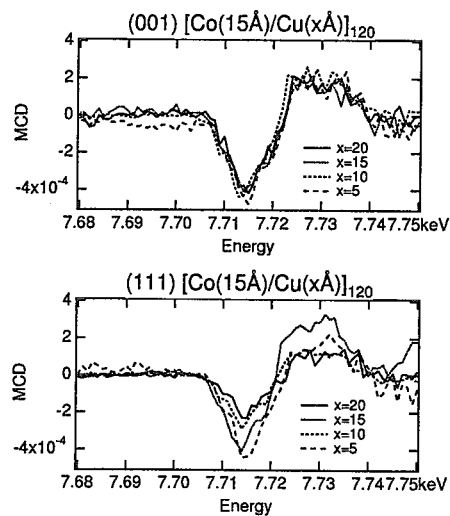


Fig. 2 XMCD spectra of the (001) and (111) grown samples taken at the Co *K*-edge

References

- 1) M. N. Baibich et al., : Phys. Rev. Lett. **61**, p. 2472-2475 (1988)
- 2) M. Suzuki et al., : Jpn. J. Appl. Phys. **37**, (1998) L1488

5.3.9 X-ray and neutron-scattering studies of orbital order in lightly doped $\text{La}_{1-x}\text{Sr}_x\text{MnO}_3$

Tatsuo FUKUDA, Kazuma HIROTA^{a)}, Kazuo TAKAHASHI^{a)}, Yasuo ENDOH^{b)}, Youichi MURAKAMI^{c)}

a) Department of Physics, Tohoku University

b) Institute for Materials Research, Tohoku University

c) Photon Factory, Institute of Materials Structure Science, KEK

1. Introduction

Doped manganese perovskites are old themes, and they are revisited more intensively these days because both fundamental and practical themes such as colossal negative magnetoresistance were found in these systems¹⁾. It is now recognized that a subtle balance among charge, spin and orbital degrees of freedom affects the physical properties of these systems. Good single crystals as a result of the progress of crystal growth techniques and the direct observation of orbital states by the synchrotron anomalous x-ray diffraction technique²⁾ have been prevailing the detailed characters of these systems. We carried out anomalous x-ray diffraction experiments of $\text{La}_{1-x}\text{Sr}_x\text{MnO}_3$ to study orbital-ordering (*OO*) states, and we also did inelastic neutron scattering measurements to establish the spin wave dispersions.

2. Experiments

Large well-characterized single crystals were grown with a floating-zone (FZ) furnace at Tohoku University, and parts from a same lot were used in x-ray and neutron experiments. Synchrotron x-ray diffraction experiments were carried out with six-axis diffractometer at 4C and 16A2 beamline of PF, KEK. Neutron scattering experiments were carried out with TOPAN neutron spectrometer installed at JRR-3M in Tokai Establishment of Japan Atomic Energy Research Institute (JAERI).

3. Results

We studied $x = 0.08, 0.10, 0.11, 0.12$ samples by synchrotron resonant x-ray diffraction experiment, which is an application of anisotropy of tensor susceptibility (ATS) scattering; anomalous scattering factor, which is anisotropic and described as a tensor, is enhanced near the Mn absorption edge. A long range antiferro *OO* is thus observable as a superlattice peak by tuning the incident x-ray energy. The *OO* peaks also have the 2-fold azimuthal angle dependence corresponding to the local symmetry of orbitals and the polarization dependence, of which features are completely different from those of fundamental Bragg peaks.

We could observe clear *OO* peaks at $(0k0)$ ($k:\text{odd}$) in the P_{bnm} orthorhombic notation³⁾. They are summarized as a structural phase diagram of $\text{La}_{1-x}\text{Sr}_x\text{MnO}_3$ in Fig. 1. In particular, we found that a little change of hole doping level around $x_c \sim 0.105$ causes large differences in the *OO*, and we also found that spin-excitation states change drastically at the same doping concentration (x_c). Furthermore, in the lower doped region, a cooperative JT distortion is associated with the *OO* and the spin wave dispersion is anisotropic. In the higher doped region, on the other hand, an *OO* state appears in the distortion released phase and the spin wave dispersion is isotropic, which indicates a novel *OO* mechanism not due to JT distortion.

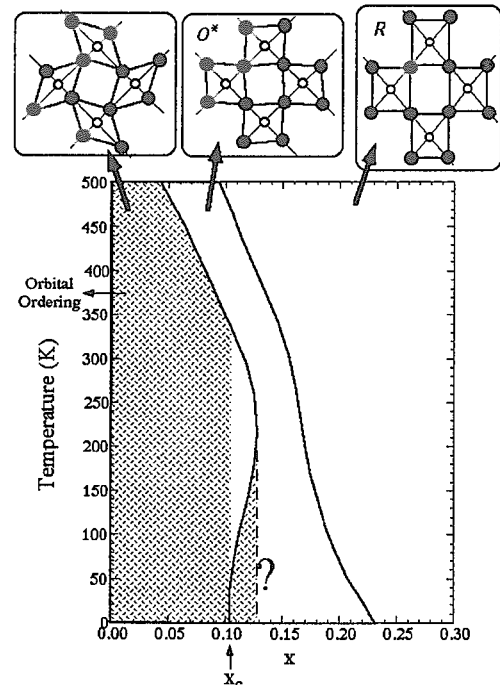


Fig. 1 Schematic structural phase diagram of $\text{La}_{1-x}\text{Sr}_x\text{MnO}_3$ ($0 < x < 0.3$)

References

- 1) Y. Tokura, *et al.*, J. Phys. Soc. Jpn. **63** (1994) 3931.; A. Urushibara, *et al.*, Phys. Rev. **B51** (1995) 14103.; A. Asamitsu, *et al.*, Nature (London) **373**
- 2) Y. Murakami, *et al.*, Phys. Rev. Lett. **80** (1998) 1932
- 3) Y. Endoh, *et al.*, Phys. Rev. Lett. **82** (1999) 4328

5.4 Surface chemistry research

5.4.1 Desorption of fragment ions from mono- and multilayered $\text{Si}(\text{OCH}_3)_4$ following localized inner-shell electron excitation

Yuji BABA, Guohua WU, Iwao SHIMOYAMA, Tetsuhiro SEKIGUCHI

1. Introduction

Photo-induced process on semiconductor surface is of great importance for the fabrication of semiconductor devices, because surface modification at low-temperature is possible using photons as a driving force of the reaction. For the deposition of silicon dioxide on silicon, silicon alkoxide is widely used for the source material. Synchrotron soft X-ray is an excellent photon source because of the potentiality of element-selective and site-selective reactions due to the localized nature of inner-shell electrons. Here we present the results for the photon-stimulated desorption of the fragment ions from tetramethoxysilane (TMS, $\text{Si}(\text{OCH}_3)_4$) adsorbed on Si(100) following the Si 1s excitation. In order to separate the photochemical process induced by substrate excitation (indirect process) from that induced by adsorbate excitation (direct process), we have prepared monolayer, bilayer, and multilayer whose thickness was precisely determined.

2. Experimental

The experiments were performed at the BL-27A station of the KEK-Photon Factory. The purified TMS was dosed on clean surface of Si(100) at 80 K. The thickness of the adsorbate was calibrated by thermal desorption spectroscopy (TDS)¹ and X-ray photoelectron spectroscopy (XPS). The desorbed ions were analyzed by a quadrupole mass spectrometer. The X-ray absorption near-edge structure (XANES) was measured by total electron yield (TEY) mode.

3. Results and discussion

Figure 1 shows the XANES spectrum for multilayer of TMS on Si(100). The thickness of TMS is 300 layers. The peak marked B corresponds to the resonant excitation from Si 1s to unoccupied σ^* orbitals for TMS, and its energy is shifted to higher energy by 6 eV than that for silicon substrate (marked A).

Figure 2 displays the photon-energy dependencies of the TEY and ion yields for bilayer. Since the total electrons emerge from deep region compared to the adsorbed layer, the TEY curve is almost the same as that for a clean surface of Si(100). However, it is noteworthy that the CH_3^+ and $\text{Si}(\text{OCH}_3)_3^+$ yields do not follow the TEY. The ion-yield curves rather follow the XANES spectrum of TMS. The results suggest that the secondary electrons produced by the Auger decay in silicon substrate scarcely contribute to the fragmentation and ion desorption. We conclude that the core-to-valence resonant excitation not in substrate but in adsorbed molecule is the main trigger of the fragment-ion desorption.

Reference

1) Y. Baba, T. Sekiguchi, Surf. Sci. 433-435, 843, 1999

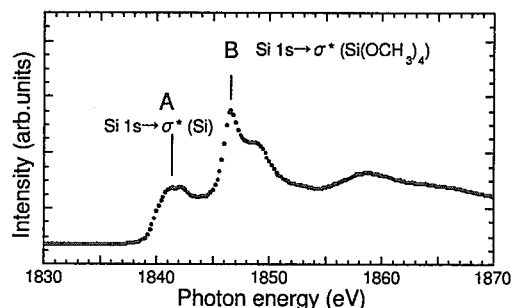


Fig. 1 XANES spectrum for multilayered $\text{Si}(\text{OCH}_3)_4$ on Si(100). The thickness is 300 layers.

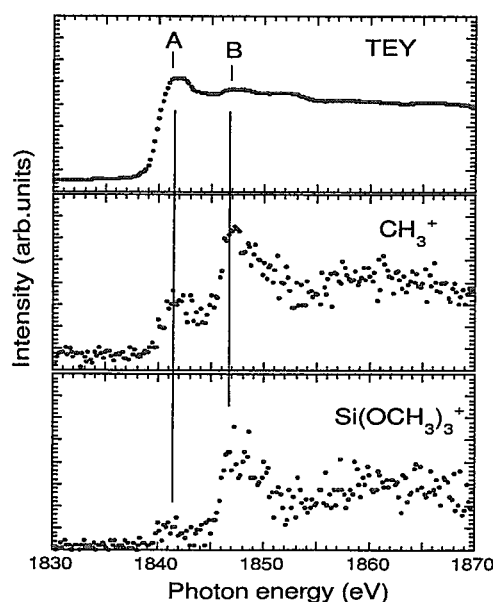


Fig. 2 Photon-energy dependencies of total electron and ion yields for bilayer of $\text{Si}(\text{OCH}_3)_4$ on Si(100)

5.4.2 Construction of surface reaction analysis apparatus and its application to initial oxidation of silicon surfaces

Yuden TERAOKA, Akitaka YOSHIGOE

1. Introduction

A new experimental apparatus for chemical reaction dynamics research on surfaces was designed in 1998 ¹⁾. It was constructed as an end-station of the BL23SU in the SPring-8 in 1999 ²⁾. The incident molecular kinetic energy and the x-ray energy are keys to develop new methods for reaction control on surfaces. The end-station has been promoting research activities on new atomic layer formation induced by the kinetic energy of incident molecules. The simultaneous use of the molecular beams and the x-rays is the most prominent character in this apparatus for achieving the real time *in situ* analysis of surface reactions, resulting in more deeper understanding for elementary processes of surface chemical reactions.

2. Description of the surface chemistry end-station

The end-station has principally the following functions: irradiation of the soft x-ray from the undulator and the conventional x-ray tube, exposure to supersonic molecular beams, reactive molecular beam scattering, photoemission spectroscopy, temperature-programmed desorption, finally scanning probe microscopy. A photograph of the end-station is shown in Fig. 1. Eight sample holders can be maintained in the load-lock chamber. A clean surface is formed by sample heating and/or argon-ion sputtering in the surface cleaning chamber. Chemical composition and periodic structure on the surface are analyzed by Auger-electron spectroscopy and a low-energy electron diffraction method. Continuous or pulsed molecular beams are fed into the surface reaction analysis chamber. Owing to low pressure in that chamber even during molecular beam operation, the electron-energy analyzer and the mass analyzers are usable simultaneously with the molecular beams for photoemission spectroscopy and mass analysis. The roles of the SR beam monitor chamber are photon beam shaping, position monitoring and x-ray intensity measurements. The surface can be observed by scanning tunnel microscopy and atomic force microscopy.

3. Analysis of initial oxidation on Si(001) surfaces by O₂ supersonic molecular beams

As the first step, initial oxidation of Si(001) surfaces with O₂ molecular beams has been investigated ²⁾ because that is not only interesting for surface reaction dynamics but also important as electronic device development. The maximum incident energy is 3 eV due to use of a high temperature nozzle. The clean Si(001) surfaces were irradiated by the O₂ beams with various incident energy to achieve saturated adsorption. The oxygen amount on the surface was evaluated by measuring O-1s photoemission intensity. The intensity depended on the incident energy and two thresholds of 1.0 eV and 2.6 eV were found. These values are very close to the predicted values of 0.8 eV and 2.4 eV from the first-principles calculation, showing potential energy barriers for dimer backbond oxidation and oxygen insertion between the second and the third Si layer. Si-2p photoemission spectra were obtained at room temperature and 870 K by using high resolution soft x-rays from the beamline. The maximum silicon oxidation number increased from Si²⁺ to Si⁴⁺ with increasing the incident energy. Even at high temperature of 870 K, the sub-oxide peak for Si³⁺ was increased with increasing the incident energy. The variation is resultant from oxidation of dimer and sub-surface silicon atoms.

References

- 1) Y. Teraoka and A. Yoshigoe : Jpn. J. Appl. Phys. **38**, Suppl. 38-1, p.642-645, 1999
- 2) Y. Teraoka, A. Yoshigoe and M. Sano : J. Vac. Soc. Jpn. **43**, p.412, 2000 (Japanese)

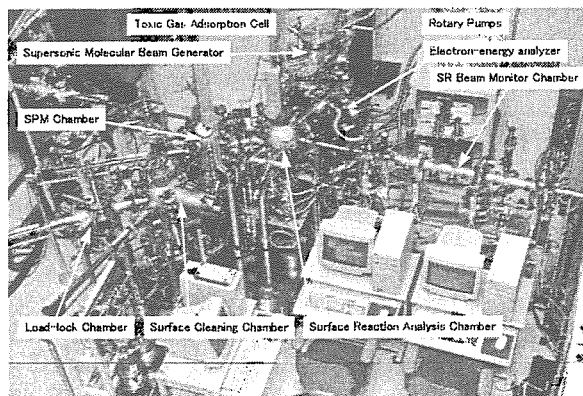


Fig. 1 Photograph of the surface reaction analysis apparatus installed at BL23SU in SPring-8

5.4.3 X-ray absorption near edge structures (XANES) spectral changes of 2-Deoxy-D-Ribose by irradiation within energy region around oxygen K-shell absorption edge

Ken AKAMATSU, Akinari YOKOYA

1. Introduction

Chemical changes in biological molecules such as DNA by γ - or X-rays are classified into two categories, 'indirect' and 'direct' effects. The 'indirect' effect is caused by hydroxyl radical or hydrated electron due to radiolysis of water¹⁾, which has been investigated in detail²⁾. However, knowledge of the 'direct' effect has been hardly developed probably because of multiplicity in the radiation chemical chain reactions initiated by the excitation. One of successful methods to clarify the 'direct' effect is the use of synchrotron radiation. It has high photon flux over a wide energy range (from infrared to g region), enough to give sufficient high-density monochromatic photons, which are essential to get high-resolution spectrum in X-ray absorption near edge structures (XANES). In this study, we selected 2-deoxy-D-ribose which is one of DNA components as the target of irradiation because the chemical change should directly lead to DNA strand breaks.

2. Experimental

XANES study was performed using a soft X-ray beamline with a variably polarizing undulator (BL23SU) in SPring-8³⁾. The aqueous solution of 2-deoxy-D-ribose (10 mg/mL) was prepared, and it was spread on a gold-coated plate to obtain a film sample by drying at room temperature. It was exposed to 3 energies of X-rays, i.e., 526.3 eV (under O $1s \rightarrow \pi^*$), 537.8 eV (an absorption peak of O $1s \rightarrow \sigma^*$) and 552.6 eV (over O $1s \rightarrow \sigma^*$) for given periods before measuring each XANES spectra to study radiation effects. The photon flux was estimated using an ion chamber for soft X-rays⁴⁾. All the XANES spectra were obtained by measuring the photo- or Auger electron current on the sample plate.

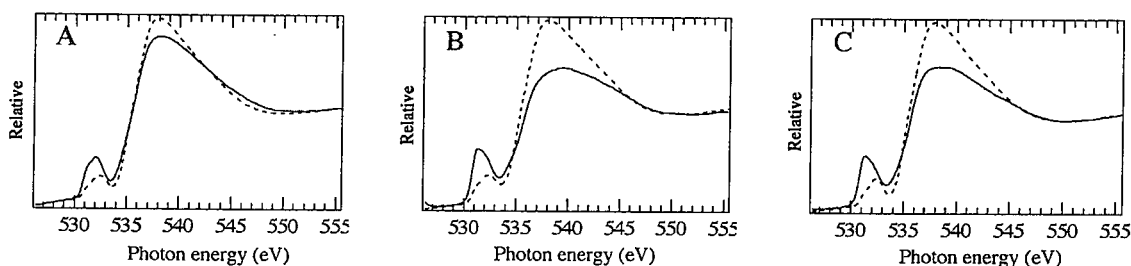


Fig. 1 XANES spectral changes of 2-deoxy-D-ribose after irradiation of monochromatic X-ray photons (A : 526.3 eV, B : 537.8 eV, C : 552.6 eV) for given periods

Total photon numbers irradiated were estimated using an ion chamber for soft X-rays⁴⁾ : A (dotted line : control, solid line : 6×10^{15}), B (dotted line : control, solid line : 1.6×10^{16}), C (dotted line : control, solid line : 3×10^{16} photons).

3. Results

In Fig. 1(A-C), a couple of overlapped peaks appeared between 530 and 533 eV and gradually increased in all irradiation energies. These two peaks were expected to be assigned to O $1s \rightarrow \pi^*$ transition resonance peaks, which indicated the production of more than two kinds of C = O bonds during de-excitation processes after energy deposition. In addition, the spectral changes approach saturation (data not shown). This phenomenon implies production of product, which is difficult to be rearranged chemically by further irradiation. These O $1s \rightarrow \pi^*$ transition resonance peaks would be not only responsible for excitation of oxygen 1s electrons, but that of oxygen nonbonding, carbon 1s and C - O valence electrons because the spectral change in irradiation at 526.3 eV (under O $1s \rightarrow \pi^*$ transition peak) was shown (Fig. 1A).

References

- 1) A. P. Breen, J. A. Murphy: *Free Radic. Biol. Med.*, **18**, p.1033-1077, 1995
- 2) J. Hüttermann *et al.*: *Effects of ionizing radiation on DNA, physical, chemical and biological aspects*, vol. I, II and III, Berlin: Springer-Verlag, 1978
- 3) A. Yokoya *et al.*: *J. Synchrotron Radiat.*, **5**, p.10-16, 1998
- 4) N. Saito, I. H. Suzuki : *J. Synchrotron Radiat.*, **5**, p.869-871, 1998

5.4.4 Orientation selective surface photochemistry using linearly polarized synchrotron radiation

Tetsuhiro SEKIGUCHI, Yuji BABA, Iwao SHIMOYAMA, Guohua WU

1. Introduction

We have investigated the mechanism of synchrotron radiation (SR) induced fragmentation of surface molecules. In general, the interaction of the top-most surface molecules with underlayers plays an important role in the surface photofragmentation^{1,2}). The bond or molecular direction on the surface is also assumed to become a key factor. To understand the molecular-orientation effect on the fragmentation, we have used polarized SR. The linearly polarized light can excite molecules with any desired direction. We have measured the photofragments induced by polarized light, using the rotatable time-of-flight mass spectrometer (TOF-MS) which has been developed recently.

Here we report data on soft X-ray induced fragmentation of solid formic acid (HCOOH). We chosen HCOOH as a sample because it has different kinds of chemical bonds, each of which can be separately activated by tuning X-ray energy. We have measured the excitation-energy dependence of fragment desorption yields as a function of polarization angles of SR. Fragmentation pathways are discussed on the basis of observed anisotropic desorption spectra.

2. Experimental

The SR-incidence-angle dependence of the fragment-ion yields was measured with the rotatable TOF-MS device [Fig. 1] which comprises a pre-electrode for ion acceleration, field-free drift tube, focusing optics, and microchannel plate detector (MCP). The polarization angle which is defined as the angle between electric field vector (E) and the surface normal can be changed by rotating the crystal around z-axis of the sample holder. The photoabsorption spectra were measured by the total electron yield (TEY) method. The thick layers of HCOOH were grown on the cleaned Si(100) substrate cooled at ~ 82 K.

3. Results and discussion

Figure 2 shows the photon-energy dependencies of H^+ -desorption probabilities as a function of the polarization angles at the carbon 1s core-excitation region. The desorption probability here means the desorption yields divided by the corresponding photoabsorption cross section. Among the fine structures the second peak (marked as $\sigma^*(C-H)$) corresponds to a transition into an unoccupied molecular orbital localized on C-H bond. Figure 2 shows that H^+ -ion yields for C 1s $\rightarrow \sigma^*(C-H)$ resonance are greatly increased when the E vector of the light becomes close to the surface normal. This indicates that C-H bonds standing upright have higher dissociation probabilities than those which lie in the surface. The present investigation will contribute to future realization of the control of chemical reaction using the polarized light.

References

- 1) T. Sekiguchi and Y. Baba, *Surf. Sci.*, **433-435**, 849 (1999)
- 2) T. Sekiguchi et al., *Surf. Sci.* **454-456**, 363 (2000); *ibid.* **454-456**, 407 (2000)

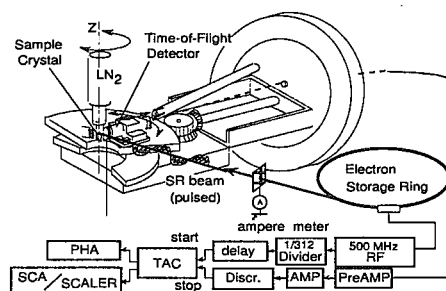


Fig. 1 Schematic drawing of a newly developed rotatable time-of-flight mass spectrometer for measuring polarization-dependent fragment-ion yields

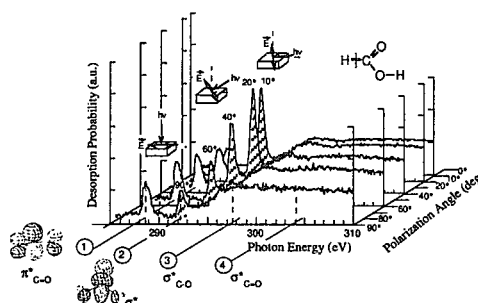


Fig. 2 The photon-energy dependence of H^+ -desorption probabilities with various polarization angles

5.5 Heavy atom science

5.5.1 Performance of soft X-ray emission spectrometer employing CCD camera

Teikichi A. SASAKI, Nobuhiko CHUGAN^{a)}, Yasuji MURAMATSU

a) Faculty of Science, Himeji Institute of Technology

1. Introduction

SXES (soft X-ray emission spectroscopy) provides a useful information on the electronic states in valence band region of solids. The spectroscopy, however, requires intense soft X-rays for the excitation because of its low spectral intensity. Thus the measurements have been mainly done by employing monochromatized soft X-rays from the third-generation SR facilities. On the other hand, improvement in the detection efficiency of the detector has been an important subject. Recently, it has been suggested that a CCD camera provides a quite high efficiency in the soft X-ray region¹⁾. We report performance of a new spectrometer employing a CCD.

2. Experimental

The optical system of the spectrometer consists of entrance micro-slit, spherical grating-monochromator and back-illuminated CCD detector which are arranged along the Rowland circle with a radius of 1m. Performance of the spectrometer was examined by the use of a low energy electron-gun as an excitation source. Density of the electron current was about 0.8 mA/cm² on a sample surface. Pressure during the irradiations was better than 4×10^{-8} Torr. In order to reduce the reflections of electrons into the analyzer chamber irradiations were done with 80° to the sample surface and angle between the incident electrons and emitted soft X-rays was 90°. Line spectrum on the detector was converted into an energy spectrum by integration of the line intensity. For the spectral references some SXES experiments using the same samples were done at BL 8.0.1 of the Advanced Light Source (ALS) in Lawrence Berkeley National Laboratory, where the MCP detector is employed for SXES.

3. Results

The spectral profiles of metal $L_{2,3}$ emission lines observed for the transition metals (Ti, V, Fe, Cr, Mn, Co, Ni, Cu and Zn) were in good agreement with those previously observed. Dependences of the FWHM values on the width of the microslit are shown in Fig. 1 for Ni L_3 line of Ni metal. It is clearly shown that 7 – 12 μm slit width is favorable for the well-resolved spectral measurements. Thus the most measurements were made by the use of the microslit with 7.3 μm or 15.0 μm width. Figure 2 shows Co $L_{2,3}$ SXES spectra of CoO crystal. The lowest profile is metal-d partial density of state (p-DOS) calculated by DV X_α method. The peak width, 4.3 eV for Co L_3 line in FWHM taken by the CCD camera, is almost the same as that by the MCP detector. The tailings in the peak profile by the CCD camera are probably due to inelastic energy loss of the incident electrons in the solid. The result suggests better resolved profile is expected for the CCD camera when combined with the SR excitation. We have also observed a phenomenon similar to elastic scattering of photons when the Ni L_3 core-level is resonantly excited by electrons with the energy of the absorption edge.

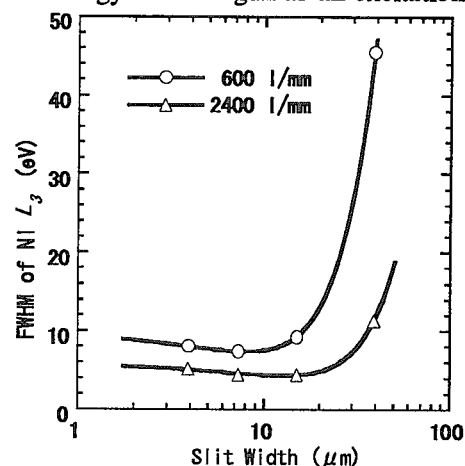


Fig. 1 Dependences of FWHM values on the width of the microslit

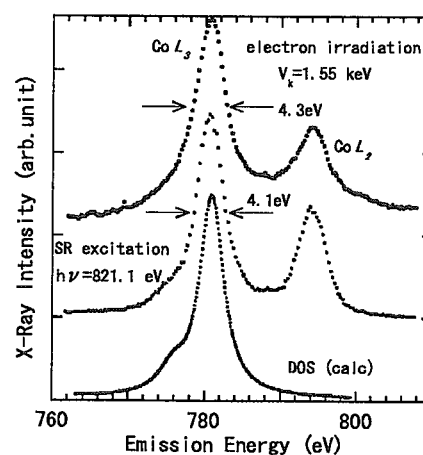


Fig. 2 Co $L_{2,3}$ SXES spectra of CoO

Reference

- 1) C.H. Skinner and J.L. Schwob, Appl. Optics 35 (1996) 4321

5.5.2 Probing bulk electronic states of solids by high-resolution photoemission spectroscopy

Yuji SAITOH, Akira SEKIYAMA ^{a)}, Shigemasa SUGA ^{a)}

a) Osaka University

1. Introduction

In this report we demonstrate the power of high-resolution Ce $3d$ - $4f$ resonant photoelectron spectroscopy (RPES) by applying it to the CeRu_2Si_2 in order to probe the bulk electronic states¹⁾. So far, various reports have been given for the studies of Ce compounds in that the hybridization of the strongly correlated $4f$ electrons with the conduction states is giving rise to unusual thermal, electric and magnetic properties partially scaled by the Kondo temperature, T_K . The CeRu_2Si_2 is a typical heavy fermion system, with $T_K \sim 22$ K. High-resolution PES provides a means of directly proving the electronic states particularly those near the Fermi level (E_F), but the short photoelectron mean free path associated with the low excitation photon energy ($h\nu$) conventionally used $4d$ - $4f$ RPES ($h\nu \sim 120$ eV) make this a surface sensitive technique. It has been reported that the Ce $4f$ states are remarkably different between the bulk and surface, originating from different strength of hybridization and a surface core-level shift. In view of its large bulk sensitivity, the Ce $3d$ - $4f$ RPES ($h\nu \sim 880$ eV) is a more direct and promising technique for revealing the bulk Ce $4f$ states. However the energy resolution of the most of the recent studies has been insufficient to obtain the detailed information in the vicinity of the E_F . In order to avoid this problem, we have constructed high-resolution photoemission system combined with a grating monochromator on the high-brilliance twin-helical undulator beamline BL25SU at SPring-8. The monochromator has been successfully commissioned in the $h\nu$ range between 200 and 1,800 eV. We have confirmed that the resolving power at 870 eV is in excess of 15,000, corresponding to the best result reported in this energy region²⁾.

2. Experimental

The high-resolution $3d$ - $4f$ RPES experiment was performed at BL25SU on single-crystal sample. The overall energy resolution was ~ 100 meV. The sample temperature was set to 20 K. The result was compared with the high-resolution $4d$ - $4f$ spectrum measured at BL-3B of Photon Factory with a resolution of 50 meV.

3. Results and discussion

The high-resolution spectra near E_F are shown in Fig. 1. As shown in the figure, the two spectra differ greatly. The two structures of $3d$ - $4f$ spectrum are assigned to the bulk $f_{5/2}^1$ and $f_{7/2}^1$ final state; in other words, from the tail of Kondo peak and spin-orbit partner, as predicted from single impurity Anderson model. The observation of such a strong tail of the bulk Kondo peak has been made possible by the bulk-sensitive $3d$ - $4f$ RPES technique with an unprecedentedly high resolution of 100 meV. The two peaks in the $4d$ - $4f$ spectrum can be assigned in the same manner, but to the surface $f_{5/2}^1$ and $f_{7/2}^1$ final states resulting from the weaker hybridization effect in the surface.

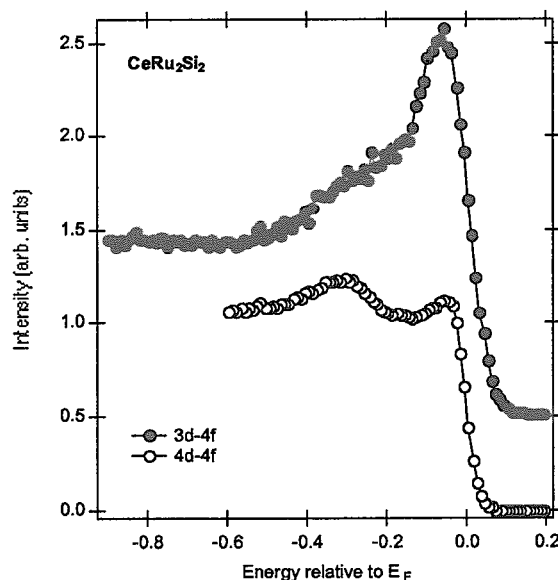


Fig. 1 High resolution RPES spectra of CeRu_2Si_2

References

- 1) A. Sekiyama, T. Iwasaki, K. Matsuda, Y. Saitoh, Y. Onuki and S. Suga, *Nature* **403**, 396 (2000)
- 2) Y. Saitoh, H. Kimura, Y. Suzuki, T. Nakatani, T. Matsushita, T. Muro, T. Miyahara, M. Fujisawa, K. Soda, T. Muro, S. Ueda, H. Harada, A. Sekiyama and S. Suga, *Rev. Sci. Instrum.*, in press (2000)

5.6 Electronic material science

5.6.1 Photoelectron spectroscopy for strongly correlated electron systems

Tetsuo OKANE, Shinichi FUJIMORI, Akihiro INO, Atsushi FUJIMORI^{a)}

a) JAERI Kansai and Department of Physics, University of Tokyo

1. Introduction

Photoelectron spectroscopy (PES) is a powerful experimental technique to investigate the electronic structure of materials. Recently, a remarkable improvement in the energy resolution of an electron energy analyzer has opened a new research field in the study of strongly correlated electron systems. For example, using PES with an energy resolution better than 10 meV one can find out very fine structures near the Fermi edge, which play a dominant role in the mechanism of the physical properties of strongly correlated electron systems.

We have constructed a photoelectron spectrometer at SPring-8, and made some measurements to estimate its performance.

2. Instrumentation

Our photoelectron spectrometer is composed of an electron energy analyzer, a vacuum-ultra-violet (VUV) photon source, a sample manipulator, a sample cooling system, a sample transfer system, and vacuum chambers. The electron energy analyzer is a commercial one; GAMMADATA-SCIENTA SES2002, which has an ultimate energy resolution of 1.5 meV. The VUV photon source GAMMADATA-SCIENTA VUV5000 provides highly brilliant radiation of He I line and He II line. Sample can be cooled down to 14 K with the sample cooling system using a closed-cycle He refrigerator.

This spectrometer will be installed in the beamline BL23SU of SPring-8, which is a special beamline to be available for actinide materials.

3. Results

We measured PES spectra of the evaporated Gold film to estimate the energy resolution of the spectrometer. The sample was cooled down to 16 K. The result is shown in Fig. 1. The achieved energy resolution of the electron energy analyzer is better than 3 meV.

To check the performance of the spectrometer in angle-resolved photoelectron spectroscopy (ARPES), we measured cleaved samples of highly-oriented pyrolytic graphite (HOPG). As shown in Fig. 2, we could simultaneously measure ARPES spectra in the range of $\pm 7^\circ$ of electron emission angle with an angular resolution better than 1° .

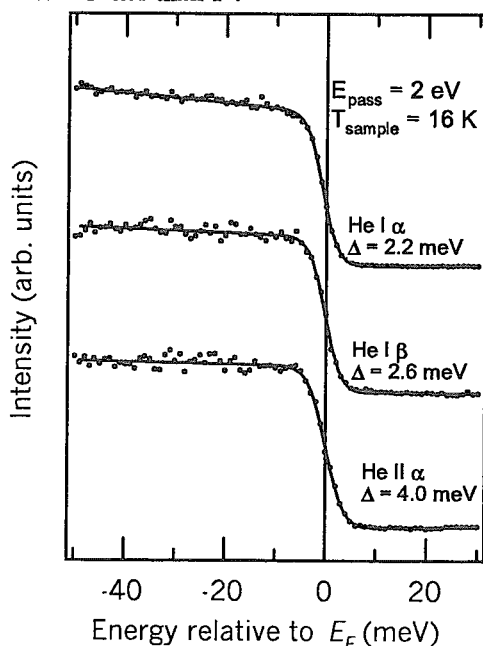


Fig. 1 PES spectra of the Gold film near Fermi edge

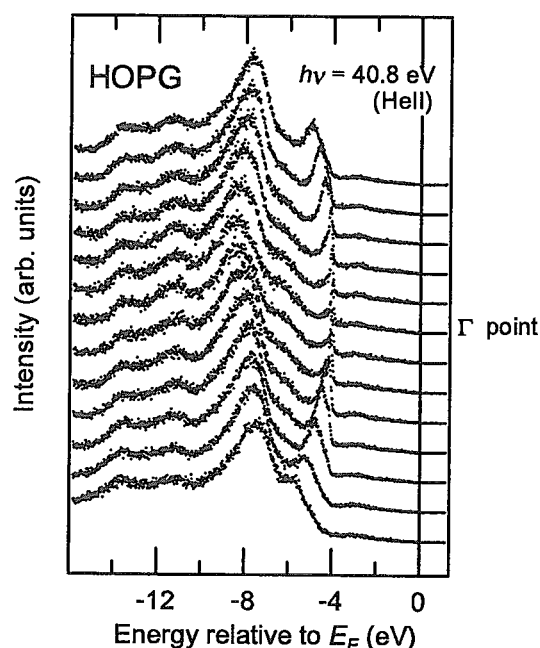


Fig. 2 ARPES spectra of HOPG

5.6.2 Synchrotron Radiation Mössbauer spectroscopy of BL11XU in SPring-8

Takaya MITSUI

1. Introduction

Synchrotron Radiation Mössbauer spectroscopy (SRMS; time spectrum and inelastic nuclear resonant scattering) enables us to study electronic state and lattice dynamics of a target material. In these experiments, we can use the excellent beam properties of synchrotron radiation. (Polarization, pulse structure, and small beam size etc.). It promises us many unique studies on material science. In order to progress these studies, the unique experimental apparatus for SRMS is installed in BL11XU of Spring-8, and some interesting experimental results are already acquired.

2. Facilities

The experimental apparatus for SRMS is composed of three devices as follows. (See Fig. 1)

(A) 14.4 KeV monochromatic X-ray generator

14.4 KeV monochromatic X-ray generator is prepared to perform SRMS experiments using ^{57}Fe nuclei without temperature instability and contact accidents during user experimental setup. It is composed of in-vacuum table and some built-in devices; high precision goniometers, and high energy-resolution monochromator (HRM). As a HRM, two channel cut crystals Si (975) x Si (511) are used. The characteristics of the X-ray beam at 14.4 KeV under 93.9 mA of ring current are as follows; the beam size is $1.8 \times 0.5 \text{ mm}^2$, the energy resolution is 3.5 meV, and the photon flux is 9.2×10^9 photons/sec.

(B) Air pad table

For multipurpose SRMS experiments, an air pad table is prepared. The air pad career to set goniometer and some experimental devices can float on the stage by compressed air, and user can move these devices to free position. It provides an advantage for the experiment, which requires complex device arrangement.

(C) Cryostat

In order to achieve SRMS experiments at low temperatures and with high magnetic fields, a liquid-He cryostat with a superconducting magnet will be installed. By using this device, the temperature of the sample can be controlled from 7 K to room temperature by a flow of gaseous He, a magnetic field up to 6 T can be applied at the sample position.

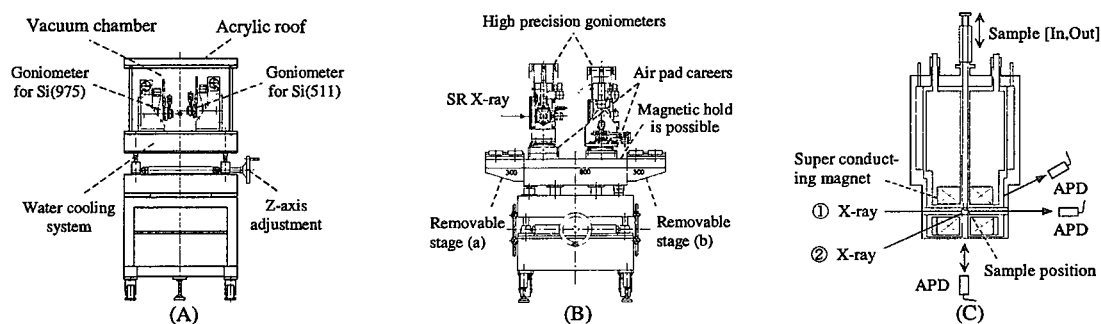


Fig. 1 A schematic view of the experimental apparatus for SRMS

3. Research activities

As recent our SRMS research group activities, the existence of local vibration mode of dilute Fe atom in the Al and Cu matrixes was proved clearly. The speed up effects of the time spectrum was studied in relation to the magnetic phase transition, too. Furthermore, our group realized the nuclear excitation of ^{40}K nuclei by using synchrotron radiation¹⁾. ^{40}K atom is one of the most important elements in material and biological sciences. But, the measurement of the traditional Mössbauer spectroscopy of ^{40}K was very difficult, because, this atom could not be populated by any radioactive parent nuclide. On the other hands, our experimental result indicates the possibility of the easy measurement of the Mössbauer spectrum for ^{40}K contained materials by using a third generation synchrotron radiation.

Reference

- 1) M.seto, S.Kitao, Y.Kobayashi, R.Haruki, T.Mitsui, Y.Yoda, X.W.Zhang, and Yu.Maeda, Phys. Rev. Lett.17, 566 (2000)

5.7 Experimental facilities development

5.7.1 Investigation of an effect of gas bremsstrahlung due to stored electron beam condition of SPring-8

Yoshihiro ASANO, Toru MATSUMURA ^{a)}

a) Advanced Science, Osaka University

1. Introduction

Gas bremsstrahlung is generated through interaction of the stored electrons with residual gas molecules in a storage ring vacuum chamber. Including high energy photons, gas bremsstrahlung directly creeping into the beamlines, can be an important issue for the safety design of the beamlines in synchrotron radiation facilities. At the straight sections for insertion devices of the 8 GeV class synchrotron radiation facility, SPring-8, the gas bremsstrahlung can be a serious radiation source because of its extremely high intensity and high energy. The detailed study of the gas bremsstrahlung is, therefore, required especially for third generation synchrotron radiation facilities. Furthermore, the gas bremsstrahlung production distribution and the dose rate due to gas bremsstrahlung should strongly depend upon the stored electron beam conditions, but the characteristics of the beam conditions were ignored until now.

2. Experiments and calculations

The gas bremsstrahlung was measured as a function of the aperture size of the photon beam, by using a new type scintillation crystal, PbWO_4 (PWO) array, shown in Fig. 1. The PWO detector has the good performance for measuring the high energy gas bremsstrahlung photon because of its short radiation length and fast decay time. The measurements were performed at the high betatron function beamline, BL11XU (average beam size and divergence of horizontal axis are $3.6_6 \times 10^{-4}$ m and $4.9_7 \times 10^{-5}$ radian, respectively), and the low betatron function beamline, BL46XU (average beam size and divergence of horizontal axis are $2.6_5 \times 10^{-4}$ m and $9.4_3 \times 10^{-5}$ radian, respectively). The measurements were compared with the Monte Carlo simulations by using EGS4 considering the electron beam sizes and beam divergences. The dose rate due to gas bremsstrahlung also estimated

3. Results

Figure 2 shows the measurements of the gas bremsstrahlung spectra as a function of the aperture size defined by using the X-Y slit of the beamline, BL11XU. The measured intensities at the beamline, BL46XU, were obtained to be about 36% lower than that of the beamline BL11XU. The calculations considering the beam size and beam divergence distribution agree fairly well with the measurements in both beamlines. Based on the measurements, the effective doses due to gas bremsstrahlung were obtained in anterior-posterior irradiation geometry considering the beam size and divergence, and the scoring area dependence were also investigated. As a result, the effective dose with the stored beam of high-betatron function at 40 m distance from the center of the straight section was estimated to be 15.8 nSv/s/10nPa/mA for scoring area with 0.023 cm in radius, 9.22 nSv/s/10nPa/mA for the low betatron function beamline1).

Reference

1) Y.Asano et al., in press (Nucl. Instr. Method in Physics Research A451 No.3 (2000))

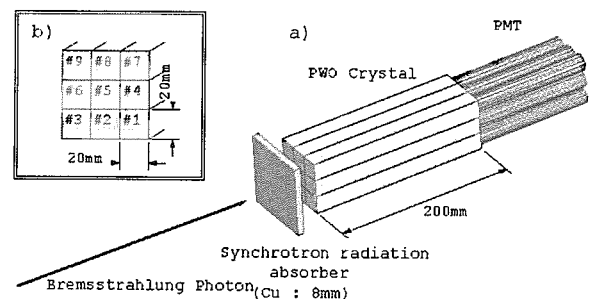


Fig. 1 Illustration of the PWO calorimeter which consists of nine crystals

The size of the crystal is 20 mm square in width and 200 mm in length.

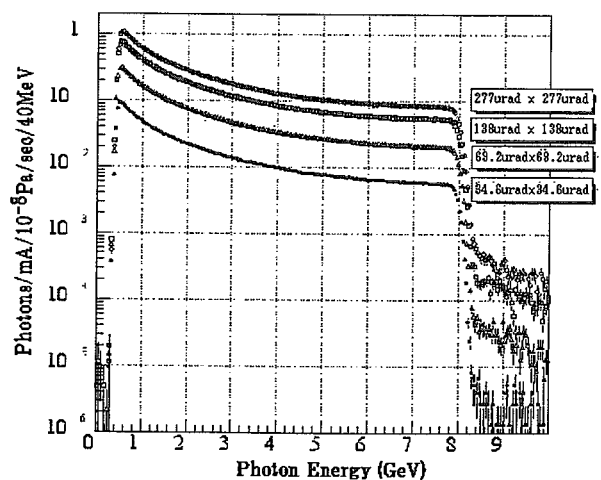


Fig. 2 The spectra of gas bremsstrahlung for the various aperture sizes of X-Y slit at the BL11XU beamline

5.7.2 Development of X-ray beam position monitor for bending magnet beamline at SPring-8

Hideaki SHIWAKU

1. Introduction

Development of an X-ray beam monitor has been studied to measure the photon beam position from bending magnet source at SPring-8. We adopted the X-ray beam monitor by use of a photoemission device because of its stability and easy to insert it into a vacuum chamber in a beamline.

The X-ray beam monitor has a type of a two-split triangular electrode made of tungsten blades as a detector¹⁾. This beam monitor also consists of a water cooling system, an electrical shielding box that is made of copper, a linear actuator, a pulse motor with a harmonic gear reducer, a rotary encoder, a vacuum chamber, and an x-axis stage. It is estimated that temperature of tungsten blades will increase to about 110 degree by X-ray irradiation of normal power density from the bending magnet at SPring-8. The beam monitors were settled in front-end of beamlines at about 12 m and/or 19 m far from X-ray source point.

Fundamental characters and capability of the X-ray beam monitor was evaluated at the beginning of the beamline commissioning.

2. Principle of detector

Figure 1 shows a principle of the detector. The two-split triangular blade is irradiated by synchrotron radiation (SR), and then photo-electron which occurred on blade was detected as a current. The blade was made of tungsten, with the size of 50 mm wide, 46 mm high and 0.3 mm thickness. Not so as to be affected by the beam direction change, the blades have slightly sloped of 2/50 against ideal beam axis.

Beam position is calculated by the following equation,

$$Y = A \frac{I_U - I_D}{I_U + I_D}$$

where Y is beam position, A is a conversion coefficient, I_U is a signal intensity from the upper blade, and I_D is a signal intensity from the lower blade.

3. Experimental and Results

Fundamental characters, for example a relation of applied bias voltage versus signal intensity, setting of optimum position of the blade, estimation of a conversion coefficient, spatial resolution, and long time stability, were measured at several beamlines.

In the relationship between the applied high voltage to the detector and the signal intensity, the signal intensity increased with applying bias voltage, and then it saturated in the region more than 200 V. The signal intensity was about 18 μ A at 18 mA R.C. The linearity of signal intensity within the position from -3 mm to +3 mm in Y-axis direction was very good.

Figure 2 shows the stability of the beam position monitor, which collected signal every 3 seconds. Standard deviation of the beam position was $\sigma = 2.2 \mu$ m.

I have designed and optimized the beam position monitor with the two-split triangular electrode. Spatial resolution was about $\sigma = \sim 3 \mu$ m, but its spatial resolution included an influence of the periodical motion noise in ~ 15 minutes interval. Original mechanical spatial resolution was less than 1 μ m. The upper and lower blades as the detector cut off SR beam about less than 0.1 mrad in this beam position monitor. I have a plane to minimize cut off area in the new beam position monitor.

Reference

- 1) T. Mitsuhashi et al., Rev. Sci. Instrum. 63, 534 (1992)

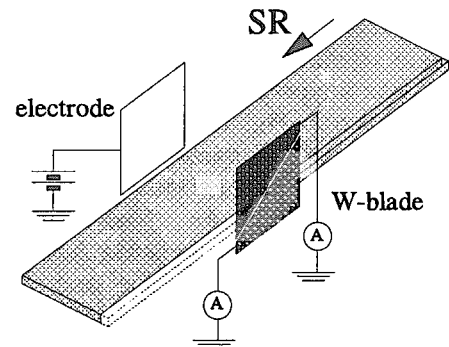


Fig. 1 Principle of the detector

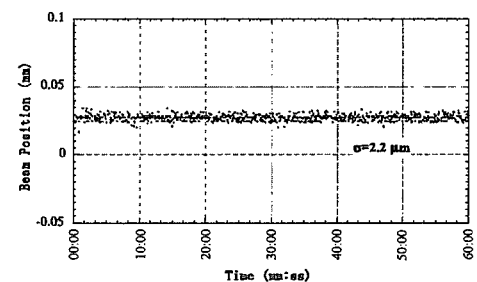


Fig. 2 Stability of the beam position monitor

6. List of publications

6.1 List of publications on Advanced Photon Research Center

High peak power laser development (Laser System Development Group)

1. Journal

- 1) Regenerative pulse shaping and amplification of ultrabroadband optical pulses
C. P. J. Barty, G. Korn, F. Raksi, C. Rose-Petruck, K. Yamakawa, et al.
Optics Letters, vol. 21, 219-221, 1996
- 2) Enhancement of soft X-ray output from a pinch plasma using a rotating plasma for pre-ionization
A. Ohzu
Optics and laser technology, 2000
- 3) Wave-front measurements of terawatt-class ultrashort laser pulses by the Fresnel phase-retrieval method
S. Matsuoka, K. Yamakawa
Journal of the Optical Society of America, B, 17, 663-667, 2000
- 4) All-solid-state mirror-dispersion controlled sub-10 fs Ti:sapphire laser
K. Yamakawa, M. Aoyama, T. Itoh, and Ch. Spielmann
Japanese Journal of Applied Physics, vol. 35, L989-991, 1996
- 5) Generation of 18-fs, multiterawatt pulses using regenerative pulse shaping and chirped pulse amplification
C. P. J. Barty, T. Guo, C. Le Blanc, F. Raksi, K. Yamakawa, et al.
Optics Letters, vol. 21, 668-670, 1996
- 6) Separation of an isotope as a precursor of a gamma ray laser medium
T. Arisawa, M. Miyabe, A. Sugiyama, K. Yamazaki, A. Ohzu, Y. Suzuki, K. Akaoka, I. Wakaida, Y. Maruyama
Hyperfine Interactions 107, 101-128, 1997
- 7) Ultra short pulse and ultra high peak power titanium sapphire laser (in Japanese)
K. Yamakawa
Laser Eng. Soc. Res. Report, 21 -27, 1997
- 8) Noise characterization of an all-solid-state mirror-dispersion-controlled 10-fs Ti:sapphire laser
M. Aoyama and K. Yamakawa
Optics Communications, vol. 140, 255-258, 1997
- 9) Laser diode-pumped high repetition rate, high energy Nd:YAG Laser
M. Kato, Y. Maruyama, S. Harayama, M. Ooba
Optical Society of America Topics Vol.19 Advanced Solid State Lasers, 19, 310-313, 1998
- 10) Ultra high-peak and high-average power chirped-pulse amplification of sub-20-fs pulses with Ti:sapphire amplifiers
K. Yamakawa, M. Aoyama, S. Matsuoka, H. Takuma, C. Barty, D. Fittinghoff
IEEE J. Sel. Top. Quantum Electron., 4(2), 385-394, 1998
- 11) Diode pumped 250-W zigzag slab Nb:YAG oscillator-amplifier system
K. Tei, M. Kato, Y. Niwa, S. Harayama, Y. Maruyama, T. Matoba, T. Arisawa
Opt. Lett., 23(7), 514-516, 1997
- 12) Sub 10fs mode lock titanium sapphire laser using chirped mirror
M. Aoyama, K. Yamakawa
Oyo-Butsuri, 67(9), 1072-1073, 1997
- 13) Effect of gas convection induced by cross-field discharge in copper vapor laser
A. Ohzu, M. Kato, Y. Maruyama
Optics and laser technology, 31, 505-509, 1999
- 14) Growth of dendrites in a large bore HyBrID copper vapor laser
A. Ohzu, M. Kato, Y. Maruyama
Optics and laser technology, 32, 101-105, 2000
- 15) Efficient discharge pumping of a copper vapor laser using a cylindrical grid electrode
A. Ohzu, M. Kato, Y. Maruyama
Rev. Sci. Instrum., 71, 2288-2291, 2000

- 16) Influence of Cs and Ag metal vapor on output characteristics of a HyBRID copper vapor laser
A. Ohzu, M. Kato, Y. Maruyama
Appl. Phys. Lett. , 76, 2979-2981, 2000
- 17) Comparative study of gas composition in a low temperature operated copper vapor laser
A. Ohzu, M. Kato, Y. Maruyama
Opt. Commun., 177, 355-361, 2000
- 18) High-repetition-rate 2-J Nd:YAG oscillator-amplifier system
K. Tei, M. Kato, F. Matsuoka, Y. Niwa, Y. Maruyama, T. Matoba, T. Arisawa
Optical Engineering 39(1), 320-322, 2000
- 19) Nd:YAG oscillator-amplifier system with a passive ring self-pumped phase-conjugate mirror
K. Tei, F. Matsuoka, M. Kato, Y. Maruyama, T. Arisawa
Optics Letters, 25(7)481-483, 2000
- 20) Generation of 16 fs, 10 TW pulses at a 10 Hz repetition rate with efficient Ti:sapphire amplifiers
K. Yamakawa, M. Aoyama, S. Matsuoka, H. Takuma, C. P. J. Barty, et al.
Optics Letters, vol. 23, 525-527, 1998
- 21) Development of a Model for Chirped-Pulse Amplification of sub-20 fs Laser Pulses
S. Matsuoka and K. Yamakawa
Japanese Journal of Applied Physics, vol.37, pp. 5997-6000, Part 1, 1998
- 22) 100 TW, sub-20 fs Ti:sapphire laser system operating at a 10 Hz repetition rate
K. Yamakawa, M. Aoyama, S. Matsuoka, T. Kase, Y. Akahane, et al.
Optics Letters, vol.23, pp. 1468-1470, 1998
- 23) Ensuring Compactness Reliability and Scalability for the Next Generation of High-Field Lasers
J. Nees, S. Biswal, F. Druon, J. Faure, M. Nantel, G. Mourou, A. Nishimura, H. Takuma, J. Itatani,
J. C. Chanteloup, C. Honninger
IEEE J. of Sel. Top. Quantum Electron., 4, 376-384, 1998
- 24) Ytterbium-doped glass regenerative chirped-pulse amplifier
S. Biswal, J. Nees, A. Nishimura, H. Takuma, G. Mourou
Opt. Commun., 160, 92, 1999
- 25) High-repetition rate 1-J green laser system
K. Tei, M. Kato, Y. Maruyama, F. Matsuoka, Y. Niwa, Y. Maruyama, T. Matoba, T. Arisawa
Appl. Opt., 38(21), 4548-4551, 1999
- 26) Contrast and phase characterization of a high-peak power 20-fs laser pulse
M. Aoyama, A. Sagisaka, K. Yamakawa, et al.
Appl. Phys., B70, S149-S153, 2000
- 27) Diffusion bonded KTiOPO₄ crystal for the second harmonic generation of high average power zigzag slab Nd:YAG laser
K. Tei, M. Kato, F. Matsuoka, Y. Niwa, Y. Maruyama, T. Matoba, T. Arisawa
JJAP, Part 2, Lett. 38 (1AB) L35-L37
- 28) Wavefront Reconstruction from Intensity Measurements Using Fresnel Phase Retrieval Method
S. Matsuoka, K. Yamakawa
Japanese Journal of Applied Physics, vol. 38, pp. 114-116, Part 2, 1999
- 29) Numerical analysis of type I third-harmonic generation through third-order and cascading second-order nonlinear optical processes
T. Zhang, K. Yamakawa
Japanese Journal of Applied Physics, 39, 91-95, 2000
- 30) A 50-EW/cm² Ti:sapphire laser system for studying relativistic light-matter interactions
B. C. Walker, C. Toth, D. Fittinghoff, T. Guo, K. Yamakawa, et al.
Optics Express, vol. 5, 196-202, 1999
- 31) Highly efficient second-harmonic generation in novel four pass quadrature frequency conversion
H. Kiriya, S. Matsuoka, Y. Maruyama, T. Arisawa
Nuclear Instruments & Methods in Physics Research, 1999
- 32) High-efficiency second-harmonic generation in four pass quadrature frequency conversion scheme
H. Kiriya, S. Matsuoka, Y. Maruyama, T. Arisawa
Optics Communications, 174(2000)499
- 33) Ring self-pumped phase conjugator for high energy pulses at 1064 nm with rhodium-doped BaTiO₃
K. Tei, Y. Niwa, M. Kato, Y. Maruyama, T. Arisawa

JJAP, 38, 5885-5887, 1999

2. Proceedings

- 1) Techniques for controlling of gain narrowing during ultrashort pulse amplification
K. Yamakawa, T. Guo, G. Korn, C. Le Blanc, F. Raksi, et al.
SPIE Proc. of Generation, Amplification, and Measurement of Ultrashort Laser Pulses III, vol. 2701, 198-208, 1996
- 2) Ultra short pulse and ultra high peak power titanium sapphire laser (in Japanese)
K. Yamakawa
JIEE Opto-Quantum device WG, OQD-96-14, pp. 29-38, 1996
- 3) Generation and amplification of 10fs in Titanium sapphire laser (in Japanese)
K. Yamakawa
J. of Laser Eng. Highly performance solid state laser and application, No. RTM-96-29, pp. 27-33, 1996
- 4) Ultrashort-pulse, ultrahigh-peak power Ti:sapphire lasers
C. P. J. Barty, T. Guo, C. Le Blanc, F. Raksi, K. Yamakawa, et al.
SPIE Proc. of Generation, Amplification, and Measurement of Ultrashort Laser Pulses III, vol. 2701, 84-96, 1996
- 5) Research Program at Kansai Advanced Photon Research Center
T. Arisawa, T. Matoba, T. Sasuga, K. Nakajima, K. Yamakawa
Proceedings of the International Conference on LASERS '96, p. 1-12, 1996
- 6) Sub-20-fs Multiterawatt Lasers and X-ray Applications
C. P. J. Barty, T. Guo, C. LeBlanc, C. Rose-Petruck, K. Yamakawa, et al.
Proc. of the 5th International Conference on X-Ray Lasers 1996, S. Svanberg and G. G. Wahlstrom Eds., Lund, Sweden: Bristol: IOP Publishing, 282-288, 1996
- 7) Multiterawatt femtosecond lasers for high field physics
C. P. J. Barty, C. L. Gordon III, S. E. Harris, B. E. Lemoff, K. Yamakawa, et al.
AIP conference Proc. of the Tamura Symposium on the Future of Accelerator Physics, No. 356, pp. 310-321, Edited by: T. Tajima, American Institute of Physics, 1996
- 8) Research program at Kansai Advanced Photon Research Center
T. Arisawa, T. Matoba, T. Sasuga, K. Nakajima, K. Yamakawa, A. Sasaki
Proc. of the International Conf. on LASERS '96, 1-12, Dec. 2-6, 1996, Portland, Oregon, USA
- 9) Development of ultra short pulse and ultra high peak power laser (in Japanese)
K. Yamakawa, Optoronica, No. 175, pp. 182-186, 1996
- 10) Regenerative pulse shaping: a new technique for ultrabroadband amplification
J. A. Squier, T. Guo, C. LeBlanc, G. Korn, K. Yamakawa, et al.
Ultrafast Phenomena X, Edited by: J. Fujimoto, W. Zinth, P. F. Barbara and W. H. Knox, Springer-Verlag, Berlin, vol. 62, 87-89, 1996
- 11) Sub-20-fs multiterawatt laser and ultrafast x-ray source
C. P. J. Barty, T. Guo, C. LeBlanc, C. Rose-Petruck, K. Yamakawa, et al.
Ultrafast Phenomena X, Edited by: J. Fujimoto, W. Zinth, P. F. Barbara and W. H. Knox, Springer-Verlag, Berlin, vol. 62, 77-78, 1996
- 12) Present status of Advanced Photon Research Program (in Japanese)
T. Matoba
Radiation, 23(3), 105-112, 1996
- 13) Present status of advanced photon science research program related to X-, and gamma-ray emission source development
T. Arisawa, T. Matoba, K. Yamakawa, Y. Maruyama, T. Sasuga, I. Wakaida, K. Nakajima, A. Sasaki, E. Minehara, M. Ohshima
Proc. of the first International Induced Gamma Emission Workshop, Aug. 16-22, 1997, Predeal, Romania
- 14) Ultra short pulse and ultra high peak power titanium sapphire laser (in Japanese)
K. Yamakawa
Laser Eng. Soc. Res. Report, 21st anniversary for Research Award, No. RTM-97-21, 21-27, 1997
- 15) Table top laser generating ultra high peak power (in Japanese)
K. Yamakawa

- JAERI Basic Science Note, vol. 4, No. 1, 2-5, 1997
- 16) LD-pumped 0.62J, 105W Nd:YAG green laser
M. Kato, Y. Maruyama, S. Harayama, Y. Niwa
Proc. of Solid State Lasers VII, 3265, 212-218, 1998
 - 17) Closed loop wavefront correction of Ti:sapphire chirped pulse amplification laser beam
Y. Maruyama, S. Harayama, K. Akaoka, K. Tei
Proc. of Solid State Lasers VII, 3265, 219-225, 1998
 - 18) Design and performance of a 100 TW, sub-20fs Ti:sapphire laser system
K. Yamakawa, S. Matsuoka, M. Aoyama, T. Kase, Y. Akahane, et al.
Proceedings of the 6th International Conference on X-Ray Lasers 1998, Institute of Physics
Conference series: No. 159, pp. 645-648, edited by Y. Kato, H. Takuma and H. Daido, Institute of
Physics, 1998
 - 19) Development of a high-peak and high-average power Ti:sapphire laser system
K. Yamakawa, M. Aoyama, S. Matsuoka, Y. Akahane, H. Takuma, et al.
AIP Conference Proceedings of the International Conference on Superstrong Fields in Plasmas, No.
426, 461-466, Edited by: M. Lontano, AIP Press, 1998
 - 20) Development of an Ultrafast High Intensity Laser Source
K. Yamakawa
Proceedings of the Environment-Conscious Innovative Materials Processing with Advanced Energy
Sources (ECOMAP-98), pp. 215-223, High Temperature Society of Japan, 1998
 - 21) Ultrahigh peak power lasers in the 10-fs regime
C. P. J. Barty, T. Guo, F. Raksi, C. Rose-Petruck, K. Yamakawa, et al.
Proceedings of Applications of High Field and Short Wavelength Sources VII, vol. 7, pp. 246-248,
OSA, 1998
 - 22) Ultrashort Pulse Amplification: A 10-fs Approach
K. Yamakawa
Proceedings of the 5th International Workshop on Femtosecond Technology, FST '98, pp. 29-32,
1998
 - 23) Generation of 100 TW, Sub-20fs Pulses at a 10 Hz Repetition Rate in Ti:Sapphire
K. Yamakawa, M. Aoyama, S. Matsuoka, T. Kase, Y. Akahane, et al.
Ultrafast Phenomena XI, W. Zinth, J. G. Fujimoto, T. Elsaesser and D. Wiersma Eds., Garmish-
Partenkirchen: Springer-Verlag, vol. 63, pp. 44-46, 1998
 - 24) High Energy Flashlamp Pumped Ti-sapphire Laser for Yb:glass CPA
A. Nishimura, A. Ohzu, A. Sugiyama, Y. Maruyama, T. Arisawa, H. Takuma, J. Nees, S. Biswal,
G. Mourou, E. Erickson, S. Owada, S. Satou
Proceedings of SPIE Symposium on Photonics West Lase1998, Vol. 3265, 234-241, 1998
 - 25) Thermal Lens Effects on Highly Pumped Yb:glass
A. Nishimura, K. Akaoka, A. Ohzu, A. Sugiyama, T. Usami, T. Matoba
SPIE-Proceedings, Vol. 3889, 414-419, 1999
 - 26) Yb:glass laser oscillation and wavefront measurements under high intensity pumping
A. Nishimura, A. Ohzu, A. Katsuaki, T. Usami, A. Sugiyama, T. Matoba
JIEE Opto-Quantum Device OQD-99-1-5, 25-28, 1999
 - 27) Present status of advanced photon science research program related to X-, and gamma-ray emission
source development
Y. Maruyama, T. Sasuga, A. Sasaki, K. Yamakawa
Proc. of the 1st International Induced Gamma Emission Workshop, 29-41, 1999
 - 28) Second harmonic generation of LD-pumped high repetition rate and high energy Nd:YAG laser using a
directly bonded KTP crystal
M. Kato, Y. Maruyama, F. Matsuoka, M. Ooba
Trends in Optics and Photonics; Advanced Solid-State Lasers, 26, 45-48, 1999
 - 29) All solid state high average power Ti:sapphire CPA laser
M. Kato, Y. Maruyama, F. Matsuoka, Y. Niwa
Trends Opt. Photo., 1999
 - 30) Development of compact and short wavelength X-ray lasers and brilliant short wavelength radiation
source based on free electron laser
T. Arisawa

- Proceedings of International Reading of Quantum Optics 99, 1999
- 31) High-efficiency, second-harmonic generation in four-pass quadrature frequency conversion
H. Kiriyaama, S. Matsuoka, Y. Maruyama, T. Matoba, T. Arisawa
Proceedings of First International Conference on Inertial Fusion Sciences and Applications IFSA'99, 1999
 - 32) Highly efficient second-harmonic generation using four pass quadrature frequency conversion
H. Kiriyaama, S. Matsuoka, Y. Maruyama, T. Matoba, T. Arisawa
Proceedings of Advanced High Power Lasers and Applications, 1999
 - 33) Development of compact and short wavelength X-ray lasers and brilliant short wavelength radiation sources based on free electron laseer
T. Arisawa
Proc. SPIE IRQO'99 Quantum Optics, 336-342, 1999
 - 34) Highly efficient second-harmonic generation in novel four pass quadrature frequency conversion
H. Kiriyaama, S. Matsuoka, Y. Maruyama, T. Arisawa
Proceedings of International Symposium on New Visions in Laser Beam Interaction, 1999
 - 35) High-efficiency second-harmonic generation in four pass quadrature frequency conversion scheme
H. Kiriyaama, S. Matsuoka, Y. Maruyama, Y.Kato, T. Arisawa
Proceedings of SPIE Symposium on Photonics West Lase 2000, 1999
 - 36) Ultra high peak femto second laser and its application
K. Yamakawa
O plus E, vol. 21, No. 9, 1137-1143, 1999

3. Patents

- 1) Frequency stabilization apparatus and method for single longitudinal frequency tunable laser oscillator, and laser oscillator and method for wavelength scanning
A. Sugiyama, T. Nakayama, M. Kato, Y. Maruyama, T. Arisawa
Application number: 08/638, 544
- 2) Power recovering apparatus
A. Ohzu
Patent number: 11-233861
- 3) Copper vapor laser oscillator
A. Ohzu
Patent number: 11-195848
- 4) Laser oscillator
A. Ohzu
Patent number: 11-220190
- 5) Multi pass wavelength conversion method
M. Ooba, Y. Maruyama, M. Kato
Patent number: 10-296803
- 6) Easy method for measurement of X-ray pulse energy
A. Ohzu
Patent number: 10-232758
- 7) Method for long path parpagation of laser beam in medium by controling wavefront
K. Akaoka, Y. Maruyama, T. Arisawa
Patent number: 10-254926
- 8) Method for pumping solido state lasers by laser diodes
H. Kiriyaama, Y. Maruyama, T. Arisawa
Patent number: 10-271570
- 9) Zig-zag slab type solid state laser oscillator and amplifier
H. Kiriyaama, Y. Maruyama, T. Arisawa
Patent number: 10-339779
- 10) Copper vapor laser oscillator
A. Ohzu
Application number: 09/181, 997
- 11) Laser oscillator

- A. Ohzu
Application number: 09/200, 865
- 12) Wavelength tuning method
H. Kiriya, Y. Maruyama, T. Arisawa
Application number: 11-231255
 - 13) Wavefront measurement method
S. Matsuoka, K. Yamakawa
Application number: 11-288301
 - 14) Method for short pulsed X-ray generation
A. Ohzu
Application number: 11-333641
 - 15) X-ray generation apparatus using metallic plasma discharge
A. Ohzu
Application number: 11-344574
 - 16) X-ray generation apparatus using rotating plasma discharge
A. Ohzu
Application number: 11-341656
 - 17) Method for correcting distorted image propagating through substances
K. Tei, F. Matsuoka, M. Kato, T. Arisawa
Application number: 200018340
 - 18) Method for detecting substance diffusing in the atmosphere using high repetition laser
Y. Maruyama, M. Kato, A. Ohzu, K. Akaoka, T. Baba
Application number: 11. 5. 26
 - 19) Method for generating short pulse light for compact and high average power apparatus
T. Arisawa, K. Deki, F. Matsuoka
Application number: 12. 5. 28
 - 20) Method for separating isotopes
T. Shibata, K. Ogura, T. Arisawa
Application number: 1972803
 - 21) Injection locking dye laser using grating as a coupler
T. Arisawa, Y. Maruyama, A. Sugiyama
Application number: 2024639
 - 22) Direct reprocessing method by laser
T. Arisawa, K. Akaoka
Application number: 2097367
 - 23) Dye laser oscillator
Y. Maruyama, M. Kato, T. Arisawa
Application number: 2059212
 - 24) Low temperature copper vapor laser
A. Ohzu, M. Kato, Y. Suzuki, T. Arisawa
Patent number: 5, 544, 191(USA)
 - 25) Laser for separating isotopes
T. Shimizu, T. Arisawa
Patent number: 2729708
 - 26) Method for generating low divergence laser beam
A. Ohzu, M. Kato, Y. Maruyama, T. Arisawa
Patent number: 2712066
 - 27) Frequency stabilization apparatus and method for single longitudinal frequency tunable laser oscillator,
and laser oscillator and method for wavelength scanning
A. Sugiyama, T. Nakayama, M. Kato, Y. Maruyama, T. Ariawa
Application number: 5, 701, 320 (USA)

X-ray laser development (X-ray Laser Research Group)

1. Journal

- 1) Propagation of a relativistic ultrashort laser pulse in a near-critical-density plasma layer
Keisuke Nagashima, Yasuaki Kishimoto, Hiroshi Takuma
Physical Review E 58 (1998) 4937
- 2) Ultrashort electron beam generation from resonantly excited nonlinear laser wakefield
Keisuke Nagashima, Yasuaki Kishimoto, Hiroshi Takuma
Physical Review E 59 (1999) 1263
- 3) The report of the 6th international conference on X-ray laser
Tetsuya Kawachi, Akira Sasaki, Hiroyuki Daido, Katsumi Midorikawa, Naohiro Yamaguchi
Journal of Plasma and Fusion Research, 75, No. 2, pp. 153-155 (1999)
- 4) Observation of X-Ray Spectra from nitrogen clusters irradiated with high-intensity ultrashort laser pulses
Sagisaka, H. Honda, K. Kondo, H. Suzuki, K. Nagashima, T. Kawachi, A. Nagashima, Y. Kato, H. Takuma
Applied Physics B70 549-554 (2000)
- 5) Fast Z-pinch optical guiding for X-ray generation and laser-plasma accelerators
T. Hosokai, M. Kando, H. Dewa, H. Kotaki, S. Kondo, N. Hasegawa, K. Horioka and K. Nakajima
Nuclear Instruments and Methode B
- 6) Optical guidance of terrawatt laser pulses by the implosion phase of fast Z-pinch discharge in a gas-filled capillary
T. Hosokai, M. Kando, H. Dewa, H. Kotaki, S. Kondo, N. Hasegawa, K. Horioka and K. Nakajima
Optics Letters (Optical Society America) vol. 25, 10 (2000)
- 7) Effect of multipulse waveform on Gains of Soft X-ray Lines of Lithium-like Aluminum in Recombining Plasmas
Kazunobu Okasaka, Tetsuya Kawachi, Hitoshi Oyama, Tamio Hara, Naohiro Yamaguchi and Kozo Ando
Jpn. J. Appl. Phys. Vol. 39 (2000) pp. 70-81

2. Proceeding

- 1) X-ray laser development activity in JAERI/Kansai
A. Nagashima, K. Nagashima, M. Kado, T. Kawachi, N. Hasegawa, M. Tanaka, T. Yamauchi, A. Sagisaka, T. Hosokai, Y. Suzuki, O. Yamashita, K. Sukegawa and Y. Kato
6th International Conference on X-ray lasers, (Kyoto Japan Aug. 1998)
Inst. Phys. Conf. Ser. No. 159 PROC X-ray Lasers 1998, P143 (1998)
- 2) X-ray Laser Gain Distribution in OFI Plasmas
M. Kado, K. Nagashima, A. Sagisaka, N. Hasegawa, M. Tanaka and Y. Kato
6th International Conference on X-ray lasers, (Kyoto Japan Aug. 1998)
Inst. Phys. Conf. Ser. No. 159 PROC X-ray Lasers 1998, P293 (1998)
- 3) Excited level populations of Li-like Aluminum Ions in a Low Temperature and Dense Recombining Plasma
T. Kawachi, C. Fujikawa, K. Ando, T. Hara and Y. Aoyagi
6th International Conference on X-ray lasers, (Kyoto Japan Aug. 1998)
Inst. Phys. Conf. Ser. No. 159 PROC X-ray Lasers 1998, P211 (1998)
- 4) Development of Plasma Waveguide using Fast Capillary Discharges
T. Hosokai, S. Kondo, M. Kando, M. Nakajima, K. Horioka and K. Nakajima
6th International Conference on X-ray lasers, (Kyoto Japan Aug. 1998)
Inst. Phys. Conf. Ser. No. 159 PROC X-ray Lasers 1998, P179 (1998)
- 5) Relaxation of Electron Energy Distributions and Population Inversion in Optical -Field -Ionized Plasmas
A. Sagisaka, K. Nagashima, M. Yamagiwa, T. Matoba and H. Takuma
6th International Conference on X-ray lasers, (Kyoto Japan Aug. 1998)
Inst. Phys. Conf. Ser. No. 159 PROC X-ray Lasers 1998, P289 (1998)
- 6) Application of fast imploding capillary discharge for laser wakefield acceleration
T. Hosokai, M. Kando, S. Kondo, H. Dewa, H. Kotaki, K. Horioka, K. Nakajima
Workshop on Beam Physics 1998 P475 (1998)
- 7) Application of fast imploding capillary discharge for laser wakefield acceleration
T. Hosokai, M. Kando, S. Kondo, H. Dewa, H. Kotaki, K. Horioka, K. Nakajima

- Yayoi Research Meeting, U. Tokyo, Proceeding p105 (1998)
- 8) Application of fast imploding capillary discharge for laser wakefield acceleration
Particle Accelerator Conference '99 (New York USA March 1999)
T. Hosokai, S. Kondo, M. Kando, H. Dewa, H. Kotaki, K. Horioka, and K. Nakajima
AIP PROC vol. 5, P3690-3692 (1999)
 - 9) Fast Z-pinch optical guiding for X-ray generation and laser-plasma accelerators
International Symposium on New Visions in Laser-Beam Interactions (October 11-15 1999 Tokyo Japan)
T. Hosokai, S. Kondo, M. Kando, H. Dewa, H. Kotaki N. Hasegawa, K. Horioka, and K. Nakajima
(Nuclear Instruments and Methode B (in press))
 - 10) Atomic processes involving doubly excited levels in a low temperature dense plasma -recombination x-ray laser-
T. Kawachi
International Seminar on Atomic Processes in Plasma, NIFS, Toki, Gifu, NIFS Report (in press)
 - 11) Atomic processes involving doubly excited levels in a recombination plasma
T. Kawachi
Symposium on Plasma effects restoration for Atomic Process, Phys. Soc. Of Japan, March, 2000, Osaka
 - 12) X-ray laser development in JAERI/Kansai
A. Nagashima, K. Nagashima, M. Kado, T. Kawachi, N. Hasegawa, M. Tanaka, T. Yamauchi, A. Sagisaka, T. Hosokai, Y. Suzuki, O. Yamashita, K. Sukegawa and Y. Kato, K. Takahashi, Y. Matsui, Y. Kato
JAERI-conf 2000-006
 - 13) Development of a CPA Nd:glass/Ti:sapphire laser system for generation of coherent x-ray laser radiation
Masataka Kado, Akira Nagashima, Keisuke Nagashima, Tetsuya Kawachi, Noboru Hasegawa, Momoko Tanaka, Tomonao Hosokai, Kota Sukegawa, Akira Sasaki, Yoshiaki Kato
Proceeding of SPIE vol. 3776, pp 242-248, 1999
 - 14) Development of tabletop transient collisional excitation x-ray lasers
Masataka Kado, Tetsuya Kawachi, Noboru Hasegawa, Momoko Tanaka, Kota Sukegawa, Keisuke Nagashima, Akira Nagashima, Yoshiaki Kato
Proceeding of SPIE vol. 3886, pp 278-284, 1999
 - 15) Design Study of High Repetition X-ray Laser Driver
K. Nagashima, A. Nishimura, H. Kiriya, Y. Kato
JAERI-conf 2000-006

3. Patent

- 1) Method of plasma channel formation for optical guiding using a Z-pinch discharge
T. Hosokai, and M. Kando
Application number: 11-202906

Free electron laser development (Free Electron Laser Research Group)

1. Journals

- 1) Optical Resonator Matching for JAERI FEL
Nobuyuki Nishimori, Eisuke Minehara, Masayoshi Sugimoto, Masaru Sawamura, Ryoji Nagai, Nobuhiro Kikuzawa
Review of Scientific Instruments, vol. 69 (1998), pp. 327-328
- 2) Precise experiment on n+d scattering at 12MeV
Nobuyuki Nishimori, Kenji Sagara, Tatsuru Fujita, Hiromichi Akiyoshi, Fumihiko Wakamatsu, Kazuhide Maeda, Hiroyuki Nakamura, Takao Nakajima
Nuclear Physics, A631 (1998), pp. 697C-700C
- 3) Recent Progresses and Preliminary Results of the Quasi-CW or Long Pulse Operation in the JAERI Superconducting rf Linac-Based FEL
Eisuke Minehara, Masayoshi Sugimoto, Masaru Sawamura, Ryoji Nagai

- Nobuhiro Kikuzawa, Nobuyuki Nishimori
Nucl. Instrum. Method., A407 (1998), II-p. 45
- 4) A Path toward the 1KW or higher FEL light output at the JAERI superconducting rf linac based FEL
Nobuyuki Nishimori, Eisuke Minehara, Masaru Sawamura, Ryoji Nagai, Nobuhiro Kikuzawa,
Masayoshi Sugimoto
Nucl. Instrum. Method. , A407 (1998), II-pp.23-24
 - 5) Path towards a 100kW class FEL using the JAERI superconducting rf linac driver
Eisuke Minehara, Masayoshi Sugimoto, Masaru Sawamura, Ryoji Nagai, Nobuhiro Kikuzawa,
Nobuyuki Nishimori, Toshihiko Yamauchi
Proceedings of SPIE Free Electron Laser Challenge 2, U.S.A., 1999, vol. 3614, pp. 62-71
 - 6) A 0.1KW class operation of the JAERI superconducting rf linac based FEL
Eisuke Minehara, Masaru Sawamura, Ryoji Nagai, Nobuyuki Nishimori, Masayoshi Sugimoto,
Nobuhiro Kikuzawa
Nucl. Instrum. Method., A429 (1999), pp. 9-11
 - 7) Design and performance of the JAERI superconducting linac for high-power free electron laser
Masaru Sawamura, Ryoji Nagai, Nobuhiro Kikuzawa, Masayoshi Sugimoto, Nobuyuki Nishimori,
Eisuke Minehara
Review of Scientific Instruments, 70(10), p. 3865-3868 (1999)
 - 8) Conceptual design of 20KW CW 1.5 micron industrial FEL
Eisuke Minehara
Proceedings of SPIE, Advanced High-Power Laser, Suita, 1999, vol. 3889, pp. 315-320
 - 9) JAERI superconducting rf linac based free electron laser facility
Eisuke Minehara, Toshihiko Yamauchi, Masayoshi Sugimoto, Masaru Sawamura, Ryoichi Hajima,
Ryoji Nagai, Nobuhiro Kikuzawa, Nobuyuki Nishimori, Toshiyuki Shizuma
Nucl. Instrum. Method., A445 (2000), pp. 183-186
 - 10) Design of energy recovery transport for the JAERI FEL driven by a superconducting linac
Ryoichi Hajima, Eisuke Minehara, Masaru Sawamura, Ryoji Nagai, Nobuhiro Kikuzawa, Nobuyuki
Nishimori, Masayoshi Sugimoto, Toshiyuki Shizuma, N. A.Vimokurov
Nucl. Instrum. Method., A445 (2000), pp. 384-388
 - 11) Improved performance of the JAERI injection and free electron laser system
Nobuyuki Nishimori, Eisuke Minehara, Masaru Sawamura, Ryoji Nagai, Nobuhiro Kikuzawa,
Masayoshi Sugimoto, Ryoichi Hajima, Toshiyuki Shizuma
Nuclear Instrument and Method, A445 (2000), pp. 432-436
 - 12) Dissociation Experiment of Dioxin by IR Laser Irradiation
Toshihiko Yamauchi, Eisuke Minehara, Nobuhiro Kikuzawa, Takehito Hayakawa, Masaru
Sawamura, Ryoji Nagai, Nobuyuki Nishimori, Ryoichi Hajima, Toshiyuki Shizuma,
Yasutaka Kamei, Hisato Ikai, Shinichi Itoh, Yukio Furukawa
Environmental Science 13(3) p. 383-390 (2000)

2. Proceedings

- 1) Measurement of variation in the micropulse spacing
Ryoji Nagai, Nobuyuki Nishimori, Masaru Sawamura, Nobuhiro Kikuzawa, Masayoshi Sugimoto,
Eisuke Minehara
Proceedings of the 22nd Linear Accelerator Meeting in Japan, Sendai, 1997, pp. 192-193
- 2) Intense Photon Generation ranging from FIR to Hard-X Rays by a High Current and Low-Energy
Electron Beam accelerated by an Electrostatic Acceleration
Eisuke Minehara
Proceedings of the 10th Tandem Accelerator and related technologies meeting, Tsukuba, 1997, pp.
56-59, Annual Report of NIES-TERRA vol. 2 1998
- 3) Pressure Control for Superconducting Accelerators at JAERI FEL
Nobuhiro Kikuzawa, Ryoji Nagai, Masaru Sawamura, Nobuyuki Nishimori, Eisuke Minehara
Proceedings of the 22nd Linear Accelerator Meeting in Japan, Sendai, 1997, pp. 194-195
- 4) Loss Monitor System for the JAERI Super Conducting RF Linac-Based FEL
Eisuke Minehara, Eiichi Tanaka, Masayoshi Sugimoto, Masaru Sawamura, Ryoji Nagai, Nobuhiro
Kikuzawa, Nobuyuki Nishimori
Proceedings of the 22nd Linear Accelerator Meeting in Japan, Sendai, 1997, pp. 343-344

- 5) Recent Progresses and Preliminary Results of the Quasi-CW Operation in the JAERI Superconducting RF Linac-Based FEL
Eisuke Minehara, Masayoshi Sugimoto, Masaru Sawamura, Ryoji Nagai, Nobuhiro Kikuzawa, Nobuyuki Nishimori, Eiichi Tanaka
Proceedings of the 22nd Linear Accelerator Meeting in Japan, Sendai, 1997, pp. 3132-3133
- 6) Measurement of energy resolution and electron beam current at JAERI FEL
Nobuyuki Nishimori, Ryoji Nagai, Masaru Sawamura, Nobuhiro Kikuzawa, Eisuke Minehara, Masayoshi Sugimoto
Proceedings of the 22nd Linear Accelerator Meeting in Japan, Sendai, 1997, pp. 341-342
- 7) Zero-Boil Off 2K and 4K cryostats and 3He and 4He refrigerator System for the JAERI superconducting rf Linac Driven FEL
Eisuke Minehara, Masayoshi Sugimoto, Masaru Sawamura, Ryoji Nagai, Nobuhiro Kikuzawa, Nobuyuki Nishimori
Proceedings of The Eighth Workshop on RF Superconductivity, Italy, 1997, pp. 233-234
- 8) Improvement of RF System of JAERI FEL Linac by Feed Forward
Masaru Sawamura, Nobuhiro Kikuzawa, Ryoji Nagai, Nobuyuki Nishimori, Masayoshi Sugimoto, Eisuke Minehara
Proceedings of the 22nd Linear Accelerator Meeting in Japan, Sendai, 1997, pp. 170-171
- 9) Intende Coherent Bremsstrahlung Light Source Utilizing Compact Electron Accelerators
Eisuke Minehara, Eiichi Tanaka
Proceedings of the 11th Symposium on Accelerator Science and Technology, Harima, 1997, pp.119-120
- 10) A Compact Closed Loop 2K He3 Refrigerator and Zero-Boil-Off Cryostat Design for the JAERI Superconducting RF Linac-Based-FEL
Eisuke Minehara, Masayoshi Sugimoto, Masaru Sawamura, Ryoji Nagai, Nobuhiro Kikuzawa, Nobuyuki Nishimori
Proceedings of the 11th Symposium on Accelerator Science and Technology, Harima, 1997, pp. 236-237
- 11) Coherent Bremsstrahlung Light Souce and FEL Driven by Small Electron Accelerators
Eisuke Minehara
Extended Abstrats of the 1997 Workshop on Beam Physics, Nishiharima, 1997, pp. 115-118
- 12) Long Pulse Operation of the JAERI Supercondunting RF Linac for FEL
Eisuke Minehara, Masayoshi Sugimoto, Masaru Sawamura, Ryoji Nagai, Nobuhiro Kikuzawa, Nobuyuki Nishimori, Eiichi Tanaka
Proceedings of the 11th Symposium on Accelerator Science and Technology, Harima, 1997, pp. 120-121
- 13) Beam Loss Monitor System for the JAERI Superconducting RF Linac-Based FEL
Eisuke Minehara, Eiichi Tanaka, Masayoshi Sugimoto, Masaru Sawamura, Ryoji Nagai, Nobuhiro Kikuzawa, Nobuyuki Nishimori
Proceedings of the 11th Symposium on Accelerator Science and Technology, Harima, 1997, pp. 444-445
- 14) Performance of Compact Refrigerators System for SRF Cavities in JAERI FEL
Nobuhiro Kikuzawa, Ryoji Nagai, Masaru Sawamura, Nobuyuki Nishimori, Eisuke Minehara, Yasuo Suzuki
Proceedings of The Eighth Workshop on RF Superconductivity, Italy, 1997, pp. 769-773
- 15) Performace of feed-forward circuit for the JAERI FEL superconducting linac
Masaru Sawamura, Nobuhiro Kikuzawa, Ryoji Nagai, Nobuyuki Nishimori, Masayosi Sugimoto, Eisuke Minehara
Proceedings of the 11th symposium on accelerator science and technology, Hyogo, 1997, pp. 200-202
- 16) First lasing of the JAERI FEL driven by the superconducting rf linac
Eisuke Minehara, Masayoshi Sugimoto, Masaru Sawamura, Ryoji Nagai, Nobuhiro Kikuzawa, Nobuyuki Nishimori
Proceedings of 19th Int. Linac Conf. (LINAC98), U. S. A., 1998, pp. 800-802
- 17) Voltage Stabilization of the Electron Gun for the JAERI FEL
Eisuke Minehara

- Proceedings of the 11th Tandem Accelerator and related technologies meeting, Tokyo, 1998, pp. 94-95.
- 18) First Lasing and Future Program of the JAERI High Power FEL Driven by the Superconducting rf Linac
Eisuke Minehara, Masayoshi Sugimoto, Masaru Sawamura, Ryoji Nagai, Nobuhiro Kikuzawa, Nobuyuki Nishimori, Toshihiko Yamauchi
Proceedings of the 23rd Linear Accelerator Meeting in Japan, Tsukuba, 1998, pp. 82-83
 - 19) Improvement of the electron gun at JAERI FEL
Nobuyuki Nishimori, Ryoji Nagai, Nobuhiro Kikuzawa, Eisuke Minehara, Masaru Sawamura, Masayoshi Sugimoto, Toshihiko Yamauchi, Takehito Hayakawa
Proceedings of the 23rd Linear Accelerator Meeting in Japan, Tsukuba, 1998, pp. 130-132
 - 20) First Lasing of JAERI FEL Driven by Superconducting RF LINAC
Ryoji Nagai, Nobuyuki Nishimori, Nobuhiro Kikuzawa, Masaru Sawamura, Masayoshi Sugimoto, Eisuke Minehara
Extended Abstracts (The 61st Autumn) Meeting 1998 The Japan Society of Applied Physics, Hiroshima, 1998, p. 925
 - 21) Improvement of RF System of JAERI FEL Superconducting Linac
Ryoji Nagai, Nobuyuki Nishimori, Nobuhiro Kikuzawa, Masaru Sawamura, Masayoshi Sugimoto, Eisuke Minehara
Proceedings of the 23rd Linear Accelerator Meeting in Japan, Tsukuba, 1998, pp. 217-218
 - 22) Optical Characteristics of the JAERI FEL
Nobuhiro Kikuzawa, Ryoji Nagai, Nobuyuki Nishimori, Toshihiko Yamauchi, Masaru Sawamura, Eisuke Minehara
Proceedings of the 23rd Linear Accelerator Meeting in Japan, Tsukuba, 1998, pp. 332-333
 - 23) Free Electron Laser Driven by the Superconducting rf Linac
Eisuke Minehara, Masayoshi Sugimoto, Masaru Sawamura, Ryoji Nagai, Nobuhiro Kikuzawa, Nobuyuki Nishimori, Takehito Hayakawa, Toshihiko Yamauchi
Bulletin of the 1998 fall meeting of the Atomic Energy Society of Japan, Fukui, 1998, I-p. 3
 - 24) Current Status and Future Plans of the JAERI Superconducting rf Linac based Free Electron Laser
Eisuke Minehara, Masayoshi Sugimoto, Masaru Sawamura, Ryoji Nagai, Nobuhiro Kikuzawa, Nobuyuki Nishimori, Toshihiko Yamauchi
Proceedings of the Eighth Topical Meeting on Free Electron Laser and High Power Radiation, Tokai, 1998, pp. 121-136.
 - 25) JAERI high power FEL driven by the superconducting rf linac
Eisuke Minehara, Masayoshi Sugimoto, Masaru Sawamura, Ryoji Nagai, Nobuhiro Kikuzawa, Nobuyuki Nishimori, Toshihiko Yamauchi
Proceedings of Int. Symp. On Environment-conscious Innovative Materials Processing with Advanced Energy Sources (ECOMAP-98), Kyoto, 1998, pp. 504-508
 - 26) Experimental Plan of Laser Application on JAERI FEL
Toshihiko Yamauchi, Eisuke Minehara, Nobuhiro Kikuzawa, Nobuyuki Nishimori, Ryoji Nagai, Takehito Hayakawa, Masaru Sawamura
Proceedings of the Eighth Topical Meeting on Free Electron Laser and High Power Radiation, Tokai, 1998, pp. 203-214
 - 27) Recent performance of the JAERI superconducting linac for FEL
Masaru Sawamura, Ryoji Nagai, Nobuhiro Kikuzawa, Nobuyuki Nishimori, Eisuke Minehara
Proceedings of the 19th Int. Linac Conf. (LINAC98), U. S. A., 1998, pp. 803-805
 - 28) Quasi-continuous wave operation of multi-mega watts electron beam in the JAERI superconducting rf linac FEL driver
Eisuke Minehara, Masayoshi Sugimoto, Masaru Sawamura, Ryoji Nagai, Nobuhiro Kikuzawa, Nobuyuki Nishimori, Toshihiko Yamauchi
Proceedings of Int. Particle Accelerator conf. (PAC99), U. S. A., 1999, pp. 2459-2461
 - 29) Development of High Average Power Infrared FEL driven by the JAERI Superconducting rf Linac
Eisuke Minehara
Bulletin of the Annual Meeting of the Applied Physics Society of Japan, Noda, 1999, III-p. 234
 - 30) Improvement of thermionic electron gun at JAERI
Nobuyuki Nishimori, Ryoji Nagai, Eisuke Minehara, Nobuhiro Kikuzawa, Masayoshi Sugimoto,

- Toshihiko Yamauchi
 Proceedings of the 1999 Workshop on New developments of electron sources, AcCLab-98-154,
 Tsukuba, 1999, pp. 28-36
- 31) Study on IR Laser Application using JAERI FEL
 Toshihiko Yamauchi, Eisuke Minehara, Nobuhiro Kikuzawa, Nobuyuki Nishimori, Ryoji Nagai,
 Takehito Hayakawa, Masaru Sawamura, Masayoshi Sugimoto
 Proceedings of 19th Annual Meeting of the Laser Society of Japan, Nagoya, 1999, p. 233
- 32) Non coherent and coherent bremsstrahlung hard X ray or γ ray sources utilizing the JAERI super-
 conducting rf linac for high power FEL's
 Eisuke Minehara, Masayoshi Sugimoto, Masaru Sawamura, Ryoji Nagai, Nobuhiro Kikuzawa,
 Toshihiko Yamauchi, Nobuyuki Nishimori
 Extended Abstracts of the 1999 Workshop on High Brightness Light Source, Tsukuba, 1999, p. 315
- 33) Recent improvements in the JAERI superconducting rf linac based free electron laser
 Eisuke Minehara, Toshihiko Yamauchi, Masayoshi Sugimoto, Masaru Sawamura, Ryoichi Hajima,
 Ryoji Nagai, Nobuhiro Kikuzawa, Nobuyuki Nishimori, Toshiyuki Shizuma
 Proceedings of 4th Asian Symp. On Free Electron Lasers, Korea, 1999, pp. 13-16
- 34) JAERI Superconducting rf Linac based Free Electron Laser Project
 Eisuke Minehara, Toshihiko Yamauchi, Masayoshi Sugimoto, Masaru Sawamura, Ryoichi Hajima,
 Ryoji Nagai, Nobuhiro Kikuzawa, Nobuyuki Nishimori, Toshiyuki Shizuma
 Proceedings of the 24th Linear Accelerator Meeting in Japan, Sapporo, 1999, pp. 25-26
- 35) Evaluation of the optical cavity with out-coupling scraper
 Ryoji Nagai, Masaru Sawamura, Ryoichi Hajima, Nobuhiro Kikuzawa, Nobuyuki Nishimori,
 Toshiyuki Shizuma, Eisuke Minehara
 Proceedings of the 24th Linear Accelerator Meeting in Japan, Sapporo, 1999, pp. 276-277
- 36) Evaluation of Optical Resonator for the JAERI Far-Infrared
 Ryoji Nagai, Masaru Sawamura, Ryoichi Hajima, Nobuhiro Kikuzawa, Nobuyuki Nishimori,
 Toshiyuki Shizuma, Eisuke Minehara
 Proceedings of the 12th Symposium on Accelerator Science and Technology, Wako, 1999, pp. 379-
 381
- 37) Study on Recirculating Beam Transport and RF Instability for the Energy-recovery Experiment at
 JAERI FEL
 Ryoichi Hajima, Toshiyuki Shizuma, Masaru Sawamura, Ryoji Nagai, Nobuhiro Kikuzawa,
 Nobuyuki Nishimori, Eisuke Minehara
 Proceedings of the 12th Symposium on Accelerator Science and Technology, Wako, 1999, pp. 116-
 118
- 38) Decomposition Experiment of Dioxin by IR Laser Irradiation
 Toshihiko Yamauchi, Eisuke Minehara, Nobuhiro Kikuzawa, Takehito Hayakawa, Masaru
 Sawamura, Ryoji Nagai, Nobuyuki Nishimori, Ryoichi Hajima, Toshiyuki Shizuma, Yasutaka
 Kamei, Hisato Ikai, Shinichi Itoh, Yukio Furukawa
 Proceedings of the Tenth Symposium on Beam Engineering of Advanced Material Syntheses, Kyoto,
 1999, pp. 213-216
- 39) JAERI Superconducting rf Linac Based FEL Program
 Eisuke Minehara, Masaru Sawamura, Ryoji Nagai, Nobuhiro Kikuzawa, Masayoshi Sugimoto,
 Ryoichi Hajima, Toshiyuki Shizuma, Toshihiko Yamauchi, Nobuyuki Nishimori
 Proceedings of the 12th Symposium on Accelerator Science and Technology, Wako, 1999, pp. 116-
 118
- 40) Industrial 1.3micron Highly-Efficient FEL Driven by the Superconducting rf Linac
 Eisuke Minehara, Toshihiko Yamauchi, Masayoshi Sugimoto, Masaru Sawamura, Ryoichi Hajima,
 Ryoji Nagai, Nobuhiro Kikuzawa, Takehito Hayakawa, Nobuyuki Nishimori, Toshiyuki Shizuma
 Bulletin of the 38th Spring Meeting Atomic Energy Society of Japan, Matsuyama, 2000, p. 119

3. Patents

- 1) Method of forming a plasma micro-undulator
 Ryoji Nagai
 Patent number: 5822342
- 2) Circular, elliptic, variably polarized planer type hybrid-undulator

Ryoji Nagai

Application number: 9-109321

- 3) High-efficiency plasma confining method, laser oscillating method and laser oscillator
Toshihiko Yamauchi
Patent number: 2683135

Optics research and development (Novel Optics Research Group)

1. Journals

- 1) Laser-induced chemical modification of the surface of fluoropolymers (In Japanese)
Shunichi Kawanishi, Nobuyuki Ichinose
Reza Kenkyu, 24, 780-786 (1996)
- 2) Excimer laser-induced surface reaction of fluoropolymers with liquid water
Nobuyuki Ichinose, Shunichi Kawanishi
Macromolecules, 29, 4155-4157 (1996)
- 3) Laser ablation dynamics of amorphous film of a Cu-phthalocyanine derivative (In Japanese)
Masahiro Hosoda, Hiroshi Furutani, Hiroshi Fukumura, Hiroshi Masuhara, Masanobu Nishii,
Nobuyuki Ichinose, Shunichi Kawanishi
Reza Kenkyu, 25, 306-311 (1996)
- 4) Micropatterning of organosilane thin layers on glass surface by laser irradiation for patterned immobilization of polyaminopolymers
Nobuyuki Ichinose
Macromol. Rep. 33 (SUPPL. 1) 33-36 (1996)
- 5) U. v. -irradiation of thin films of polystyrene derivatives; Formation of carboxylic group and crosslinking from 4-trimethylsilylmethyl substituent
Toshiyuki Tamai, Isao Hashida, Nobuyuki Ichinose, Shunichi Kawanishi, Hiroo Inoue,
Kazuhiko Mizuno
Polymer, 37, 5525-5528 (1996)
- 6) Non-linear laser intensity dependence of the formation of carboxylic acid groups at the surface of polymer films; The effect of coupling of radical intermediates
Nobuyuki Ichinose, Toshiyuki Tamai, Shunichi Kawanishi, Isao Hashida, Kazuhiko Mizuno
Langmuir, 13, 2603-2605 (1997)
- 7) Photochemical introduction of superacidic sites on fluoropolymer surfaces
Nobuyuki Ichinose, Shunichi Kawanishi
Langmuir, 13, 5805-5807 (1997)
- 8) Patterning of SnO₂ thin films by combination of lithographic photoirradiation and pyrolysis of an organotin polymer
Toshiyuki Tamai, Nobuyuki Ichinose, Shunichi Kawanishi, Masanobu Nishii, Tsuneo Sasuga,
Isao Hashida, Kazuhiko Mizuno
Chem. Mater. 9, 2674-2675 (1997)
- 9) Generation of polyphenylene radical cations and their cosensitization ability in the 9, 10 - dicyanoanthracene-sensitized photochemical chain reactions of 1, 2-bis (4-methoxyphenyl) cyclopropane
Toshiyuki Tamai, Nobuyuki Ichinose, Tomoko Tanaka, Tsuneo Sasuga, Isao Hashida, Kazuhiko Mizuno
J. Org. Chem. 63, 3204-3212 (1998)
- 10) Laser induced molecular transfer using ablation of a triazeno-polymer
D. M. Karnakis, T. Lippert, Nobuyuki Ichinose, Shunichi Kawanishi, Hiroshi Fukumura
Appl. Surf. Sci. 127-129, 781-786 (1998)
- 11) Effect of hydrogen bonding on laser-induced transfer of 1-pyrenebutyric acid in solid polymers
K. Saitow, nobuyuki Ichinose, Shunichi Kawanishi, Hiroshi Fukumura
Chem. Phys. Lett. 29, 433-437 (1998)
- 12) Laser implantation of photochromic molecules into polymer films; A new approach towards molecular device fabrication
Hiroshi Fukumura, H. Ujii, H. Banjo, H. Masuhara, D.M. Karnakis, Nobuyuki Ichinose, Shunichi

- Kawanishi, K. Uchida, M. Irie
Appl. Surf. Sci. 127-129, 761-766 (1998)
- 13) Implantation of organic molecules into biotissue by pulsed laser irradiation
Masahiro Goto, Nobuyuki Ichinose, Shunichi Kawanishi, Hiroshi Fukumura
Jpn. J. Appl. Phys. Part 2, 38, L87-L88 (1999)
 - 14) Laser implantation of molecular aggregates into poly (methyl methacrylate)
Masahiro Goto, Nobuyuki Ichinose, Shunichi Kawanishi, Hiroshi Fukumura
Appl. Surf. Sci. 137-139, 471-476 (1999)
 - 15) Laser-induced fluorescence of 1, 3, 5-trimethoxybenzene radical cation in solution at room temperature
Nobuyuki Ichinose, Tomoko Tanaka, Shunichi Kawanishi, Tomoe Suzuki, Kazunaka Endo
J. Phys. Chem. A, 103, 7923-7926 (1999)
 - 16) Forward-transfer laser implantation of pyrene molecules in a solid polymer
D.M. Karnakis, M. Goto, Nobuyuki Ichinose, Shunichi Kawanishi, Hiroshi Fukumura
Appl. Phys. Lett. 73, 1439-1441 (1999)
 - 17) Application of hybrid design method to VUV double-element optical systems equipped with holographic gratings recorded with aspheric wavefronts
M. Koike, Y. Ueno, T. Namioka
Proc. SPIE 3150, 31-39 (1997)
 - 18) Design of imaging system for EUVL
H. Kinoshita, T. Watanabe, M. Koike, T. Namioka
Proc. SPIE 3152, 211-220 (1997)
 - 19) Plane gratings for high-resolution grazing incidence monochromators: holographic grating versus mechanically ruled varied-line-spacing grating
M. Koike, T. Namioka
Appl. Opt. 36, 6308-6318 (1997)
 - 20) Direct bonding of Ti:sapphire laser crystals
A. Sugiyama, H. Fukuyama, T. Sasuga, T. Arisawa, H. Takuma
Appl. Opt. 37, 2407-2410 (1998)
 - 21) High energy flash lamp pumped Ti-sapphire laser for Yb:glass CPA
A. Nishimura, A. Ohzu, A. Sugiyama, Y. Maruyama, T. Arisawa, H. Takuma, J. Nees, S. Biswal, G. Mourou, E. Erickson, S. Owada, S. Satou
Proc. SPIE 3265, 234-241 (1998)
 - 22) Comparison of mechanically ruled versus holographically varied-spacing gratings for a soft x-ray flat field spectrograph
T. Yamazaki, E. Gullikson, N. Miyata, M. Koike, Y. Harada, S. Mrowka, U. Kleineberg, J. H. Underwood, M. Yamagihara, K. Sano
Appl. Opt. 38, 4001-4003 (1999)
 - 23) Design of holographic gratings recorded with aspheric wave-front recording optics for soft X-ray flat field spectrographs
M. Koike, T. Yamazaki, Y. Harada
J. Electron Spectroscopy and Related Phenomena, 101-103, 913-918 (1999)
 - 24) Laser site selective excitation of KY3F10 doped with samarium
J. P. R. Wells, A. Sugiyama, T. P. J. Han, H. G. Gallagher
J. Luminescence 85, 91-102 (1999)
 - 25) X-ray scattering study of interfacial roughness correlation in Mo/Si multilayers fabricated by ion beam sputtering
A. Ulyanenkova, R. Matsuo, K. Omote, K. Inaba, J. Harada, M. Ishino, M. Nishii, O. Yoda
J. Appl. Phys. 87, 7255-7260 (2000)
 - 26) A spectroscopic comparison of samarium doped LiYF₄ and KY₃F₁₀
P. R. Wells, A. Sugiyama, T. P. J. Han, H. G. Gallagher
J. Luminescence 87-89, 1029-1031 (2000)
 - 27) Varied-line-spacing laminar-type holographic grating for the standard soft X-ray flat-field spectrograph
M. Koike, T. Namioka, E. Gullikson, Y. Harada, S. Ishikawa, T. Imazono, S. Mrowka, N. Miyata, M. Yamagihara, J. H. Underwood, K. Sano, T. Ogiwara, O. Yoda, S. Nagai
to be published in Proc. SPIE 4146

2. Reports

- 1) Studies of laser crystals
A. Sugiyama, Y. Anzai, M. Katsurayama, T. Yamazaki, K. Yamagishi, T. Sasuga, T. Arisawa, H. Takuma
JAERI-Tech 97-049 (1997)
- 2) Crystal growth of $\text{Li}^{10}\text{B}_3\text{O}_5$
A. Sugiyama, H. G. Gallagher, T. P. J. Han
JAERI-Tech 99-069 (1999)
- 3) Development of high quality large laser crystals for a CPA laser system
A. Sugiyama, H. Fukuyama, S. Nagai, M. Katsurayama, Y. Anzai
JAERI-Conf 2000-006, 71-74 (2000)
- 4) Fabrication of soft X-ray multilayer mirrors by means of ion beam sputtering
M. Ishino, M. Nishii, O. Yoda
JAERI-Conf 2000-006, 270-272 (2000)
- 5) Fabrication and evaluation of holographically varied line-spacing gratings for soft X-ray flat field spectrographs
M. Koike, T. Yamazaki, S. Ishikawa, T. Imazono, N. Miyata, M. Yanagihara, Y. Harada, K. Sano
JAERI-Conf 2000-006, 289-292 (2000)

3. Patents

- 1) Apparatus and method of stabilizing oscillation frequency for single axial mode frequency tunable laser oscillator and apparatus and method of frequency sweepable laser oscillation
A. Sugiyama, T. Nakayama, M. Kato, Y. Maruyama, T. Arisawa
Patent number: 08/638544
- 2) Direct bonding method for laser crystals
A. Sugiyama, H. Fukuyama, T. Sasuga, T. Arisawa
Application number: 9-186662
- 3) Plane diffraction grating based on surface normal rotation and its application to an optical system
M. Koike, Y. Harada, K. Sano
Application number: 10-207722
- 4) Activation of cryopump and cryopump system
Y. Ikeda, K. Sukanuma
Application number: 10-2761171
- 5) Method and apparatus for generating laser plasma X-ray
K. Ogura
Application date: 98.11.6
- 6) Plane diffraction grating based on surface normal rotation and its application to an optical system
M. Koike, Y. Harada, K. Sano
Application number: 11-231255
- 7) Apparatus for extension of pulse width for a pulsed laser
A. Sugiyama, Y. Maruyama
Patent number: 3002998

4. Book

- 1) Monochromators and Spectrometers: Normal incidence
M. Koike
Section 2.5.1., Method of Vacuum Ultraviolet Physics, Eds: J. A. Samson, D. L. Ederer,
Experimental Methods in the Physical Sciences Vol. 32, (Academic Press, New York, 1998)

Laser driven particle acceleration research (Laser Acceleration Research Group)

1. Journals

- 1) Femtosecond Single-Bunched Linac for Pulse Radiolysis Based on Laser Wake field Acceleration
A. Ogata, K. Nakajima, T. Kozawa and Y. Yoshida

- IEEE Trans Plasma Sci. 24 (1996) 453-459
- 2) Generation, Measurement and Application of Synchronized 700 fs Electron, 100 fs Laser and Picosecond X-ray Single Pulses
M. Uesaka, T. Ueda, T. Watanabe, M. Kando, K. Nakajima, H. Kotaki and A. Ogata
Advanced Accelerator Concepts (AIP Conf. Proc. 398), 687-692 (1997)
 - 3) Recent Results of Laser Wakefield Acceleration in KEK/U. Tokyo/JAERI
K. Nakajima, M. Kando, H. Ahn, H. Kotaki, T. Watanabe, T. Ueda, M. Uesaka, H. Nakanishi, A. Ogata, T. Kawakubo and K. Tani
7th Workshop on Advanced Accelerator Concepts, Lake Tahoe, Cal., AIP Conf. Proc. 398 (1997) 83-95
 - 4) Formation of Self-Channeling and Electron Jet in an Underdense Plasma Excited by Ultrashort High Intensity Laser Pulses
M. Kando, H. Ahn, H. Kotaki, K. Tani, T. Watanabe, T. Ueda, M. Uesaka, Y. Kishimoto, K. Nakajima, M. Arinaga, H. Nakanishi and A. Ogata
7th Workshop on Advanced Accelerator Concepts, Lake Tahoe, Cal., AIP Conf. Proc. 398 (1997) 390-399
 - 5) Production and utilization of synchronized femtosecond electron and laser single pulses
M. Uesaka, T. Watanabe, T. Ueda, M. Kando, K. Nakajima, H. Kotaki, A. Ogata
Journal of Nuclear Materials, 248, 380-385 (1997)
 - 6) Experiments of high energy gain laser wakefield acceleration
H. Dewa, H. Ahn, H. Harano, M. Kando, K. Kinoshita, S. Kondoh, H. Kotaki, K. Nakajima, H. Nakanishi, A. Ogata, H. Sakai, M. Uesaka, T. Ueda, T. Watanabe, K. Yoshii
Nuclear Instruments and Methods in Physics Research A 410 (1998) pp. 357-363
 - 7) Femtosecond Electron Beam Generation and Measurement for Laser Synchrotron Radiation
M. Uesaka, K. Kinoshita, T. Watanabe, T. Ueda, K. Yoshii, H. Harano, K. Nakajima, A. Ogata, F. Sakai, H. Kotaki, M. Kando, H. Dewa, S. Kondo, Y. Shibata, K. Ishi, M. Ikezawa
Nucl. Instrum. & Meth.A, Vol.410(1998), pp. 424-430
 - 8) Experimental Results of Laser Wakefield Acceleration Using a Femtosecond Terawatt Laser Pulse
M. Kando, H. Ahn, H. Dewa, H. Kotaki, T. Ueda, M. Uesaka, T. Watanabe, H. Nakanishi, A. Ogata, K. Nakajima
Jpn. J. Appl. Phys. Vol.38 (1999) pp. L967-L969
 - 9) Subpicosecond electron single-beam diagnostics by a coherent transition radiation and a streak camera
Takahiro Watanabe, Mitsuru Uesaka, Jun Sugahara, Koji Yoshii, Yukio Shibata, Fumio Sakai, Shuji Kondo, Masaki Kando, Hideyuki Kotaki, Kazuhisa Nakajima
Nuclear Instruments and Methods in Physics Research A 437 (1999) pp. 1-11
 - 10) Femtosecond Quantum Beam Science and New Pump-and-Probe Analysis
Mitsuru Uesaka, Takahiro Watanabe, Hideki Harano, Kenichi Kinoshita, Jun Sugahara, T. Ueda, Koji Yoshii, Kazuhisa Nakajima, Atsushi Ogata, Fumio, Sakai, Masaki Kando, Hideyuki Kotaki, Hideki Dewa, Shuji Kondo
Femtosecond Quantum Beam Science, V-7, p313, 1999
 - 11) Optical guidance of terrawatt laser pulses by the implosion phase of fast Z-pinch discharge in a gas-filled capillary
T.Hosokai, M.Kando, H.Dewa, H.Kotaki, S.Kondo, N.Hasegawa, K.Horioka and K.Nakajima
Optics Letters (Optical Society America) vol.25, 10 (2000)
 - 12) Generation, Measurement and Application of Femtosecond electron Beam
M. Uesaka, T. Watanabe, K. Kinoshita, J. Sugahara, H. Harano, T. Ueda, K. Yoshii, K. Nakajima, F. Sakai, H. Kotaki, H. Dewa, M. Kando, S. Kondo
Journal of The Atomic Energy Society of Japan, April, 2000
 - 13) Fast Z-pinch optical guiding of high peak power laser
T. Hosokai, M. Kando, H. Dewa, H. Kotaki, S. Kondo, S. Kanazawa, N. Hasegawa, K. Horioka, K. Nakajima
The Transaction of The Institute of Electrical Engineers of Japan, Vol. 120-A, No. 5, pp. 575-582, May, 2000
 - 14) Fast Z-pinch optical guiding for X-ray generation and laser-plasma accelerators
T. Hosokai, M. Kando, H. Dewa, H. Kotaki, S. Kondo, N. Hasegawa, K. Horioka and K. Nakajima
Nuclear Instruments and Methods B (to be published)

- 15) Compact X-Ray Sources by Intense Laser Interaction with Beams and Plasmas
Hideyuki Kotaki, Masaki Kando, Hideki Dewa, Syuji Kondo, Takahiro Watanabe, Toru Ueda,
Kenichi Kinoshita, Koji Yoshii, Mitsuru Uesaka, Kazuhisa Nakajima
Nuclear Instruments and Method B (to be published)
- 16) Generation and Application of Femtosecond X-ray Pulse
Mitsuru Uesaka, Hideyuki Kotaki, Kazuhisa Nakajima, Hideki Harano, Kenichi Kinoshita, Takahiro
Watanabe, Toru Ueda, Koji Yoshii, Masaki Kando, Hideki Dewa, Shuji Kondo,
Fumio Sakai
Nuclear Instruments and Method B (to be published)
- 17) Particle Acceleration by Ultraintense Laser Interactions with Beams and Plasmas
Kazuhisa Nakajima,
LASER AND PARTICLE BEAMS to be published
- 18) Recent Progress on Laser Acceleration
Kazuhisa Nakajima
Nuclear Instruments and Methods in Physics Research to be published
- 19) Experimental Verification of Laser Photocathode RF Gun as an Injection for a Laser Plasma
Accelerator
Mitsuru Uesaka, Kenichi Kinoshita, Takahiro Watanabe, Jun Sugahara, Toru Ueda, Koji Yoshii,
Tetsuya Kobayashi, Nasr Hafz, Kazuhisa Nakajima, Fumio Sakai, Masaki Kando, Hideki Dewa,
Hideyuki Kotaki, Shuji Kondo
IEEE Trans. on Plasma Science to be published

2. Proceedings

- 1) High resolution synchronization between sub-picosecond electron beam and femtosecond laser
T. Watanabe, M. Uesaka, T. Kozawa, T. Ueda, M. Kando, H. Kotaki, K. Nakajima, A. Ogata
Proceedings of The 21st Linear Accelerator Meeting in Japan, Tokyo, September 30-October 2,
1996, pp.296-298
- 2) Generation, Measurement and Application of Synchronized 700fs Election, 100fs T3 laser and
Picoseconds X-ray Single Pulses
M. Uesaka, T. Ueda, T. Watanabe, M. Kando, K. Nakajima, H. Kotaki, A. Ogata
The 7th Advanced Accelerator Concepts, Lake Tahoe, U. S. A., October 12-18, 1996, AIP
Conference Proceedings 398, pp. 687-692
- 3) Formation of Self-Channeling and Electron Jet in an Under dense Plasma Excited by Ultra short High
Intensity Laser Pulses
M. Kando, K. Nakajima, H. Ahn, H. Kotaki, K. Tani, M. Arinaga, T. Kawakubo, H. Nakanishi, A.
Ogata, Y. Kishimoto, J. Koga, H. Watanabe, T. Watanabe, T. Ueda, and M. Uesaka
The 7th Advanced Accelerator Concepts, Lake Tahoe, U. S. A., October 12-18, 1996, AIP
Conference Proceedings 398, pp. 390-399
- 4) Recent Results of Laser Wake field Acceleration in KEK/JAERI/U.Tokyo
K. Nakajima, M. Kando, H. Ahn, H. Kotaki, K. Tani, M. Arinaga, T. Kawakubo, H. Nakanishi, A.
Ogata, T. Watanabe, T. Ueda, M. Uesaka
The 7th Advanced Accelerator Concepts, Lake Tahoe, U.S.A., October 12-18, 1996, AIP Conference
Proceedings 398, pp. 83-95
- 5) Femtosecond Dynamic Microspectroscopy Using Synchronized Femtosecond Electron, Laser and X-
ray Pulses
M. Uesaka, T. Watanabe, T. Ueda, M. Kando, K. Nakajima, H. Kotaki, A. Ogata
Abstracts of the Fourth International Workshop on Femtosecond Technology (FST T97), Tsukuba,
Japan, February 13-14, 1997, pp. 54-57
- 6) Laser Wakefield Acceleration Experiments
H. Kotaki, K. Nakajima, M. Kando, H. Ahn, T. Watanabe, T. Ueda, M. Uesaka, H. Nakanishi, A.
Ogata, K. Kinoshita, K. Tani
Applications of High Field and Short Wavelength VII, Santa Fe, U.S.A., March 19-22, 1997, p251
- 7) A Short Pulse X-ray Generation by Thomson Scattering of Ultrashort Laser Pulses by Relativistic
Electron Beams
H. Kotaki, M. Kando, H. Ahn, K. Nakajima, H. Nakanishi, A. Ogata, T. Watanabe, T. Ueda, M.
Uesaka

- Particle Accelerator Conference '97, Vancouver, B.C., Canada, 12-16 May 1997
- 8) High Energy Gain Laser Wakefield Acceleration
M. Kando, H. Ahn, H. Kotaki, K. Nakajima, H. Nakanishi, A. Ogata, T. Watanabe, T. Ueda, M. Uesaka
Particle Accelerator Conference '97, Vancouver, B.C., Canada, 12-16 May 1997
 - 9) Femtosecond electron beam generation by S-band linac at the University of Tokyo
K. Kinoshita, M. Uesaka, T. Watanabe, T. Ueda, K. Yoshii, H. Harano, F. Sakai, H. Kotaki, K. Nakajima, H. Nakanishi, A. Ogata
Proceeding of the 22nd Linear Accelerator Meeting in Japan, Sendai 1997, pp. 187-188 (1997)
 - 10) Beam evaluation by coherent transition radiation
T. Watanabe, K. Yoshii, H. Harano, T. Ueda, K. Kinoshita, M. Uesaka, Y. Shibata, K. Ishi, S. Ono, Y. Inoue, S. Sasaki, M. Ikezawa, F. Sakai, S. Kondo, M. Kando, H. Kotaki, H. Dewa, K. Nakajima, A. Ogata
Proceeding of the 22nd Linear Accelerator Meeting in Japan, Sendai 1997, pp. 335-337 (1997)
 - 11) A short Pulse X-ray Generation via Laser Thomson Scattering on Relativistic Electron Beams
H. Kotaki, K. Nakajima, M. Kando, H. Ahn, H. Dewa, S. Kondo, F. Sakai, T. Watanabe, T. Ueda, K. Kinoshita, K. Yoshii, H. Nakanishi, A. Ogata, M. Uesaka
Proceedings of the 11th Symposium on Accelerator Science and Technology, Harima Science Garden City, October 22 1997, p449-451
 - 12) Development of High Duty Operation RF Photoinjector
F. Sakai, X. Wang, H. Kotaki, K. Nakajima, T. Watanabe, K. Kinoshita, S. Kondo, M. Kando, H. Dewa, T. Ueda, K. Yoshii, M. Uesaka, A. Ogata, H. Nakanishi, M. Washio, A. Endo
Proceedings of the 11th Symposium on Accelerator Science and Technology, Harima Science Garden City, October 22 1997, pp. 473-475
 - 13) Generation of Femtosecond Electron Single Pulse at the S-band Linac
K. Kinoshita, M. Uesaka, T. Watanabe, T. Ueda, K. Yoshii, H. Harano, F. Sakai, H. Kotaki, K. Nakajima, H. Nakanishi, A. Ogata
Proceedings of the 11th Symposium on Accelerator Science and Technology, Harima Science Garden City, October 22 1997, pp. 479-480
 - 14) Laser Wakefield Acceleration Experiments
M. Kando, H. Kotaki, H. Dewa, H. Ahn, F. Sakai, S. Kondo, T. Ueda, T. Watanabe, M. Uesaka, H. Nakanishi, K. Nakajima and A. Ogata
Proceedings of the 11th Symposium on Accelerator Science and Technology, Harima Science Garden City, pp. 513-515 (1997)
 - 15) A Short Pulse X-ray Generation via Laser Thomson Scattering on Relativistic Electron Beams
H. Kotaki, K. Nakajima, M. Kando, H. Ahn, H. Dewa, S. Kondo, F. Sakai, T. Watanabe, T. Ueda, H. Nakanishi, A. Ogata, M. Uesaka
Proceedings of The International Conference on Lasers'97, New Orleans, USA, December 15-19, 1997, pp. 68-70
 - 16) All Solid State Picosecond UV Source for RF Photocathode
F. Sakai, K. Nakajima
Proceedings of The International Conference on Lasers'97, New Orleans, USA, December 15-19, 1997, pp. 63-67
 - 17) Experiment of Laser Wakefield Accelerator and Laser Synchrotron Radiation
K. Nakajima
Proceedings of The International Conference on Lasers'97, New Orleans, USA, December 15-19, 1997, pp. 778-784
 - 18) Recent Progress of Laser Wakefield Acceleration Experiments at KEK / U. Tokyo / JAERI
K. Nakajima, H. Dewa, M. Kando, H. Kotaki, F. Sakai, S. Kondo, A. Ogata, M. Uesaka
6th European Particle Accelerator Conference, Sweden, June, 1998
 - 19) Femtosecond Electron Beam Generation by the S-band Laser Photocathode RF Gun and Linac
M. Uesaka, H. Harano, K. Kinoshita, T. Ueda, T. Watanabe, A. Ogata, H. Dewa, S. Kondo, H. Kotaki, F. Sakai, M. Kando, A. Endo, M. Washio, K. Nakajima, H. Nakanishi, K. Yoshii
Proc. of 6th European Particle Accelerator Conference, Sweden, June, 1998, p. 776
 - 20) Subpicosecond Electron Beam Diagnostics by Coherent Transition Radiation Interferometer
T. Watanabe, M. Uesaka, J. Sugahara, T. Ueda, K. Yoshii, Y. Shibata, K. Ishi, M. Ikezawa, F. Sakai,

- S. Kondo, M. Kando, H. Kotaki and K. Nakajima
 Proc. of The Asian Particle Accelerator Conference (APAC) '98 (KEK, Japan), p. 740
- 21) Generation of Femtosecond Electron Single Pulse using Laser Photocathode RF Gun
 M. Uesaka, K. Kinoshita, T. Watanabe, T. Ueda, K. Yoshii, H. Harano, F. Sakai, H. Kotaki, K. Nakajima, H. Nakanishi, A. Ogata
 Proc. of The Asian Particle Accelerator Conference (APAC) '98 (KEK, Japan), p. 737
- 22) Recent Developments of 2nd Generation LWFA Experiments
 H. Dewa, T. Hosokai, M. Kando, S. Kondo, H. Kotaki, F. Sakai, K. Nakajima, H. Nakanishi, A. Ogata
 8th Workshop on Advanced Accelerator Concepts, Baltimore, July 5-11, 1998
- 23) Self-interaction of subpico-second electron bunch traveling through a chicane based bunch-compressor
 Ryoichi Hajima, Koji Yoshii, Toru Ueda, Fumio Sakai, Hideyuki Kotaki, Shuji Kondoh, Masaki Kando, Kenichi Kinoshita, Hideki Harano, Takahiro Watanabe, Mitsuru Uesaka, Hideki Dewa, Kazuhisa Nakajima
 Proc. 20th International Free-Electron Laser Conference, Aug.16-21, 1998, Williamsburg, Virginia USA
- 24) Development of plasma waveguide using fast capillary discharges
 T. Hosokai, S. Kondo, M. Kando, M. Nakajima, K. Horioka, and K. Nakajima
 6th International Conference on X-ray lasers (Kyoto Japan Aug. 1998)
 Inst. Phys. Conf. Ser. No.159 PROC X-ray Lasers 1998 P179 (1998)
- 25) Short Pulse X-ray Generation via Backward Thomson Scattering on Relativistic Electron Beam
 Hideyuki Kotaki, Kazuhisa Nakajima, Masaki Kando, Hideki Dewa, Shuji Kondo, Fumio Sakai, Takahiro Watanabe, Toru Ueda, Hiroshi Nakanishi, Koji Yoshii, Atsushi Ogata, Kenichi Kinoshita and Mitsuru Uesaka
 6th International Workshop on X-ray Lasers, Kyoto, 1998. 9, Inst. Phys. Conf. Ser. No. 159 PROC X-ray Lasers 1998 P565 (1998)
- 26) High repetition rate photocathode RF-gun
 F. Sakai, H. Kotaki, M. Kando, H. Dewa, S. Kondo, K. Nakajima, T. Ueda, K. Yoshii, H. Harano, T. Watanabe, M. Uesaka, A. Ogata, H. Nakanishi, A. Endo, T. Hori
 Proc. Of the 23rd Linear Accelerator Meeting in Japan, pp. 43-45
- 27) 50Hz Operation Results of Photo-Cathode RF-GUN
 T. Ueda, K. Yoshii, H. Harano, T. Watanabe, M. Uesaka, A. Ogata, H. Nakanishi, K. Nakajima, H. Kotaki, S. Kondo, F. Sakai, H. Dewa, M. Kando, T. Hosokai
 Proc. Of the 23rd Linear Accelerator Meeting in Japan, pp. 139-141, 1998
- 28) Application of fast imploding capillary discharge for laser wakefield acceleration
 T. Hosokai, S. Kondo, M. Kando, H. Dewa, H. Kotaki, K. Horioka and K. Nakajima
 Particle Accelerator Conference '99 (New York, USA, March, 1999), AIP PROC vol. 5, P3690-3692 (1999)
- 29) DESIGN OF ELECTRON BEAM INJECTION SYSTEM FOR LASER ACCELERATION EXPERIMENTS AT JAERI-KANSAI
 M. Kando, H. Kotaki, H. Dewa, S. Kondo, T. Hosokai, F. Sakai, J. Yang, and T. Hori, K. Nakajima
 1999 Particle Accelerator Conference, New York, Mar.- Apr., 1999
- 30) Performance Tests of BNL/KEK/SHI Photocathode RF Gun
 M. Kando, H. Kotaki, H. Dewa, S. Kondo, T. Ueda, K. Yoshii, T. Watanabe, M. Uesaka, F. Sakai, A. Ogata, H. Nakanishi, K. Nakajima
 Proceedings of The 24th Linear Accelerator Meeting in Japan, July 9 (1999), pp. 128-129
- 31) Recent progress on Laser-Driven Particle Accelerators
 Kazuhisa Nakajima
 First International Conference on Internal Fusion Science and Applications (IFSA'99), Bordeaux, France, 12-17 September, 1999
 Proceedings of Inertial Fusion and Sciences and Applications 99, ELSEVIER, pp. 1145-1150 (2000)
- 32) Recent Progress on Laser Acceleration
 Kazuhisa Nakajima
 International Symposium on New Visions in Laser-Beam Interactions, Tokyo Metropolitan University, Tokyo, Japan, 11-15 October, 1999, Proceedings : now printing
- 33) Fast Z-pinch optical guiding for X-ray generation and laser-plasma accelerators

- T. Hosokai, S. Kondo, M. Kando, H. Dewa, H. Kotaki N. Hasegawa, K. Horioka and K. Nakajima
International Symposium on New Visions in Laser-Beam Interactions, Tokyo Metropolitan
University, Tokyo, Japan, 11-15 October, 1999, Proceedings : now printing
- 34) Compact X-Ray Sources by Intense Laser Interaction with Beams and Plasmas
Hideyuki Kotaki, Masaki Kando, Hideki Dewa, Shuji Kondo, Takahiro Watanabe, Toru Ueda,
Kenichi Kinoshita, Koji Yoshii, Mitsuru Uesaka, Kazuhisa Nakajima
International Symposium on New Visions in Laser-Beam Interactions, Tokyo Metropolitan
University, Tokyo, Japan, 11-15 October, 1999, Proceedings : now printing
- 35) Development of Recent Laser Acceleration
K. Nakajima
Proc. of the First Symp. on APR (JAERI-Conf 2000-006), November 9 (1999)
- 36) Development of High Quality Electron Beam Accelerator
M. Kando, H. Dewa, H. Kotaki, S. Kondo, T. Hosokai, S. Kanazawa, T. Yokoyama, K. Nakajima
Proc. of the First Symp. on APR (JAERI-Conf 2000-006), November 9 (1999), pp. 218-221
- 37) Generation of Electron Jet from Intense Laser Plasma
Hideki Dewa, Takako Fukuda, Noboru Hasegawa, Tomonao Hosokai, Masaki Kando, Yasuteru
Kodaka, Shuji Kondo, Hideyuki Kotaki, Nasr A. Mohamed Hafz, Kazuhisa Nakajima, Kimio Niwa
and Mitsuru Uesaka
Proc. of the First Symp. on APR (JAERI-Conf 2000-006), November 9 (1999), pp. 242-245
- 38) Z-pinch plasma wave guide for Laser Wakefield Acceleration
T. Hosokai, M. Kando, H. Dewa, H. Kotaki, S. Kondo, S. Kanazawa, K. Nakajima
Proc. of the First Symp. on APR (JAERI-Conf 2000-006), November 9 (1999), pp. 250-253
- 39) Compact X-Ray Sources by Intense Laser Interaction with Beams and Plasmas
Hideyuki Kotaki, Masaki Kando, Hideki Dewa, Shuji Kondo, Takahiro Watanabe, Toru Ueda,
Kenichi Kinoshita, Koji Yoshii, Mitsuru Uesaka, Kazuhisa Nakajima
Photonics WEST LASER2000 (SPIE) January 22-28, 2000, San Jose, Proceedings of SPIE, Vol.
3935, pp. 149-155
- 40) Z-pinch Optical Guiding for 1GeV Electron Acceleration by Laser wakefields
T. Hosokai, M. Kando, H. Dewa, H. Kotaki, S. Kondo, K. Horioka and K. Nakajima
13th International Conference on High-Power Particle Beams "BEAMS2000" (Nagaoka, JAPAN
JUNE25-30)
- 41) Commissioning of Photocathode RF Gun Based Microtron at JAERI-Kansai
M. Kando, H. Kotaki, S. Kondo, T. Hosokai, T. Yokoyama, S. Kanazawa, K. Nakajima, T. Ishizuka,
F. Sakai, T. Hori
Proceedings of The 25th Linear Accelerator Meeting in Japan, Himeji, July 12-14, pp. 9-11
- 42) Conditioning of Photocathode RF-Gun at JAERI-Kansai
H. Kotaki, M. Kando, S. Kondo, S. Kanazawa, T. Yokoyama. T. Hosokai, K. Nakajima
Proceedings of The 25th Linear Accelerator Meeting in Japan, Himeji, July 12-14, pp. 147-149

3. Patents

- 1) Method of plasma channel formation for optical guiding using a Z-pinch discharge
T. Hosokai, and M. Kando
Application number: 11-202906
- 2) Method of electron beam monitoring in the microtron
T. Hori, F. Sakai, and M. Kando
Application number: 2000-206277

Advanced photon simulation research (Simulation Group for Advanced Photon Science)

1. Journals

- 1) Differential algebraic hydrodynamics solver with cubic-polynomial interpolation
T. Utsumi
Comput. Fluid Dyn. J., Vol. 4, No. 2, pp. 225-238 (1995)
- 2) Application of the differential algebraic-cubic interpolated propagation scheme to the heat conduction
equations

- T. Utsumi, T. Kunugi
Comput. Fluid Dyn. J., Vol. 4, No. 3, pp. 265-277 (1995)
- 3) Solving wave equations with the differential algebraic-cubic interpolated propagation scheme
 T. Utsumi, T. Kunugi
Comput. Model. Simul. Eng., Vol. 1, No. 4, pp. 452-476 (1996)
 - 4) Numerical analysis for thermal waves in gas generated by impulsive heating of a boundary surface
 T. Utsumi, T. Kunugi
Therm. Sci. Eng., Vol. 4, No. 3, pp. 1-7 (1996)
 - 5) Advanced photon simulation
 K. Tani
J. Plasma and Fusion Res., Vol. 72, No. 9, pp. 935-940 (1996)
 - 6) Observation of ASE in soft x-ray region from the recombining lithiumlike aluminium plasma pumped by multi-pulse irradiation
 T. Kawachi, K. Ando, M. Aoyama, T. Hara, Y. Aoyagi, A. Sasaki
J. Opt. Soc. Am., B, Vol. 14, pp. 1863-1869 (1997)
 - 7) Stability and accuracy of the cubic interpolated propagation scheme
 T. Utsumi, T. Kunugi, T. Aoki
Comput. Phys. Commun., Vol. 101, No. 1-2, pp. 9-20 (1997)
 - 8) Modeling of ultra-short-pulse laser pumped X-ray lasers
 A. Sasaki
J. Quant. Spectrosc. Radiat. Transfer, Vol. 58, No. 4-6, pp. 879-885 (1997)
 - 9) Convective amplification of wake field due to self-modulation of a laser induced by field ionization
 S. Kato, Y. Kishimoto, J. Koga
Phys. Plasmas, Vol. 5, No. 1, pp. 292-299 (1998)
 - 10) Optical field ionization effects on the generation of wakefields with short pulse lasers
 J. Koga, S. Kato, Y. Kishimoto, S.P. LeBlanc, M.C. Downer
Nucl. Instrum. Methods in Phys. Res. A, Vol. 410, pp. 499-504 (1998)
 - 11) A Numerical method for solving the one-dimensional Vlasov-Poisson equation in phase space
 T. Utsumi, J. Koga, T. Kunugi
Comput. Phys. Commun., Vol. 108, No. 2-3, pp. 159-179 (1998)
 - 12) Ultrafast X-ray processes with hollow atoms
 K. Moribayashi, A. Sasaki, T. Tajima
Phys. Rev., A, Vol. 58, No. 3, pp. 2007-2015 (1998)
 - 13) Unified description of liquid metals and strongly coupled plasmas
 J. Chihara
RIST News, No. 25, pp.13-20 (1998)
 - 14) Stochastic cooling of atoms using lasers
 M.G. Raizen, J. Koga, B. Sundaram, Y. Kishimoto, H. Takuma, T. Tajima
Phys. Rev., A, Vol. 58, No. 6, pp. 4757-4760 (1998)
 - 15) Structure factor and electronic structure of compressed liquid rubidium
 J. Chihara, G. Kahl
Phys. Rev., B, Vol. 58, No. 9, pp. 5314-5321 (1998)
 - 16) A story of our experience on developing a massive parallel program
 Y. Ueshima, T. Arakawa, A. Sasaki, W. Yokota
RIST News, No. 26, pp. 49-56 (1998)
 - 17) Guide to massive scalar parallel program on the paragon
 Y. Ueshima, T. Arakawa, A. Sasaki, W. Yokota
Computer Jyoho, No. 65, pp. 49-55 (1998)
 - 18) Laser Larmor X-ray radiation from low-Z matter
 Y. Ueshima, Y. Kishimoto, A. Sasaki, T. Tajima
Laser Part. Beams, Vol. 17, pp. 45-58 (1999)
 - 19) Lyapunov exponent of dilute gas, liquid and solid plasmas
 K. Nishihara, Y. Ueshima
Plasma Phys. Control. Fusion, Vol. 41, No. 3A, pp. A257-A266 (1999)
 - 20) Formulation for multi-phase/multi-component flow analysis
 T. Utsumi, S. Fujii

- Therm. Sci. Eng., Vol. 7, No. 1, pp. 21-30 (1999)
- 21) Collisional relaxation of an electron velocity distribution function in ultra-fast laser irradiation
M. Yamagiwa, J. Koga, A. Sagisaka, K. Nagashima
Plasma Phys. Control. Fusion, Vol. 41, No. 2, pp. 265-270 (1999)
 - 22) Calculation of ion abundance of collisional X-ray lasers using thin foil targets
A. Sasaki, T. Utsumi, K. Moribayashi, T. Tajima, H. Takuma
Rev. Laser Eng., Vol. 27, No. 3, pp. 185-189 (1999)
 - 23) Collisional effects on population inversion in optical-field-ionized plasmas
A. Sagisaka, K. Nagashima, M. Yamagiwa, T. Matoba, H. Takuma
J. Phys. Soc. Jpn., Vol. 68, No. 4, pp. 1221-1227 (1999)
 - 24) Subpicosecond pulse laser absorption by an overdense plasma with variable ionization
A. Zhidkov, A. Sasaki
Phys. Rev., E, Vol. 59, No. 6, pp. 7085-7095 (1999)
 - 25) X-ray emission by ultrafast inner-shell ionization from vapors of Na, Mg, and Al
K. Moribayashi, A. Sasaki, T. Tajima
Phys. Rev., A, Vol. 59, No. 4, pp. 2732-2737 (1999)
 - 26) Simulation model for the effects of nonlinear polarization on the propagation of intense pulse lasers
J. Koga
Opt. Lett., Vol. 24, No. 6, pp. 408-410 (1999)
 - 27) Spectrum analysis of three-body recombination rates for no-Maxwellian electron distributions under ultra-fast laser irradiation
M. Yamagiwa, J. Koga, A. Sagisaka
J. Phys., B, Vol. 32, No. 12, pp. 2881-2887 (1999)
 - 28) Animation analysis of plasma X-ray lasers
A. Sasaki, H. Yoneda
J. Plasma and Fusion Res., Vol. 75, No. 5, p. 507 (1999)
 - 29) Numerical study of solids irradiated with high-peak-power ultrashort laser pulse
T. Utsumi, A. Sasaki, T. Kunugi, S. Fujii, M. Akamatsu
Comput. Fluids Dyn. J., Vol. 8, No. 1, pp. 128-134 (1999)
 - 30) 1D plasma simulation in phase space with the differential algebraic cubic interpolated propagation scheme
T. Utsumi
Comput. Fluids Dyn. J., Vol. 8, No. 1, pp. 135-141 (1999)
 - 31) Simulation of transient collisional X-ray lasers using 2D parallelized CIP hydrodynamics code
A. Sasaki, T. Utsumi, T. Tajima, H. Takuma
Comput. Fluids Dyn. J., Vol. 8, No. 1, pp. 142-148 (1999)
 - 32) Direct spectroscopic observation of multiple-charged-ion acceleration by an intense femtosecond-pulse laser
A. Zhidkov, A. Sasaki, T. Tajima, T. Auguste, P. D'Olivera, S. Hulin, P. Monot, A. Y. Faenov, T. A. Pikuz, I. Y. Skoblev
Phys. Rev., E, Vol. 60, No. 3, pp. 3273-3278 (1999)
 - 33) Pressure-variation of structure factor of liquid Rb
J. Chihara, G. Kahl
Jpn. J. Appl. Phys., Vol. 38 (SUPPL. 38-1), pp. 492-495 (1999)
 - 34) Ion acceleration by super intense laser in plasmas
T. Zh. Esirkepov, Y. Sentoku, T. V. Liseikina, F. Califano, N. M. Naumova, Y. Ueshima, V. A. Vshirkov, Y. Kato, K. Mima, K. Nishihara, F. Pegoraro, S. V. Bulanov
JETP Lett., Vol. 70, No. 2, p. 82 (1999)
 - 35) Particle modeling of ionization and three-body recombination in fully ionized plasmas
K. Nanbu, S. Yonemura, A. Sasaki
Jpn. J. Appl. Phys., Vol. 38, No. 7B, pp. 4460-4464 (1999)
 - 36) MeV ion generation by an ultra-intense short-pulse laser; Application to positron emitting radionuclide production
M. Yamagiwa, J. Koga
J. Phys., D: Appl. Phys., Vol. 32, No. 19, pp. 2526-2528 (1999)
 - 37) Nucleus-electron model for states changing from a liquid metal to a plasma and the Saha equation

- J. Chihara, Y. Ueshima, S. Kiyokawa
Phys. Rev., E, Vol. 60, No. 3, pp. 3262-3272 (1999)
- 38) Ion explosion and multi-mega-electron-volt ion generation from an underdense plasma layer irradiated by a relativistically intense short-pulse laser
M. Yamagiwa, J. Koga, L.N. Tsintsadze, Y. Ueshima, Y. Kishimoto
Phys. Rev., E, Vol. 60, No. 5, pp. 5987-5990 (1999)
- 39) Collisional radiative model of complex ions
A. Sasaki
J. Plasma and Fusion Res., Vol. 75, No. 10, pp. 1138-1144 (1999)
- 40) Radiation hydrodynamics
A. Sasaki, T. Utsumi
J. Plasma and Fusion Res., Vol. 75, Suppl-II, pp. 12-15 (1999)
- 41) Stationary periodic and solitary waves induced by a strong short laser pulse
L. N. Tsintsadze, K. Nishikawa, T. Tajima, J. T. Mendonca
Phys. Rev., E, Vol. 60, No. 6, pp. 7435-7440 (1999)
- 42) Optical properties of cluster plasmas
T. Tajima, Y. Kishimoto, M. C. Downer
Phys. Plasmas, Vol. 6, No. 10, pp. 3759-3764 (1999)
- 43) Generation of low-frequency electromagnetic waves by spectrally broad intense laser pulses in a plasma
L. N. Tsintsadze, T. Tajima, K. Nishikawa, J. Koga, K. Nakagawa, Y. Kishimoto
Physica Scripta, Vol. T84, pp. 94-97 (2000)
- 44) Interaction of photons with plasmas and liquid metals; Photoabsorption and scattering
J. Chihara
Journal of Physics, Condensed Matter, Vol. 12, No. 3, pp. 231-247 (2000)
- 45) Energetic-multiple-charged-ion sources on short-laser-pulse irradiated foils
A. Zhidkov, A. Sasaki, T. Tajima
Rev. Sci. Instrum., Vol. 71, No. 2, pp. 931-934 (2000)
- 46) Emission of MeV multiple-charged ions from metallic foils irradiated with an ultrashort laser pulse
A. Zhidkov, A. Sasaki, T. Tajima
Phys. Rev., E, Vol. 61, No. 3, pp. R2224-2227 (2000)

2. Reports

- 1) Quantum and molecular dynamics study on the light interaction with matter
M. Shibahara, S. Kotake, T. Kunugi
JAERI-memo 07-188, 48P. (1995)
- 2) QMD study of energy transfer mechanism of diatomic molecules to solid surfaces
T. N. Zolotoukhina
JAERI-memo 07-194, 50P. (1995)
- 3) Excitation of a wake field driven by an ionization induced self-modulated intense short laser pulse
S. Kato, Y. Kishimoto, J. Koga
JAERI-memo 08-179, 15P. (1996)
- 4) Parallelization of plasma 2-D hydrodynamics code using message passing interface (MPI)
A. Sasaki
JAERI-Data/Code 97-048, 49P. (1997)
- 5) Vectorization, parallelization and implementation of quantum molecular dynamics codes [QQQF, MONTEV]
K. Kato, T. Kunugi, S. Kotake, M. Shibahara
JAERI-Data/Code 98-007, 104P. (1998)
- 6) Parallelization of quantum molecular dynamics simulation code
K. Kato, T. Kunugi, M. Shibahara, S. Kotake
JAERI-Research 98-008, 25P. (1998)
- 7) A Numerical method for solving the one-dimensional Vlasov-Poisson equation in phase space
T. Utsumi, T. Kunugi, J. Koga
JAERI-memo 09-115, 31P. (1997)
- 8) Signatures of a short-pulse stimulated Raman backscattering at high laser intensities for X-ray laser

applications

- M. M. Skoric, A. Maluckov, A. Sasaki, T. Tajima, K. Tani
JAERI-memo 09-200, 37P. (1997)
- 9) Reports on 6th international conference on X-ray lasers
N. Yamaguchi, H. Daido, T. Kawachi, T. Tomie, K. Midorikawa, A. Sasaki
J. Plasma and Fusion Res., Vol. 75, No. 1, pp. 153-154 (1999)
 - 10) Ultrafast atomic process in X-ray emission by using inner-shell ionization method for sodium and carbon atoms
K. Moribayashi, A. Sasaki, T. Tajima
JAERI-Research 98-034, 37P. (1998)
 - 11) Generation of ultra-short pulse hard X-rays with ultra-short pulse intense laser
Y. Ueshima, Y. Kishimoto, A. Sasaki, K. Moribayashi, K. Nagashima, M. Kado, A. Sagisaka, T. Tajima
JAERI-Research 98-048, 46P. (1998)
 - 12) Hybrid particle-in-cell (PIC) simulation of heat transfer and ionization balance in overdense plasmas irradiated by subpicosecond pulse lasers
A. Zhidkov, A. Sasaki
JAERI-Research 98-068, 50P. (1998)
 - 13) Guide to development of a scalar massive parallel programming on Paragon
Y. Ueshima, T. Arakawa, A. Sasaki, W. Yokota
JAERI-Data/Code 98-030, 69P. (1998)
 - 14) Stationary periodic and solitary waves induced in an isotropic plasma by a strong short laser pulse
L.N. Tsintsadze, K. Nishikawa, T. Tajima, J.T. Mendonca
JAERI-Research 99-030, 16P. (1999)
 - 15) Guide to the programming of I/O on the paragon
Y. Ueshima, T. Arakawa, A. Sasaki, W. Yokota
JAERI-Data/Code 99-051, 23P, (2000)
 - 16) Procedures of grasp92 code to calculate accurate Dirac-Coulomb energy for the ground state of helium atom
T. Utsumi, A. Sasaki
JAERI-Data/Code 2000-003, 30P, (2000)

3. Proceedings

- 1) Energy transfer of diatomic molecules to solid surfaces; QMD study
T. N. Zolotoukhina
Molecular and Microscale Heat transfer in Materials Processing and Other Applications, Vol. 1, pp. 32-39 (1996)
- 2) Recent progress in lithiumlike aluminium recombining plasma laser in RIKEN
T. Kawachi, K. Ando, T. Hara, Y. Aoyagi, A. Sasaki
Inst. Phys. Conf. Ser., No. 151, Section 3, pp. 102-106 (1996)
- 3) Development of hydrodynamics and atomic kinetics codes for recombination x-ray lasers
A. Sasaki, K. Akaoka, H. Takuma, H. Yoneda, H. Nakayama, K. Ueda
Inst. Phys. Conf. Ser., No. 151, Section 3, pp. 130-132 (1996)
- 4) Reports on 5th international colloquium on X-ray lasers
Y. Kato, H. Daido, T. Kawachi, K. Midorikawa, S. Kubodera, A. Sasaki, K. Murai, T. Tomie
Rev. Laser Eng., Vol. 24, p. 1239 (1996)
- 5) Solver with the differential algebraic cubic interpolated propagation scheme on massively parallel computer
T. Utsumi, K. Tani
Proc. on Parallel Algorithms/Architecture Synthesis, pp. 200-205 (1997)
- 6) Simulation of intense laser-dense matter interactions; X ray production and laser absorption
Y. Ueshima, Y. Kishimoto, A. Sasaki, Y. Sentoku, T. Tajima
Proceedings of the First JAERI-Kansai International Workshop on Ultrashort-Pulse Ultrahigh-Power Lasers and Simulation for Laser-Plasma Interactions, July 14-18, 1997, Kyoto, JAERI-Conf 98-004, pp. 31-36 (1998)
- 7) Ultrafast atomic process in X-ray emission by inner-shell ionization

- K. Moribayashi, A. Sasaki, T. Tajima
 Proceedings of the First JAERI-Kansai International Workshop on Ultrashort-Pulse Ultrahigh-Power Lasers and Simulation for Laser-Plasma Interactions, July 14-18, 1997, Kyoto, JAERI-Conf 98-004, pp. 58-63 (1998)
- 8) Stimulated Raman backscattering at high laser intensities
 M. M. Skoric, T. Tajima, A. Sasaki, A. Maluckov, M. Jovanovic
 Proceedings of the First JAERI-Kansai International Workshop on Ultrashort-Pulse Ultrahigh-Power Lasers and Simulation for Laser-Plasma Interactions, July 14-18, 1997, Kyoto, JAERI-Conf 98-004, pp. 64-69 (1998)
- 9) Plasma simulation with the differential algebraic CIP scheme
 T. Utsumi
 Proceedings of the First JAERI-Kansai International Workshop on Ultrashort-Pulse Ultrahigh-Power Lasers and Simulation for Laser-Plasma Interactions, July 14-18, 1997, Kyoto, JAERI-Conf 98-004, pp. 70-75 (1998)
- 10) Correlations in a partially degenerate electron plasma
 J. Chihara
 Proceedings of the First JAERI-Kansai International Workshop on Ultrashort-Pulse Ultrahigh-Power Lasers and Simulation for Laser-Plasma Interactions, July 14-18, 1997, Kyoto, JAERI-Conf 98-004, pp. 76-81 (1998)
- 11) Modeling of collisional excited x-ray lasers using short pulse laser pumping
 A. Sasaki, K. Moribayashi, T. Utsumi, T. Tajima
 Proceedings of the First JAERI-Kansai International Workshop on Ultrashort-Pulse Ultrahigh-Power Lasers and Simulation for Laser-Plasma Interactions, July 14-18, 1997, Kyoto, JAERI-Conf 98-004, pp. 96-101 (1998)
- 12) Optical properties of cluster plasma
 Y. Kishimoto, T. Tajima, M.C. Downer
 Proceedings of the First JAERI-Kansai International Workshop on Ultrashort-Pulse Ultrahigh-Power Lasers and Simulation for Laser-Plasma Interactions, July 14-18, 1997, Kyoto, JAERI-Conf 98-004, pp. 102-111 (1998)
- 13) Relaxation of electron energy distributions and population inversion in optical-field-ionized plasmas
 A. Sagisaka, K. Nagashima, M. Yamagiwa, T. Matoba, H. Takuma
 Inst. Phys. Conf. Ser., No. 159, pp. 289-292 (1999)
- 14) Anomalous plasma heating by intense ultra-short laser pulse for optical field ionization x-ray lasers
 S. Kato, J. K. Koga, K. Kato, Y. Ueshima, T. Utsumi, Y. Kishimoto, Y. Owadano
 Inst. Phys. Conf. Ser., No. 159, pp. 297-300 (1999)
- 15) Inner-shell ionization X-ray laser and hollow atom X-ray laser
 K. Moribayashi, A. Sasaki, Y. Ueshima, T. Tajima
 Inst. Phys. Conf. Ser., No. 159, pp. 317-320 (1999)
- 16) X-ray pumping source for inner-shell ionization X-ray laser
 K. Moribayashi, A. Sasaki, Y. Ueshima, T. Tajima
 Inst. Phys. Conf. Ser., No. 159, pp. 321-324 (1999)
- 17) Giga-particle simulation on short pulse X ray generation with ultrashort pulse relativistic laser
 Y. Ueshima, T. Arakawa, Y. Kishimoto, A. Sasaki, T. Tajima
 Inst. Phys. Conf. Ser., No. 159, pp. 325-328 (1999)
- 18) Modeling of electron collisional excited X-ray lasers using short pulse laser pumping
 A. Sasaki, T. Utsumi, K. Moribayashi, M. Kado, N. Hasegawa, T. Tajima, H. Takuma
 Inst. Phys. Conf. Ser., No. 159, pp. 387-390 (1999)
- 19) Particle modelling of ionization and three-body recombination in an x-ray laser medium
 K. Nanbu, S. Yonemura, A. Sasaki
 Inst. Phys. Conf. Ser., No. 159, pp. 403-406 (1999)
- 20) Hybrid particle-in-cell simulation, the absorption and ionization dynamics of an overdense plasma heated by subpicosecond pulse laser
 A. Zhidkov, A. Sasaki
 Inst. Phys. Conf. Ser., No. 159, pp. 407-410 (1999)
- 21) The Numerical simulation of melting and evaporation due to ultrashort pulse laser irradiation
 T. Utsumi, A. Sasaki, T. Kunugi, S. Fujii, M. Akamatsu

- Inst. Phys. Conf. Ser., No. 159, pp. 451-454 (1999)
- 22) Calculation of K-absorption edge in laser-shocked aluminum
J. Chihara, S. Kiyokawa, T. Utsumi
Inst. Phys. Conf. Ser., No. 159, pp. 455-458 (1999)
 - 23) Special purpose computer for X-ray scattering analysis of macromolecule in solution
N. Masuda, M. Oikawa, T. Itoh, H. Ihara
Inst. Phys. Conf. Ser., No. 159, pp. 703-706 (1999)
 - 24) Simulation of various ionization effects in overdense plasmas irradiated by a subpicosecond pulse laser
A. Zhidkov, A. Sasaki, T. Tajima
J. Plasma and Fusion Res. SERIES, Vol.2, Proceedings of 9th International, Toki Conference on Plasma Physics and Controlled Nuclear Fusion (ITC-9), New Frontiers in Plasma Physics, December 7-11, 1998, pp. 414-417 (1999)
 - 25) Report on the 8th international workshop on radiative properties of hot dense matter
A. Sasaki
Rev. Laser Eng., Vol. 27, No. 6, pp. 430-434 (1999)
 - 26) Inner-shell ionization and hollow atom x-ray lasers driven by high-intensity laser
K. Moribayashi, A. Sasaki, Y. Ueshima
Proceeding of SPIE, High-Power Lasers in Energy Engineering, Vol. 3886, pp.634-641 (2000)
 - 27) Numerical analysis of high-gain transient collisional x-ray lasers
A. Sasaki, A. Zhidkov, T. Utsumi, K. Moribayashi, T. Tajima, H. Takuma
Proceeding of SPIE, High-Power Lasers in Energy Engineering, Vol. 3886, pp.642-649 (2000)
 - 28) Simulation of intense short-pulse laser-plasma interaction
M. Yamagiwa, Simulation Group for Advanced Photon Science
Proceedings of the 1st Symposium on Advanced Photon Research (Kyoto, 1999.11) JAERI-Conf 2000-006, pp. 37-40 (2000)
 - 29) Simulation on interaction of an ultra short-pulse intense laser with foil; Proton acceleration with sub peta-watt laser
Y. Ueshima, Y. Kishimoto, Y. Sentoku
Proceedings of the 1st Symposium on Advanced Photon Research (Kyoto, 1999.11) JAERI-Conf 2000-006, pp. 169-172 (2000)
 - 30) Wavelengths of the Ni-like 4d to 4p x-ray laser lines
T. Utsumi, A. Sasaki
Proceedings of the 1st Symposium on Advanced Photon Research (Kyoto, 1999.11) JAERI-Conf 2000-006, pp. 173-176 (2000)
 - 31) Simulation of transient collisional x-ray lasers
A. Sasaki, T. Utsumi, K. Moribayashi, A. Zhidkov, T. Kawachi, M. Kado, N. Hasegawa
Proceedings of the 1st Symposium on Advanced Photon Research (Kyoto, 1999.11) JAERI-Conf 2000-006, pp. 189-192 (2000)
 - 32) Interaction of intense femtosecond laser pulses with high-Z solids
A. Zhidkov, A. Sasaki, T. Utsumi, I. Fukumoto, T. Tajima, M. Yoshida, K. Kondo
Proceedings of the 1st Symposium on Advanced Photon Research (Kyoto, 1999.11) JAERI-Conf 2000-006, pp. 193-196 (2000)
 - 33) State analysis of high power laser induced hot electrons by simulation of x-ray radiation
I. Fukumoto, T. Utsumi, A. Sasaki, A. Zhidkov
Proceedings of the 1st Symposium on Advanced Photon Research (Kyoto, 1999.11) JAERI-Conf 2000-006, pp. 199-202 (2000)
 - 34) Simulation of solids irradiated with high power ultrashort laser pulse
S. Fujii, T. Utsumi, A. Sasaki, T. Kunugi
Proceedings of the 1st Symposium on Advanced Photon Research (Kyoto, 1999.11) JAERI-Conf 2000-006, pp. 203-206 (2000)
 - 35) Short-wavelength inner-shell ionization x-ray laser simulation
K. Moribayashi, A. Sasaki, Y. Ueshima, T. Tajima
Proceedings of the 1st Symposium on Advanced Photon Research (Kyoto, 1999.11) JAERI-Conf 2000-006, pp. 207-210 (2000)

6.2 List of publications on Synchrotron Radiation Research Center

Experimental facilities development (Experimental Facilities Development Group)

1. Journals

- 1) Conceptual design of SPring-8 front ends
Y. Sakurai, M. Oura, H. Sakae, T. Usui, H. Kimura, Y. Oikawa, H. Kitamura, T. Konishi, H. Shiwaku, A. Nakamura, H. Amamoto and T. Harami
Rev. Sci. Instrum., 66 (2) (1995) 1771-1773
- 2) A wire scanning type position monitor for an undulator radiation
X. W. Zhang, H. Sugiyama, M. Ando, S. J. Xia and H. Shiwaku
Rev. Sci. Instrum., 66 (2) (1995) 1990-1992
- 3) Synchrotron radiation time gate quartz device for nuclear resonant scattering
C. K. Suzuki, X. W. Zhang, M. Ando, Y. Yoda, T. Ishikawa, S. Kikuta, T. Harami, H. Shiwaku and H. Ohno
Rev. Sci. Instrum., 66 (2) (1995) 2235-2237
- 4) Synchrotron radiation beamline to study radioactive materials at the PF
H. Konishi, A. Yokoya, H. Shiwaku, H. Motohashi, T. Makita, Y. Kashihara, S. Hashimoto, T. Harami, T. A. Sasaki, H. Maeta, H. Ohno, H. Maezawa, S. Asaoka, N. Kanaya, K. Ito, N. Usami and K. Kobayashi
Nucl. Instrum. Methods Phys. Res. A, 372 (1995) 322-332
- 5) Large-aperture TV detector with a beryllium-windowed image intensifier for X-ray diffraction
Y. Amemiya, T. Ito, N. Yagi, Y. Asano, K. Wakabayashi, T. Ueki and T. Endo
Rev. Sci. Instrum., 66 (2) (1995)
- 6) Compton scattering of 20-40 keV photons
Y. Namito, S. Ban, H. Hirayama, N. Nariyama, H. Nakashima, Y. Nakane, Y. Sakamoto, N. Sasamoto, Y. Asano and S. Tanaka
Phys. Rev., A51 (1995) No.4
- 7) Characteristics of a vacuum-type micro calorimeter for synchrotron radiation measurement
H. Nakashima, Y. Nakane, Y. Sakamoto, Y. Asano, S. Tanaka, S. Ban, Y. Namito, H. Hirayama and N. Nariyama
Nucl. Instrum. Method Phys. Res., A365 (1995) 553-558
- 8) Characteristic feature in XANES of uranium intermetallics and alloys with noble metals
T. Ogawa, M. Akabori, A. Ito, H. Hayashi, H. Motohashi, and H. Shiwaku
Phys. Rev. B, (1996)
- 9) Carbon wire type beam profile monitor for synchrotron radiation (in Japanese)
H. Shiwaku
J. Japanese Soc. Synchro. Rad. Res., 10 (2) (1997) 161-165
- 10) Beam position monitor using diamond (in Japanese)
H. Sakae, H. Aoyagi, M. Oura, H. Kimura, T. Ohata, H. Shiwaku, S. Yamamoto, H. Sugiyama, K. Tanabe, H. Kobashi and H. Kitamura
J. Japanese Soc. Synchro. Rad. Res., 10 (2) (1997) 165-169
- 11) Responses and glow curves of $\text{Li}_2\text{B}_4\text{O}_7$: Cu, BeO and CaSO_4 : Tm TLDs to 10-40 keV monoenergetic photons from synchrotron radiation
N. Nariyama, S. Tanaka, Y. Nakane, Y. Asano, H. Hirayama, S. Ban, H. Nakashima and Y. Namito
Rad. Protec. Dosimet., 74 (1997) 155-161
- 12) Shielding design calculation of SPring-8 beamline using STAC8
Y. Asano
J. Synchro. Rad., 5 (1998) 615-617
- 13) Mössbauer time spectra of the nuclear forward scattering from coherently vibrating resonant nuclei
M. Mitsui, T. Shimizu, Y. Imai, Y. Yoda, X. W. Zhang, H. Takei, T. Harami and S. Kikuta
Jpn. J. Appl. Phys., 36 (1997) 6525
- 14) Inelastic X-ray scattering by electrons and nuclei in hemoglobin solution
T. Harami, G. Miyazaki, T. Mitsui, Y. Yoda, Y. Kobayashi, S. Kitao and X. W. Zhang
Hyperfine Interactions (C), 3 (1998) 61
- 15) Time spectra of the nuclear forward scattering from a $^{57}\text{FeBO}_3$ single crystal exposed to the RF

- magnetic field synchronized with synchrotron radiation
 M. Mitsui, T. Shimizu, Y. Imai, Y. Yoda, X. W. Zhang, H. Takei, T. Harami and S. Kikuta
 Hyperfine Interactions (C), 3 (1998) 429
- 16) Characteristics of shielding design calculation for synchrotron radiation beamline of SPring-8
 Y. Asano and N. Sasamoto
 Rad. Protec. Dosimet., 82 (1999) 167-174
- 17) Electronics for SPring-8 X-ray beam monitors
 T. Kudo, H. Aoyagi, H. Shiwaku, Y. Sakurai and H. Kitamura
 J. Synchro. Rad., 5 (1998) 630-631
- 18) Structural study of holmium (III) and uranium (VI) organic ligand complex by extended X-ray
 absorption fine-structure spectroscopy
 T. Yaita, H. Narita, S. Suzuki, S. Tachimori, H. Shiwaku, H. Motohashi
 J. Alloyss Compounds, 271-273 (1998) 184-188
- 19) Benchmark experiment for radiation shielding around the beam dump of the SPring-8 injector
 Y. Asano and N. Sasamoto
 J. Nucl. Sci. Technol., Suppl. 1 (2000) 535-539
- 20) Shielding design calculations for laser electron photon beamline of SPring-8
 Y. Asano, T. Nakano, T. Hotta and Y. Ohashi
 J. Nucl. Sci. Technol., Suppl. 1 (2000) 217-221

2. Proceedings

- 1) Shielding design calculation for SPring-8 insertion device beamline
 Y. Asano and N. Sasamoto
 Proceedings of 9th Int. Conf. on Radiation Protection, 1996 (1996) 4. 582-584
- 2) Measurement of glass dosimeter response for low energy photon using synchrotron radiations
 Y. Asano, N. Sasamoto, H. Nakashima, Y. Nakane, Y. Sakamoto, S. Tanaka, Y. Namito, S. Ban, H.
 Hirayama and N. Nariyama
 Proceedings of 9th Int. Conf. on Radiation Protection, 1996 (1996) 4. 253-255
- 3) Inelastic nuclear resonant scattering by hemoglobin CO at room temperature
 T. Harami, G. Miyazaki, M. Seto, X. W. Zhang, Y. Kobayashi, Y. Yoda, H. Shiwaku, S. Nasu and S.
 Kikuta
 Conference Proceedings Vol.50 of "ICAME-95", (1996) 831
- 4) X-ray beam position monitor for insertion device beamline --- wire type beam position monitor ---
 H. Shiwaku, X. W. Zhang, H. Sugiyama, S. Yamamoto, Y. Kagoshima, T. Harami, H. Ohno and M.
 Ando
 KEK Proceedings 96-8 (1997) 102-105
- 5) Development of beam position monitor --- diamond type beam position monitor ---
 H. Sakae, M. Oura, H. Shiwaku, T. Ohata, H. Kitamura, H. Aoyagi, H. Kimura, S. Yamamoto and H.
 Sugiyama
 KEK Proceedings 96-8 (1997) 106-120
- 6) Charge-integrating position-sensitive proportional counter
 A. Muto, K. Hesagawa, N. Yagi and Y. Asano
 Proceedings of the 11th Workshop on Radiation Detectors and Their Uses KEK (1997)
- 7) Synchrotron radiation shielding calculation using STAC8
 Y. Asano
 Proceedings of technical workshop on accelerator safety, Taiwan Synchrotron Radiation Research
 Center, Hsin-chu, Taiwan, (1997) 11p
- 8) Estimation of synchrotron radiation dose outside the hutch of SPring-8 beamline
 Y. Asano
 Proceedings of the 10th International Congress of the International Radiation Protection Association,
 Hiroshima, p6a-330 (1-6) (2000)

3. Reports

- 1) X-ray beam position monitor at SPring-8
 H. Shiwaku, H. Sakae and H. Kitamura
 SR Science and Technology Information, 5(2/3) (1995) 19-23

- 2) From user of photoreaction data (Application to shielding calculation of SR beamline)
Y. Asano
Proceedings of Nuclear Data Seminar in 1995, JAERI-conf 96-008 (1996) 44-49
- 3) Build-up effect on obliquely incident pencil beam photon from 15 to 500keV into lead shield (in Japanese)
Y. Asano and T. Sugita
JAERI—research 96-001 (1996)
- 4) Leakage dose distribution due to scattered photon from concrete floor of synchrotron radiation beamline (in Japanese)
Y. Asano
JAERI-research 97-058 (1997)
- 5) Present status of JAERI soft X-ray beamline BL23SU (in Japanese)
A. Yokoya, Y. Teraoka, Y. Saitoh, T. Okane, T. Nakatani, T. Shimada, Y. Miyahara, et al.
SPring-8 Information, 2 (1) (1997) 30-35
- 6) JAERI hard X-ray beamline for material science: BL14B1 (in Japanese)
H. Konishi, W. Utsumi and J. Mizuki
SPring-8 Information, 2 (4) (1997) 20-23
- 7) Present status of JAERI bending magnet beamline: BL14B1 (in Japanese)
H. Konishi
SPring-8 Information, 3 (3) (1998) 13-15
- 8) Outline of the JAERI hard X-ray undulator beamline, BL11XU
H. Shiwaku, T. Mitsui, Y. Katayama, T. Inami and M. Takahasi
SPring-8 Information, 3 (6) (1998) 29-33
- 9) Radiation shielding and safety analysis of SPring-8 (in Japanese)
Y. Asano and N. Sasamoto
JAERI-tech 98-009 (1998)
- 10) Pulse shape measurement of scintillation emission (in Japanese)
H. Yagi, H. Ito, Y. Asano and S. Usuda
JAERI-tech 98-043 (1998)
- 11) Present status of JAERI X-ray beamline; BL14B1 and BL11XU
H. Konishi, H. Shiwaku, Y. Yoneda, T. Mitsui and Y. Nishihata
SPring-8 Information, 4 (5) (1999) 4-8
- 12) Simulation of gas bremsstrahlung on SPring-8 beamline (in Japanese)
Y. Asano
JAERI-research 99-022 (1999)
- 13) A study of neutron standard field for workplace (in Japanese)
Y. Asano
JAERI-research 99-45 (1999)
- 14) Safety design of synchrotron radiation beamline (in Japanese)
Y. Asano
SR Science and Technology Information, 6 (3) (1996)
- 15) Environmental neutron spectrum due to cosmic-ray (in Japanese)
Y. Asano
The report of the committee of the environmental radiation monitoring, Japan Atomic Energy Industry Forum-Kansai (1997)

4. Book

- 1) Beamlines for medical applications on the SPring-8
Medical Application User Group of SPring-8: C. Uyama, T. Takeda, F. Toyofuku, K. Tokumori, M. Ando, K. Hyodo, Y. Itai, H. Shiwaku, K. Nishimura, and SPring-8 Project Team: H. Kamitsubo
Medical Applications of Synchrotron Radiation (Ed. by M. Ando and C. Uyama), Springer-Verlag, p. 149-157, 1998

High pressure science (High Pressure Science Group)

1. Journals

- 1) Effect of nonhydrostaticity on the pressure induced phase transformation of rhombohedral boron nitride
T. Taniguchi, T. Sato, W. Utsumi, T. Kikegawa and O. Shimomura
Appl. Phys. Lett., 70 (1997) 2392-2394
- 2) In-situ X-ray observation of phase transformation of rhombohedral boron nitride under static high pressure and high temperature
T. Taniguchi, T. Sato, W. Utsumi, T. Kikegawa and O. Shimomura
Diamond and Related Materials, 6 (1997) 1806-1815
- 3) High-pressure high-temperature XAFS investigation on HgTe
Y. Katayama, M. Mezouar, J. P. Itie, J. M. Besson, G. Syfosse, P. LeFevre, and A. Di Cicco
J. de Phys. IV Colloque, C2 (1997) 1011-1012
- 4) Angle-dispersive diffraction measurement system for high-pressure experiments using a multi-channel collimator
K. Yaoita, Y. Katayama, K. Tsuji, T. Kikegawa and O. Shimomura
Rev. Sci. Instrm. 68 (1997) 2106
- 5) Density measurements under high temperature and high pressure by means of X-ray absorption
Y. Katayama
Rev. High Pressure Sci. Technol. 6 (1997) 216-221 (in Japanese)
- 6) The postspinel phase boundary in Mg_2SiO_4 determined by in situ X-ray diffraction
T. Irifune, N. Nishiyama, K. Kuroda, T. Inoue, M. Isshiki, W. Utsumi, K. Funakoshi, S. Urakawa, T. Uchida, T. Katsura and O. Shimomura
Science, 279 (1998) 1698-1700
- 7) X-ray diffraction studies of expanded fluid mercury using synchrotron radiation
K. Tamura, M. Inui, Y. Oh'ishi, K. Funakoshi and W. Utsumi
J. Phys.: Condens.Matter, 10 (1998) 11405-11417
- 8) SPring-8 beamlines for the high pressure science with multi-anvil apparatus
W. Utsumi, K. Funakoshi, S. Urakawa, M. Yamakata, K. Tsuji, H. Konishi and O. Shimomura
Rev. High Pressure Sci. Technol., 7 (1998) 1484-1486
- 9) EXAFS study on tellurium under high pressure and temperature
Y. Katayama, S. Hattori, Y. Morimoto, N. Toda, H. Mori, T. Kobayashi and K. Tsuji
Rev. High Pressure Sci. Technol., 7 (1998) 251-253
- 10) Structure of liquid rubidium and liquid sodium under pressure
Y. Morimoto, S. Kato, N. Toda, Y. Katayama, K. Tsuji, K. Yaoita and O. Shimomura
Rev. High Pressure Sci. Technol., 7 (1998) 245-247
- 11) Amorphization from the quenched high-pressure phase in III-V and II-VI compounds
Y. Mori, S. Kato, H. Mori, Y. Katayama and K. Tsuji
Rev. High Pressure Sci. Technol., 7 (1998) 353-355
- 12) Effects of pressure on hopping conduction in amorphous Ge alloys
N. Toda, Y. Katayama and K. Tsuji
Rev. High Pressure Sci. Technol., 7 (1998) 647-649
- 13) Density measurements of liquid under high pressure and high temperature
Y. Katayama, K. Tsuji, O. Shimomura, T. Kikegawa, M. Mezouar, D. Martinez-Garcia, J. M. Besson, D. Hausermann and M. Hanfland
J. Synchro. Rad., 5 (1998) 1023-1025
- 14) Extended X-ray absorption fine structure study on liquid selenium under high pressure
Y. Katayama, K. Tsuji, H. Oyanagi and O. Shimomura
J. Non-Crystal. Sol., 234 (1998) 93-98
- 15) Volume measurement of MgO under high pressures and high temperatures
W. Utsumi, D. Weidner, R. Liebermann and M. Vaughn
High Pressure-Temperature Research: Properties of Earth and Planetary Materials at High Pressure and Temperature, (1998) 327-333
- 16) Structure of liquid selenium and liquid tellurium under pressure
K. Tsuji and Y. Katayama
The physics of complex liquid. ed. F. Yonezawa, K. Tsuji, K. Kaji, M. Doi and T. Fujiwara, World Scientific, (1998) 83-97

- 17) Introduction of the synchrotron radiation facility, SPring-8: Investigation of earth's interior with high pressure-temperature x-ray experiments
W. Utsumi, K. Funakoshi, and T. Irifune
Industry and Electricity 554 (1998) 11-16, 216-221 (in Japanese)
- 18) High-pressure and high temperature X-ray diffraction experiments at SPring-8 beamline
K. Funakoshi and W. Utsumi
Journal of the Mineralogical Society of Japan 27 (1998) 5-10 (in Japanese)
- 19) Structural studies of expanded fluid mercury using synchrotron radiation
K. Tamura, M. Inui, I. Nakoso, Y. Oh'ishi, K. Funakoshi and W. Utsumi
J. Non-Crystal. Sol., 250-252 (1999) 148-153
- 20) X-ray diffraction measurements for expanded fluid-Se using synchrotron radiation
M. Inui, K. Tamura, Y. Oh'ishi, I. Nakoso, K. Funakoshi and W. Utsumi
J. Non-Crystal. Sol., 250-252, (1999) 519-524
- 21) EXAFS study on liquid selenium and liquid tellurium under high pressure
Y. Katayama, O. Shimomura and K. Tsuji
J. Non-Crystal. Sol., 250-252 (1999) 537-541
- 22) Optical ionization of DX center in AlGaAs:Se by inner-shell excitation
Y. Yoshino, K. Takarabe, M. Ishii, Y. Katayama and O. Shimomura
Phys. B, 273-274 (1999) 781-783
- 23) X-ray diffraction studies of expanded fluid mercury using synchrotron radiation at SPring-8
K. Tamura, M. Inui, I. Nakoso, Y. Oh'ishi, K. Funakoshi and W. Utsumi
Jpn. J. Appl. Phys., 38 (1999) 452-455
- 24) High temperature research beamline (BL04B1) at SPring-8
W. Utsumi, K. Funakoshi, S. Urakawa, T. Irifune, K. Tamura, M. Inui, K. Tsuji and O. Shimomura
J. Japanese Soc. Synchrotron Radiation Research 12 (1999) 17-23 (in Japanese)
- 25) Magnetic properties and single crystal growth of a spin gapped compound, high pressure phase of $(\text{VO}_2)_\text{P}_2\text{O}_7$
T. Saito, M. Azuma, M. Takano, Z. Hiroi, Y. Narumi, K. Kindo and W. Utsumi
J. Japan Soc. Powder and Powder Metallurgy 46 (1999) 1014-1019 (in Japanese)
- 26) Structure of liquids under high-pressure and high-temperature studied by synchrotron radiation
Y. Katayama
J. Japanese Soc. Synchrotron Radiation Research 12 (1999) 375-383 (in Japanese)
- 27) Structural phase transitions of endohedral metallofullerene $\text{La}@\text{C}_{82}$ studied by single crystal X-ray diffraction
T. Watanuki, A. Fujiwara, K. Ishii, Y. Matsuoka, H. Suematsu, K. Ohwada, H. Nakao, Y. Fujii, T. Kodama, K. Kikuchi and Y. Achiba,
Mol. Cryst. Liq. Cryst., 340 (2000) 639-642
- 28) A first-order liquid-liquid phase transition in phosphorus
Y. Katayama, T. Mizutani, W. Utsumi, O. Shimomura, M. Yamakata and K. Funakoshi
Nature, 403 (2000) 170-173
- 29) Second-order phase transition of FeS under high pressure and temperature
K. Kusaba, W. Utsumi, M. Yamakata, O. Shimomura and Y. Syono
J. Phys. Chem. Solid, 61 (2000) 1483-1487
- 30) In situ X-ray diffraction experiments under high pressures and high temperatures at BL14B1 beamline
W. Utsumi, Y. Katayama, T. Mizutani, O. Shimomura, M. Yamakata, M. Azuma, and T. Saito
J. Crystallographic Soc. Japan 42 (2000) 59-67 (in Japanese)
- 31) Structural studies of metallic fluids at SPring-8
K. Tamura, M. Inui, K. Tsuji, K. Funakoshi, and W. Utsumi
J. Crystallographic Soc. Japan 42 (2000) 33-40 (in Japanese)
- 32) On the researchs of the high-pressure mineral physics experimental station at BL04B1 in SPring-8
S. Urakawa, O. Ohtaka, K. Funakoshi, and W. Utsumi
J. Crystallographic Soc. Japan 42 (2000) 24-32 (in Japanese)
- 33) Ultrahigh-pressure research with 8GeV-SR X-ray at BL10XU
N. Hamaya and T. Watanuki
J. Crystallographic Soc. Japan 42 (2000) 51-58 (in Japanese)

2. Proceedings

- 1) In situ x-ray observation of the graphite-diamond transition using synchrotron radiation
W. Utsumi, T. Yagi, T. Taniguchi and O. Shimomura
Advanced Materials '96, edit by M. Akaishi et. al. Published by NIRIM Ibaraki, Japan, (1996) 257-261
- 2) Multi-anvil high pressure apparatus for an in situ X-ray diffraction study using synchrotron radiation
W. Utsumi
Proceeding of the 3rd China-Japan High Pressure Conference, (1998) 56-59
- 3) In situ x-ray observation of graphite-diamond transition using carbonate catalysts under high pressures and high temperatures
W. Utsumi, T. Taniguchi, T. Mizutani, N. Nishiyama, S. Nakano, K. Funakoshi and O. Shimomura
Proc. of the 6th NIRIM International symposium on Advanced Materials (ISAM99), (1999) 67-68
- 4) Structural phase transitions of endohedral metallofullerene La@C82 studied by single crystal X-ray diffraction
T. Watanuki, A. Fujiwara, K. Ishii, Y. Matsuoka, H. Suematsu, K. Ohwada, H. Nakao, Y. Fujii, T. Kodama, K. Kikuchi and Y. Achiba,
Electronic Properties of Novel Materials-Science and Technology of Molecular Nanostructures, edited by H. kuzmany et al., American Institute of Physics, (1999) 124-127

3. Report

- 1) Observation of the materials in the high pressure-temperature vessels -- In situ observation with synchrotron radiation
W. Utsumi
Mukizai Now, 180 (2000) 5 (in Japanese)

Structural physics research (Structural Physics Research Group)

1. Journals

- 1) Semiconductor Interface Studies Using X-ray Anomalous Dispersion
J. Mizuki and D. J. Tweet
Surface Investigation, 12 (1997) 459-468
- 2) Intermediate-range order in lead metasilicate glass
K. Suzuya, D. L. Price, Marie-Louise Saboungi and H. Ohno
Nucl. Instr. Meth. Phys. B, 133 (1997) 57-61
- 3) Magnetic and structural studies of $\text{La}_{1-x}\text{Sm}_x\text{TiO}_3$ ($0 < x < 1$)
K. Yoshii and A. Nakamura
J. Solid State Chem., 133 (1997) 584-586
- 4) Desorption of molecular and atomic fragment-ions from solid CCl_4 and SiCl_4 by resonant photoexcitation at chlorine K-edge
Y. Baba, K. Yoshii and T. A. Sasaki
Surf. Sci., 376 (1997) 330-338
- 5) Element-specific desorption from molecular adsorbates by core-to-valence resonant photoexcitation
Y. Baba, K. Yoshii, H. Yamamoto, T. A. Sasaki and W. Wurth
Surf. Sci., 377-379 (1997) 699-704
- 6) P-KL_{2,3}L_{2,3} resonant Auger spectra in solid phosphorus compounds
K. Yoshii, Y. Baba and T. A. Sasaki
J. Phys.: Condens. Matter, 9 (1997) 2839-2847
- 7) On some problems of EXAFS data analysis - Report on the Workshop of EXAFS Data Analysis -
Y. Nishihata and H. Maeda
J. Japanese Soc. Synchro. Rad. Res., 10 (1997) 45-50 (in Japanese)
- 8) Study of local structure by DAFS
J. Mizuki
J. Cryst. Soc. Jpn., 39 (1997) 31-36 (in Japanese)
- 9) An additional axis for the surface X-ray diffractometer

- M.Takahasi and J.Mizuki
J. Synchrotron Radiat., 5 (1998) 893-895
- 10) Structure of P_2O_5 and alkali phosphate glasses
 K. Suzuya, D. L. Price, Chun-Keung Loong and S. W. Martin
J. Non-Cryst. Solids, 232-234 (1998) 650-657
 - 11) Structure and dynamics of phosphate glasses: from ultra- to orthophosphate composition
 C. K. Loong, K. Suzuya, D. L. Price, B. C. Sales and L. A. Boatner
Physica B, 241-243 (1998) 890-896
 - 12) Growth of ultrathin $BaTiO_3$ films on $SrTiO_3$ and MgO substrates
 Y. Yoneda, T. Okabe, K. Sakaue and H. Terauchi
Surf. Sci., 410 (1998) 62-69
 - 13) Structural characterization of $BaTiO_3$ films grown by molecular beam epitaxy
 Y. Yoneda, T. Okabe, K. Sakaue and H. Terauchi
J. Appl. Phys., 83 (1998) 2458-2461
 - 14) Substrate effects on the Growth of epitaxial $BaTiO_3$ films
 Y. Yoneda, T. Okabe, K. Sakaue and H. Terauchi
J. Korean Phys. Soc., 32 (1998) S1393-S1396
 - 15) X-ray diffraction of $SrTiO_3/BaTiO_3$ multilayer films
 Y. Yoneda, T. Okabe, K. Sakaue and H. Terauchi
J. Korean Phys. Soc., 32 (1998) S1636-S1638
 - 16) Magnetic and structural studies of orthotitanate $Ln_{1-x}Nd_xTiO_3$ ($Ln=Ce$ and Pr ; $0 < x < 1$)
 K. Yoshii and A. Nakamura
J. Solid State Chem., 137 (1998) 181-183
 - 17) Resonant Auger transitions and ion desorption following S-1s excitation in condensed CS_2
 K. Yoshii, Y. Baba and T. A. Sasaki
J. Electron Spectrosc. Relat. Phenom., 93 (1998) 105-108
 - 18) Resonant Auger electron spectra at Si-, P-, S-, and Cl-1s thresholds of condensed molecules
 K. Yoshii, Y. Baba and T. A. Sasaki
Phys. Stat. Sol. (b), 206 (1998) 811-822
 - 19) Structural and optical characterization of porous 3C-SiC
 T. Monguchi, H. Fujioka, K. Ono, M. Oshima, T. Serikawa, T. Hayashi, K. Horiuchi, S. Yamashita,
 K. Yoshii and Y. Baba
J. Electrochemical Soc., 145 (1998) 2241-2243
 - 20) Resonant Auger electron spectroscopy for analysis of the chemical state of phosphorus segregated at SiO_2/Si interfaces
 M. Oshima, Y. Yoshimura, K. Ono, H. Fujita, Y. Sato, Y. Baba, K. Yoshii and T. A. Sasaki
J. Electron Spectrosc. Relat. Phenom. 88-91 (1998) 603-607
 - 21) Desorption of fragment ions from mono- and multilayered CCl_4 on Cu (100) by inner-shell photoexcitation
 Y. Baba, K. Yoshii and T. A. Sasaki
Surf. Sci., 402-404 (1998) 115-119
 - 22) Magnetic studies of orthotitanate $Ln_{1-x}Nd_xTiO_3$ ($Ln=Ce$ and Pr ; $0 < x < 1$)
 K. Yoshii and A. Nakamura
J. Solid State Chem., 137 (1998) 181-183
 - 23) Characterization of porous 3C-SiC
 T. Monguchi, H. Fujioka, K. Ono, M. Oshima, T. Serikawa, T. Hayashi, K. Horiuchi, S. Yamashita,
 K. Yoshii and Y. Baba
J. Electrochemical Soc., 145 (1998) 2241-2243
 - 24) Resonant Auger electron spectroscopy for chemical state analysis of phosphorus segregated at SiO_2/Si interfaces
 M. Oshima, Y. Yoshimura, K. Ono, H. Fujioka, Y. Sato, Y. Baba, K. Yoshii and T. A. Sasaki
J. Electron Spectrosc. Relat. Phenom. 88-91 (1998) 603-607
 - 25) XAFS in the high-energy region
 Y. Nishihata, O. Kamishima, Y. Kugozono, M. Maeda and S. Emura
J. Synchrotron Rad., 5 (1998) 1007-1009
 - 26) XAFS in the high-energy region

- Y. Nishihata
J. Japanese Soc. Synchro. Rad. Res. 11 (1998) 314-316 (in Japanese)
- 27) Surface Structure Studies by X-Ray Diffraction
J. Mizuki
Radioisotopes, 47 (1998) 344-352 (in Japanese)
- 28) Surface and Interface Structure Analysis by X-ray Diffraction
J. Mizuki
Zairyoukagaku, 35 (1998) 155-163 (in Japanese)
- 29) Materials characterization with SR X-rays
J. Mizuki
Kagakukougyou, 49 (1998) 521-529 (in Japanese)
- 30) EXAFS study on local structural changes in amorphous Fe-Zr-B alloys
N. Nakata, N. Hara, Y. Hirotsu, S. Emura, A. Makino, T. Uruga, M. Harada, Y. Nishihata, Y. Yoneda and Y. Kubozon
Jpn. J. Appl. Phys., 38 (1999) suppl.38-1, 404-407
- 31) Structure of 1-ethyl-3-methylimidazolium chloroaluminates: Neutron diffraction measurements and ab initio calculations
S. Takahashi, K. Suzuya, S. Kohara, N. Koura, L. A. Curtiss and M. L. Saboungi
Z. Phys. Chem., 209 (1999) 209-222
- 32) Magnetic studies of $\text{La}_{1-x}\text{Sm}_x\text{TiO}_3$ and $\text{Ln}_{1-x}\text{Nd}_x\text{TiO}_3$ ($\text{Ln}=\text{Ce}$ and Pr ; $0 < x < 1$)
K. Yoshii and A. Nakamura
Physica B, 259-261 (1999) 900-901
- 33) High energy XAFS study of Sm: K-edge in $\text{Sm}_2\text{Fe}_{17}\text{N}_x$
H. Kasatani, M. Ohmura, K. Yokoyama, K. Kobayashi, Y. Nishihata, K. Yagi and H. Terauchi
Jpn. J. Appl. Phys., 38 (1999) suppl. 38-1, 433-435
- 34) XAFS spectra in the high-energy region measured at SPring-8
Y. Nishihata, S. Emura, H. Maeda, Y. Kubozono, M. Harada, T. Uruga, H. Tanida, Y. Yoneda, J. Mizuki and T. Emoto
J. Synchrotron Rad., 6 (1999) 149-151
- 35) Structure of $\text{K}_2\text{O-B}_2\text{O}_3$ glasses and melts
N. Umesaki, Y. Kita, K. Handa, S. Kohara, K. Suzuya, T. Fukunaga, M. Misawa and T. Iida
Electrochem. 67 (1999) 541-546
- 36) The Structure of lead-indium phosphate and lead-scandium phosphate glasses
K. Suzuya, C. K. Loong, D. L. Price, B. C. Sales and L. A. Boatner
J. Non-Crystal. Solids, 258 (1999) 48-56
- 37) Structure of magnesium phosphate glasses
K. Suzuya, D. L. Price, C. K. Loong and S. Kohara
J. Phys. Chem. Solids, 60 (1999) 1457-1460
- 38) Structure of $\text{M}_2\text{O-B}_2\text{O}_3$ ($\text{M}: \text{Na}$ and K) glasses and melts by neutron diffraction
K. Handa, Y. Kita, S. Kohara, K. Suzuya, T. Fukunaga, M. Misawa, T. Iida, H. Iwasaki and N. Umesaki
J. Phys. Chem. Solids, 60 (1999) 1465-1471
- 39) A reverse Monte Carlo study of lead metasilicate glass
K. Suzuya, S. Kohara, D. L. Price, Marie-Louise Saboungi and H. Ohno
J. J. Appl. Phys., 38 suppl. 38-1 (1999) 144-147
- 40) The reverse Monte Carlo study of molten alkali carbonate
S. Kohara, K. Suzuya and H. Ohno
Plasmas & Ions, 2 (1999) 79-83
- 41) Magnetic studies of $\text{La}_{1-x}\text{Sm}_x\text{TiO}_3$ and $\text{Ln}_{1-x}\text{Nd}_x\text{TiO}_3$ ($\text{Ln}=\text{Ce}$ and Pr ; $0 < x < 1$)
K. Yoshii and A. Nakamura
Physica B, 259-261(1999) 900-901
- 42) Charge ordering in $\text{La}_{1-x}\text{Sr}_x\text{MnO}_3$ ($X=0.12$)
T. Inami, N. Ikeda, Y. Murakami, I. Koyama, Y. Wakabayashi and Y. Yamada
Jpn. J. Appl. Phys., 38 suppl. 38-1 (1999) 212-214
- 43) Magnetic study of the mixed orthotitanate $\text{La}_{1-x}\text{Sm}_x\text{TiO}_3$ ($0 < x < 1$)
K. Yoshii, A. Nakamura and H. Abe

- J. Alloys Compd., 290 (1999) 234-243
- 44) Magnetic structure of the kagome lattice antiferromagnet potassium jarosite $\text{KFe}_3(\text{OH})_6(\text{SO}_4)_2$
T. Inami, M. Nishiyama, S. Maegawa and Y. Oka
Phys. Rev., B61 (2000) 12181-12186
- 45) Synthesis and magnetic properties of $\text{Ln}_{2/3}\text{TiO}_3$ (Ln=Pr and Nd)
K. Yoshii
J. Solid State Chem., 149 (2000) 354-359
- 46) Magnetic properties of $\text{Pr}_{1-x}\text{Sr}_x\text{CoO}_3$
K. Yoshii and A. Nakamura
Physica B, 281&282 (2000) 514-515
- 47) Structural, magnetic and transport properties of $\text{Ce}_{1-x}\text{TiO}_3$
K. Yoshii, A. Nakamura and H. Abe
Trans. Mater. Res. Soc. Jpn., 25 [1] (2000) 241-244
- 48) Theoretical and experimental study of resonant 3d X-ray photoemission and resonant $\text{L}_3\text{M}_{4,5}\text{M}_{4,5}$ Auger transition of PdO
T. Uozumi, T. Okane, K. Yoshii, T. A. Sasaki and A. Kotani
J. Phys. Soc. Jpn., 69 (2000) 1226-1233
- 49) Structural and magnetic studies of the lanthanide deficient perovskite $\text{Ce}_{2/3}\text{TiO}_3$
K. Yoshii
J. Alloys. Compd., 305/1-2 (2000) 72-75
- 50) Magnetic transition in the perovskite $\text{Ba}_2\text{CoNbO}_6$
K. Yoshii
J. Solid State Chem., 151 (2000) 294-297
- 51) Magnetic order in perovskite $\text{Pr}_{1-x}\text{Ba}_x\text{CoO}_3$ studied by magnetic circular dichroism (MCD) spectroscopy
K. Yoshii, M. Mizumaki, Y. Saitoh and A. Nakamura
J. Solid State Chem., 152 (2000) 577-581
- 52) Magnetic behaviors of $\text{Pr}_{1-x}\text{Nd}_x\text{TiO}_3$
K. Yoshii, A. Nakamura and H. Abe
J. Alloys Compd., 307/1-2 (2000) 25-30
- 53) Structural and magnetic properties of the perovskites $\text{Sm}_{n+1}(\text{Co}_{0.5}\text{Nb}_{0.5})_n\text{O}_{3n+1}$ ($n=\infty, 2$ and 1)
K. Yoshii
J. Alloys Compd., 307/1-2 (2000) 119-123
- 54) Magnetic properties of $\text{Ce}_{1-x}\text{Nd}_x\text{TiO}_3$ and some solid solution orthotitanates $\text{Ln}_{1-x}\text{Ln}'_x\text{TiO}_3$ (Ln and $\text{Ln}'=\text{La}$ to Sm ; $0 < x < 1$)
K. Yoshii, A. Nakamura, H. Abe and Y. Morii
J. Solid State Chem., 153 (2000) 145-151
- 55) Pseudomorphic growth of Pd monolayer on Au (111) electrode surface
M. Takahashi, Y. Hayashi, J. Mizuki, K. Tamura, T. Kondo, H. Naohara and K. Uosaki
Surf. Sci., 461 (2000) 213-218
- 56) Study of structural physics at BL-14B1 JAERI beamline
J. Mizuki, H. Konishi, Y. Nishihata, M. Takahashi, K. Suzuya, N. Matsumoto and Y. Yoneda
J. Cryst. Soc. Jpn., 42 (2000) 68-75 (in Japanese)

Surface chemistry research (Surface Chemistry Research Group)

1. Journals

- 1) Comparison between electron yield, PSD ion yield, and surface PIPICO yield in near C and O K-edge XAFS in condensed methyl formate-D
T. Sekiguchi, H. I. Sekiguchi, K. Obi and K. Tanaka
J. de Phys. IV (Colloq.), 7 C2 (1997) 505-506
- 2) Surface and bulk $\sigma^*(\text{C-D})$ states in NEXAFS spectra of condensed formic acid layers
H. I. Sekiguchi, T. Sekiguchi and K. Tanaka
J. de Phys. IV(Colloq.), 7 C2 (1997) 499-500
- 3) Stimulated etching of Si (100) by Cl_2 molecular beams with hyperthermal translational energies

- Y. Teraoka and I. Nishiyama
J. Appl. Phys., 82 (1997) 3137-3142
- 4) Applications of a photoion-photoion-coincidence technique to the study of photon-stimulated ion-desorption process following K-shell excitation
 T. Sekiguchi, H. I. Sekiguchi and K. Tanaka
Surf. Sci., 390 (1997) 199-203
 - 5) Photon-stimulated ion desorption from DCOO/Si(100) near the O K-edge
 H. I. Sekiguchi, T. Sekiguchi and K. Tanaka
Surf. Sci., 390 (1997) 214-218
 - 6) Site-specific fragmentation in condensed (CH₃S)₂ by sulfur K-edge photoexcitation
 Y. Baba, K. Yoshii and T. A. Sasaki
J. Chem. Phys., 105 (1996) 8858-8864
 - 7) Desorption of molecular and atomic fragment-ions from solid CCl₄ and SiCl₄ by resonant photoexcitation at chlorine K-edge
 Y. Baba, K. Yoshii and T. A. Sasaki
Surf. Sci., 376 (1997) 330-338
 - 8) Element-specific desorption from molecular adsorbates by core-to-valence resonant photoexcitation
 Y. Baba, K. Yoshii, H. Yamamoto, T. A. Sasaki and W. Wurth
Surf. Sci., 377-379 (1997) 699-704
 - 9) P KL_{2,3}L_{2,3} resonant Auger spectra in solid phosphorus compounds
 K. Yoshii, Y. Baba and T. A. Sasaki
J. Phys.: Condens. Matter, 9 (1997) 2839-2847
 - 10) Spectroscopy on biological systems using synchrotron soft X-rays
 A. Yokoya
J. Jpn. Soc. Synchrotron Rad. Res., 10 (1997) 392-412 (in Japanese)
 - 11) Auger electron spectrometry
 Y. Baba
Radioisotopes, 47 (1998) 240-247 (in Japanese)
 - 12) Dissociation thresholds of low-energy molecular ions on a Cu (100) surface
 H. Yamamoto, Y. Baba and T. A. Sasaki
Jpn. J. Appl. Phys., 37 (1998) 5008
 - 13) Resonant Auger transitions and ion desorption following S-1s excitation in condensed CS₂
 K. Yoshii, Y. Baba and T. A. Sasaki
J. Electron Spectrosc. Relat. Phenom., 93 (1998) 105
 - 14) Structural and optical characterization of porous 3C-SiC
 T. Monguchi, M. Oshima, K. Yoshii and Y. Baba, et al.
J. Electrochem., Soc. 145 (1998) 2241
 - 15) Electronic structures of phosphates studied by TEY-XANES and resonant AES
 N. Okude, H. Noro, M. Nagoshi, H. Yamamoto, Y. Baba and T. A. Sasaki
J. Electron Spectrosc. Relat. Phenom., 88-91 (1998) 467
 - 16) Resonant Auger electron spectroscopy for analysis of the chemical state of phosphorus segregated at SiO₂/Si interface
 M. Oshima, Y. Baba, K. Yoshii and T. A. Sasaki, et al.
J. Electron Spectrosc. Relat. Phenom., 88-91 (1998) 603
 - 17) Soft X-ray beamline specialized for actinides and radioactive materials equipped with a variably polarizing undulator
 A. Yokoya, T. Sekiguchi, Y. Saitoh, T. Okane, Y. Teraoka, et al.
J. Synchrotron Rad., 5 (1998) 10-16
 - 18) Emission of silicon cluster ions by molecular ion bombardment
 H. Yamamoto and Y. Baba
Appl. Phys. Lett. 72 (1998) 2406
 - 19) Resonant Auger electron spectra at Si-, P-, S-, and Cl-1s thresholds of condensed molecules
 K. Yoshii, Y. Baba and T.A. Sasaki
Phys. St. Sol. (b), 296 (1998) 811
 - 20) Construction of the JAERI soft X-ray beamline for actinide material sciences
 T. Nakatani, Y. Saitoh, Y. Teraoka, T. Okane, A. Yokoya

- J. Synchrotron Rad., 5 (1998) 536-538
- 21) Design of surface chemistry end-station of BL23SU in SPring-8
Y. Teraoka and A. Yoshigoe
Jpn. J. Appl. Phys., 38 Suppl. 38-1 (1999) 642-645
 - 22) Adsorbate-substrate interaction in photofragmentation of trimethylsilyl fluoride ($\text{Si}(\text{CH}_3)_3\text{F}$) physisorbed on Cu(111) following Si K-shell excitation
T. Sekiguchi and Y. Baba
Surf. Sci., 433-435 (1999) 849-853
 - 23) Adsorption structure of formic acid on Si (100) studied by surface NEXAFS
H. I. Sekiguchi and T. Sekiguchi
Surf. Sci., 433-435 (1999) 549-553
 - 24) Emission of silicon clusters by high-density excitation
H. Yamamoto and Y. Baba
Surf. Sci., 433-435 (1999) 890
 - 25) Screening effect of metal, semiconductor and insulator surfaces on the photo-fragmentation of physisorbed molecules
Y. Baba and T. Sekiguchi
Surf. Sci., 433-435 (1999) 843
 - 26) XANES and XPS analyses of silicon irradiated by deuterium ions
T. Yoshida, T. Tanabe, H. Yoshida, Y. Yazawa, T. Hara, M. Sakai, H. Yamamoto and Y. Baba
Jpn. J. Appl. Phys., 38, Suppl.38-1 (1999) 305
 - 27) Chemical states of piled-up phosphorus and arsenic atoms at the SiO_2/Si interface
Y. Yoshimura, K. Ono, H. Fujioka, S. Hayakawa, Y. Sato, M. Uematsu, Y. Baba, K. Hirose and M. Oshima
Jpn. J. Appl. Phys. 38, Suppl. 38-1 (1999) 552
 - 28) P and S K-edge XANES of transition-metal phosphates and sulfates
N. Okude, M. Nagoshi, H. Noro, Y. Baba, H. Yamamoto and T.A. Sasaki
J. Electron Spectrosc. Relat. Phenom., 101-103 (1999) 607
 - 29) Study of radiation damage induced by inner-shell excitation in aromatic hydrocarbon solids
I. Shimoyama
Radiation Chemistry, 68 (1999) 17-21 (in Japanese)
 - 30) Study of inner shell excitation effect on C-H dissociation in aromatic hydrocarbon solids
I. Shimoyama
J. Jpn. Soc. Synchrotron Rad. Res., 12 (1999) 59-60 (in Japanese)
 - 31) Site-specific fragmentation of acetone adsorbates on Si (100) in the carbon 1s absorption edge
T. Sekiguchi, H. I. Sekiguchi and Y. Baba
Surf. Sci., 454-456 (2000) 363-368
 - 32) Site-specific ion desorption from formamide adsorbates near the carbon and nitrogen K-edge
H. I. Sekiguchi, T. Sekiguchi, M. Imamura, N. Matsubayashi, H. Shimada and Y. Baba
Surf. Sci., 454-456 (2000) 407-411
 - 33) X-ray absorption studies of anodized monocrystalline 3C-SiC
T. Monguchi, H. Fujioka, T. Uragami, H. Ohuchi, K. Ono, Y. Baba and M. Oshima
J. Electrochem. Soc., 147 (2000) 741-743
 - 34) Stress field dependence of the silicon oxidation rate
H. Noma, H. Fujioka, Y. Baba and M. Oshima
Transactions Mater. Res. Soc. Jpn., 25 (2000) 151-154
 - 35) Desorption of fragment ions from condensed $\text{Si}(\text{OCH}_3)_4$ by localized inner-shell electron excitation at the silicon, oxygen and carbon K-edges
Y. Baba and T. Sekiguchi
J. Vac. Sci. Technol., A18 (2000) 334-337
 - 36) Non-destructive depth profile analysis of SiO_2/Si layer by high-energy XPS
H. Yamamoto and Y. Baba
J. Surf. Anal., 7 (2000) 122-127 (in Japanese)
 - 37) Soft X-ray photochemistry in solid surfaces
T. Sekiguchi and Y. Baba
J. Jpn. Soc. Synchrotron Rad. Res., 13 (2000) 147-155 (in Japanese)

2. Proceedings

- 1) Mechanism of fragmentation and desorption pathways via multi-hole states of chemisorbates as studied by ion-ion-coincidence method
T. Sekiguchi, H. I. Sekiguchi and K. Tanaka
Atomic Collision Research in Japan Progress Report, 23 (1997) 84-85
- 2) Fragmentation of methyl formate following carbon 1s electron excitation
H. I. Sekiguchi and T. Sekiguchi
Atomic Collision Research in Japan Progress Report, 23 (1997) 80-81
- 3) The role of adsorbate-substrate interaction and adsorbate-adsorbate interaction in core-hole induced fragmentation
T. Sekiguchi and Y. Baba
Atomic Collision Research in Japan Progress Report, 24 (1998) 118-119
- 4) The orientation of chemisorbed formate using K-edge photoabsorption spectroscopy
H. I. Sekiguchi and T. Sekiguchi
Atomic Collision Research in Japan Progress Report, 24 (1998) 116-117
- 5) Site-specific fragmentation of acetone adsorbates by selective excitation of inequivalent carbons
T. Sekiguchi, H. I. Sekiguchi and Y. Baba
Atomic Collision Research in Japan Progress Report, 25 (1999) 82-83
- 6) Design of beamline end-station at BL23SU in SPring-8 for surface reaction dynamics study
Y. Teraoka and A. Yoshigoe
Atomic Collision research in Japan Progress Report, 25 (1999) 97-98

3. Report

- 1) Design and manufacture of a testing device for the evaluation of optical elements
Y. Shimizu, O. Yoda, T. Sasuga, Y. Teraoka, A. Yokoya, Y. Yanagihara
JAERI-Tech, 2000-021(2000)

4. Patents

- 1) Dry etching method
Y. Teraoka
Application number: 05-266643
- 2) Evaluation method for semiconductor device fabrication process
Y. Teraoka
Patent number: 334-06816
Allowance date: 98.12.15

Heavy atom science (Heavy Atom Science Group)

1. Journals

- 1) P-KL_{2,3}L_{2,3} Resonant Auger Spectra in Solid Phosphorus Compounds
K. Yoshii, Y. Baba and T. A. Sasaki
J. Phys: Condens. Matter 9 (1997) 2839-2847
- 2) Desorption of Molecular and Atomic Fragment-ions from Solid CCl₄ and SiCl₄ by Resonant Photoexcitation at Chlorine K-edge
Y. Baba, K. Yoshii and T. A. Sasaki
Surf. Sci., 376 (1997) 330-338
- 3) Element-specific Desorption from Molecular Adsorbates by Core-to-valence Resonant Excitation
Y. Baba, K. Yoshii, H. Yamamoto, T. A. Sasaki and W. Wurth
Surf. Sci., 377-379 (1997) 699-704
- 4) Magnetic linear dichroism in angle-resolved photoemission of nickel
Y. Saitoh, S. Ueda, T. Muro, S. Imada, S. Suga, A. Kimura and A. Kakizaki
Physica B, 237-238 (1997) 397-399
- 5) High resolution photoemission study of CeRu₂Si₂
M. Tsunekawa, S. Suga, A. Kimura, T. Matsushita, T. Muro, S. Ueda, H. Daimon, S. Imada, T.

- Nakatani, Y. Saitoh, T. Iwasaki, A. Sekiyama, Fujimori, H. Ishii, T. Miyahara, T. Hanyu, H. Namatame, M. Taniguchi, E. Shigemasa, O. Sakai, R. Takayama, R. Settai, H. Azuma and Y. Onuki
Solid State Commun., 103 (1997) 659-662
- 6) Core photoemission spectra of U_3P_4 and U_3As_4 single crystal
S. Suga, H. Harada, H. Matsubara, Y. Saitoh, A. Kimura, S. Imada, S. Ogawa, A. Ochiai, and T. Suzuki
J. Phys. Soc. Jpn., 66 (1997) 3566-3569
 - 7) Soft X-ray beamline specialized for actinides and radioactive materials equipped with a variably polarizing undulator
A. Yokoya, T. Sekiguchi, Y. Saitoh, T. Okane, T. Shimada, H. Kobayashi, M. Takao, T. Teraoka, S. Sasaki, Y. Miyahara, T. Harami and T. A. Sasaki
J. Synchrotron Rad., 5 (1998) 10-16
 - 8) Resonant Auger electron spectra at Si-, P-, S- and Cl-1s thresholds of codensed molecules
K. Yoshii, Y. Baba and T. A. Sasaki
Phys. Stat Sol. (b), 206 (1998) 811-822
 - 9) Dissociation thresholds of low energy molecular ions on a Cu (100) surface
H. Yamamoto, Y. Baba and T. A. Sasaki
Jpn. J. Appl. Phys., 37 (1998) 5008-5010
 - 10) Desorption of fragment ions from mono- and multilayered CCl_4 on Cu (100) by inner-shell photoexcitation
Y. Baba, K. Yoshii and T. A. Sasaki
Surf. Sci., 402-404 (1998) 115-119
 - 11) Resonant Auger transitions and ion desorption following S-1s excitation in condensed CS_2
K. Yoshii, Y. Baba and T. A. Sasaki
J. Electron Spectrosc. Relat. Phenom. 93 (1998) 105-108
 - 12) Electronic structures of phosphates studied by TEY-XANES and resonant AES
N. Okude, H. Noro, M. Nagoshi, H. Yamamoto, Y. Baba and T. A. Sasaki
J. Electron Spectrosc. Relat. Phenom. 88-91 (1998) 467-471
 - 13) Resonant Auger electron spectroscopy for analysis of the chemical state of phosphorus segregated at SiO_2/Si interface
M. Oshima, Y. Baba, K. Yoshii and T. A. Sasaki, et al.
J. Electron Spectrosc. Relat. Phenom., 88-91 (1998) 603-607
 - 14) Magnetic dichroism in angle-resolved photoemission of ferromagnetic nickel
S. Ueda, S. Imada, Y. Saitoh, T. Muro, M. Kasashima, A. Kimura, A. Kakizaki and S. Suga
J. Electron Spectrosc. Relat. Phenom. 88 (1998) 191-194
 - 15) Electron correlation effects in ferromagnetic Ni observed by spin resolved photoemission
K. Ono, A. Kakizaki, K. Tanaka, K. Shimada, Y. Saitoh and T. Sendohda
Solid State Commun. 107 (1998) 153-157
 - 16) Construction of the JAERI soft X-ray beamline for actinide material sciences
T. Nakatani, Y. Saitoh, Y. Teraoka, T. Okane and A. Yokoya
J. Synchrotron Rad., 5 (1998) 536-538
 - 17) Twin helical undulator beamline for soft X-ray spectroscopy at SPring-8
Y. Saitoh, T. Nakatani, T. Matsushita, T. Miyahara, M. Fujisawa, K. Soda, T. Muro, S. Ueda, H. Harada, A. Sekiyama, S. Imada, H. Daimon and S. Suga
J. Synchrotron Rad., 5 (1998) 542-544
 - 18) Soft X-ray beamline specialized for actinides and radioactive materials equipped with a variably polarizing undulator
A. Yokoya, T. Sekiguchi, Y. Saitoh, T. Okane, Y. Teraoka et.al.
J. Synchrotron Rad., 5 (1998) 10-16
 - 19) P and S K-edge XANES of transition-metal phosphates and sulfates
N. Okude, M. Nagoshi, H. Noro, Y. Baba, H. Yamamoto and T. A. Sasaki
J. Electron Spectrosc. Relat. Phenom. 101-103 (1999) 607-610
 - 20) High resolution Ce 3d-4f resonant photoemission study of $CeNiSn$ and $CePdSn$
A. Sekiyama, S. Suga, Y. Saitoh, S. Ueda, H. Harada, T. Matsushita, T. Nakatani, T. Iwasaki, K. Matsuda, M. Kotsugi, S. Imada, T. akabatake, T. Yoshino, D. T. Adroja, R. Takayama, O. Sakai, H. Harima and T. Nanba

- Solid State Commun., 111 (1999) 373-378
- 21) Importance of measurements of small MCD signals at temperatures higher than T_c : Distinction between itinerant and localized magnetism
T. Miyahara, H. Ishii, S. Imada, Y. Saitoh, R. J. Jung, H. Kimura, S. Suga, H. Sugawara and H. Sato
Jpn. J. Appl. Phys., 38 (1999) 396-399
 - 22) Photoemission study of D03-related $(\text{Fe}_{1-x}\text{V})_3\text{Al}$ alloys
K. Soda, T. Takeuchi, Y. Yanagida, U. Mizutani, M. Kato, Y. Nishino, A. Sekiyama, S. Imada, S. Suga, T. Matsushita and Y. Saitoh
Jpn. J. Appl. Phys., 38 (1999) 496-499
 - 23) Probing bulk states of correlated electron systems by high-resolution resonance photoemission
A. Sekiyama, T. Iwasaki, K. Matsuda, Y. Saitoh, Y. Onuki and S. Suga
Nature 403 (2000) 396-398
 - 24) Bulk and surface electronic structures of CePdX ($X=\text{As, Sb}$) studied by 3d-4f resonance photoemission
T. Iwasaki, S. Suga, S. Imada, A. Sekiyama, K. Matsuda, M. Kotsugi, K. S. An, T. Muro, S. Ueda, T. Matsushita, Y. Saitoh, T. Nakatani, H. Ishii, O. Sakai, R. Takayama, T. Suzuki, T. Oguchi, K. Kato and A. Ochiai
Phys. Rev., B61 (2000) 4621-4628
 - 25) Magnetic order in perovskite $\text{Pr}_{1-x}\text{Ba}_x\text{CoO}_3$ studied by magnetic circular dichroism (MCD) spectroscopy
K. Yoshii, M. Mizumaki, Y. Saitoh, and A. Nakamura
J. Solid State Chem., 152 (2000) 577-581
 - 26) Theoretical and experimental study of resonant 3d X-ray photoemission and resonant $\text{L}_3\text{M}_{4,5}\text{M}_{4,5}$ Auger transition of PdO
T. Uozumi, T. Okane, K. Yoshii., T. A. Sasaki and A. Kotani
J. Phys. Soc. Jpn., 69 (2000) 1226-1233

2. Reports

- 1) Resonant photoemission of deep core-shells
T. A. Sasaki
Notes Basic Sci., 4 (1997) 45-48
- 2) Report on highlights in X-ray synchrotron radiation research
T. A. Sasaki
SPring-8 Information, 3 (1) (1998) 27—29
- 3) Present status of solid state soft X-ray spectroscopy station at BL25SU
Y. Saitoh
SPring-8 Information, 3 (4) (1998) 15-18
- 4) BL25SU experimental station
Y. Saitoh
SPring-8 Information, 4 (3) (1999) 46-49

Electric material science (Electronic Material Science Group)

1. Journals

- 1) Atomic diffusion and electronic structures of Ce/Ni (110) and Ce/Cu (110) systems
T. Okane, M. Yamada, S. Suzuki, S. Sato, A. Kakizaki, T. Kobayashi, S. Shimoda, M. Iwaki and M. Aono
J. Phys. Soc. Jpn., 67 (1997) 264-271
- 2) Resonant photoemission study of single crystalline NdB_6 clean surface
A. Tanaka, K. Tamura, K. Takahashi, M. Hatano, T. Okane, S. Suzuki, S. Sato, S. Kunii, A. Harasawa, A. Kimura and A. Kakizaki
Physica B, 240 (1997) 123-127
- 3) Anisotropy of spin-orbit branching ratio in angle-resolved photoemission from adsorbed layers
H-W. Yeom, T. Abukawa, Y. Takakuwa, S. Fujimori, T. Okane, Y. Ogura, T. Miura, S. Sato, A. Kakizaki and S. Kono
Surf. Sci. Lett., 395 (1998) L236-241

- 4) Soft x-ray beamline specialized for radioactive materials equipped with variably-polarizing undulator
A. Yokoya, T. Sekiguchi, Y. Saitoh, T. Okane, T. Nakatani, T. Shimada, H. Kobayashi, M. Takao, Y. Teraoka, Y. Hayashi, S. Sasaki, Y. Miyahara, T. Harami and T. A. Sasaki
J. Synchrotron Rad., 5 (1998) 10-16
- 5) X-ray photoelectron spectroscopy study of $U(Rh_{1-x}Pd_x)_3$
S. Fujimori, Y. Saito, N. Sato, T. Komatsubara, S. Suzuki, S. Sato, and T. Ishii
J. Phys. Soc. Jpn., 67 (1998) 4164-4168
- 6) Absence of U 5f band states in resonant photoemission spectrum of UPd_2Al_3
S. Fujimori, Y. Saito, M. Seki, K. Tamura, M. Mizuta, K. Yamaki, K. Sato, T. Okane, A. Tanaka, N. Sato, T. Komatsubara, Y. Tezuka, S. Shin, S. Suzuki, S. Sato and T. Ishii
Phys. Rev. B, 59 (1999) 10469-10472
- 7) Photoemission and inverse-photoemission study of heavy-fermion uranium compounds
S. Fujimori, Y. Saito, K. Yamaki, T. Yamamoto, K. Taniguchi, Y. Haga, Y. Onuki, N. Sato, T. Komatsubara, S. Suzuki, and S. Sato
Jpn. J. Appl. Phys. Ser., 11 (1999) 215-217
- 8) The U 5f states in the heavy fermion uranium compound UPd_2Al_3 studied by resonant and X-ray photoelectron spectroscopy
S. Fujimori, Y. Saito, M. Seki, K. Tamura, M. Mizuta, K. Yamaki, K. Sato, T. Okane, A. Tanaka, N. Sato, T. Komatsubara, Y. Tezuka, S. Shin, S. Suzuki and S. Sato
J. Electron Spectrosc. Relat. Phenom., 101-103 (1999) 439-442
- 9) Inelastic nuclear resonant scattering of Fe-Cl₃-graphite intercalation compounds
S. Kitao, T. Mitsui, T. Harami, Y. Yoda and M. Seto
Jpn. J. Appl. Phys., 38 (1999) 535-537
- 10) Experimental study of the influence of magnetic phase transition on the Mossbauer time spectra of nuclear forward scattering
T. Mitsui, S. Kitao and M. Seto
J. Phys. Soc. Jan., 68 (1999) 4049-4050
- 11) Local vibrational densities of states of dilute Fe atoms in Al and Cu metals
M. Seto, Y. Kobayashi, S. Kitao, R. Haruki, T. Mitsui, Y. Yoda, S. Nasu and S. Kikuta,
Phys. Rev., B61 (2000) 11420-11424
- 12) Nuclear resonant scattering of synchrotron radiation by 40K
M. Seto, S. Kitao, Y. Kobayashi, R. Haruki, T. Mitsui, Y. Yoda, X. W. Zhang and Yu. Maeda
Phys. Rev. Lett. 84 (2000) 566-569
- 13) Nuclear resonant scattering of synchrotron radiation by ¹²¹Sb and ¹⁴⁹Sm
S. Kitao, T. Mitsui and M. Seto
J. Phys. Soc. Jan., 69 (2000) 683-685
- 14) Multiple nuclear Bragg scattering
Y. Yoda, H. Igarashi, X. W. Zhang, Y. Imai, T. Mitsui, I. Koyama and S. Kikuta
Hyperfine Interaction, 126 (2000) 435-441
- 15) Photoemission study of the U/Si (111) interface
S. Fujimori, Y. Saito, K. Yamaki, T. Okane, N. Sato, T. Komatsubara, S. Suzuki and S. Sato
Surf. Sci., 444 (2000) 180-186
- 16) Theoretical and experimental study of resonant 3d X-ray photoemission and resonant $L_3M_{4,5}M_{4,5}$ Auger transition of PdO
T. Uozumi, T. Okane, K. Yoshii, T. A. Sasaki and A. Kotani
J. Phys. Soc. Jpn., 69 (2000) 1226-1233

Appendix A Activities of the Research Committee

A research committee was organized in FY1996 to promote activities on advanced photon and synchrotron radiation research in Kansai Research Establishment, JAERI. There are three technical subcommittees for Laser System, Laser Utilization and Synchrotron Radiation Utilization, under the committee.

Committee for Advanced Photon and Synchrotron Radiation Research

First meeting	March 21	1997	Tokyo
Second meeting	February 3	1998	Tokyo
Third meeting	March 9	1999	Tokyo
Fourth meeting	February 10	2000	Tokyo

Technical Subcommittee for Laser System

First meeting	December 8	1997	Tokyo
Second meeting	July 30	1998	Tokyo
Third meeting	December 13	1999	Tokyo

Technical Subcommittee for Laser Utilization

First meeting	December 10	1997	Tokyo
Second meeting	December 3	1998	Tokyo
Third meeting	December 24	1999	Tokyo

Technical Subcommittee for Synchrotron Radiation Utilization

First meeting	December 9	1997	Tokyo
Second meeting	November 27	1998	Harima (SPring-8)
Third meeting	February 8	2000	Harima (SPring-8)

Member of Committee

Committee for Advanced Photon and Synchrotron Radiation Research (FY1999)

Chairman	Chiyoe	Yamanaka	Director General, Institute for Laser Technology
Vice-Chairman	Susumu	Namba	Professor, Technical Research Center, Nagasaki Institute of Applied Science
	Katunobu	Aoyagi	Chief Scientist, Semiconductors Laboratory, The Institute of Physical and Chemical Research
	Fumio	Inaba	Professor, Faculty of Engineering, Tohoku Institute of Technology
	Nobutsugu	Imanishi	Professor, Graduate School of Engineering, Kyoto University
	Seishi	Kikuta	Executive Director, Deputy Director General, Japan Synchrotron Radiation Research Institute
	Yoshitaka	Kimura	Director, Institute of Materials Structure Science, High Energy Accelerator Research Organization
	Yukio	Sugiura	Director, Institute for Chemical Research, Kyoto University
	Hiroshi	Takata	Director, Harima Research Laboratory, Sumitomo Electric Industries, Ltd.
	Harushige	Tsubakino	Laboratory Chair, Laboratory of Advanced Science and Technology for Industry, Himeji Institute of Technology
	Yasuki	Nagai	Director, Research Center for Nuclear Physics, Osaka University
	Takeshi	Namioka	Professor Emeritus, Tohoku University
	Tatsuhiko	Yamanaka	Director, Institute of Laser Engineering, Osaka University
	Hiroyoshi	Lang	Professor, Faculty of Technology, Tokyo University of Agriculture and Technology
	Shuntaro	Watanabe	Professor, Institute for Solid State Physics, The University of Tokyo
	Yukio	Sudo	Director, Office of Planning, JAERI
	Hideo	Ohno	Director General, Kansai Research Establishment, JAERI
	Hiroshi	Takuma	Invited Researcher, JAERI
Secretary	Masahiro	Mori	Senior Staff, Office of Planning, JAERI
	Yoshiaki	Kato	Director, Advanced Photon Research Center, JAERI
	Osamu	Shimomura	Director, Department of Synchrotron Radiation Research, JAERI
	Takashi	Arisawa	Prime Scientist, Advanced Photon Research Center, JAERI
	Siro	Nagai	Deputy Director, Kansai Research Establishment, JAERI
	Yoichiro	Maruyama	Sub-Group Leader, Advanced Photon Research Center, JAERI
	Norio	Ogiwara	Principal Scientist, Advanced Photon Research Center, JAERI
	Tadashi	Aoki	Deputy General Manager, Department of Synchrotron Radiation Research, JAERI

Technical Subcommittee for Laser System (FY1999)

Chief	Shuntaro	Watanabe	Professor, Institute for Solid State Physics, The University of Tokyo	
	Shinichiro	Aoshima	Central Research Laboratory, Mahatmas Photonics K.K.	
	Ichita	Endo	Professor, Graduate School of Advanced Sciences of Matter, Hiroshima University	
	Ichiro	Katayama	Professor, Center for Nuclear Study, School of Science, The University of Tokyo	
	Hiroo	Kinoshita	Professor, Laboratory of Advanced Science and Technology for Industry, Himeji Institute of Technology	
	Takatomo	Sasaki	Professor, Faculty of Engineering, Osaka University	
	Hiroyuki	Daido	Assistant Professor, Institute of Laser Engineering, Osaka University	
	Toshihisa	Tomie	Principal Scientist, Electro technical Laboratory	
	Masahiro	Nakatsuka	Professor, Institute of Laser Engineering, Osaka University	
	Takashi	Fujimoto	Professor, Graduate School of Engineering, Kyoto University	
	Katsumi	Midorikawa	Chief Scientist, Laser Technology Laboratory, The Institute of Physical and Chemical Research	
	Kenzo	Miyazaki	Professor, Institute of Advanced Energy Laboratory, Kyoto University	
	Tetsuo	Yamazaki	Professor, Institute of Advanced Energy Laboratory, Kyoto University	
	Hironori	Yamashita	Professor, Graduate School of Science, Nagoya University	
	Masanobu	Yamanaka	Assistant Professor, Institute of Laser Engineering, Osaka University	
	Kuniyoshi	Yokoo	Professor, Research Institute of Electrical Communication, Tohoku University	
	Kunio	Yoshida	Professor, Faculty of Engineering, Osaka Institute of Technology	
	Yoshiaki	Kato	Director, Advanced Photon Research Center, JAERI	
	Secretary	Siro	Nagai	Deputy Director, Kansai Research Establishment, JAERI
		Yoichiro	Maruyama	Principal Scientist, Advanced Photon Research Center, JAERI

Technical Subcommittee for Applied Photon Research (FY1999)

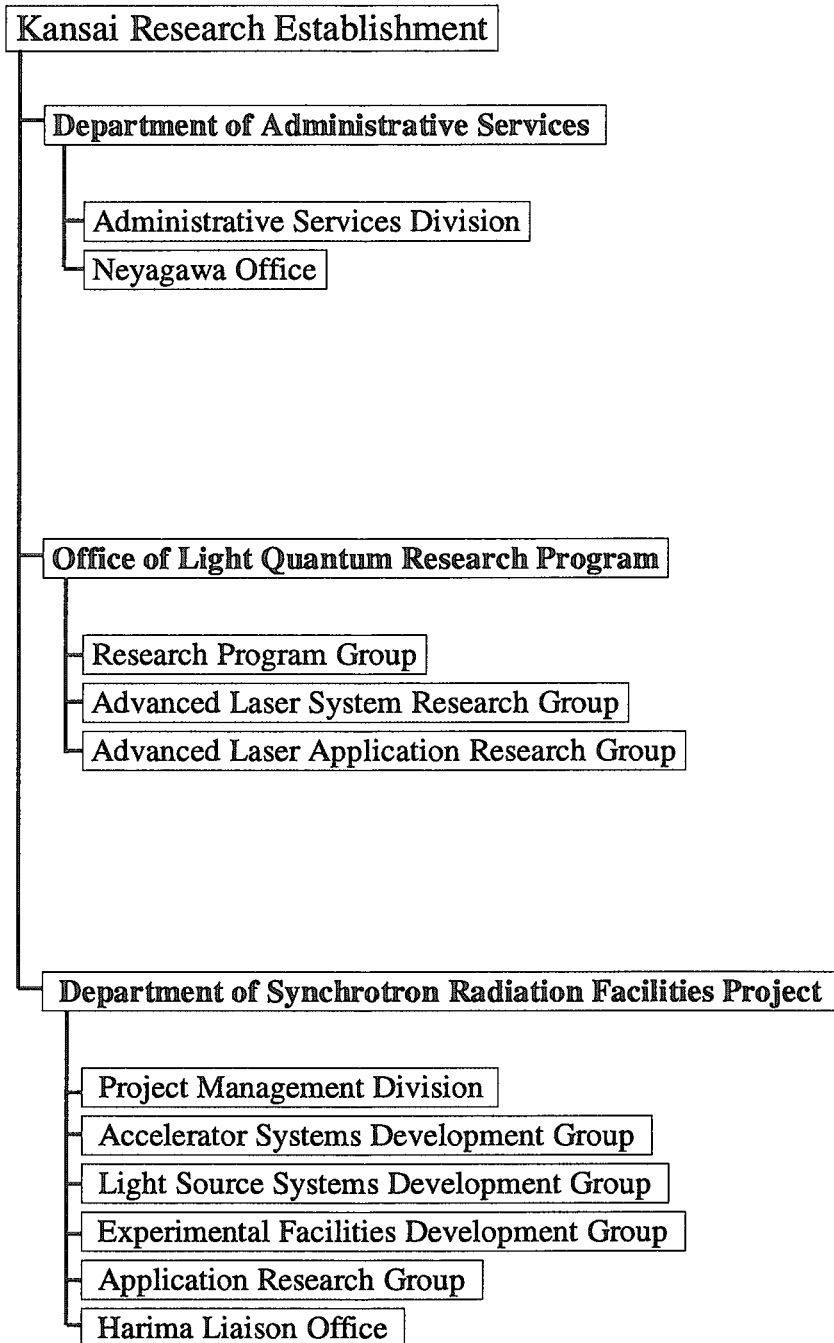
Chief	Susumu	Namba	Professor, Technical Research Center, Nagasaki Institute of Applied Science	
	Atsushi	Ogata	Professor, Graduate School of Advanced Sciences of Matter, Hiroshima University	
	Yoneyoshi	Kitakawa	Assistant Professor, Institute of Laser Engineering, Osaka University	
	Nobuhiro	Gemma	Research & Development Center, Toshiba Corporation	
	Hideomi	Koinuma	Director, Materials and Structures Laboratory, Tokyo Institute of Technology	
	Takayoshi	Kobayashi	Professor, Faculty of Science, The University of Tokyo	
	Naoki	Sato	Professor, Institute for Chemical Research, Kyoto University	
	Seiichi	Tagawa	Professor, Institute of Scientific and Industrial Research, Osaka University	
	Yasushi	Nishida	Professor, Faculty of Engineering, Utsunomiya University	
	Katsunobu	Nishihara	Professor, Institute of Laser Engineering, Osaka University	
	Tatsuo	Nogi	Professor, Graduate School of Informatics, Kyoto University	
	Hiroshi	Masuhara	Professor, Faculty of Engineering, Osaka University	
	Takayasu	Mochiduki	Professor, Laboratory of Advanced Science and Technology for Industry, Himeji Institute of Technology	
	Tsutomu	Yabusaki	Professor, Graduate School of Science, Kyoto University	
	Kazuhisa	Nakajima	Invited Researcher, Advanced Photon Research Center, JAERI	
			Assistant Professor, Accelerator Laboratory, High Energy Accelerator Research Organization	
	Secretary	Siro	Nagai	Deputy Director, Kansai Research Establishment, JAERI
		Norio	Ogiwara	Principal Scientist, Advanced Photon Research Center, JAERI

Technical Subcommittee for Synchrotron Radiation (FY1999)

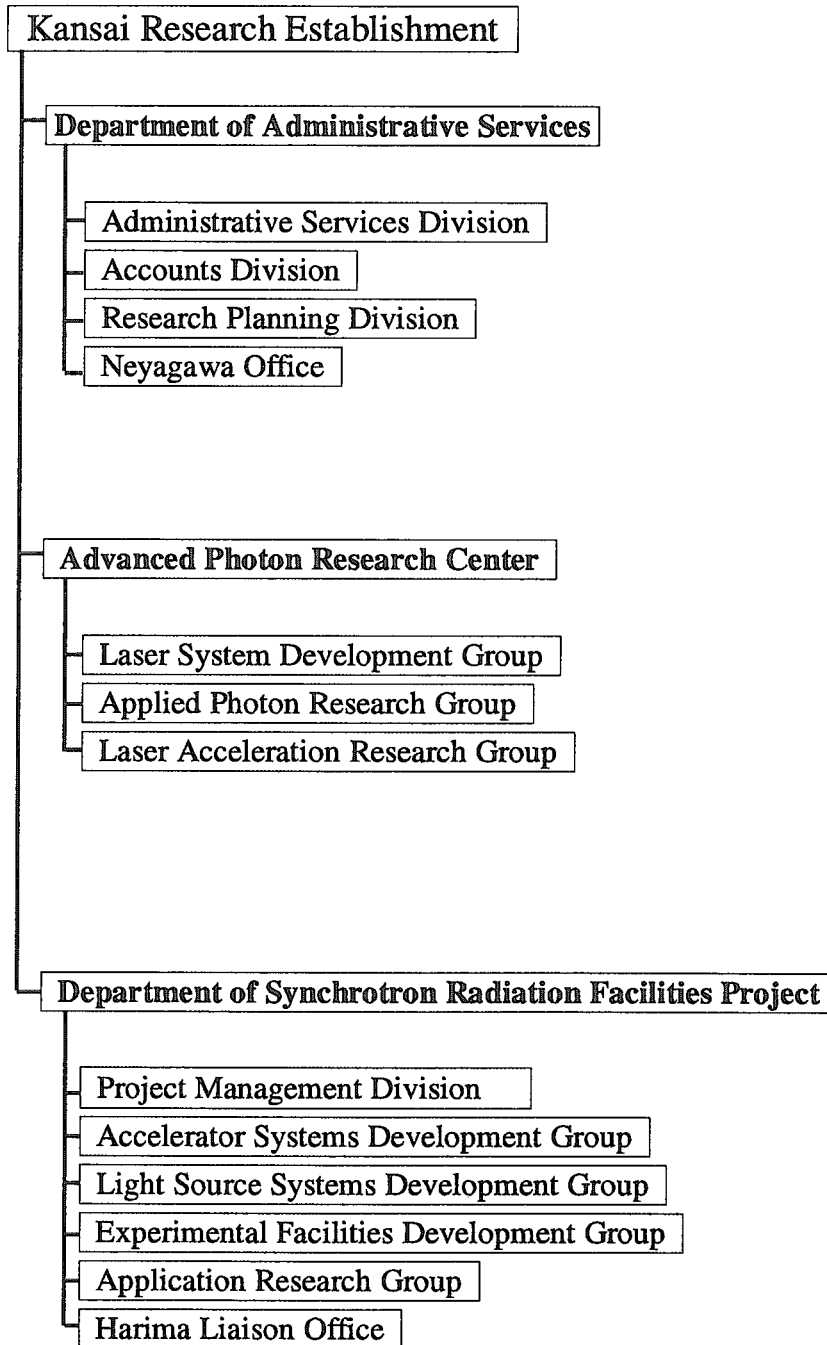
Chief	Koshi	Kikuta	Executive Director, Deputy Director General, Japan Synchrotron Radiation Research Institute
	Tatsuo	Ueki	Director, Japan Synchrotron Radiation Research Institute
	Yoshichika	Ohnuki	Professor, Faculty of Science, Osaka University
	Shik	Shin	Assistant Professor, Institute for Solid State Physics, The University of Tokyo
	Toshio	Takahashi	Assistant Professor, Institute for Solid State Physics, The University of Tokyo
	Kenichiro	Tanaka	Professor, Faculty of Science, Hiroshima University
	Kazuhiko	Tsuji	Professor, Faculty of Science and Technology, Keio University
	Saburo	Nasu	Professor, Faculty of Engineering Science
	Kotaro	Hieda	Professor, Faculty of Science, Rikkyo University
	Yoichi	Murakami	Assistant Professor, Institute of Materials Structure Science, High Energy Accelerator Research Organization
	Osamu	Shimomura	Director, Department of Synchrotron Radiation Research, JAERI
Secretary	Siro	Nagai	Deputy Director, Kansai Research Establishment, JAERI
	Tadashi	Aoki	Deputy General Manager, Department of Synchrotron Radiation Research, JAERI

Appendix B Organization of Kansai Research Establishment

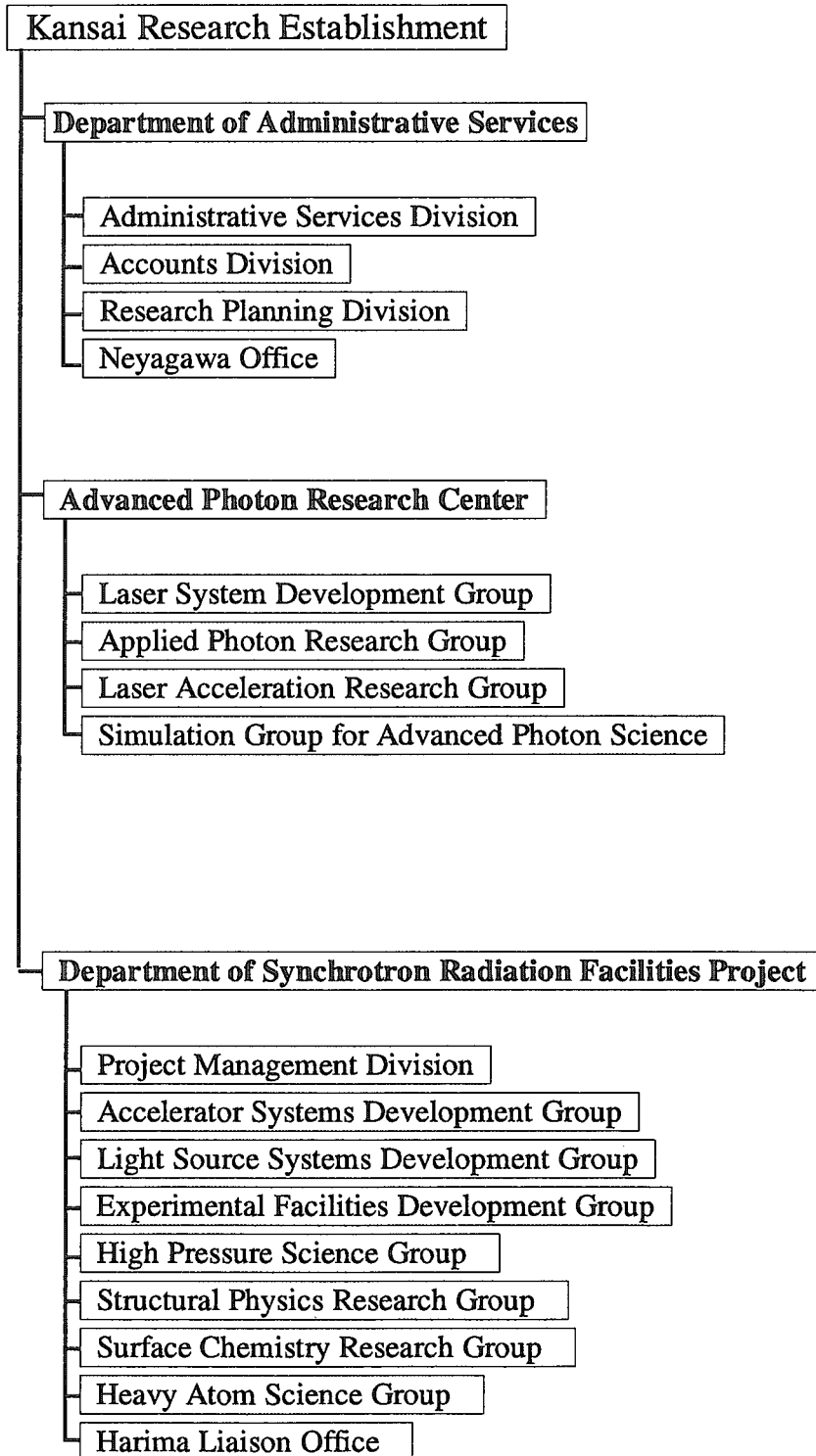
October 1, 1995 ~ March 31, 1996



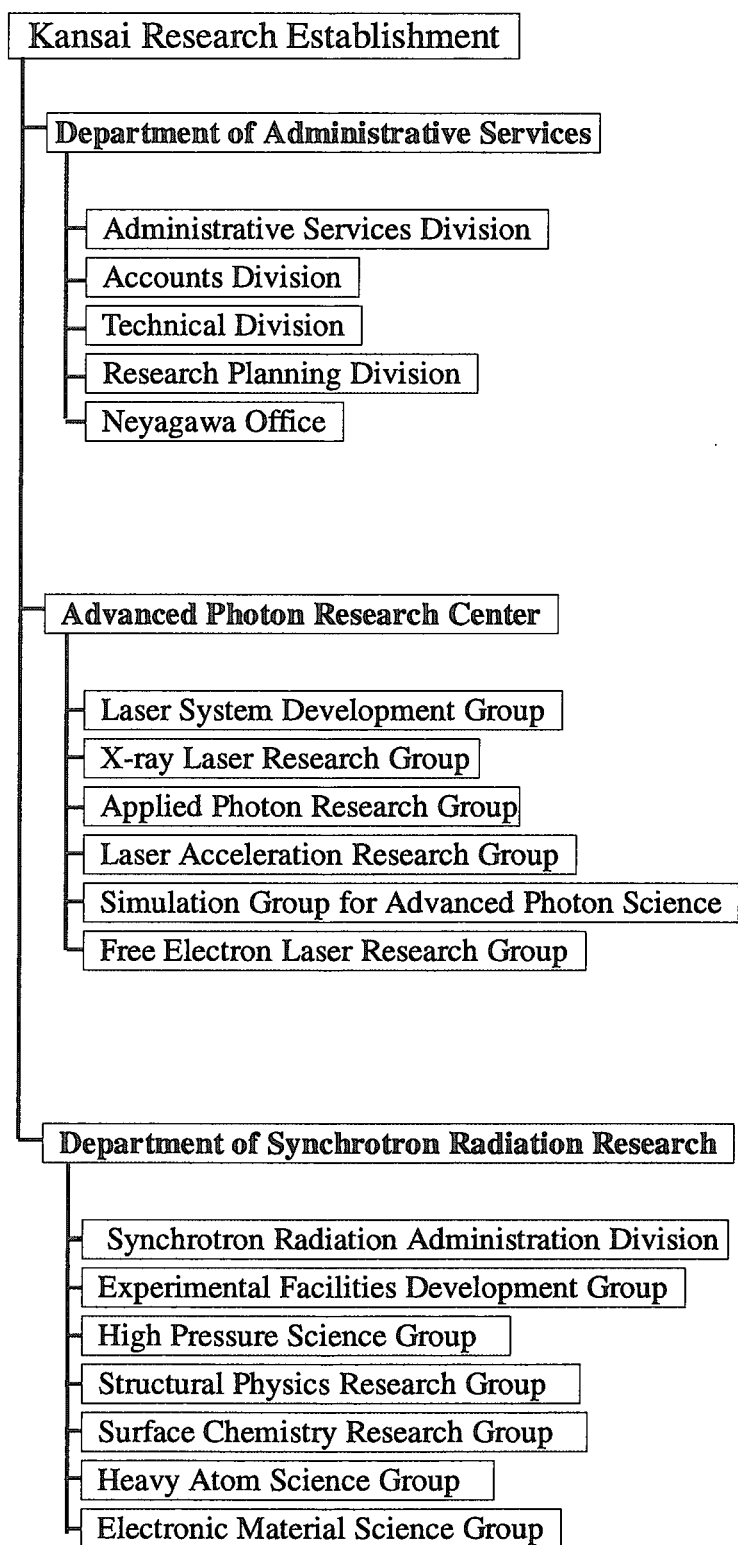
April 1, 1996 ~ March 31, 1997



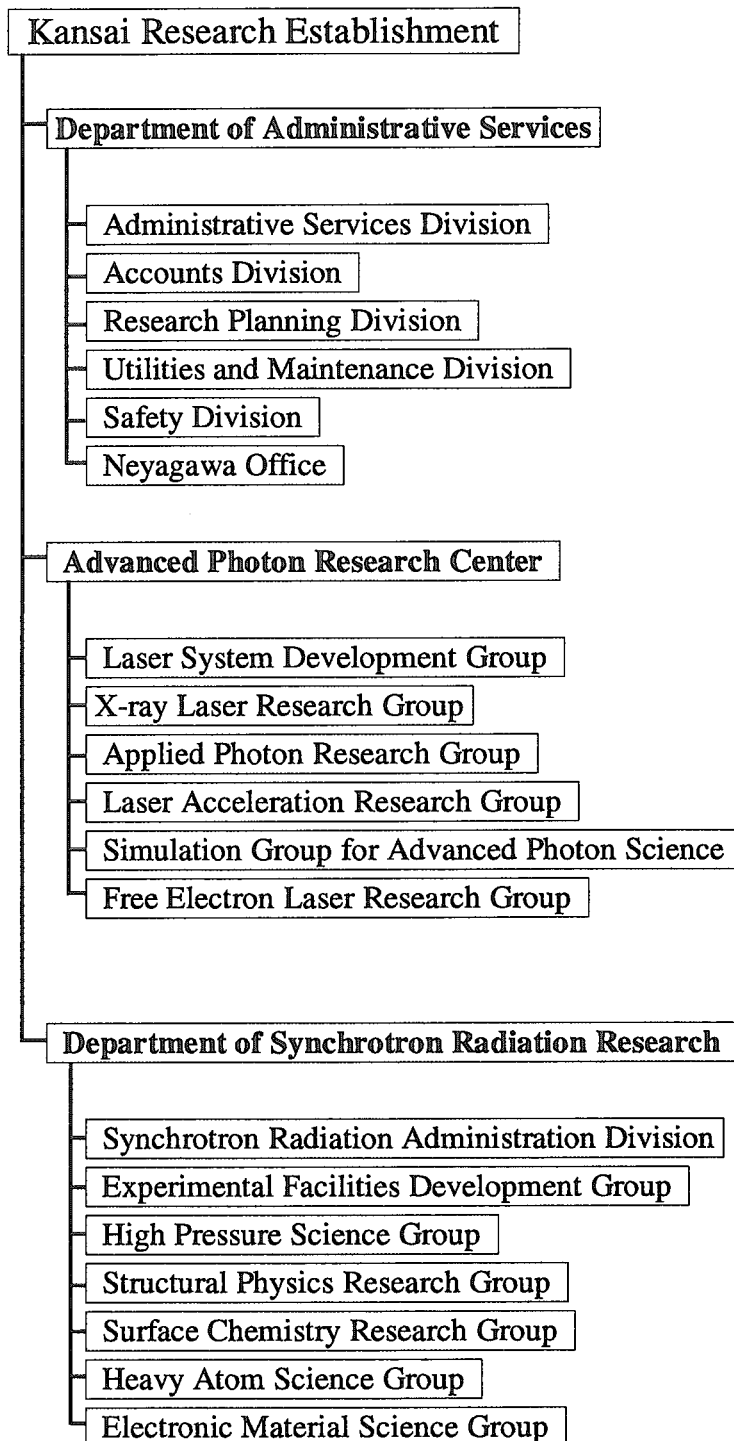
April 1, 1997~March 31, 1998



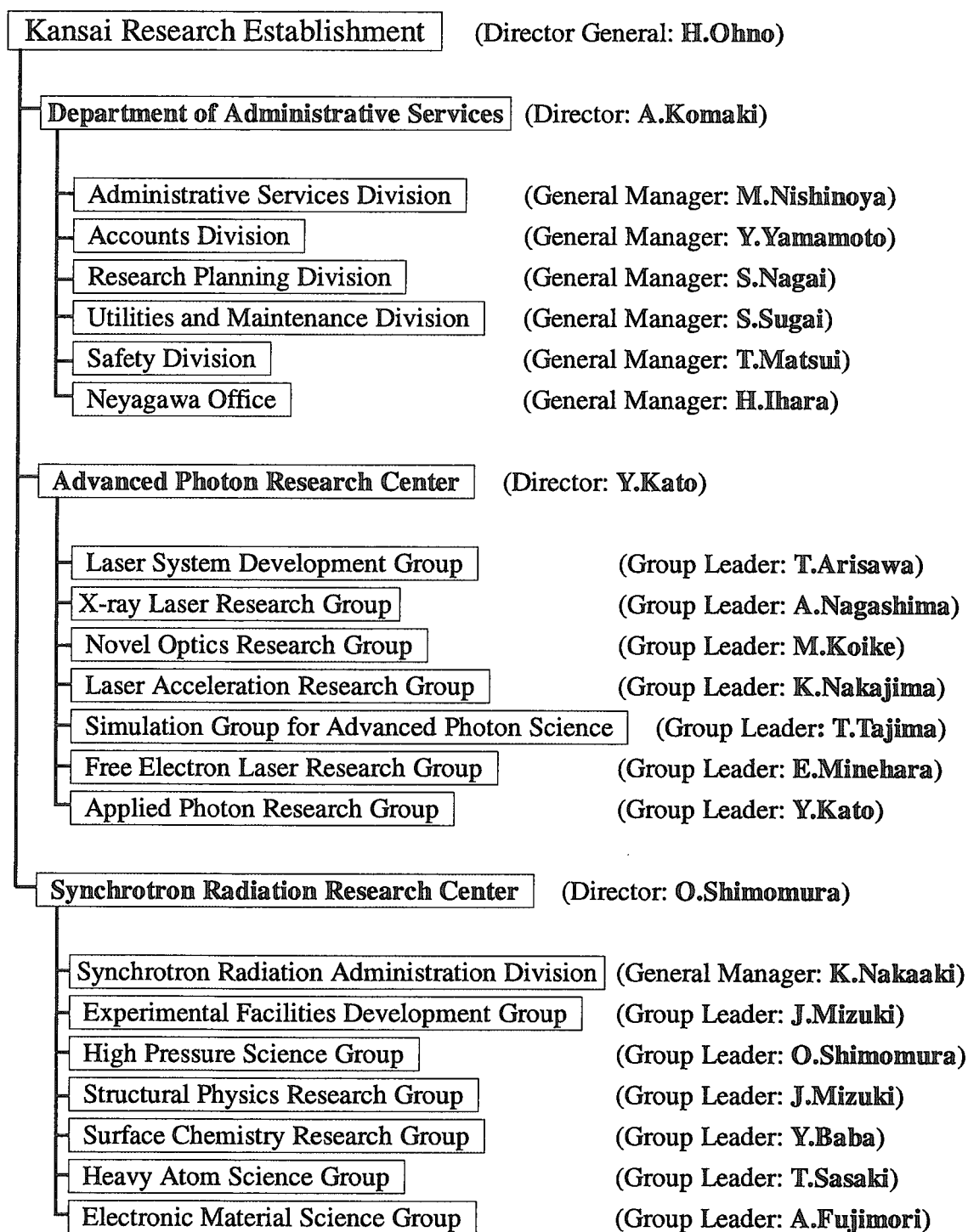
April 1, 1998~March 31, 1999



April 1, 1999 ~ March 31, 2000



April 1, 2000



Appendix C Personnel

March 31, 2000

Personnel at Advanced Photon Research Center

Yoshiaki Kato
 Takashi Arisawa
 Hiroshi Takuma
 Tohru Matoba
 Osamu Yamashita
 Tsutomu Watanabe
 Kazunori Kikuchi
 Jun Nakajima
 Kotomi Waki
 Kiyomi Endoh
 Masako Shigenari

Laser System Development Group

Takashi Arisawa
 Yoichiro Maruyama
 Akihiko Nishimura
 Katsuaki Akaoka
 Masaaki Kato
 Akira Ozu
 Koichi Yamakawa
 Junji Kawanaka
 Kazuaki Suganuma
 Fumiaki Matsuoka
 Hiromitsu Kiriyama
 Yutaka Akahane
 Tsutomu Usami
 Fumihiko Nakano
 Shinichi Matsuoka
 Makoto Aoyama

X-ray Laser Research Group

Yoshiaki Kato
 Akira Nagashima
 Keisuke Nagashima
 Yoji Suzuki
 Masataka Kado
 Tetsuya Kawachi
 Noboru Hasegawa
 Momoko Tanaka
 Kouta Sukegawa
 Akito Sagisaka
 Tomonao Hosokai
 Kenjiro Takahashi
 Lu Peixiang
 Yoshinori Matsui

Applied Photon Research Group

Siro Nagai
 Osamu Yoda
 Norio Ogiwara
 Masato Koike
 Yuichi Shimizu
 Akira Sugiyama
 Koichi Ogura
 Yuzuru Kurosaki

Hiroshi Murakami
 Satoshi Orimo
 Hiroyasu Fukuyama
 Masahiko Ishino
 Naoji Moriya
 Yukio Hayashi
 Hiroshi Masuhara

Laser Acceleration Research Group

Kazuhiisa Nakajima
 Shuhei Kanazawa
 Hideyuki Kotaki
 Shuji Kondo
 Takashi Yokoyama
 Masaki Kando
 Hideki Dewa

Simulation Group for Advanced Photon Science

Toshiki Tajima
 Hitoshi Ihara
 Mitsuru Yamagiwa
 Akira Sasaki
 James Koga
 Takayuki Utsumi
 Kengo Moribayashi
 Takuya Arakawa
 Keisuke Nakagawa
 Yutaka Ueshima
 Ichirou Fukumoto
 Alexei Zhidkov
 Levon Tsintsadze
 Hiroo Totsuji

Free Electron Laser Research Group

Eisuke Minehara
 Toshihiko Yamauchi
 Masaru Sawamura
 Ryoichi Hajima
 Ryoji Nagai
 Nobuhiro Kikuzawa
 Takehito Hayakawa
 Nobuyuki Nishimori
 Toshiyuki Shizuma

March 31, 2000

Personnel at Synchrotron Radiation Research Center

Osamu Shimomura
Fujiyasu Nomura
Teikichi Sasaki

Experimental Facilities Development Group

Jun'ichiro Mizuki
Hiroyuki Konishi
Yoshihiro Asano
Hideaki Shiwaku
Takaya Mitui
Motoharu Marushita
Yukio Hayashi

High Pressure Science Group

Osamu Shimomura
Nozomu Hamaya
Wataru Utsumi
Yoshinori Katayama
Tetsu Watanuki
Takeshi Mizutani
Naoki Ishimatsu

Structural Physics Research Group

Jun'ichiro Mizuki
Yasuo Nishihata
Kentaro Suzuya
Norimasa Matsumoto
Kenji Yoshii
Masamitsu Takahashi
Toshiya Inami
Yasuhiro Yoneda
Tatsuo Fukuda
Hiroyuki Kawamura

Surface Chemistry Research Group

Yuji Baba
Tetsuhiro Sekiguchi
Yuden Teraoka
Akinari Yokoya
Akitaka Yoshigoe
Ken Akamatsu
Mutsumi Sano
Iwao Shimoyama

Heavy Atom Science Group

Teikichi Sasaki
Yuji Saitoh
Akane Agui

Electronic Material Science Group

Atsushi Fujimori
Makoto Seto
Tetsuo Okane
Shin'ichi Fujimori
Akihiro Ino

Synchrotron Radiation Administration Division

Katsuhiko Nakaaki
Hironobu Ogawa
Kunihiro Suzuki
Tadashi Aoki
Shoichi Ono
Satoshi Furuta
Kensin Doi

March 31, 2000

Personnel at Department of Administrative Services

Akira Komaki
Tetsuo Kanazawa
Siro Nagai

Administrative Services Division

Yoshinori Nishinoya
Seizo Hosaka
Yoshimi Kurata
Syoji Odauchi
Yutaka Fukuda
Masako Tanaka
Shinji Komata

Accounts Division

Yoshio Yamamoto
Isamu Okabe
Masahiko Matsumoto
Hiroyuki Yamano
Taiki Ikejima
Kazumi Takeda
Takanori Kawasaki
Norito Hiramatsu

Research Planning Division

Siro Nagai
Noboru Tsuchida
Sayaka Harayama
Shuichi Fujita
Noriko Uehara

Utilities and Maintenance Division

Seiji Sugai
Tadashi Hanawa
Takashi Yamaguchi
Taketomo Abe
Tsutomu Tomiya

Safety Division

Tomoaki Matsui
Yaichi Fukushima
Masayuki Ueno
Masayuki Kabutou
Yuko Hasegawa
Sanae Kita

Neyagawa Office

Hitoshi Ihara
Atsuko Hayashi

Appendix D Symposia

- (1) **The first JAERI-Kansai International Workshop on Ultrashort-pulse Ultrahigh-power Lasers and Simulation for Laser-plasma Interactions** (held as “Joint ICFA/JAERI-Kansai International Workshop ‘97”, organized by International Committee for Future Accelerators, hosted by Japan Atomic Energy Research Institute and High Energy Accelerator Research Organization)
July 14-18, 1997, Kyoto, Japan
JAERI-Conf 98-004, “Proceedings of The first JAERI-Kansai International Workshop on Ultrashort-pulse Ultrahigh-power Lasers and Simulation for Laser-plasma Interactions July 14-18, 1997, Kyoto Research Park, Kyoto, Japan”, March 1998.
- (2) **The 6th International Conference on Synchrotron Radiation Instrumentation** (cosponsored by Japan Atomic Energy Research Institute, Japanese Society for Synchrotron Radiation Research, RIKEN and Japan Synchrotron Radiation Research Institute)
August 4—8, 1997, Himeji, Japan
J. Synchrotron Radiation, 5 part 3, “SRI’97 Proceedings”, May 1998.
- (3) **6th International Conference on X-Ray Lasers** (cosponsored by Japan Atomic Energy Research Institute and Osaka University)
August 31-September 4, 1998, Kyoto, Japan
Institute of Physics Conference Series Number 159, “Proceedings of the 6th International Conference on X-Ray Lasers held in Kyoto, Japan, August 31-September 4, 1998”
- (4) **The Second International Conference on Synchrotron Radiation in Materials Science** (cosponsored by Japan Atomic Energy Research Institute, RIKEN and Japan Synchrotron Radiation Research Institute)
October 31—November 3, 1998, Kobe, Japan
Jpn. J. Appl. Phys. Suppl., 38-1, “Proceedings of the SRMS—2”, June 1999.
- (5) **The First Symposium on Advanced Photon Research**
November 8-9, 1999, Kyoto, Japan
JAERI-Conf 2000-006, “Proceedings of The First Symposium on Advanced Photon Research November 8-9, 1999, Keihanna Plaza/Advanced Photon Research Center, Kyoto, Japan”, March 2000.
- (6) **Workshop on Surface and Interface Using Synchrotron Radiation**
March 16-17, 2000, SPring-8, Japan.

This is a blank page.

国際単位系 (SI) と換算表

表1 SI基本単位および補助単位

量	名称	記号
長さ	メートル	m
質量	キログラム	kg
時間	秒	s
電流	アンペア	A
熱力学温度	ケルビン	K
物質質量	モル	mol
光度	カンデラ	cd
平面角	ラジアン	rad
立体角	ステラジアン	sr

表3 固有の名称をもつSI組立単位

量	名称	記号	他のSI単位による表現
周波数	ヘルツ	Hz	s ⁻¹
力	ニュートン	N	m·kg/s ²
圧力, 応力	パスカル	Pa	N/m ²
エネルギー, 仕事, 熱量	ジュール	J	N·m
工率, 放射束	ワット	W	J/s
電気量, 電荷	クーロン	C	A·s
電位, 電圧, 起電力	ボルト	V	W/A
静電容量	ファラド	F	C/V
電気抵抗	オーム	Ω	V/A
コンダクタンス	ジーメンズ	S	A/V
磁束	ウェーバ	Wb	V·s
磁束密度	テスラ	T	Wb/m ²
インダクタンス	ヘンリー	H	Wb/A
セルシウス温度	セルシウス度	°C	
光束流	ルーメン	lm	cd·sr
照射度	ルクス	lx	lm/m ²
放射線量	ベクレル	Bq	s ⁻¹
吸収線量	グレイ	Gy	J/kg
線量当量	シーベルト	Sv	J/kg

表2 SIと併用される単位

名称	記号
分, 時, 日	min, h, d
度, 分, 秒	°, ', "
リットル	l, L
トン	t
電子ボルト	eV
原子質量単位	u

1 eV = 1.60218 × 10⁻¹⁹ J
1 u = 1.66054 × 10⁻²⁷ kg

表4 SIと共に暫定的に維持される単位

名称	記号
オングストローム	Å
バ	b
バ	bar
ガ	Gal
キュリー	Ci
レントゲン	R
ラ	rad
レ	rem

1 Å = 0.1 nm = 10⁻¹⁰ m
1 b = 100 fm² = 10⁻²⁸ m²
1 bar = 0.1 MPa = 10⁵ Pa
1 Gal = 1 cm/s² = 10⁻² m/s²
1 Ci = 3.7 × 10¹⁰ Bq
1 R = 2.58 × 10⁻⁴ C/kg
1 rad = 1 cGy = 10⁻² Gy
1 rem = 1 cSv = 10⁻² Sv

表5 SI接頭語

倍数	接頭語	記号
10 ¹⁸	エクサ	E
10 ¹⁵	ペタ	P
10 ¹²	テラ	T
10 ⁹	ギガ	G
10 ⁶	メガ	M
10 ³	キロ	k
10 ²	ヘクト	h
10 ¹	デカ	da
10 ⁻¹	デシ	d
10 ⁻²	センチ	c
10 ⁻³	ミリ	m
10 ⁻⁶	マイクロ	μ
10 ⁻⁹	ナノ	n
10 ⁻¹²	ピコ	p
10 ⁻¹⁵	フェムト	f
10 ⁻¹⁸	アト	a

(注)

- 表1-5は「国際単位系」第5版, 国際度量衡局 1985年刊行による。ただし, 1 eV および 1 uの値は CODATA の1986年推奨値によった。
- 表4には海里, ノット, アール, ヘクトールも含まれているが日常の単位なのでここでは省略した。
- barは, JISでは流体の圧力を表わす場合に限り表2のカテゴリーに分類されている。
- EC閣僚理事会指令では bar, barn および「血圧の単位」mmHgを表2のカテゴリーに入れている。

換算表

力	N (=10 ⁵ dyn)	kgf	lbf
	1	0.101972	0.224809
	9.80665	1	2.20462
	4.44822	0.453592	1

粘度 1 Pa·s (N·s/m²) = 10 P (ポアズ) (g/(cm·s))

動粘度 1 m²/s = 10⁴ St (ストークス) (cm²/s)

圧	MPa (=10 bar)	kgf/cm ²	atm	mmHg (Torr)	lbf/in ² (psi)
	1	10.1972	9.86923	7.50062 × 10 ³	145.038
力	0.0980665	1	0.967841	735.559	14.2233
	0.101325	1.03323	1	760	14.6959
	1.33322 × 10 ⁻⁴	1.35951 × 10 ⁻³	1.31579 × 10 ⁻³	1	1.93368 × 10 ⁻²
	6.89476 × 10 ⁻³	7.03070 × 10 ⁻²	6.80460 × 10 ⁻²	51.7149	1

エネルギー・仕事・熱量	J (=10 ⁷ erg)	kgf·m	kW·h	cal (計量法)	Btu	ft·lbf	eV
	1	0.101972	2.77778 × 10 ⁻⁷	0.238889	9.47813 × 10 ⁻⁴	0.737562	6.24150 × 10 ¹⁸
	9.80665	1	2.72407 × 10 ⁻⁶	2.34270	9.29487 × 10 ⁻³	7.23301	6.12082 × 10 ¹⁹
	3.6 × 10 ⁶	3.67098 × 10 ⁵	1	8.59999 × 10 ⁵	3412.13	2.65522 × 10 ⁶	2.24694 × 10 ²⁵
	4.18605	0.426858	1.16279 × 10 ⁻⁶	1	3.96759 × 10 ⁻³	3.08747	2.61272 × 10 ¹⁹
	1055.06	107.586	2.93072 × 10 ⁻⁴	252.042	1	778.172	6.58515 × 10 ²¹
	1.35582	0.138255	3.76616 × 10 ⁻⁷	0.323890	1.28506 × 10 ⁻³	1	8.46233 × 10 ¹⁸
	1.60218 × 10 ⁻¹⁹	1.63377 × 10 ⁻²⁰	4.45050 × 10 ⁻²⁶	3.82743 × 10 ⁻²⁰	1.51857 × 10 ⁻²²	1.18171 × 10 ⁻¹⁹	1

1 cal = 4.18605 J (計量法)
= 4.184 J (熱化学)
= 4.1855 J (15 °C)
= 4.1868 J (国際蒸気表)
仕事率 1 PS (仏馬力)
= 75 kgf·m/s
= 735.499 W

放射能	Bq	Ci
	1	2.70270 × 10 ⁻¹¹
	3.7 × 10 ¹⁰	1

吸収線量	Gy	rad
	1	100
	0.01	1

照射線量	C/kg	R
	1	3876
	2.58 × 10 ⁻⁴	1

線量当量	Sv	rem
	1	100
	0.01	1

